博士論文

A study on the properties of sustainable concrete with various industrial by-product

各種産業副産物を用いたサステナブルコンクリートの特性に関する研究

2023 年 6 月

劉 子浩 リュウ　ジハオ

LIU ZIHAO

The University of Kitakyushu
Graduate Programs in Environmental Engineering
Architecture Course,
Takasu Laboratory

CONTENTS

Chapter 1

RESEARCH BACKGROUND AND PURPOSE

1.1 Background

1.1.1 Current situation of cement application

With the rapid worldwide development of urbanization in recent years, concrete, one of the most widely used materials in the construction industry, is consumed in large quantities every year. It is known for its high compressive strength, durability, and versatility. The key ingredient in concrete is cement, which binds the other components of concrete together. Cementitious materials play a crucial role in determining the strength and durability of concrete. Ordinary Portland cement (OPC) is used as the main cementitious material in concrete. The global cement demand is estimated at over 4.216 billion metric tons in 2018 as per International Cement Review Research Report which further requires nearly 9.476 107 Joules/ton of energy consumption in its production process[1]. Among them, 1 kg Portland cement production process produces 0.66 ~ 0.82 kg of carbon emissions, and the carbon dioxide produced by global cement production accounts for 5% ~ 7% of anthropogenic carbon dioxide emissions. In 2017, the carbon dioxide emissions of the cement industry exceeded all the trucks on the road. (Fig 1.1) Cement consumption is expected to rise from its present annual value of roughly 4.2 billion tons to around 5.2 billion tons by 2050, according to current projections [2]. In recent years, there has been a growing interest in exploring alternative cementitious materials that can reduce the carbon footprint of concrete production and enhance its performance.

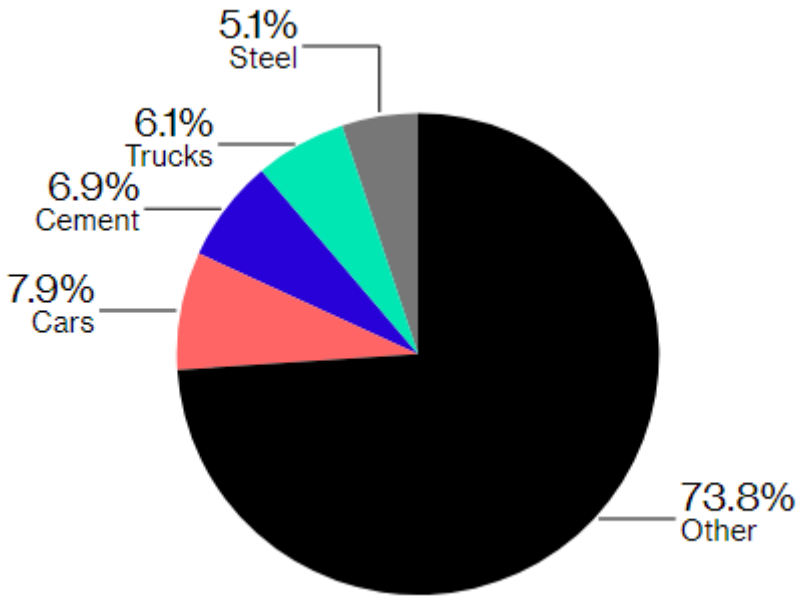

Fig1.1 the carbon dioxide emissions of the cement industry in 2017[1]

1.1.2 Physical and chemical properties of fly ash

Fly ash is the finely divided residue that results from the combustion of pulverized coal and is transported from the combustion chamber by exhaust gases. It has been reported that the global annual output of fly ash exceeds 900 million tons[22], of which the annual output of China is about 580 million tons[23], India is 169.25 million tons[24], the United States is 43.5 million tons[25], and Australia is 14 million tons[26]. However, the effective utilization rate of fly ash currently accounts for only about 53.5% of the total[22]. Fly ash particles contain high concentrations of potentially toxic trace elements that are condensed from flue gas, making them a significant source of contamination. The research conducted on the potential applications of fly ash waste holds both industrial and environmental significance. Currently, a large portion of fly ash generated is disposed of in landfills, but this practice is being critically evaluated due to its environmental implications. The increasing costs and potential prohibitions associated with fly ash disposal have necessitated extensive global research on waste material utilization. The aim is to address the escalating environmental risks and optimize waste disposal techniques to make them more economically viable. An effective solution to this problem involves the utilization of waste materials for the creation of new products, rather than relying solely on land disposal. This approach not only helps mitigate the growing toxic threat to the environment but also offers an opportunity to improve waste management practices and affordability. By embracing the use of waste materials, we can minimize the impact of fly ash contamination and work towards a more sustainable future. This shift towards resource utilization and recycling is crucial for reducing reliance on landfills and aligning with environmental goals. Extensive research and innovation in this field are key to finding economically viable and environmentally friendly solutions[8].

Fly ash is primarily composed of small, powder-like particles that are mostly spherical in shape, whether solid or hollow, and primarily exhibit a glassy (amorphous) structure. The carbonaceous components within the fly ash consist of angular particles. While sub-bituminous coal fly ash shares a similar silt-like particle size as bituminous coal fly ash, it typically exhibits a slightly coarser texture. The specific gravity of fly ash generally falls within the range of 2.1 to 3.0, while its specific surface area can vary between 170 and 1000 m^2/kg [9]. The color of fly ash can range from tan to gray to black, contingent upon the quantity of unburned carbon present in the ash.

The characteristics of fly ash are significantly impacted by the properties of the combusted coal and the methods employed for its handling and storage. Coal can be categorized into four types, or ranks, based on their heating value, chemical composition, ash content, and geological origin. These four coal types (ranks) encompass anthracite, bituminous, sub-bituminous, and lignite. Furthermore, in addition to its classification based on its form, whether dry, conditioned, or wet, fly ash is occasionally categorized according to the specific type of coal from which it originated. Bituminous coal fly ash primarily comprises silica, alumina, iron oxide, and calcium as its main constituents, alongside varying quantities of carbon determined by the loss on ignition (LOI). In contrast, lignite and sub-bituminous coal fly ash exhibit higher concentrations of calcium and magnesium oxide, lower proportions of silica and iron oxide, and reduced carbon content when compared to bituminous coal fly ash. Due to the limited utilization of anthracite coal in utility boilers, the quantity of anthracite coal fly ash generated is relatively small. By referring to Table 1, a comparison can be made between the typical chemical

constituents of bituminous coal fly ash and those of lignite coal fly ash and sub-bituminous coal fly ash. The table demonstrates that lignite and sub-bituminous coal fly ash exhibit a greater concentration of calcium oxide and lower loss on ignition when compared to fly ash derived from bituminous coals. Moreover, lignite and sub-bituminous coal fly ash may contain a higher proportion of sulfate compounds in comparison to bituminous coal fly ash[8].

Table 1.1 Normal range of chemical composition for fly ash produced from different coal types.[8]

Component (wt.%)	Bituminous	Sub-bituminous	Lignite
SiO_2	20–60	40–60	15–45
Al_2O_3	5–35	20–30	10–25
Fe_2O_3	10–40	4–10	4–15
CaO	1–12	5–30	15–40
MgO	0–5	1–6	3–10
SO_3	0–4	0–2	0–10
Na_2O	0–4	0–2	0–6
K_2O	0–3	0–4	0–4
LOI	0–15	0–3	0–5

As per the guidelines outlined by the American Society for Testing Materials (ASTM C618), fly ash is classified into two categories based on its composition. Class F fly ash is defined as ash with more than 70 wt% combined SiO_2 + Al_2O_3 + Fe_2O_3 and low lime content. On the other hand, Class C fly ash is characterized by a SiO2 + Al_2O_3 + Fe_2O_3 content ranging from 50 to 70 wt% and high lime content. Generally, high-calcium Class C fly ash is produced by burning low-rank coals (such as lignite or sub-bituminous coals) and possesses cementitious properties, capable of self-hardening upon contact with water. In contrast, low-calcium Class F fly ash is typically derived from the combustion of higher-rank coals (bituminous coals or anthracites), exhibiting pozzolanic characteristics and requiring the presence of $Ca(OH)_2$ and water to harden.[10]

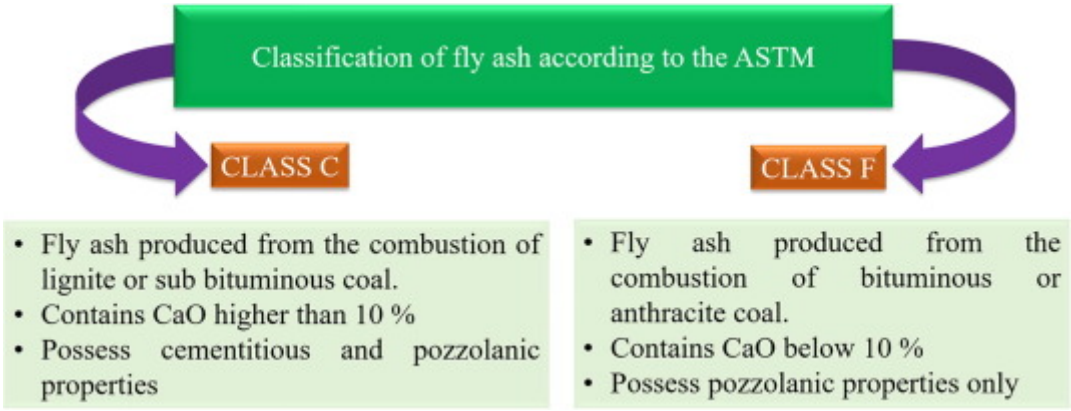

Fig. 1.2. FA classification according to ASTM illustrating the main differences.[10]

1.1.3 Physical and chemical properties of GGBS

GGBS (Ground Granulated Blast Furnace Slag) is a significant byproduct generated during steel and iron production processes. The blast furnace operates at a temperature of approximately 1500 degrees Celsius. It receives a precisely controlled mixture of limestone, iron ore, and coke. Within the blast furnace, the combination of limestone, iron ore, and coke undergoes melting, resulting in the formation of molten iron and slag. To produce GGBS, the molten slag from the blast furnace is rapidly cooled using high-pressure water jets, causing it to solidify into a fine, granular, and glassy substance. The global annual output of blast furnace slag is about 530 million tons, but only about 65% of the total is recycled[27].

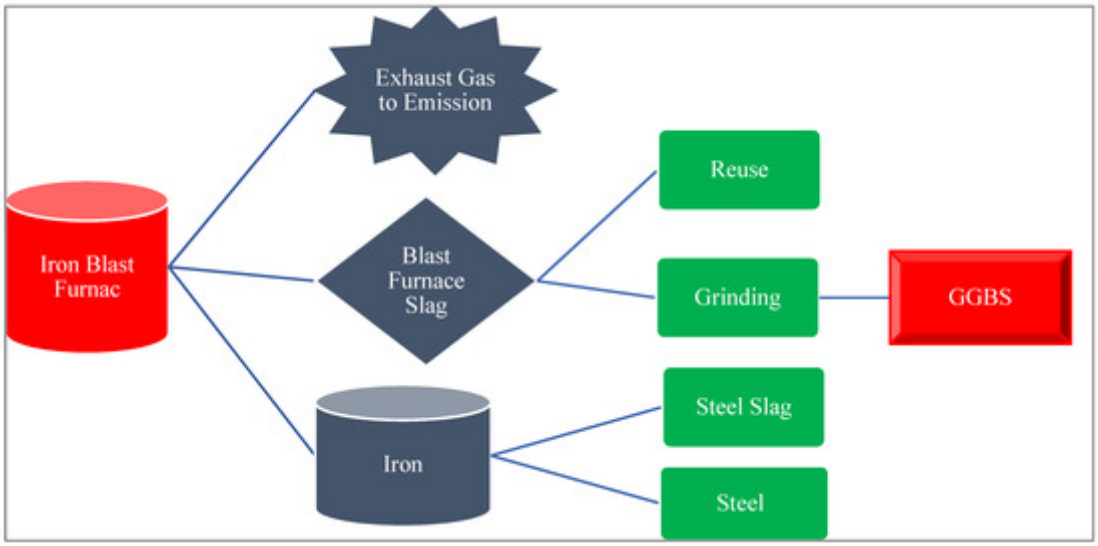

Fig. 1.3 Manufacturing Process of GGBS[11]

The specific gravity of GGBS typically falls within the range of 2.5 to 2.9, similar to that of cement. It has been reported to have an absorption capacity of 1.2%, which can negatively impact the flowability of concrete. GGBS possesses a grain size range of 1.18 mm to 0.10 mm, with approximately 62% of the material falling between these sizes [12]. The bulk density of GGBS ranges from 1200 to 1670 kg/m3, which is roughly equivalent to the density of cement at 1440 kg/m3. In

terms of surface area, GGBS exhibits a range of 4250 to 4700 cm2/g, significantly higher than the surface area of cement at 3310 cm2/g. The larger surface area of GGBS requires a greater amount of mortar to cover it, resulting in less accessible paste for lubrication, ultimately reducing the flowability of concrete. However, it is worth noting that different research studies have reported varying physical properties of GGBS, which could be attributed to the diverse sources of GGBS from different locations[11].

Figure 1.4 presents a scanning electron microscope (SEM) image of GGBS, which serves as a valuable tool for examining the surface morphology of the material. The SEM analysis revealed angular fragments and a rough surface texture of the GGBS particles. These angular shapes and surface roughness contribute to increased internal friction between the GGBS particles and other components of concrete. Consequently, this phenomenon adversely affects the flowability of the concrete mixture.

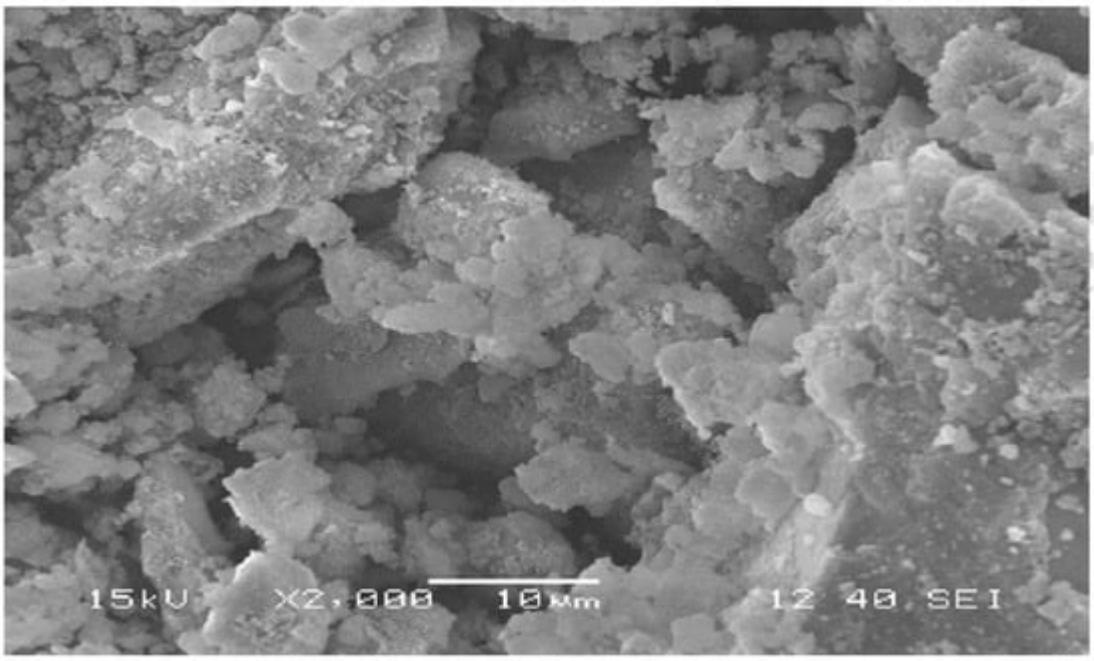

Fig. 1.4 SEM of GGBS[13]

The structure of blast furnace slag varies depending on the composition of the ore, fluxing stone, and impurities present in the coke used in the blast furnace. GGBS primarily consists of silica, calcium, aluminum, magnesium, and oxygen. Table1.2 shows the chemical properties of several GGBS that were used in the experiments. As per the ASTM guidelines, pozzolanic materials are formed when certain chemical components, including silica, calcium, alumina, magnesia, and iron, accumulate to a concentration exceeding 70%. GGBS has accumulated significant amounts of silica, calcium, alumina, magnesia, and iron, surpassing the 70% threshold. Consequently, GGBS is a reliable pozzolanic material that can be effectively used as a substitute for OPC (Ordinary Portland Cement) in concrete applications.

Table1.2 Chemical Compounds of GGBS.[11]

SiO_2	39.41	39.66	34	35.6	91
Al_2O_3	11.63	12.94	14	11.74	-
Fe_2O_3	3.35	1.58	4	0.8	-
MgO	5.52	6.94	7	10.7	7.73
CaO	36.56	34.20	23	41.7	-
Na_2O	0.32	0.20	-	-	0.12
K_2O	1.21	1.44	-	-	-

1.1.4 Physical and chemical properties of Biomass fly ash

In the coming decades, the transition to more sustainable fuels is crucial due to the non-renewable nature of traditional fossil fuels and their significant contribution to greenhouse gas emissions. The global energy consumption supplied by fossil fuels has decreased from approximately 95% in 1970 to around 80% in 2016, owing to advancements in alternative energy technologies and increased public awareness regarding the necessity for change. Sustainable biomass-based bioenergy represents the largest and most important category, contributing approximately 70% to the total renewable energy supply. In 2017, solid biomass combustion accounted for 91% of the biomass energy supply, while liquid biofuels and biogas contributed 7% and 2%, respectively. Biomass-based electricity generation accounted for roughly 15% of biomass consumption. Common methods involve the combustion of biomass in fixed, fluidized, or pulverized bed boilers to generate high-pressure steam, which in turn drives turbines for electricity generation.[16][17][18]

The biomass sources used for heat and electricity generation encompass various materials, including agricultural and forestry residues, dedicated energy crops, wood fuel, charcoal, chips, pellets, municipal solid waste, sewage sludge, and paper sludge. However, the combustion of fuels derived from these renewable resources or waste materials produces ash with distinct physical and chemical properties compared to ash produced from more conventional fuels like coal. Therefore, alternative reuse or disposal strategies are necessary to manage the generated ash effectively.[4]

The utilization of wood fly ash (WFA) as a partial replacement for cement in construction materials offers several advantages, including reduced reliance on natural resources in cement production, mitigation of greenhouse gas emissions, and improved ash management practices. Several studies have demonstrated promising results when incorporating blends of coal and WFA or solely biomass ash into concrete. However, there are still technical challenges to address, such as commercial barriers and concerns regarding the availability and quantity of biomass ash, especially when considering large-scale industrial applications.

Wood fly ash exhibits a diverse and irregular morphology, characterized by variations in particle size and shape (Fig. 1.5). The particles display a wide range of shapes and sizes, with some particles being angular and possessing rough textures, while others are spherical and may have impurities adhering to their surfaces. Additionally, there are particles with smooth surfaces present in the ash

sample.[3] [19]

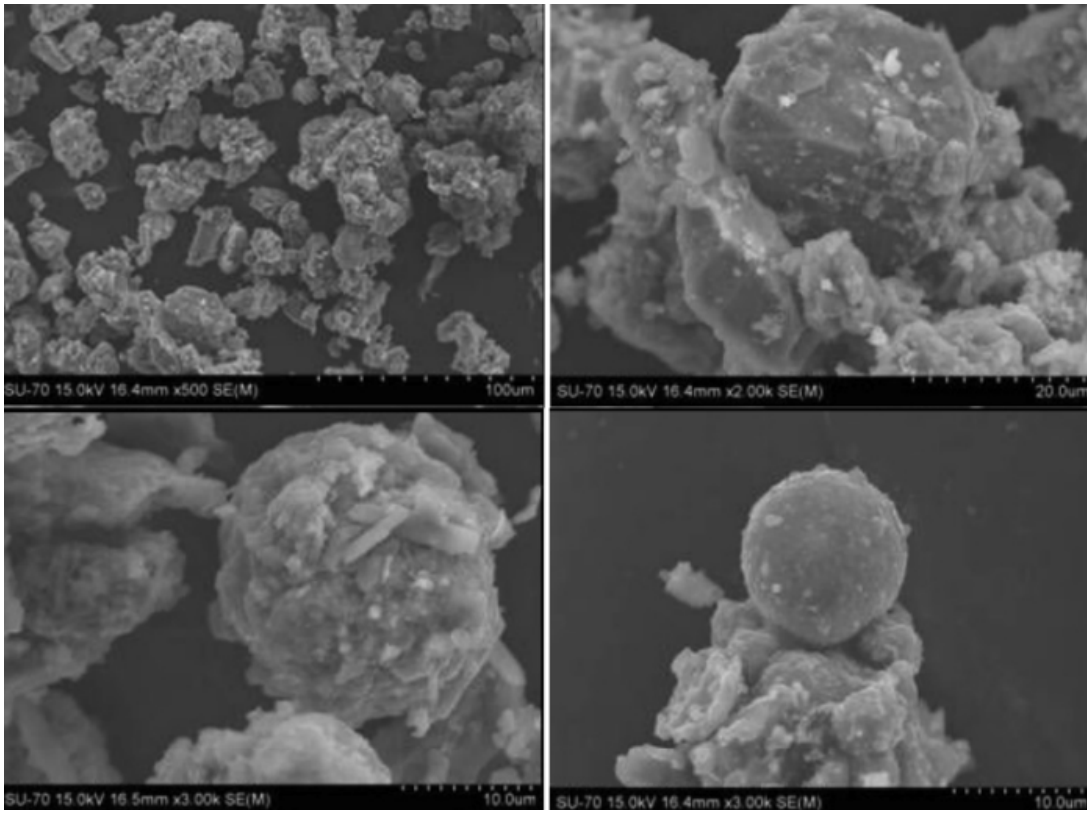

Fig 1.5 Microscopic aspect (SEM images) of the wood fly ash from fluidized bed[3]

The density of wood fly ash has been found to vary between 2.35 and 2.76 g/cm3, as reported in several studies [20]. In the case of two wood fly ash samples collected from different Portuguese facilities, one obtained from a biomass thermal power plant and the other from a biomass co-generation plant, researchers observed different specific surface area and bulk density values. Specifically, one sample had a specific surface area of 40 m^2/g and a bulk density of 2.59 g/cm^3, while the other sample exhibited a specific surface area of 8 m^2/g and a bulk density of 2.54 g/cm^3, as reported in studies conducted by researchers [15][14] In a study conducted by researchers [3], two different wood fly ashes were examined, one obtained from wood combustion in a fluidized bed reactor and the other from wood combustion in a grate combustor. The specific surface areas determined by the BET method were found to be 13 and 14 m^2/g, respectively, while the bulk density measured was 2.23 g/cm^3. These findings indicate that the bulk density of wood fly ashes generally falls within the range of 2200 to 2800 kg/m^3. Additionally, the surface area exhibits a wider variation, which is influenced by the type of combustor equipment used, ranging from 8 to 40 m^2/g.

The analysis revealed that the wood fly ashes comprised predominantly fine particles, with the mass distribution observed across three distinct size ranges[21]. Specifically, 48% of the mass was found within the 20-50 μm range, 36.3% within the 50-200 μm range, and 10.5% within the 200-500 μm range. This particle size distribution highlights the predominance of smaller particles in the ashes, contributing to their overall composition. Nevertheless, it is important to note that the particle size of wood fly ash can vary significantly due to several factors, including the specific combustion

technology employed and the origin of the biomass used. These factors play a crucial role in determining the resulting particle size distribution of wood fly ash.

In a comprehensive study conducted by researchers [6][7], the particle size distribution of five distinct types of ashes was analyzed and the findings are depicted in Figure 1.6 and Figure 1.7. The investigation revealed that Class C and Class F coal fly ash, in accordance with ASTM C618-15 (2015) standards, exhibited similar particle size distributions, with the majority of particles falling within the range of 3 to 50 μm [6]. In contrast, wood fly ash (WFA) displayed significantly larger particle sizes compared to the other types of fly ash examined. This observation aligns with the findings reported by Lessard et al., who also noted the presence of larger particles in WFA in comparison to the particle size distribution of cement[7].

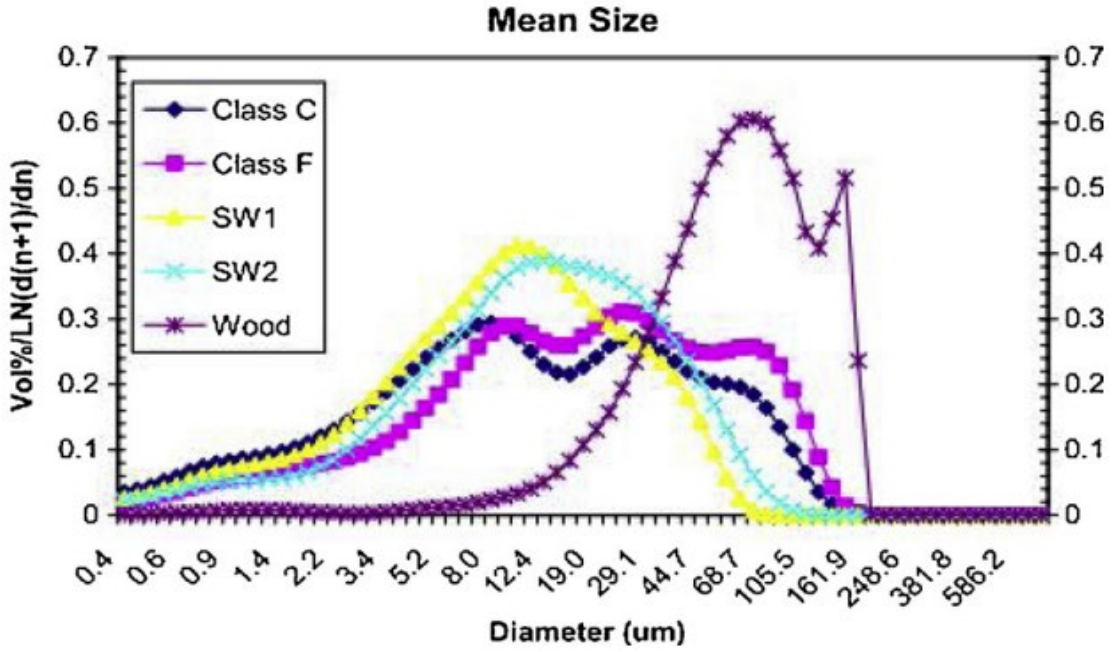

Fig.1.6 Particle size distribution of fly ashes wi th different origins: coal (Class C and Class F), sawdust (SW1 and SW2) and wood[6]

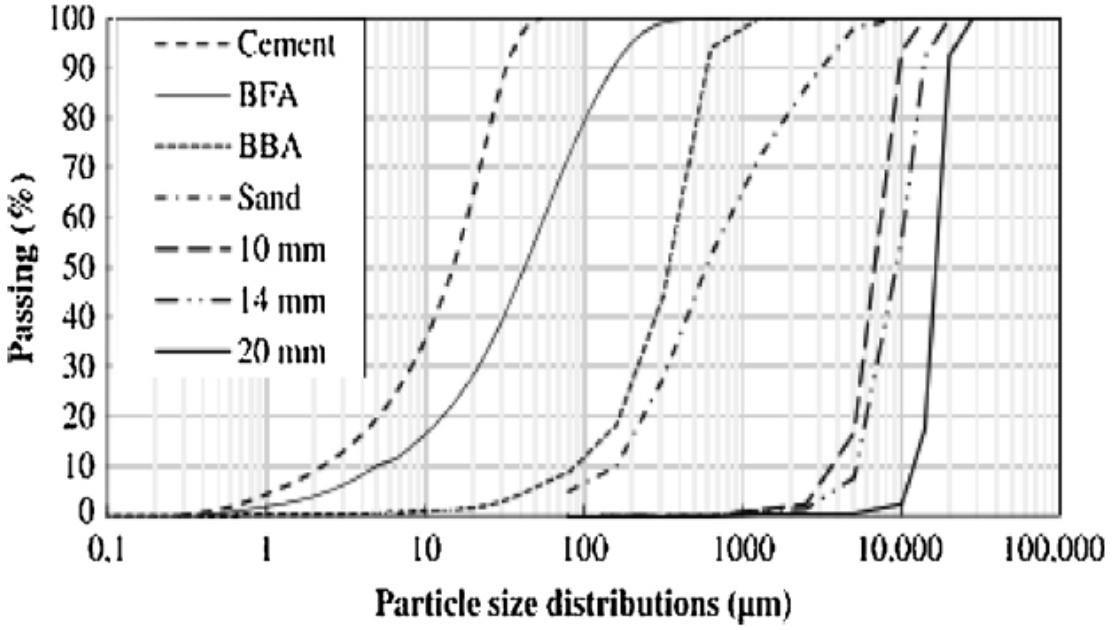

Fig. 1.7 Particle size distribution of wood fly ash (WFA), biomass bottom fly ash (BBA), cement, sand and aggregates (10, 14 and 20 mm)[7]

Table 1.3 provides a comprehensive comparison of the loss of ignition (LOI) content between wood fly ash and coal fly ash. Notably, wood fly ash exhibits a considerably higher range of LOI values (0.5–25.0% wt) in comparison to coal fly ash. The LOI content serves as a crucial parameter, as it is widely acknowledged that fly ash with elevated LOI values can potentially impact the properties of concrete. Therefore, careful consideration must be given to the LOI content when incorporating wood fly ash in concrete applications. Fly ashes with high LOI absorbed more water and chemical admixtures, for example the superplasticizer resulting in increasing the slump loss, decreasing the air-entraining effect and bleeding and decreasing the strength of concrete[5].

Table1.3 highlights the chemical composition of ashes, revealing that lime and quartz are the predominant oxides with higher concentrations. The silica (SiO_2) content ranges from 4.8% to 52.1% by weight, while the calcium oxide (CaO) content ranges from 8.5% to 53.4% by weight. It is worth noting the considerable dispersion in the content of these elements across the samples. Additionally, the ashes contain significant concentrations of other oxides, including aluminium, potassium, iron, sodium, magnesium, chloride, and sulphur. These findings underscore the diverse range of oxides present in the ashes, contributing to their overall chemical composition[5].

Type of fuel ash	Nomenclature of fly ash	Combustion Technology	LOI %wt	SiO_2	CaO	K_2O	Al_2O_3	MgO	Fe_2O_3	SO_3	Cl	Na_2O	MnO	P_2O_5	TiO_2
Class C	FA	–	0.7	37.3	24.2	0.4	19.6	5.4	6.1	1.8	–	1.5	0.01	1.2	1.5
Class F	FA	–	1.7	54.9	1.1	2.4	27.8	0.8	7.5	0.4	–	0.2	0.02	0.3	1.6
Coal	FA	CFB	34.0	11.0	15.2	0.6	3.4	0.4	5.0	2.8	0.1	0.3	0.03	–	–
Wood	WFA	–	7.9	48.9	13.6	3.4	12.5	3.2	5.5	1.3	–	1.7	0.1	1.0	0.8
Forest waste	WFA	Grate	25.0	41.0	11.4	3.9	9.3	2.3	2.6	–	–	0.9	0.3	0.9	0.4
Forest waste	WFA	BFB	20.0	28.0	25.4	3.2	6.2	5.0	2.2	–	–	3.3	0.7	0.9	0.3
Forest waste	WFA	BFB	< 0.5	–	53.4	4.2	–	5.5	–	3.7	–	0.6	0.6	0.1	–
Wood	WFA	BFB	9.4	45.8	25.7	8.2	4.6	3.6	2.9	4.2	0.6	0.6	–	3.4	0.3
Virgin wood	WFA	BFB	4.5	29.9	33.1	3.6	9.6	3.5	5.8	2.9	1.1	1.3	0.8	2.3	–
Virgin wood	WFA	BFB	3.6	36.4	23.8	6.7	9.0	3.5	6.4	4.7	1.9	1.5	0.5	1.9	–
Treated wood	WFA	BFB	10.3	40.4	20.8	2.1	9.5	3.0	6.1	9.3	1.7	3.0	0.2	0.7	–
–	WFA	Power Plant	0.8	16.4	33.7	13.0	5.9	11.7	3.6	–	1.7	1.4	2.8	3.3	0.7
Wood	WFA	–	13.5	31.0	24.0	2.7	8.5	4.8	3.0	2.3	–	6.6	–	–	–
Forest waste	WFA	Grate	10.4	52.1	15.9	4.1	13.3	3.3	5.3	0.5	0.1	–	–	–	–
Forest waste	WFA	BFB	3.5	25.1	40.1	2.1	11.3	6.6	5.2	1.1	0.3	–	–	–	–
90% Bituminous coal + 10% Biomass	90FA-10WFA	–	0.9	48.7	8.7	2.4	21.2	5.4	10.1	1.1	–	3.1	–	0.002	–
Wood waste, peat, waste from board	Blend	CFB	–	4.8	12.8	3.7	2.1	1.4	1.4	0.9	0.1	1.2	1.3	0.7	3.0
Wood chips, peat	Blend	CFB	–	11.5	8.5	3.6	2.5	1.0	2.0	0.5	0.1	0.7	0.7	0.2	0.1
Wood chips	WFA	CFB	–	9.3	12.0	3.6	1.9	1.1	1.1	0.2	0.3	0.7	0.9	0.4	0.1
Wood	WFA	CFB	6.2 (550 °C)	13.7	12.0	4.7	3.0	1.2	3.2	4.0	1.0	0.7	0.9	–	–

BFB, bubbling fluidised bed; CFB, circulated fluidised bed.

In comparison to coal fly ashes, wood fly ashes (WFA) exhibit distinct characteristics[5]. They generally contain higher levels of Ag, B, Br, Ca, Cl, Cu, Ga, Hg, I, Mg, Mn, Mo, Na, P, Rb, Sr, Te, Zn, and K, while showing reduced amounts of Al. Furthermore, WFA display a greater diversity in composition and inorganic content. They demonstrate elevated levels/values of dry water-soluble

residue, pH, carbonates, chlorides, oxyhydroxides, phosphates, and water-soluble components. Conversely, they exhibit lower contents/values of Al, As, Au, Ba, Be, Bi, Cd, Ce, Co, Cs, Dy, Er, Eu, F, Fe, Gd, Ge, Li, Ni, as well as lower ash-fusion temperatures, lower bulk density, and decreased amounts of silicates, sulphates, and sulphides. These disparities emphasize the distinctive characteristics and chemical composition of wood fly ashes compared to coal fly ashes.
Grass crop residues exhibit significant pozzolanic activity and have the potential to serve as a viable substitute for cement in construction materials. On the other hand, other virgin biomass ashes exhibit lower pozzolanic activity but can still be effectively employed as fillers in cement-based materials[28].

1.1.5 The prediction model of concrete creep

It is critical to predict delayed strain in concrete structures in order to assess their durability and serviceability. Deformation of concrete often leads to cracks in the concrete, and early-stage cracks may hasten the deterioration of the concrete, leading to the corrosion of the embedded reinforcement by facilitating the passage of contaminants and moisture. The load-carrying capacity of a structure is reduced as a result of such damage that develops over time.

ACI Committee 209 showed that the effect of supplementary cementitious materials has not been considered in many existing prediction models of concrete creep and drying shrinkage, such as the ACI 209 model, CEB-FIP 1990 model, Gardner and Lockman (GL-2000), AIJ Model, JSCE model, and CEB MC90-99 model.[29][30][31][32][33]
AIJ Model is presented in Equation (1)

$$C(t,t_0) = CR \cdot log_e(t - t_0 + 1)$$

$$CR = (6.8X - 0.12G + 17.5)(t_0)^{-0.33}(1 - \frac{h}{100})^{0.36}(V/S)^{-0.43} \quad (1)$$

Where $C(t,t_0)$ is specific creep strain(×10-6/(N/mm2), t is the age of concrete (day), t_0 is age of concrete at beginning of load (day), G is specific coarse aggregate amount (kg/m^3), X is water binder ratio (%), h is relative humidity, V/S is volume surface area ratio .
JSCE Model is presented in Equation (2)

$$C_r(t,t_0) = \frac{4W(1-h)+350}{12+f_c(t_0)} log_e(t - t_0 + 1) \quad (2)$$

Where $C_r(t,t')$ is specific creep strain(×10-6/(N/mm2), t is the age of concrete (day), t_0 is age of concrete at beginning of load (day), h is relative humidity, W is specific water amount (kg/m3), $f_c(t_0)$ is compressive strength of age at the start of loading.
ACI209 Model is presented in Equation (3)

$$\varphi(t,t_0) = \frac{(t-t_0)^{\psi}}{d+(t-t_0)^{\psi}}\varphi_u \quad (3)$$

where $\varphi(t,t_0)$ is the creep coefficient; d (in days) and ψ are considered constants for a given member shape and size that define the time-ratio part; t is the age of concrete (day), t_0 is the age of load applied (day), and φ_u is the ultimate creep coefficient. For the standard conditions, φ_u is 2.35, ACI-209R-92 recommends, an average value of 10 and 0.6 for d and ψ, respectively.
CEB MC90-99 is presented in Equation (4)

$$\varphi_{28}(t,t_0) = \varphi_0\beta_c(t-t_0)$$
$$\varphi_0 = \varphi_{RH}(h)\beta(f_{cm28})\beta(t_0)$$
$$\varphi_{RH} = \left[1 + \frac{1-h/h_0}{\sqrt[3]{0.1[(V/S)/(V/S)_0]}}\alpha_1\right]\alpha_2$$
$$\beta(f_{cm28}) = \frac{5.3}{\sqrt{f_{cm28}/f_{cmo}}}$$
$$\beta(t_0) = \frac{1}{0.1 + (t_0/t_1)^{0.2}}$$
$$\beta_c(t-t_0) = \left[\frac{(t-t_0)/t_1}{\beta_H + (t-t_0)/t_1}\right]^{0.3}$$
$$\beta_H = 150[1 + (1.2\cdot h/h_0)^{18}](V/S)/(V/S)_0 + 250\alpha_3$$
$$\alpha_1 = \left[\frac{3.5f_{cmo}}{f_{cm28}}\right]^{0.7} \quad \alpha_2 = \left[\frac{3.5f_{cmo}}{f_{cm28}}\right]^{0.2} \quad \alpha_3 = \left[\frac{3.5f_{cmo}}{f_{cm28}}\right]^{0.5} \qquad (4)$$

where t is the age of concrete(day), t_0 is the age of concrete at beginning of load (day), f_{cm28} is compressive strength at the age of 28 days (MPa), f_{cmo} is 10 MPa, V/S is the volume surface ratio, $(V/S)_0$ is 50mm, h is the relative humidity, ho = 1, t_1 is 1 day.

GL200 Model is presented in Equation (5)

$$\varphi_{28}(t,t_0) = \Phi(t_c)\left[2\frac{(t-t_0)^{0.3}}{(t-t_0)^{0.3}+14} + \left(\frac{7}{t_0}\right)^{0.5}\left(\frac{(t-t_0)}{(t-t_0)+7}\right)^{0.5} + 2.5(1-1.086h^2)\left(\frac{(t-t_0)}{(t-t_0)+0.12(V/S)^2}\right)^{0.5}\right]$$

$$\Phi(t_c) = \left[1 - \left(\frac{(t_0-t_c)}{(t_0-t_c)+0.12(V/S)^2}\right)^{0.5}\right]^{0.5} \qquad (5)$$

Where t is the age of concrete, t_0 is the age of concrete at beginning of load (day), t_c is the age of concrete at beginning of drying, V/S is the volume surface ratio, h is the relative humidity.

CEB-FIP 1990 Model is presented in Equation (6)

$$\varphi(t,t_0) = \varphi_0\beta_c(t-t_0)$$
$$\varphi_0 = \varphi_{RH}(h)\beta(f_{cm28})\beta(t_0)$$
$$\varphi_{RH} = 1 + \frac{\text{1-RH/RH}_0}{\sqrt[3]{0.46[h/h_0]}}$$
$$\beta(f_{cm28}) = \frac{5.3}{\sqrt{f_{cm28}/f_{cmo}}}$$
$$\beta(t_0) = \frac{1}{0.1 + (t_0/t_1)^{0.2}}$$
$$\beta_c(t-t_0) = \left[\frac{(t-t_0)/t_1}{\beta_H + (t-t_0)/t_1}\right]^{0.3}$$
$$\beta_H = 150 \times [1 + \{1.2\cdot h/h_0\}^{18}] \times \frac{h}{h_0} + 250$$
$$h = 2A_C/u \qquad (6)$$

where t is the age of concrete(day), t_0 is the age of concrete at beginning of load (day), f_{cm28} is compressive strength at the age of 28 days (MPa), f_{cmo} is 10 MPa, V/S is the volume surface ratio,

A_C is the cross-section and u is the perimeter of the member in contact with the atmosphere, h_0 is 100mm, RH is the relative humidity, RH0 = 1, t_1 is 1 day.

1.2 The purpose of this study

This study seeks to address the growing concerns over environmental sustainability in the construction industry. By investigating the properties of sustainable concrete with various industrial by-products, it aims to provide a comprehensive understanding of their performance and potential applications. The evaluation of engineering properties, such as compressive strength, flexural strength, and durability, will help assess the viability of sustainable concrete as a suitable replacement for conventional concrete.

Additionally, the research will explore the influence of different cementitious materials on the pore structure of concrete containing recycled fine aggregate. By examining the pore structure, the study aims to identify the effects of these materials on the concrete's permeability, porosity, and overall durability. This knowledge can contribute to the development of optimized mix designs that enhance the performance and longevity of sustainable concrete structures.

The investigation of the creep behavior of concrete with fly ash and various renewable aggregates will shed light on the long-term deformation characteristics of sustainable concrete. Understanding how these materials affect creep can provide valuable insights for structural design, ensuring the safe and reliable performance of sustainable concrete structures over time.

Furthermore, the study will explore the properties of concrete incorporating biomass fly ash and limestone powder. By examining their impact on mechanical properties, durability, and sustainability aspects, the research aims to highlight the potential benefits and challenges associated with these materials. This information can guide engineers and researchers in making informed decisions regarding the use of biomass fly ash and limestone powder in sustainable concrete production.

Lastly, the investigation of fly ash, biomass fly ash, and GGBS-based geopolymer concrete will contribute to expanding the knowledge base on alternative binder systems. Geopolymer technology offers a promising avenue for sustainable concrete production, as it reduces the reliance on cement and utilizes industrial by-products. Understanding the properties and performance of these geopolymer concrete mixtures can pave the way for their wider adoption in the construction industry, promoting sustainable practices and reducing the carbon footprint associated with traditional cement production.

Overall, this research aims to provide valuable insights into the properties and potential applications of sustainable concrete with various industrial by-products and geopolymer technology. By contributing to the understanding of sustainable construction materials, this study seeks to support the transition towards more environmentally friendly and sustainable practices in the construction industry.

1.3 Research structure

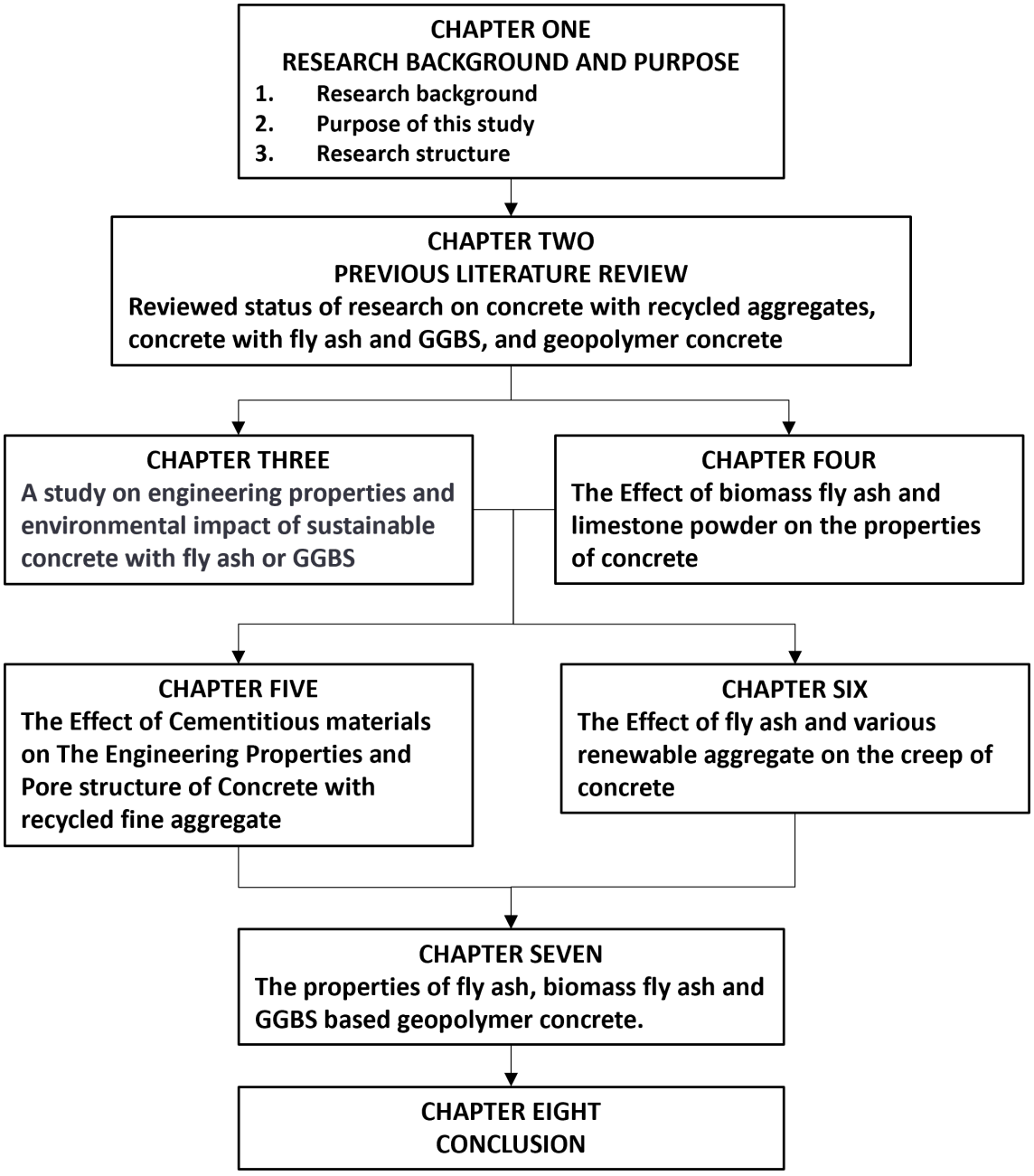

Reference

[1] P.K. Mehta, Development, High-performance, high-volume fly ash concrete: materials, mixture proportioning, properties, construction practice, and case histories, Suppementary Cementing Materials for Sustainable Development, 2002

[2] Ecra (European Cement Research Academy). Calcined Clay: A Supplementary Cementitious Material with a Future. Available online: https://ecra-online.org/file admin/ecra/newsletter/ECRA_Newsletter_3_2019.pdf

[3] Tarelho, L. A. C., Coelho, A. M. S. L., Teixeira, E. R., & Ferreira, V. M. (2012). Characteristics of ashes from two Portuguese biomass co-generation plants. *TC*.

[4] Zhai, J., Burke, I. T., & Stewart, D. I. (2021). Beneficial management of biomass combustion ashes. *Renewable and Sustainable Energy Reviews*, *151*, 111555.

[5] Teixeira, E. R., Camões, A., & Branco, F. G. (2019). Valorisation of wood fly ash on concrete. *Resources, Conservation and Recycling*, *145*, 292-310.

[6] Wang, S., Miller, A., Llamazos, E., Fonseca, F., & Baxter, L. (2008). Biomass fly ash in concrete: Mixture proportioning and mechanical properties. *Fuel*, *87*(3), 365-371.

[7] Lessard, J. M., Omran, A., Tagnit-Hamou, A., & Gagne, R. (2017). Feasibility of using biomass fly and bottom ashes to produce RCC and PCC. *Journal of Materials in Civil Engineering*, *29*(4), 04016267.

[8] Ahmaruzzaman, M. (2010). A review on the utilization of fly ash. *Progress in energy and combustion science*, *36*(3), 327-363.

[9] Roy, W. R., Thiery, R. G., Schuller, R. M., & Suloway, J. J. (1981). Coal fly ash: a review of the literature and proposed classification system with emphasis on environmental impacts. *Environmental geology no. 096*.

[10] Alterary, S. S., & Marei, N. H. (2021). Fly ash properties, characterization, and applications: A review. *Journal of King Saud University-Science*, *33*(6), 101536.

[11] Ahmad, J., Kontoleon, K. J., Majdi, A., Naqash, M. T., Deifalla, A. F., Ben Kahla, N., ... & Qaidi, S. M. (2022). A comprehensive review on the ground granulated blast furnace slag (GGBS) in concrete production. *Sustainability*, *14*(14), 8783.

[12] Bilir, T. Effects of Non-Ground Slag and Bottom Ash as Fine Aggregate on Concrete Permeability Properties.*Constr. Build. Mater.* **2012**, *26*, 730–734.

[13] Patra, R.K.; Mukharjee, B.B. Influence of Incorporation of Granulated Blast Furnace Slag as Replacement of Fine Aggregate on Properties of Concrete. *J. Clean. Prod.* **2017**, *165*, 468–476.

[14]Rajamma, R., Senff, L., Ribeiro, M. J., Labrincha, J. A., Ball, R. J., Allen, G. C., & Ferreira, V. M. (2015). Biomass fly ash effect on fresh and hardened state properties of cement based materials. *Composites Part B: Engineering*, *77*, 1-9.

[15]Rajamma, R., Ball, R. J., Tarelho, L. A., Allen, G. C., Labrincha, J. A., & Ferreira, V. M. (2009). Characterisation and use of biomass fly ash in cement-based materials. *Journal of hazardous materials*, *172*(2-3), 1049-1060.

[16]Trading Economics. World - fossil fuel energy consumption (% of total).

https://tradingeconomics.com/world/fossil-fuel-energy-consumption-percent-of-total-wb-data.html2020.

[17] Dawson L. 'Our Waste, our Resources; A Strategy for England'–Switching to acircular economy through the use of extended producer responsibility. EnvironLaw Rev 2019;21:210–8.

[18] World Bioenergy Association. Global bioenergy statistics 2019. Stockholm,Sweden: World Bioenergy Association; 2019.

[19] Lessard, J. M., Omran, A., Tagnit-Hamou, A., & Gagne, R. (2017). Feasibility of using biomass fly and bottom ashes to produce RCC and PCC. Journal of Materials in Civil Engineering, 29(4), 04016267.

[20] Berra, M., Mangialardi, T., & Paolini, A. E. (2015). Reuse of woody biomass fly ash in cement-based materials. Construction and Building Materials, 76, 286-296.

[21] Barbosa, R., Dias, D., Lapa, N., Lopes, H., & Mendes, B. (2013). Chemical and ecotoxicological properties of size fractionated biomass ashes. *Fuel Processing Technology*, *109*, 124-132.

[22] C. Heidrich, H.J. Feuerborn, A. Weir, Coal combustion products: a global perspective, in: World of Coal Ash Conference, 2013, pp. 22–25.

[23] NDRC, Annual Report on Comprehensive Utilization of Resources in China (2014),China, National Development and Reform Commission, 201.

[24] CEA, Fly ash generation at coal/lignite based thermal power stations and its utilization in the country for the year 2015-16, New Delhi, Central Electricity Authority, 2016.

[25] ACAA, Coal Combustion Product (CCP) Production and Use Survey Report, American Coal Ash Association, Farmington Hills, 2016, p. 2016.

[26] ADAA, Annual Membership Survey Results, in H. G. P. Ltd, ed. Ash Development Association of Australia, 2016.

[27] Association of Australia, 2016. A. Gholampour, T. Ozbakkaloglu, Performance of sustainable concretes containing very high-volume Class-F fly ash and ground granulated blast furnace slag, J. Cleaner Prod. 162 (2017) 1407–1417.

[28] Zhai, J., Burke, I. T., & Stewart, D. I. (2021). Beneficial management of biomass combustion ashes. Renewable and Sustainable Energy Reviews, 151, 111555.

[29] ACI Committee. ACI 209.2 R-08: guide for modeling and calculating shrinkage and creep in hardened concrete. American Concrete Institute Committee, 2008.

[30] COMITE EURO-INTERNATIONAL DU BETON: CEB-FIP Model Code 90, Thomas Telford 1990

[31] Gardner, N. J., & Lockman, M. J. (2001). Design provisions for drying shrinkage and creep of normal-strength concrete. Materials journal, 98(2), 159-167.

[32] Sato, Y., et al. "Study on the prediction formula for time-dependent strain of concrete: Prediction formula of total creep strain" Journal of Structural and Construction Engineering (Transactions of AIJ) 71.599 (2006): 9-15. (In Japanese)

[33] Standard specifications for concrete structures-2007, Japan Society of Civil Engineers (JSCE)

Chapter 2

PREVIOUS LITERATURE REVIEW

2.1 Research status of recycled aggregate concrete

Recycled concrete aggregates (RAC) are derived from construction and demolition waste (CDW) and typically consist of two parts: natural aggregates (NA) and the old mortar layer attached to the surface of the NA (Fig. 2.1). As a result, RAC contains two interfacial transition zones (ITZs): the old ITZ between natural coarse aggregate and the old mortar (light blue line) and the new ITZ between RA and the new mortar (dark blue line). Compared to natural aggregate concrete (NAC) with only one new ITZ, RAC generally has a larger volume of ITZ, resulting in higher porosity and inferior mechanical properties (e.g., compression, bending, and splitting tensile) for RAC. Increased porosity can also affect the permeability of RAC, leading to different concentration gradients (e.g. for water, chloride ion, or carbon dioxide) than those in corresponding NAC, which can impact rebar corrosion protection and ageing. Furthermore, the NA enclosed by a layer of old mortar has lower compressive strength than pure NA and may easily develop additional cracks during the RA manufacturing process. The propagation of these pre-existing cracks under service load can result in the final crushing of RAC[3][4].

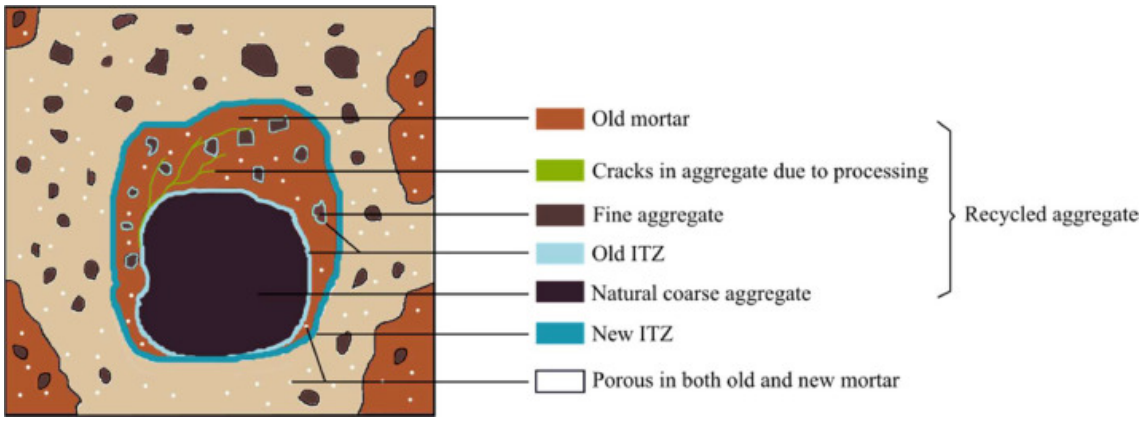

Fig. 2.1 Depicts a visualization of recycled aggregates (RA) in recycled aggregate concrete [4]

2.1.1 The fresh properties of recycled aggregates concrete

Dhir et al. [5]conducted a study to examine the impact of incorporating both coarse and fine recycled concrete aggregate (RCA) on concrete production. The compaction factor of different mixtures, including those with 100% coarse RCA, 50% fine RCA, and varying water-to-cement (w/c) ratios, was presented in Figure 2.2. It is worth noting that all RCA materials were added in a saturated surface dry (SSD) state. Initially, all mixtures demonstrated comparable compaction factors regardless of the level of replacement. However, as time progressed, the control mixtures exhibited a more significant decrease in the compaction factor compared to those containing 100% coarse RCA. The mixtures incorporating 100% coarse RCA and 50% fine RCA displayed intermediate values between the two aforementioned scenarios. This observation suggests that the RCA, being in an SSD state, might have experienced some bleeding, leading to a higher effective w/c ratio over time and improved compaction characteristics.

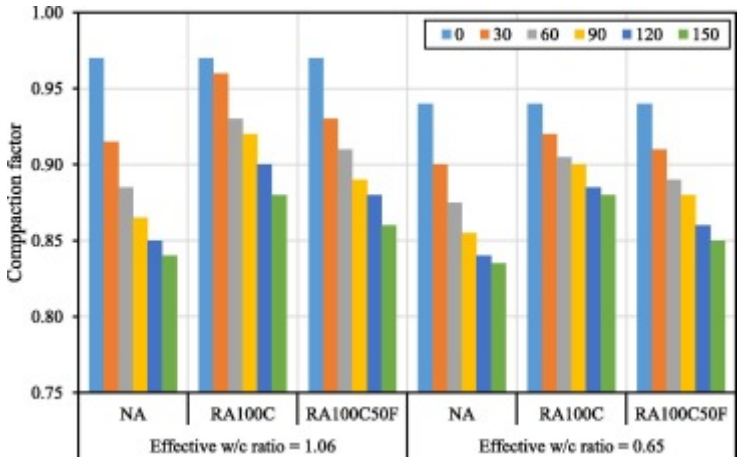

Fig. 2.2 Compaction factor over time of mixes with different effective w/c ratios and replacement levels.[5]

In the study conducted by Yang et al.[26] , it was observed that the initial slump of the concrete mixtures varied significantly, indicating notable differences in workability. As time progressed, there were considerable losses in slump, which is typically expected in mixes containing partially dry recycled aggregate (RA). These findings highlight the influence of RA characteristics on the workability of concrete. (Fig. 2.3)

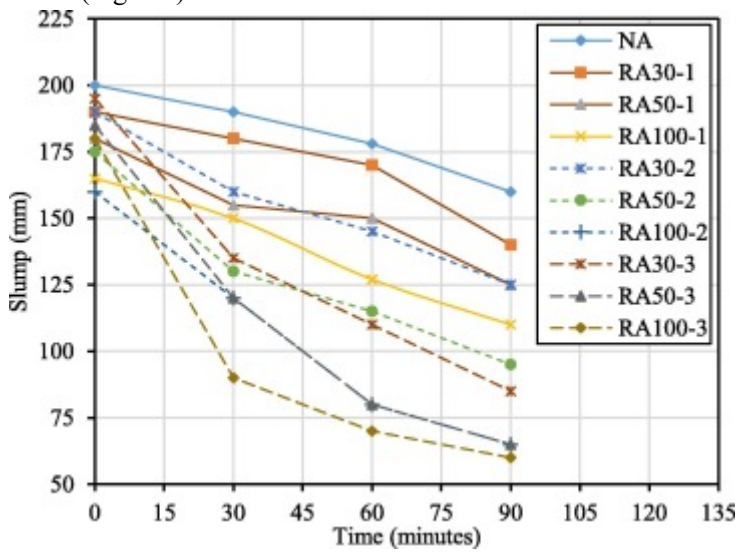

Fig. 2.3 Slump loss over time of concrete mixes with varying replacement levels and RCA with varying quality[26]

It has been reported[6] that the relationship between the density of fresh concrete and the ratio of RA replacement to NA for RCBA sized between 5 and 10 mm, as shown in Figure 2.4. Two types of recycled ceramic bricks, Brick A and B, were used in the study, obtained from local industrial plants in Portugal. The water absorption of Brick A and B were 15.8% and 18.9%, respectively, while that of natural aggregate was less than 1.33%. The results indicated that the density of fresh concrete decreased with an increase in the replacement ratio of RCBA, regardless of the water/cement ratio. It is important to note that the reduction in density of fresh concrete when the replacement ratio changed from 0% to 50% or 50% to 100% was relatively small (approximately 6%).

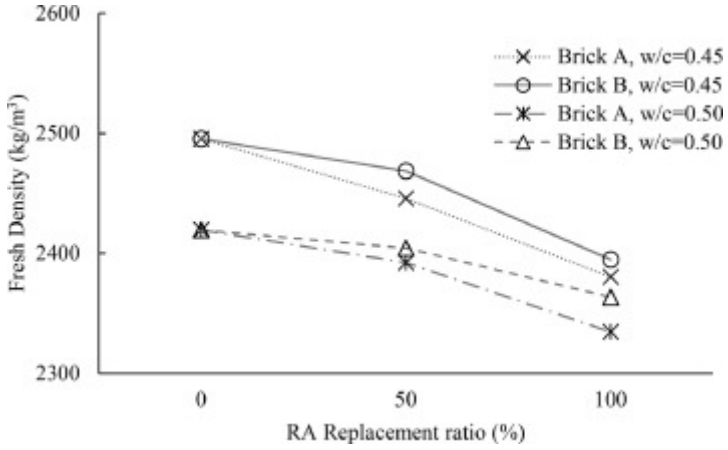

Fig. 2.4. Relationship between RA replacement ratio and the concrete fresh density[6]

2.1.2 The mechanical properties of recycled aggregate concrete

Gholampour et al.[1] conducted a study on the effect of incorporating a combination of foundry sand (FS)/ recycled fine aggregate (RFA) and FA/GGBS on the properties of concrete. The results of the study indicate that an increase in the content of FS and RFA up to 100% leads to a reduction in the compressive strength of the concrete (Fig 2.5). However, incorporating RFA at 25% sand replacement leads to slightly higher compressive strength compared to conventional concrete. Replacement of cement with FA at different levels negatively affects the concrete strength but replacing cement with 23% FA and 47% GGBS results in higher concrete strength compared to that of the companion cement-based concrete with the same sand replacement level.

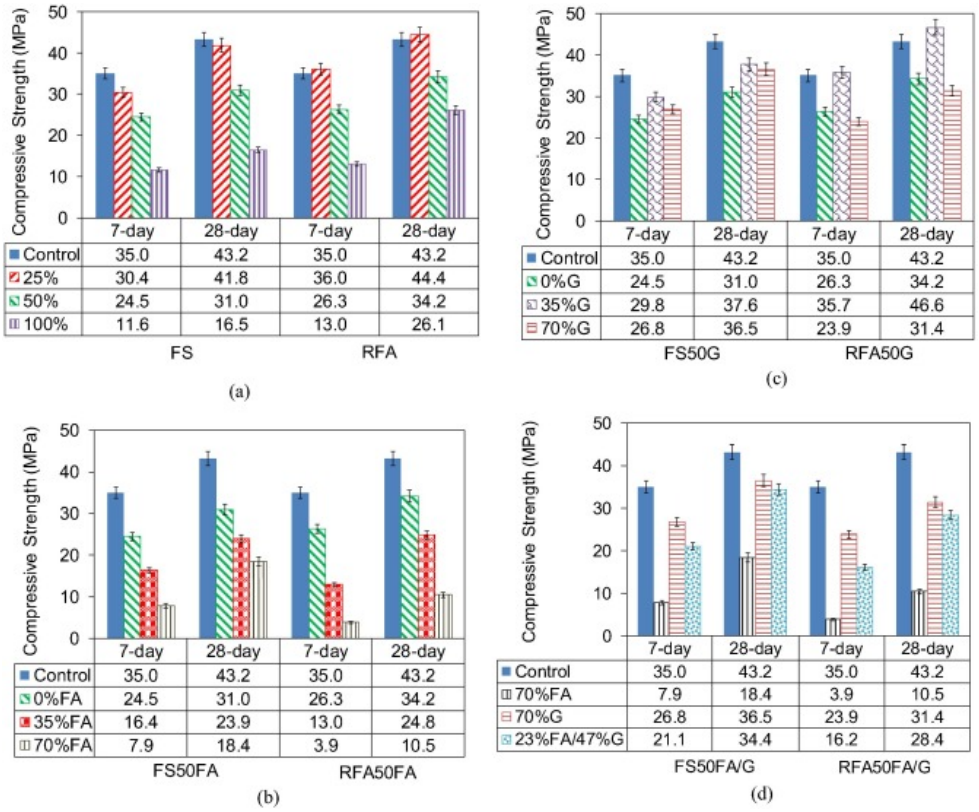

Fig. 2.5 Compressive strength of different mixes with replacement of: (a) sand with FS and RFA, (b) cement with FA in FS50 and RFA50 mixes, (c) cement with GGBS in FS50 and RFA50 mixes, and (d) cement with FA/GGBS in FS50 and RFA50 mixes.[1]

A review of research on recycled aggregate concrete was conducted by Bai et al[13], it indicates a general agreement, which the compressive strength of concrete decreases with an increase in the replacement rate of RA, regardless of the quality or type of aggregate. The findings suggest that an increase in the proportion of RA has a negative impact on the compressive strength of concrete. Nevertheless, some studies have reported instances where the addition of a small amount of recycled aggregate can actually enhance the concrete's strength[14][15]. The superior compressive strength observed in recycled aggregate concrete was primarily attributed to the effective regulation of the RA's grading. The relative compressive strength of concrete with varying replacement ratios of RA is illustrated in Fig. 2.6, disregarding aggregate type and quality. The trend is evident that the inclusion of RCA results in lower compressive strengths compared to those of the control concrete[13].

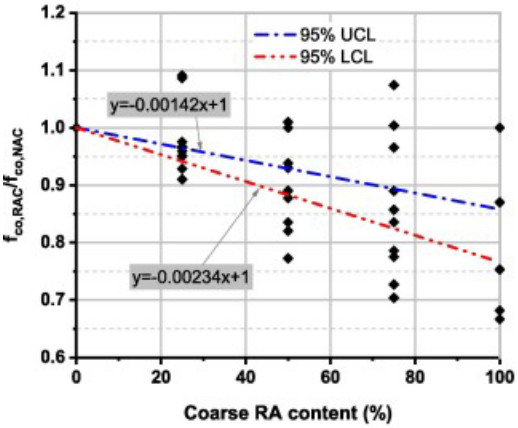

Fig. 2.6 The relative compressive strength of concrete with varying replacement ratios of RA[13]

Thomas and others[16] analyzed the effect of effective w/c ratio on the properties of RAC. The relationship between the compressive strength of RAC and normal concrete, at 28 days (a), 180 days (b), and 365 days (c) of age, as well as the effective w/c ratio, is presented in Fig. 2.7.

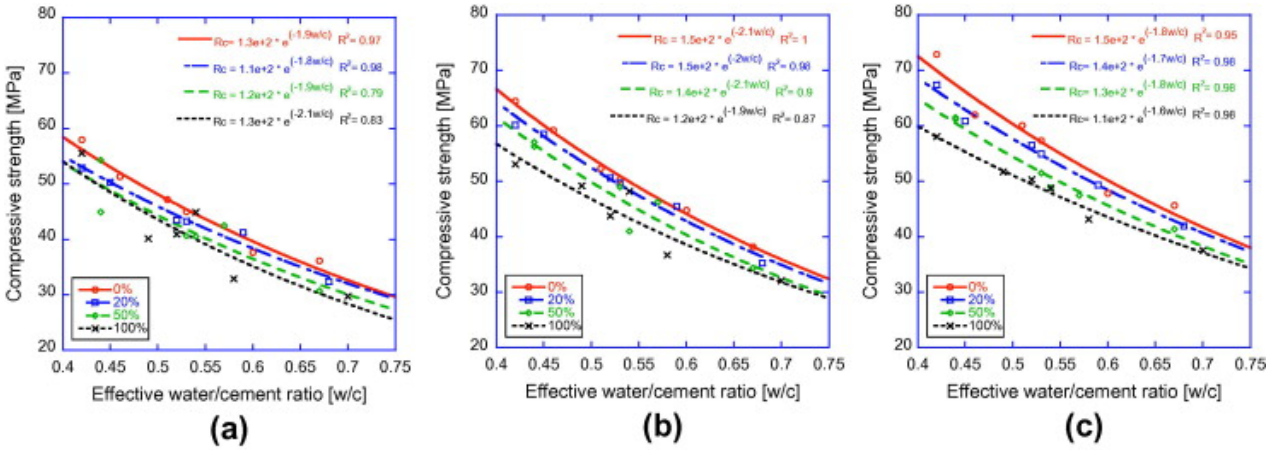

Fig. 2.7 Compressive strength versus the water/cement ratio of different degrees of substitution after 28 days (a), 180 days (b) and 365 days (c)[16].

The results of 28 days indicate that there is no significant difference in compressive strength between RAC with 20% RA substitution and normal concrete. However, a significant loss in compressive strength is observed when the substitution rate reaches 100%, and a reduction of 0.05 in w/c ratio is required to achieve comparable strength. After 180 days, the difference in compressive strength between normal concrete and RAC is more pronounced for higher strength concretes. A linear correlation between the compressive strength of RAC and the corresponding CC is demonstrated in Fig. 2.8. The results displayed the compressive strength values of all tested RAC compared to their respective normal concrete, indicating a positive correlation between the two.

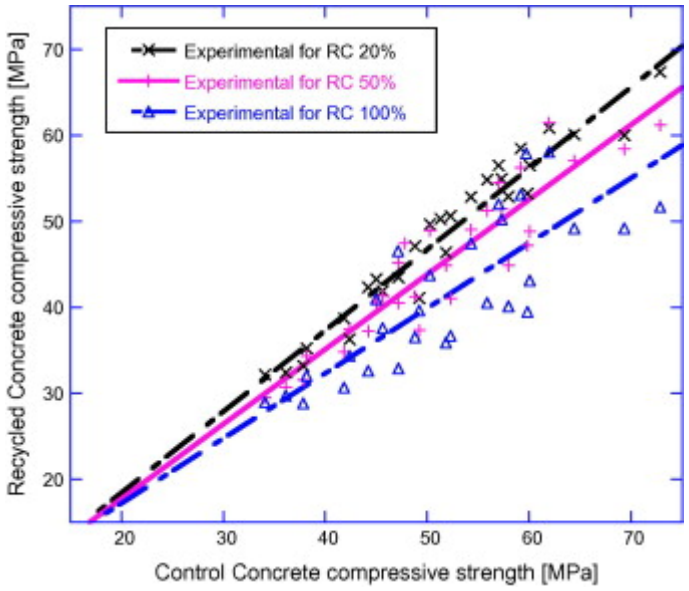

Fig. 2.8 Compressive strength of all tested RAC versus the corresponding normal concrete.[16]

The results show that the strength correlation equation between recycled aggregate concrete and normal concrete is as follows:

$F_{RAC} = -0.323 + 0.022X + (1 - 0.0025X) * F_C$ [16]

where F_{RAC} is the RAC compressive strength and F_c the CC compressive strength in MPa, X is substitution ratio %.

Katar et al. [19] studied the properties of self-compact concrete produced by substituting natural aggregate (NA) with recycled coarse aggregate (RCA) at replacement levels of 0%, 25%, 50%, and 75%. The use of RCA results in a decrease in the compressive strength of concrete at 7, 14, and 28 days. As the replacement ratio increases, the reduction in compressive strength becomes more significant. The 28-day compressive strength reduction was observed to be 21%, 24%, and 25% for 25%, 50%, and 75% replacement levels, respectively (Fig. 2.9). However, the minimum 28-day strength achieved was 41.8 MPa, which is still deemed acceptable for structural purposes. As the replacement level of RCA increases, the water absorption of the self-compact concrete also increases. The absorption ratio was found to increase by 28%, 68%, and 72% for 25%, 50%, and 75% replacement levels, respectively.

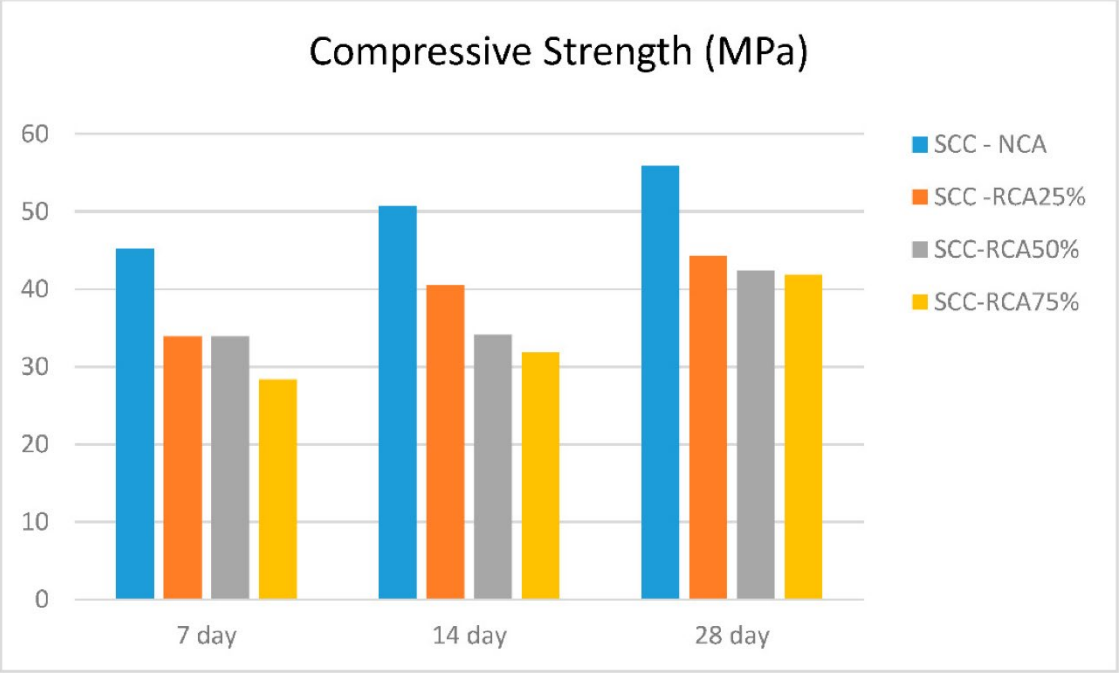

Fig. 2.9 The compressive strength of self-compact concrete (SCC) [19]

According to the findings of De Brito et al. [21], the replacement rate of recycled aggregate had minimal impact on the compressive strength, particularly when the original concrete used to produce the recycled aggregate exhibited higher strength than the recycled aggregate concrete. (Fig. 2.10)

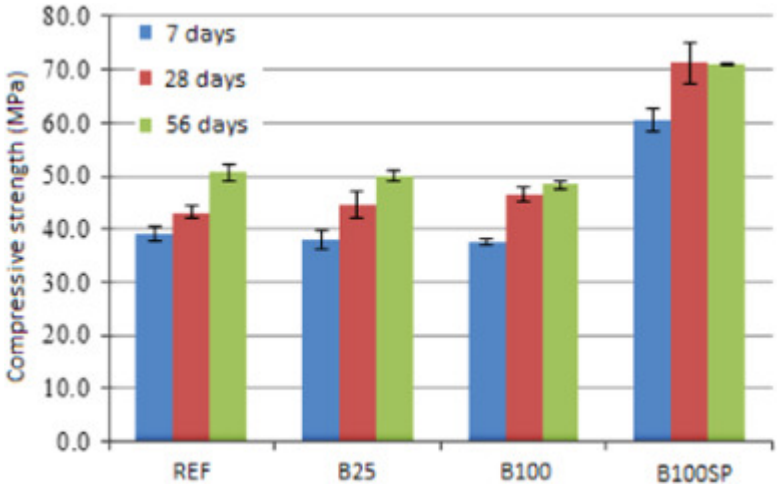

Fig. 2.10 The compressive strength of recycled aggregate concrete[21]

2.1.3 The durability of recycled aggregate concrete

Kirthik et al.[2] conducted a study on the properties of concrete made with recycled fine aggregate (RFA). Their findings suggest that increasing the amount of RFA in the concrete has a negative impact on its durability. However, the optimal replacement of river sand with RFA was found to be 30% (RFA30). This resulted in a reduction in shrinkage and porosity by approximately 14% and 25%

(Fig.2.12 and Fig.2.13), respectively. Moreover, the RFA30 concrete exhibited 21.25% higher resistance to chlorine penetration compared to the control concrete. As the age of the concrete increases, a decrease in total porosity was observed. This can be attributed to the formation of additional hydration compounds that occupy the voids, as depicted in Fig. 2.11, as well as the dense structure of the recycled fine aggregate concrete.

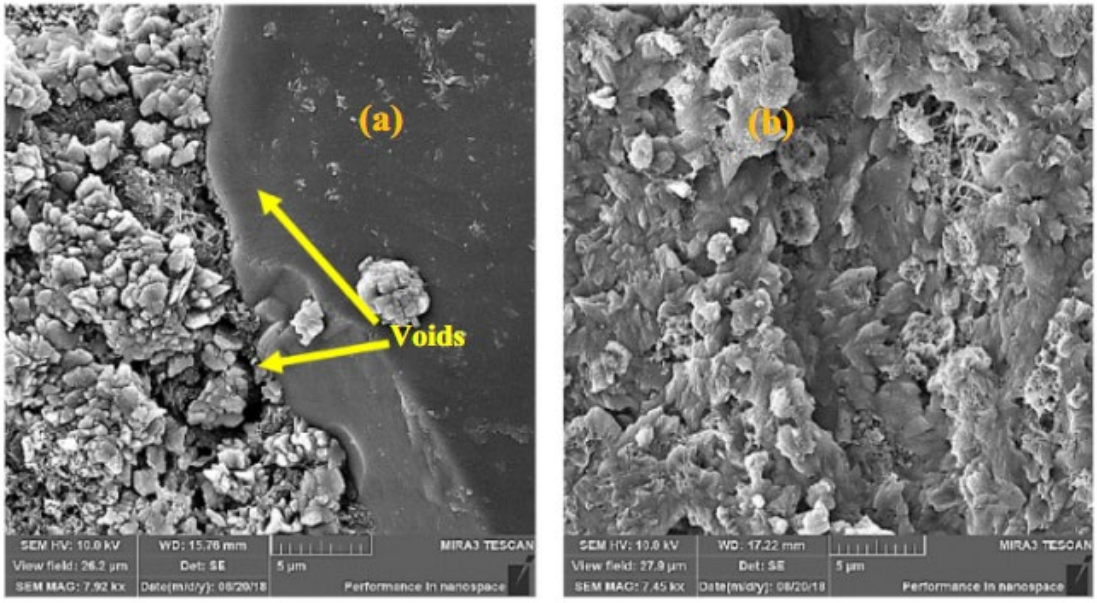

Fig. 2.11 Microstructure of RFA 30 at (a) 28 days (b) 56 day

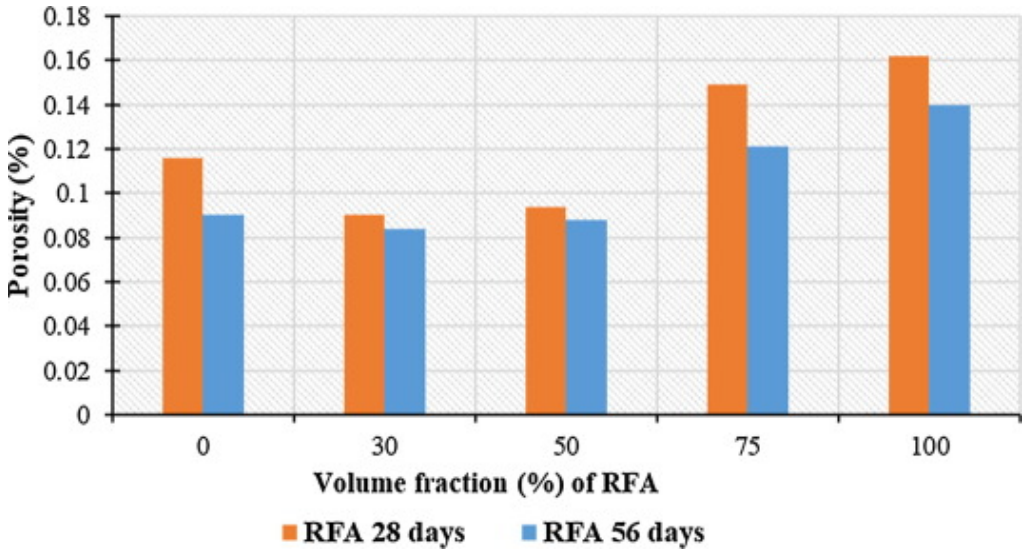

Fig. 2.12 The porosity of recycled fine aggregate concrete

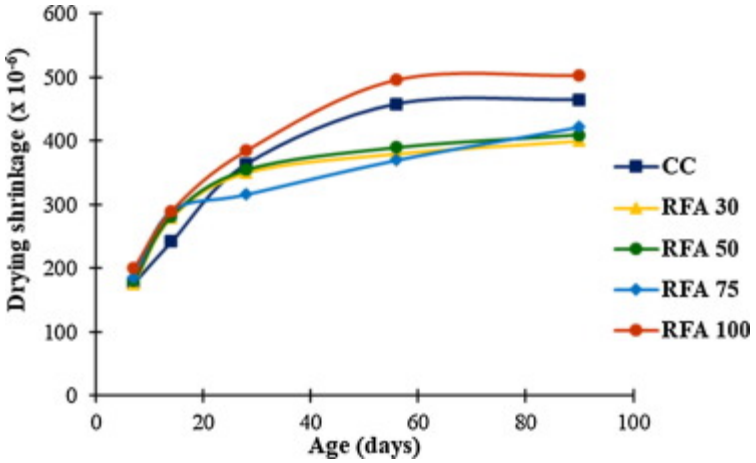

Fig. 2.13 The drying shrinkage of recycled fine aggregate concrete

In recent years some scholars have studied the creep of recycled aggregate concrete. Creep is a permanent deformation of a solid material over time when subjected to a constant stress. In concrete, this deformation can be characterized by changes in length or volume under compressive stress that is less than 40% of the concrete's strength, as defined by ASTM C 512. Several previous research works have examined the creep characteristics of RAC. The results indicate that the relative creep tends to increase as the replacement ratio of RA increases[4]. Experimental evidence supporting the relationship between porosity and relative creep strain has been provided by He et al.[7], as illustrated in Fig.2.14. The abbreviation NA represents natural aggregate, while RCA30 and RCA80 denote the original concrete of strength classes C30 and C80, respectively. SRA refers to the inclusion of shrinkage reducing admixture. The average relative creep and its fluctuations are determined based on the creep strain data of each sample type obtained over 25 testing periods up to 180 days.

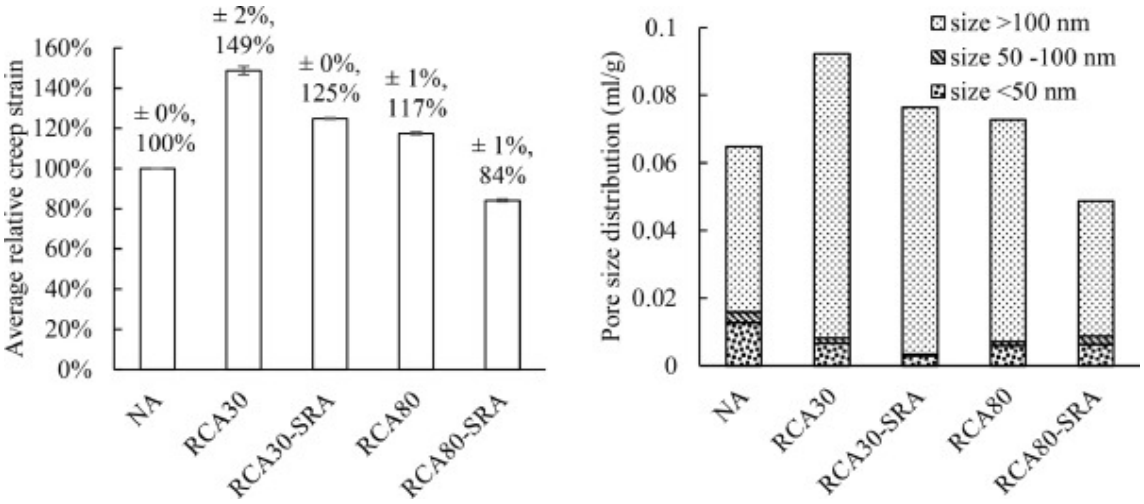

Fig. 2.14 The correlation between testing groups and two factors: (a) the average relative creep and (b) pore size distribution[4]

The decrease in concrete volume caused by the evaporation of internal moisture results in drying shrinkage. Many researchers have studied the relationship between the shrinkage of RAC and the replacement ratio of RA, and their findings suggest that as the replacement ratio of RA increases, the

shrinkage of RAC also increases [8][9][10]. This can be attributed to the fact that a higher amount of water is needed in the production of RAC. Previous studies [8] have reported that pre-soaking RA for 24 hours can lead to an increase in dry shrinkage, possibly due to the entrainment of excess water in the RAC. These findings indicate that the moisture condition of RA can also have an impact on the drying shrinkage of RAC. In addition, studies have shown that the addition of auxiliary cementitious materials to concrete can effectively reduce the shrinkage of recycled aggregate concrete[11][12]. According to Domingo-Cabo et al. [10], RAC with a lower RA replacement ratio of 20% exhibited comparable shrinkage to NAC at 28 days. Nonetheless, after 6 months, the shrinkage of RAC with replacement ratios of 20%, 50%, and 100% was found to be 4%, 12%, and 70% higher than that of NAC, respectively. It has been presented the variation of drying shrinkage of RAC over time in Figure 2.15. The graph shows a tendency for the variation to flatten out as time progresses, suggesting that the shrinkage of RAC reduces over time[13].

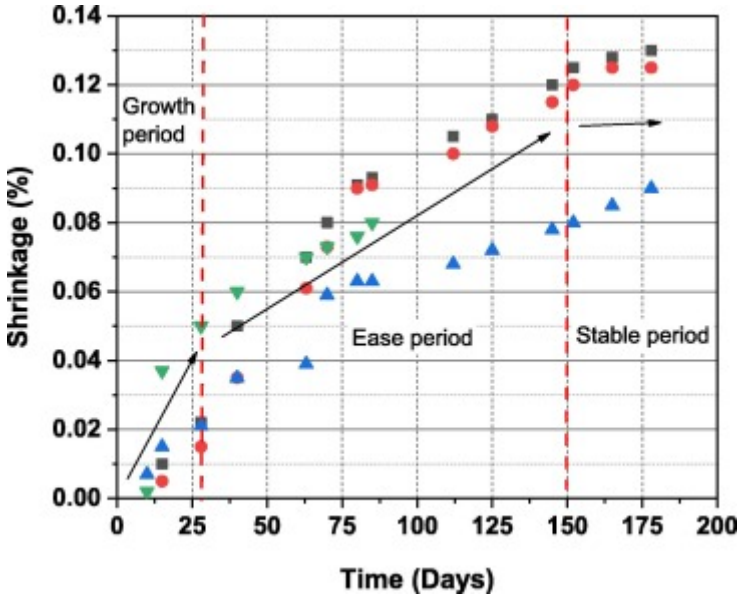

Fig.2.15 Shrinkage rate of RAC for different experimental researches[13]

Sosa and others[17] investigated the drying shrinkage and drying prediction model of recycled fine aggregate concrete. The outcomes showed that, at early ages, a rapid and higher increase in shrinkage was observed in the recycled concrete compared to the reference concrete. However, after 56 days, this trend reversed, and the increase in shrinkage was higher in the reference concrete than in the recycled concrete. This phenomenon is likely due to the water stored in the pores of recycled fine aggregate concrete, which is slowly released and contributes to internal curing. In addition, the results showed that the drying shrinkage of concrete is primarily affected by factors such as the w/c ratio, coarse aggregate mineralogy, and total water content, rather than the use of recycled fine aggregate. Therefore, the quality of recycled fine aggregate and the method of compensating for water absorption of aggregates have little impact on drying shrinkage. As a result, shrinkage prediction models remain valid even when recycled fine aggregates are used.

Yu and others [18] studied the effects of recycled coarse aggregate on the shrinkage of concrete. In this study, various types of recycled coarse aggregate (RCA) were used to prepare recycled aggregate concrete (RAC), and the shrinkage behavior of RAC was investigated. The concrete waste

is first crushed and screened to create simple-crushed recycled coarse aggregate (SCRCA). This is followed by particle shaping to produce primary particle-shaped recycled coarse aggregate (PPRCA). Further particle shaping of the PPRCA yields the secondary particle-shaped recycled coarse aggregate (SPRCA). The results (Fig 2.16) showed that as the RCA replacement ratio increased, the shrinkage of PP-RAC and SC-RAC compared to SP-RAC also increased. Specifically, at a 25% RCA replacement ratio, PP-RAC and SC-RAC experienced 11.4% and 21.8% increases in shrinkage, respectively, compared to SP-RAC. At a 50% RCA replacement ratio, the increase in shrinkage was 12.3% for PP-RAC and 25.5% for SC-RAC compared to SP-RAC. At a 75% RCA replacement ratio, the increase in shrinkage was 15% for PP-RAC and 33.2% for SC-RAC compared to SP-RAC. When SCRCA completely replaced NCA, the shrinkage of SC-RAC reached a maximum of 178.2 × 10−6, which is about 40% higher than that of NAC. When PPRCA completely replaced NCA, the shrinkage of PP-RAC was about 15% higher than that of NAC. However, when SPRCA completely replaced NCA, the shrinkage of SP-RAC was approximately the same as that of NAC. These findings suggest that the quality of RCA plays a significant role in the shrinkage of green recycled concrete, with a greater impact observed at higher replacement ratios. Nonetheless, when configured with SPRCA completely replacing NCA, the shrinkage performance of green recycled concrete was essentially the same as that of NAC.

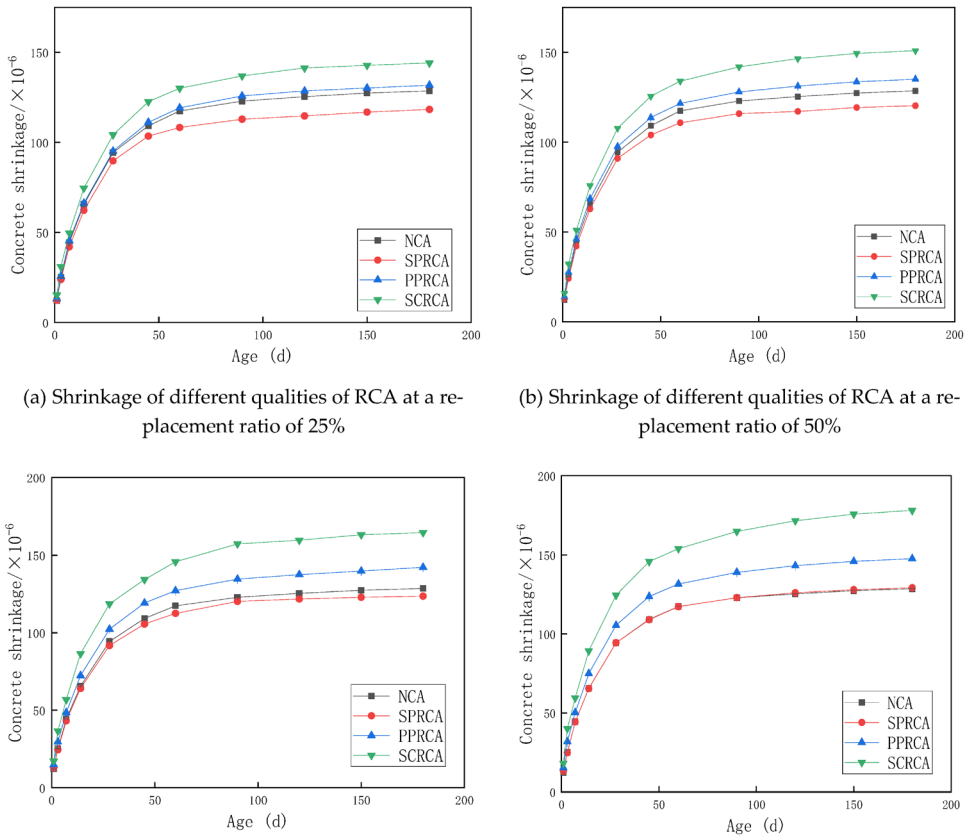

(a) Shrinkage of different qualities of RCA at a replacement ratio of 25%

(b) Shrinkage of different qualities of RCA at a replacement ratio of 50%

(c) Shrinkage of different qualities of RCA at a replacement ratio of 75%

(d) Shrinkage of different qualities of RCA at a replacement ratio of 100%

Fig. 2.16 Effect of RCA quality on concrete shrinkage[18]

Lv et al. [20]conducted a comprehensive investigation on the shrinkage and creep behavior of recycled aggregate concrete, employing water-cement ratios of 0.527 and 0.4. The shrinkage behavior

of recycled aggregate concrete was found to be comparable to that of ordinary concrete. In the case of w/c =0.527, RAC with 50% and 100% substitution rates exhibited increased shrinkage of 26% and 48% respectively, at 180 days compared to ordinary concrete. Similarly, in case of w/c=0.4, RAC with 50% and 100% substitution rates showed increased shrinkage of 22% and 47% respectively, compared to ordinary concrete (Fig. 2.17). As the replacement rate of recycled aggregate increased, the shrinkage of RAC also increased. Initially, RAC experienced rapid and pronounced shrinkage, followed by a gradual reduction in the shrinkage rate. By 120 days, the shrinkage became gentler, and approximately 95% of the total shrinkage was achieved. The findings suggest that the shrinkage of RAC tends to stabilize by 180 days.

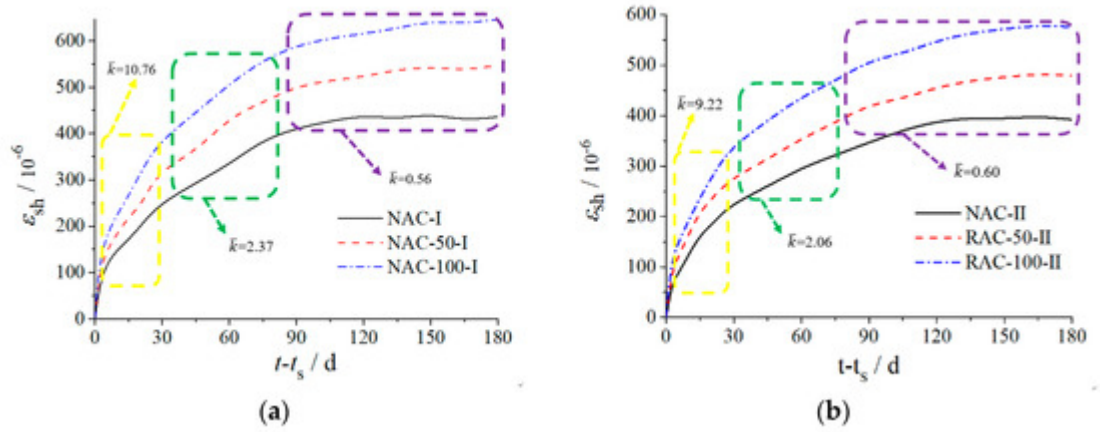

Fig. 2.17. Shrinkage deformation curve of RAC (a) *w/c* = 0.527; (b) *w/c* = 0.4.[20]

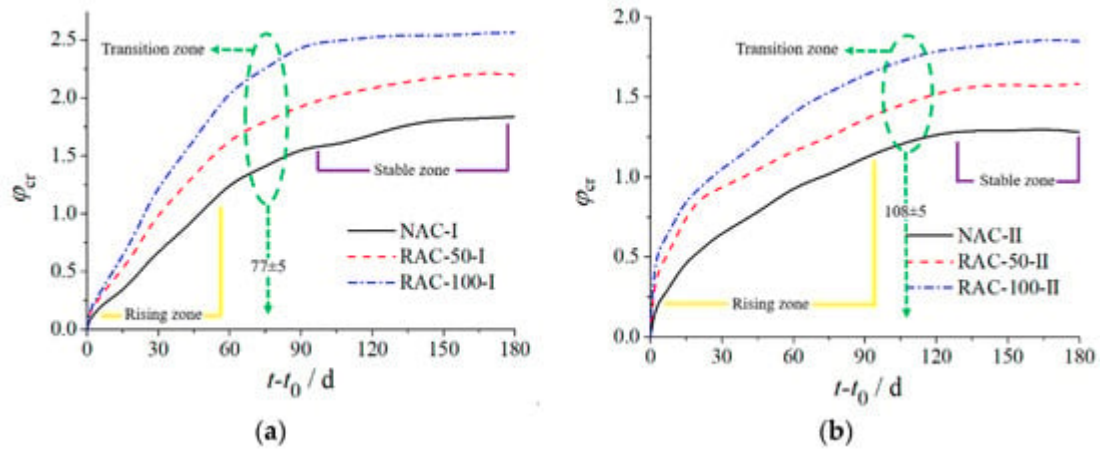

Fig. 2.18 Creep coefficient curve of RAC. (a) w/c = 0.527; (b) w/c = 0.4.[20]

At the 180-day loading period, it was observed that the creep behavior of recycled aggregate concrete (RAC) exhibited notable differences compared to ordinary concrete (Fig. 2.18). In Group I, where the water-to-cement ratio (w/c) was 0.527, RAC with a substitution rate of 50% and 100% displayed increased creep rates of 19.6% and 39.6% respectively, when compared to ordinary concrete. Similarly, in Group II, with a w/c of 0.4, RAC with 50% and 100% substitution rates showed increased creep rates of 23.6% and 44.3% respectively. These findings indicate that the increase in the replacement rate of recycled aggregate has a significant influence on the shrinkage and creep behavior of RAC[20].

In the study conducted by Lei et al.[22], it was observed that an increase in the replacement ratio of

recycled aggregate (RA), particularly when the RA had a higher content of adhered mortar (approximately 40%), led to a decrease in carbonation depth. This can be attributed to the higher presence of adhered mortar in RA, which results in an overall higher cement content and subsequently slows down the rate of carbonation. In the investigation conducted by Silva et al. [23], the influence of recycled aggregate (RA) content on the relative carbonation depth of recycled aggregate concrete (RAC) compared to natural aggregate concrete (NAC) was examined. The findings suggested that there was a 95% probability that the relative carbonation depth of RAC with 100% coarse RA was 2.5 times higher than that of NAC. Furthermore, for concrete incorporating the same amount of fine RA, the relative carbonation depth increased by approximately 8.7 times, potentially due to the higher water absorption capacity of fine RA. However, when the replacement ratio of coarse RA increased, it was possible to achieve comparable strength and carbonation depth between RAC and NAC by reducing the water-to-cement ratio of RAC. (Fig. 2.19)

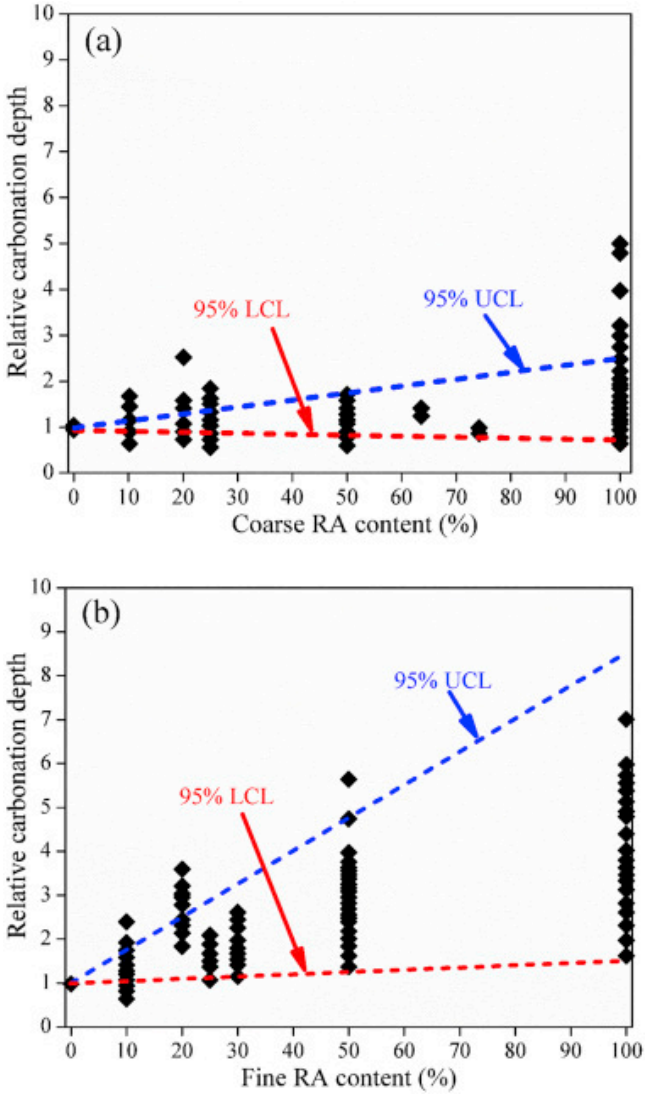

Fig. 2.19 Relative carbonation depth versus replacement level[23]

In a related study by Kou et al.[24], it was observed that incorporating fly ash as a cement replacement in recycled aggregate concrete (RAC) could lead to an increased carbonation depth. In a

case where samples were exposed for 10 years, the RAC with 55% fly ash content demonstrated approximately 1.68 times and 1.89 times higher carbonation coefficient compared to natural aggregate concrete (NAC) and RAC without fly ash. This phenomenon can primarily be attributed to the reduced calcium hydroxide content in high volume fly ash concrete, which influences the carbonation process.

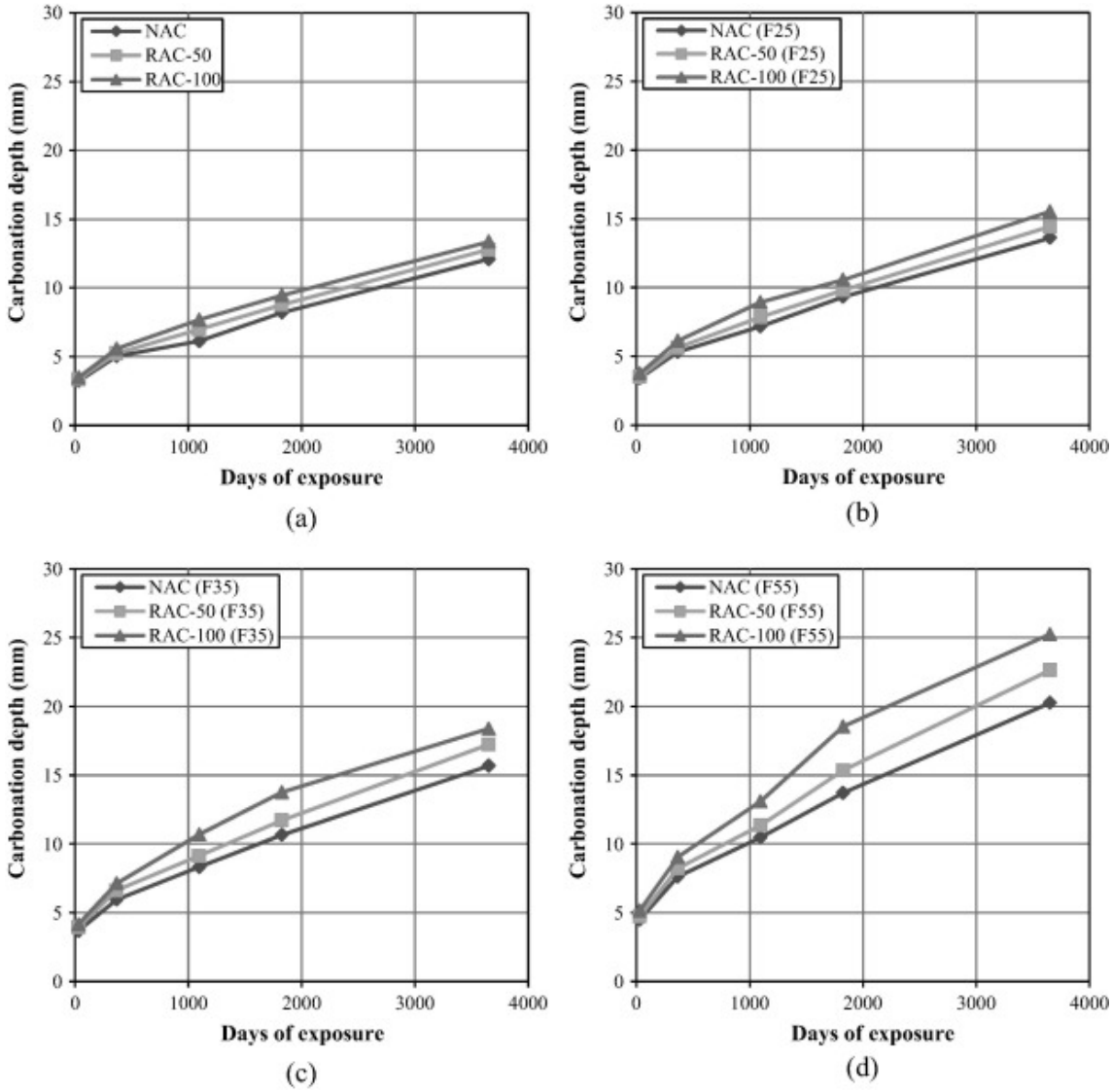

Fig. 2.20 Carbonation depth over time of concrete mixes with increasing coarse RCA content and varying fly ash content: (a) No fly ash; (b) 25% fly ash; (c) 35% fly ash; 55% fly ash[23][24]

In a comprehensive investigation by Amorim et al. [25], the impact of environmental conditions on the durability characteristics of concrete incorporating varying amounts of coarse recycled concrete aggregate (RCA) was examined. Notably, the laboratory environment, characterized by a relatively low average relative humidity of 60% and a temperature of 20 °C, resulted in greater carbonation depth compared to other environments considered in the study (see Fig. 2.21). Furthermore, the specimens cured in this environment exhibited a clear correlation between carbonation depth and the level of coarse RCA replacement, with a 30% increase observed when 100% coarse RCA was utilized after a curing period of 91 days. These findings highlight the influence of both environmental conditions and the extent of RCA incorporation on the carbonation performance of concrete.

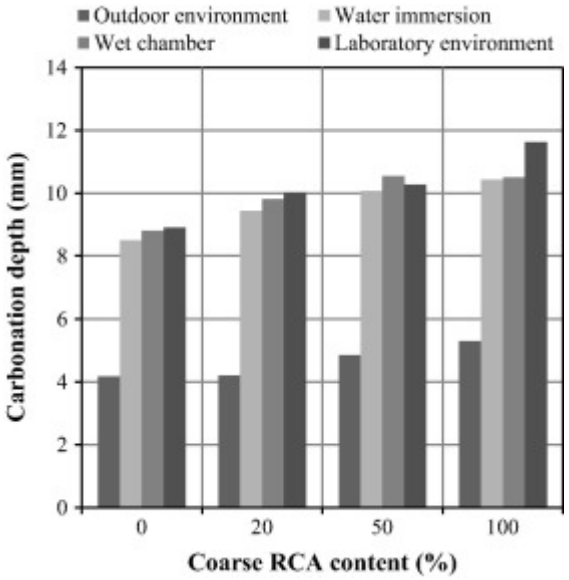

Fig. 2.21 Carbonated depth of concrete cured in different environments[25]

2.2 Research status of concrete with fly ash or GGBS

2.2.1 The mechanical properties of fly ash concrete

Alvin Harison [27] studied that cement has been replaced by fly ash accordingly in the range of 0% (without fly ash), 10%, 20%, 30%, 40%, 50% and 60% by weight of cement for M-25 mix with 0.46 water cement ratio. Concrete mixtures were produced, tested and compared in terms of compressive strength. The results of compressive strength of referral concrete as well as fly ash concrete at 7, 28 and 56 d are given in Fig. 1. It is evident that beyond 28 d, the strength increased with the addition of fly ash.

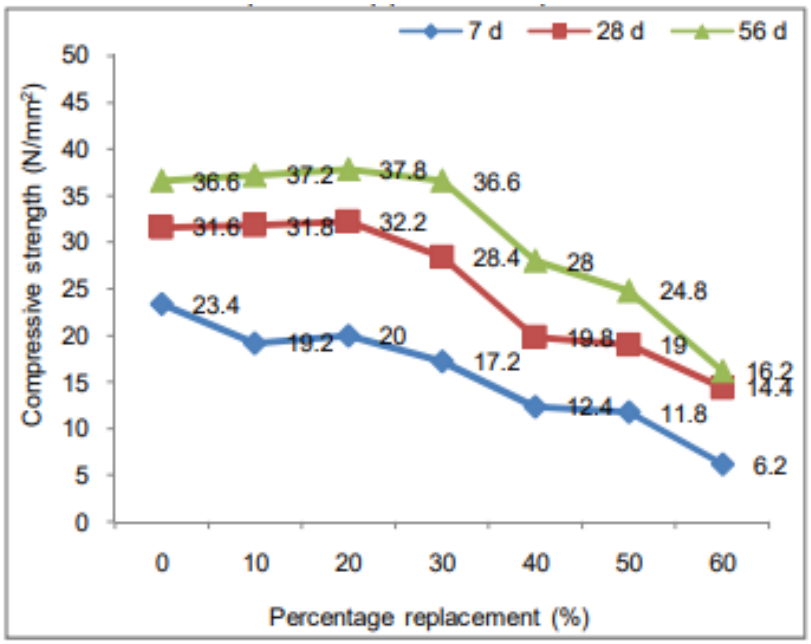

Fig. 2.22 The compressive strength of concrete with fly ash[27]

Strength was comparable up to 30% fly ash content and after that it decreased. However, increase in strength was more prominent at 20% replacement level. It was also observed that on addition of fly ash, 7 d strength was decreased at all replacement level. The results about that decrease of compressive strength may be due to slow hydration process since fly ash is a slow reactive pozzolans which delays the hydration process. From the findings it was seen that the compressive strength decreased above 30% replacement level at all the ages. It was observed that at 30% replacement with fly ash, compressive strength at 7 d curing is decreased 27% than that of referral concretes. Decrease in compressive strength at 7d curing was 47, 50 and 73% at replacement level of 40, 50 and 60% respectively. Inaddition, it was also observed that up to 30% replacement level, the prepared mix were sticky. Beyond 30% replacement level, workability and finish ability of mix was decreased. It may be since up to 30% replacement level, fly ash particles also worked as filler material to fill the pores between fine aggregate particles, resulting in a dense sticky mix since, more water was available for lubrication. However, beyond 30% replacement level, more water was needed for lubrication due to more surface area. As such workability and finish ability of mix was decreased beyond 30% replacement. From this paper can know that when use fly ash to replace cement in concrete. the compressive strength of fly ash concretes up to 30% replacement level is more or equal to cement concrete at 28 and 56 d. and the optimum replacement level of fly ash is 20%.[27]

R. D. Padhye [28] studied the effect of cement replacement by fly ash in concrete. He through the experiment to see the effect of fly-ash on compressive strength of different high grades concrete for different proportions of fly ash and different curing periods. The replacement of fly ash in this paper is 10%, 20%, 30%, 40%, 50%, 60%. Table 2.1 shows the compressive strength of different concrete mixes for 7, 28 and 45 Days. The results show that the compressive strength of concrete mixes decrease with increase in fly ash. The fly ash can be replaced up to maximum of 40% and replacements above 40% may not be safe for different concrete mixes. With the increase of fly ash there is steep increase in strength from 7 to 28 days indicating that early strength of concrete is reduced with increase in fly ash. Also, the variation in early strength is more than the variation in later strength. Thus, fly ash has an adverse effect on early strength of concrete.

Table 2.1 the compressive strength of different concrete mixes for 7, 28 and 45 Days. [28]

% of fly ash	grade M30			grade M40			Grade M50		
	compressive strength in N/mm²			compressive strength in N/mm²			compressive strength in N/mm²		
	7	28	45	7	28	45	7	28	45
0	28.22	49.11	52.15	36.88	53.11	58.07	41.77	61	63.56
10	27.18	46.33	49.49	40.88	53.66	58.00	40.00	60.23	62.23
20	21.55	42.92	49.45	31.55	50.33	54.44	27.11	58.66	60.44
30	22.88	40.74	42.22	32.51	47.74	48.87	29.54	57.47	58.64
40	18.66	32.44	34.67	26.22	40.00	40.89	31.21	52.17	56.45
50	13.77	24.88	32.89	20.11	31.33	35.11	31.21	45.19	48.54
60	9.77	17.89	22.23	15.22	26.66	30.22	12.23	35.15	40.29

A total of 28 mixtures with different mix designs were studied to obtain the efficiency and the maximum content of fly ash that gives the maximum compressive strength [29]. Four groups of mixtures were prepared, each group containing six mix designs and using the cement content of one of the control mixtures as the base for the mix design. In each group 20% of the cement content of the control mixture was removed, resulting in starting mixtures with 200, 240, 280, and 320 kg/m3 cement content. Fly ash in the amount of approximately 15%, 25%, 33%, 42%, 50%, and 58% of the rest of the cement content was added as partial cement replacement. All specimens were moist cured for 28 and 180 days before compressive strength testing. The results of workability and compressive strength are shown in Table 2.2. This study showed that strength increases with increasing amount of fly ash up to an optimum value, beyond which strength starts to decrease with further addition of fly ash. The optimum value of fly ash for the four test groups is about 40% of cement. Fly ash/cement ratio is an important factor determining the efficiency of fly ash. As the cement content in the concrete mixture increases, hydration product Ca(OH)2 will also increase and hence the amount of Ca(OH)2 with which the fly ash will enter into reaction will increase, then an increased amount of C–S–H will result.

Table 2.2 The results of workability and compressive strength.[29]

Workability (mm) and compressive strength (N/mm^2) of the concrete

Concrete	Workability	Compressive strength (N/mm^2)	
	Slump (mm)	28 days (N/mm^2)	180 days (N/mm^2)
C250FA00	12	23.1	26.6
C200FA30	12	21.3	25.0
C200FA50	11.5	22.4	26.7
C200FA65	11.5	22.9	27.2
C200FA85	12	22.7	27.1
C200FA100	12.5	21.4	25.7
C200FA115	12.5	20.0	24.2
C300FA00	12	29.5	34.2
C240FA35	12	27.1	32.2
C240FA60	11.5	29.2	34.6
C240FA80	11.5	29.6	35.3
C240FA100	12	29.8	35.6
C240FA120	12	28.5	34.2
C240FA140	12.5	26.9	32.6
C350FA00	12	35.7	41.4
C280FA40	11.5	33.0	38.9
C280FA70	12	35.6	42.2
C280FA95	11.5	36.2	43.3
C280FA120	12	36.5	43.4
C280FA140	12.5	35.5	42.5
C280FA165	12.5	33.6	40.8
C400FA00	12	41.5	48.0
C320FA50	11.5	39.3	46.3
C320FA80	11.5	41.4	49.3
C320FA105	11.5	42.5	50.7
C320FA135	12	42.7	50.9
C320FA160	12.5	41.2	49.7
C320FA185	12.5	39.5	48.3

Dinakar P [30] studied the influence of including fly ash (FA) on the properties of self-compacting concrete (SCC). Portland pozzolana cement (PPC) was partially replaced with 10–70%

fly ash. The water to binder ratio was maintained constant at 0.30 for all mixes. Compressive strength tests were carried out at 3, 7, 28 and 56 days and the results are presented in Table 2.3 Fig. 2.23 shows the variation of compressive strengths at 28 and 56 days with respect to the fly ash replacement.

Table 2.3 Mechanical properties of the concretes investigated.[30]

Concrete name	Compressive strength (MPa)				Splitting tensile strength (MPa)		Modulus of elasticity (GPa)	
	3 day	7 day	28 day	56 day	28 day	56 day	28 day	56 day
10% FA	44.42	58.37	78.97	87.85	5.62	5.55	43.24	42.14
30% FA	48.33	51.20	88.06	99.43	5.93	6.06	45.42	46.24
50% FA	27.1	35.91	60.83	66.20	4.12	4.20	36.63	36.01
70% FA	18.14	21.77	44.21	50.21	2.61	2.84	31.56	32.78

As noted from the results shown in Fig. 2, the compressive strength, of SCC increased drastically from 10% to 30% replacement of fly ash but started to decline at 50% and 70% replacement. High compressive strength of nearly 100 MPa has been obtained at 30% replacement at 56 days than the other fly ash mixes including the 10% replacement, where a high strength of approximately 88 MPa at 56 days is obtained. Generally, and at the same water to binder ratio, there is a strength reduction for concretes containing fly ash compared with that of the control. However, and even at high fly ash content (70%), a long-term high strength of about 50 MPa is achieved at the same water to binder ratio. Higher strength would be expected in the fly ash mixes if the w/b ratio was lowered to achieve similar workability to that of the control.

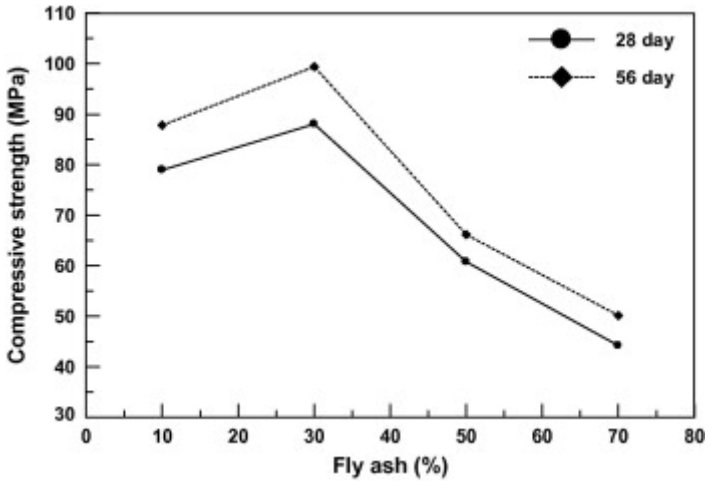

Fig. 2.23 Variation of compressive strength with respect to fly ash replacement.[30]

The results of split tensile strength tests at 28 and 56 days are presented in Table 4. The split tensile strength ranges from 2.61 to 5.93 MPa and 2.84 to 6.06 MPa at 28 and 56 days, respectively. The split tensile strength of all SCC mixtures increased with age. The results showed that, an increase in the FA content decreased the split tensile strength of the SCC especially at 28 days. SCC mixtures containing 10–30% FA replacement showed higher split tensile strength than SCC mixtures containing 50–70% FA replacement. This indicates that up to a 30% of FA replacement may have positive effects

on the interfacial bond between the paste and aggregates. The mixtures containing 50– 70% FA showed lower tensile strength probably due to the weaker bond between the matrix and the aggregates[30].

The relationship between the splitting tensile strength (fsp) and compressive strength (fck) for the SCC mixtures is presented in Fig. 2.24. For the tested mixtures the tensile strength can be calculated by using the following equation:

$$F_{SP} = 0.0264 f_{ck}^{1.21919} \quad [30]$$

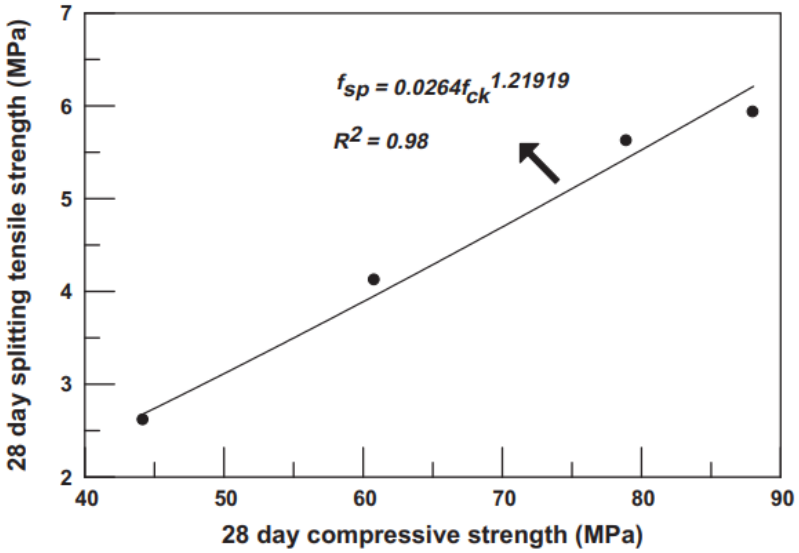

Fig. 2.24 Relationship between compressive strength and splitting tensile strength.[30]

Conclusion above results, we can get that fly ash replacements of around 30–50% will be ideal for developing SCCs when Portland pozzolana cement was used. High percentage of fly ash (more than 50%) cannot be used to produce SCC when cement was used, and 30% replacement of fly ash exhibited the highest compressive strength, splitting tensile strength and elastic modulus. At 30% fly ash as cement replacement can produce SCC with a very high compressive strength of 100 MPa.

2.2.2 The durability of fly ash concrete.

DeMaeijer, P. K. et al. reported that replacing cement with fly ash can improve resistivity, the chloride migration coefficient, and alkali-silicon reactions, but reduces the carbonization resistance of concrete [31].

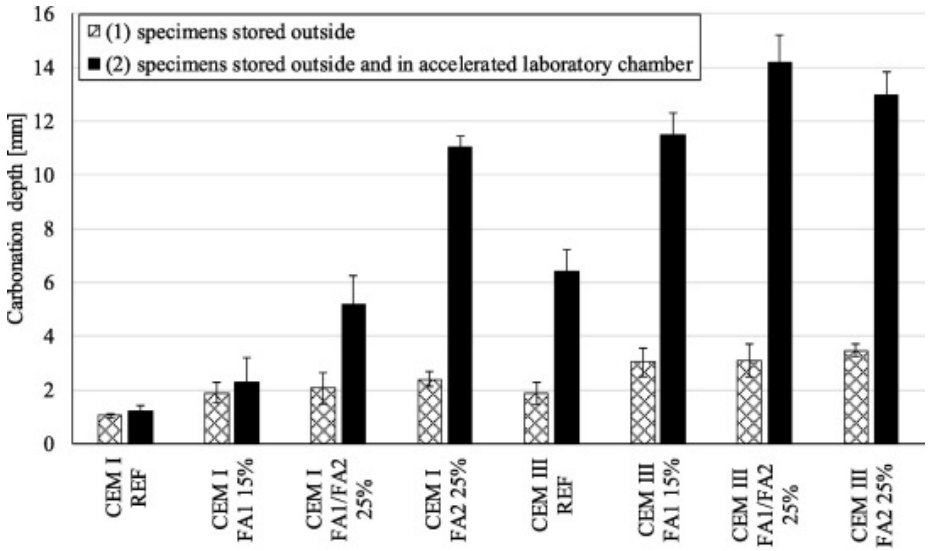

Fig. 2.25 Carbonation test results.[31]

Chindaprasirt et al. found that replacing OPC with fly ash can increase the porosity but decrease the average pore size. Furthermore, as the fly ash content increases, the gel pore volume (5.7–10 nm) increases [32]. Saha studied concrete incorporating fly ash, and the results showed that drying shrinkage decreases with increasing fly ash content (Fig. 2.26). The incorporation of fly ash reduced the porosity of concrete, resulting in concrete with better water sorptivity and chloride permeability (Fig.2.27)[33].

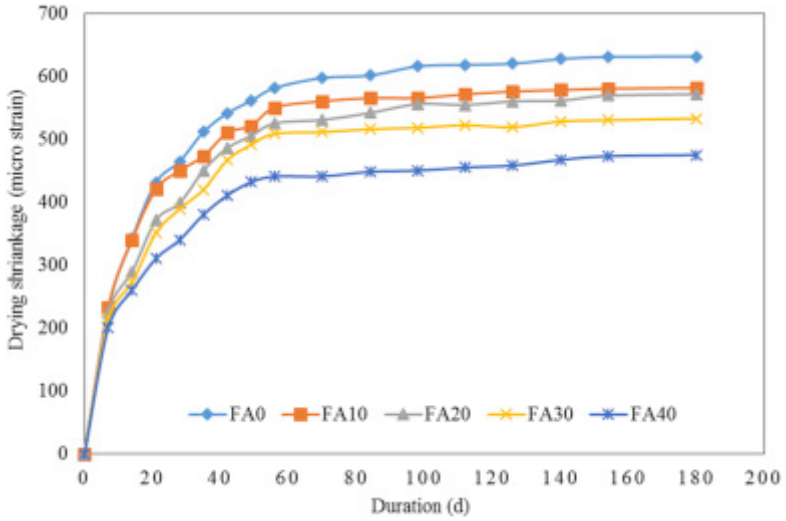

Fig. 2.26 Effect of fly ash on drying shrinkage of concrete.[33]

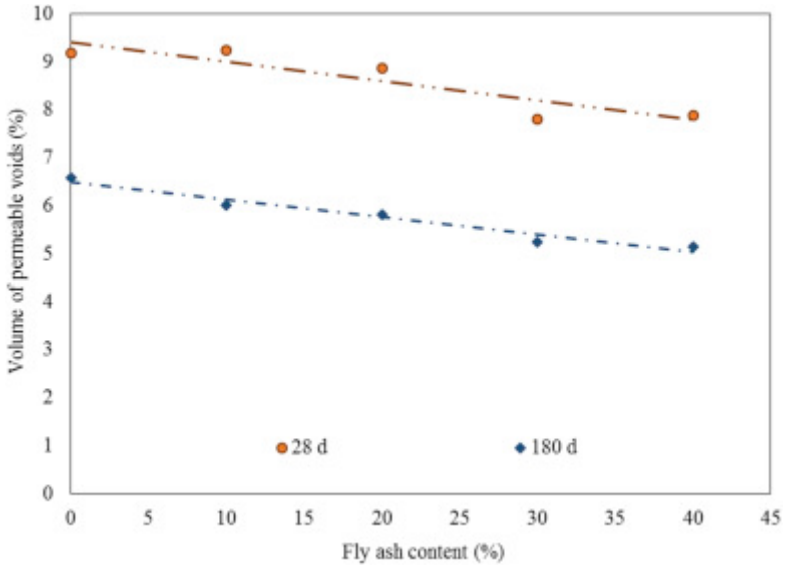

Fig. 2.27 Effect of fly ash on volume of permeable voids.[33]

Moffatt and others found that resistance to chloride-ion penetration was considerably enhanced when high replacement amounts of fly ash were used[34]. It has been reported that concrete with fly ash replacing 25% of the cement has a 15% lower creep compared with conventional concrete [35]. Bamforth reported that concrete containing 30% fly ash replacing cement exhibited 50% reduced creep strain compared with concrete without fly ash [36]. Lohtia et al. studied the creep of concrete containing 0%–25% fly ash replacing cement and found an increase in creep for concrete with replacement of more than 15% fly ash compared with conventional concrete[37]. It has also been reported that self-compacting concrete with a higher fly ash content in place of cement tends to reduce both drying and autogenous shrinkage [38]. However, one study reported that shrinkage increases with percentage of fly ash content [39].

2.2.3 The properties of GGBS concrete

Molten slag is a by-product of the iron production process gotten from the blast furnaces; the product obtained when it is cooled and ground into very a fine powder is called GGBS [40]. GGBS has the most hydraulic property owing to its high CaO content; this reinforces its potential as an SCM. Many scholars have studied the possibility of using GGBS in concrete from the perspective of mechanical properties. Gupta et al.[41] studied the strength development of ultrahigh performance mortar when 60% of the PC was replaced with GGBS of different fineness. In this study, cement is replaced by slag at 20% and 60% by weight. Slag of three different fineness is used: 400±4 m2/kg, 556±5 m2/kg and 750± 5 m2/kg at constant water-binder ratio of 0.25 for all mixes. Compressive and flexural strength were measured for mechanical performance. Results show that early and late compressive strength and flexural strength are improved significantly by incorporation of slag with fineness 556 ± 5 m2/kg compared to reference and slag of 400 m2/kg fineness. However, at similar fineness 20% slag incorporation is found to produce higher early strength compared to 60% slag although 90-day strength for both replacement percentages are similar.

Dai et al.[42] carried out a similar study using six different grades of GGBS. To improve the properties

of ground granulated blast furnace slag (GGBS) and utilize ground granulated blast furnace slag efficiently, this study investigates the effect of fineness on the hydration activity index (HAI) of ground granulated blast furnace slag. The hydration activity index of GGBS with six specific surface areas (SSAs) was characterized by the ratio of compressive strength of the prismatic mortar test block. The compressive strength of the specimen at 1 day, 3 days, 7 days, 14 days and 28 days is presented in Table 2.4. It can be seen that the compressive strength of the specimens increases with the increasing of its age. The compressive strength of the reference mortar at the same age increases with the increase of the specific surface area of the GGBS.

Table.2.4 Compressive strength of specimen(MPa).

Age	Cement	KA	KB	KC	KD	KE	KF
1 d	23.32	5.80	6.15	6.96	8.24	8.38	8.58
3 d	24.94	12.99	16.24	17.98	19.37	20.11	21.23
7 d	34.45	21.00	24.71	28.07	32.25	33.13	34.45
14 d	36.31	27.61	30.86	35.50	40.14	42.18	45.24
28 d	42.92	35.38	41.99	46.28	48.37	50.00	52.43

P. Ganesh experimentally evaluated various properties such as flowability, compressive strength, tensile strength, fracture, and durability of Ultra high-performance concrete（UHPC） with a high volume GGBS under two curing conditions (Standard water and elevated temperature curing). UHPC specimens are subjected to a compressive strength test at 7, 28, 56, and 90 days after standard water curing and other specimens are subjected to elevated temperature. Compressive strength results of UHPC with high volume GGBS under different curing conditions are presented in Fig. 2.28. An average compressive strength of G-0, G-20, G-40, G-60, and G-80 UHPC specimens cured under elevated temperature are 151, 160, 168, 152 and 143 MPa, respectively. These values for 28 days standard water cured specimens are 116, 121, 118, 110, and 101 MPa, respectively. From the results, it is observed that the compressive strength under elevated temperature curing is improved significantly with an increase in cement replacement level by GGBS upto 40%. Compressive strength of specimens at 28 days standard water curing is increased marginally for G-20 mix, slightly close for G-40 mix, and starts decreasing for the G-60 and G-80 mixes with respect to control mix. From the result, it is evident that the early age compressive strength for a high volume of GGBS highly relies on temperature curing. Since, the 7 days standard water cured specimens do not exhibit significant strength development with respect to GGBS incorporation. The compressive strength of 7 days standard water curing specimen is slightly close to G-20 mix and lesser for G-40, G-60 and G-80 mixes with respect to control mix. The strength may not be appreciable at an early age due to the dilution effect of GGBS in place of cement, since the reactivity of GGBS is very slow compared to Portland cement. Therefore, a compressive strength of UHPC mix with high volume GGBS under water curing is relatively slow at an early age, whereas the elevated temperature exposure condition accelerates the strength at an early age with respect to higher cement replacement level by GGBS.

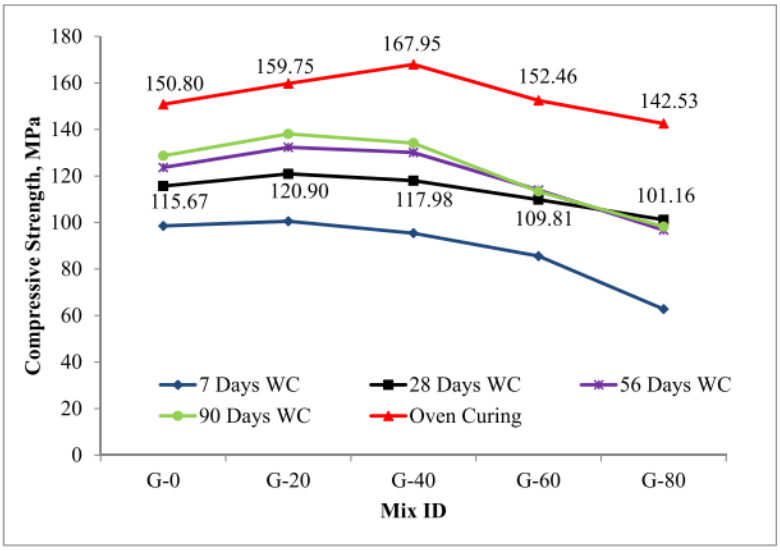

Fig.2.28 Compressive strength of UHPC under standard water curing (WC) and elevated temperature curing (Oven).[43]

Split tensile strength results for the UHPC mixes with high volume GGBS under varying curing conditions are presented in Fig. 2.29. Similar to compressive strength, split tensile strength also carried out on standard water cured cylinders at the age of 7, 28, 56, and 90 days and on the specimens exposed to elevated temperature. The average split tensile strength of G-0, G-20, G-40, G-60, and G-80 UHPC specimens cured under elevated temperature are 22.2, 23.3, 24.5, 22.8, and 20.0 MPa, respectively. These values for 28 days standard water cured specimens are 19.5, 20.4, 19.2, 17.7, and 14.9 MPa, respectively. The split tensile strength results show that the early age strength of high volume GGBS doesn't show any significant improvement compared to later age results at 56 and 90 days.

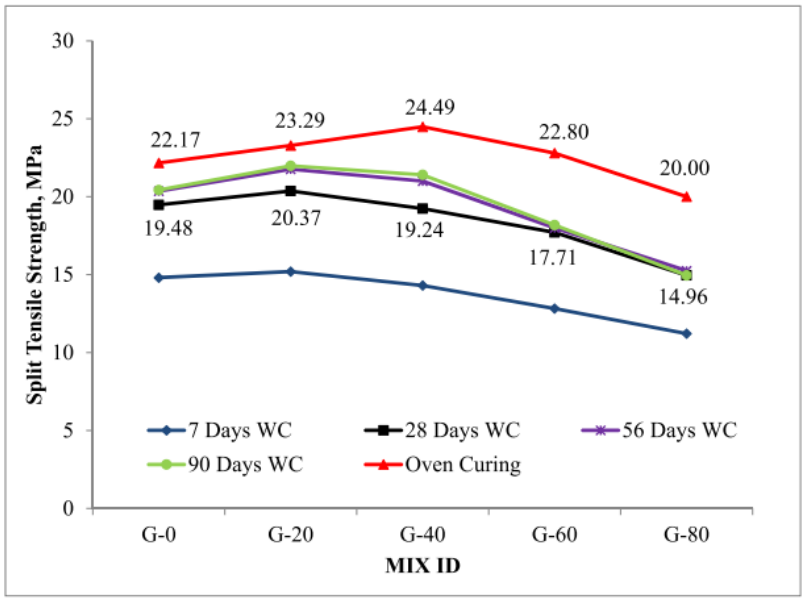

Fig.2.29 Split tensile strength of UHPC under standard water curing (WC) and elevated temperature curing (Oven).[43]

Based on the results of the above mechanical properties, it can be found that, The compressive strength and split tensile strength are improved significantly with the increase of GGBS level up to 40% against elevated curing approach and 20% with standard water curing. The early age compressive strength is not significant with respect to a high volume of GGBS due to the poor hydration reactivity of GGBS under water curing at early age. Temperature curing improves the hydration reaction and exhibit faster strength attainment with respect to higher GGBS level.

It has been reported that in self-consolidating concrete made with high volumes of GGBS, replacing up to 70% of the cement with GGBS reduces the shrinkage of concrete by more than 45% compared with conventional concrete[44]. Darquennes et al. studied the free shrinkage of concrete incorporating 75% GGBS and found that for a GGBS concentration of ≤50% of the volume of the binder, the overall shrinkage evolution rate and amplitude were lower over time than those for conventional concrete[45]. Brooks et al. found that GGBS concrete exhibited equivalent or greater long-term strength and shrinkage, relatively less basic creep, and comparable or less total creep compared with ordinary concrete[46]. It has also been reported that at an early age, the creep of GGBS-blended concrete is less than that of ordinary concrete. However, creep was higher in the long term compared with ordinary concrete [47]. Khatri et al. reported the opposite result, indicating that concrete with less slag in its binder has less creep [48].

2.3 Research status of geopolymer concrete

Geopolymer Concrete (GPC) exhibits its mechanical properties through a unique process called geo-polymerization, which distinguishes it from Ordinary Portland Cement Concrete (OPCC) and lime concrete. The mechanical properties of GPC are influenced by various factors, including the type and composition of its constituents, the presence or absence of calcium silicate hydrate (CSH) gel and the curing conditions[49].

Mechanical properties are the physical properties exhibited by a material when subjected to external loads. In the case of both Ordinary Portland Cement Concrete (OPCC) and Geopolymer Concrete (GPC), they are often subjected to significant structural loading, and therefore their performance is evaluated based on their mechanical properties. The key mechanical properties of a material typically include compressive strength, tensile strength, flexural strength, modulus of elasticity, fire resistance, and durability. A material with superior mechanical properties is generally expected to perform better under typical structural loading conditions[50].

2.3.1 The mechanical properties of geopolymer concrete

Compressive strength is a fundamental mechanical property that represents the maximum stress a material or structural element can withstand before experiencing crushing failure. In structural concrete, compressive strength is of paramount importance as it is primarily responsible for bearing compressive loads under normal loading conditions. Furthermore, many other mechanical properties of geopolymer concrete (GPC) are directly linked to its compressive strength. Even a slight variation in compressive strength can have a significant impact on these associated properties.

The compressive strength of GPC is typically influenced by several factors, including the type of parent geopolymer material, type and concentration of alkaline liquid, water-to-binder ratio, and curing conditions. However, it is generally observed that the compressive strength of GPC is equal to

or higher than that of Ordinary Portland cement concrete (OPCC)[50].

(1) Different precursor materials

1. Fly ash

Fly ash is a hazardous byproduct primarily generated from the combustion of coal in coal-fired power plants. It is formed when finely ground coal is burned in a boiler to generate electricity and is then collected from the power plant's chimney using particulate control devices such as electrostatic precipitators or fabric filters. Fly ash predominantly comprises tiny glassy spheres with silt-sized and clay-sized particles, imparting a texture similar to that of talcum powder. It can be classified into two types: Class C and Class F, which are determined by the specific type and origin of the coal being burned[51]. Fly ash is available in two types: Class F, commonly referred to as low calcium, and Class C, which has a high calcium content[52]. In terms of composition, fly ash primarily consists of silica, calcium, alumina, iron, and magnesium. The Fly ash properties and the chemical composition are shown below in Table 2.5[54].

Table 2.5 Fly Ash Physical Properties and Chemical composition.[54]

Chemical composition	% by weight	Physical properties	
SiO_2	57.95	Fineness	522 m^2/kg
Al_2O_3	31.78	Specific gravity	2.2
Fe_2O_3	4.30	Residue on 45μ sieve	25%
Ca_2O	1.2		
MgO	0.5		
Na_2O	1.29		
K_2O	0.3		
SO_3	0.08		
LOI	2.6		

2. Ground Granulated Blast furnace slag (GGBS)

The steel industry produces a molten residue known as Blast furnace slag, which possesses non-metallic properties and primarily consists of calcium, silica, and alkane[55]. In certain cases, Ground Granulated Blast Furnace Slag (GGBS) is utilized as a source material in the development of Geopolymer Concrete (GPC), yielding satisfactory strength and moment outcomes[56]. When compared to fly ash, the use of GGBS leads to a reduction in the slump value due to its high calcium content[57][58]. This phenomenon contributes to the formation of Ca-Al-Si gel and enhances geopolymerization[59][60].

Table 2.6 Chemical composition of slag (Nippon Slag Association, 2012).

Type component	Blast furnace slag (slag cement)
CaO	41.7
SiO_2	33.8
T-Fe	0.4
MgO	7.4
Al_2O_3	13.4
S	0.8
P_2O_5	<0.1
MnO	0.3

3. Metakaolin

Metakaolin refers to an anhydrous calcined form of the clay mineral kaolinite. The average particle size of metakaolin falls between 1 to 2 micrometers, which is smaller than Portland cement particles but larger than silica fume particles. The chemical composition of metakaolin, as presented in Table 2.7, consists of approximately 92.6% silica and alumina[61].

Table 2.7 Chemical composition of metakaolin[60]

Chemical composition	Percentage
Silica (SiO_2)	54.3
Alumina (Al_2O_3)	38.3
Ferric oxide (Fe_2O_3)	4.28
Calcium oxide (CaO)	0.39
Magnesium oxide	0.08
Sodium oxide	0.12
Potassium oxide (K_2O)	0.50

(2) Alkaline solution

The alkaline activator solution utilized in the development of GPC primarily comprises soluble alkalis, typically sodium or potassium-based. The commonly employed alkaline activator consists of sodium hydroxide (NaOH) in conjunction with sodium silicate (Na2SiO3) to facilitate the formation of Geopolymer Concrete (GPC)[62].

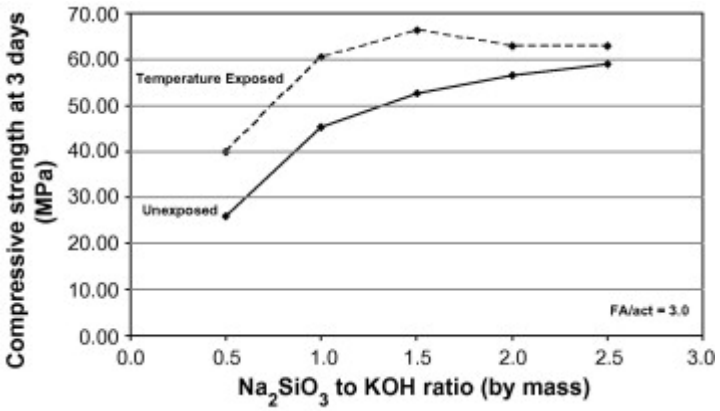

Fig. 2.30 Effect of sodium silicate-to-potassium hydroxide ratio on compressive strength.[62]

Fig.2.30 illustrates the 3-day compressive strength measurements of fly ash-based geopolymer samples prepared with different Na2SiO3/KOH ratios ranging from 0.5 to 2.5, while maintaining a constant curing temperature of 80 °C. It is evident that the strength of the geopolymer notably improved with an increase in the Na2SiO3/KOH ratio. This increase in ratio leads to a higher sodium content in the mixtures, consequently contributing to more stable strength properties. Geopolymers with higher sodium concentrations, particularly within the Na2SiO3 component, exhibit rapid strength development[63]. However, it is anticipated that the compressive strength will decrease with the addition of more silicate to the system. This is due to the excess sodium silicate impeding water evaporation and structure formation[64]. An intriguing observation is that the compressive strength of the geopolymer specimens unexpectedly increased when exposed to elevated temperatures. This increase in strength can be attributed to the low diffusion coefficient of K+ ions at elevated temperatures, resulting in a higher melting temperature of the geopolymer.

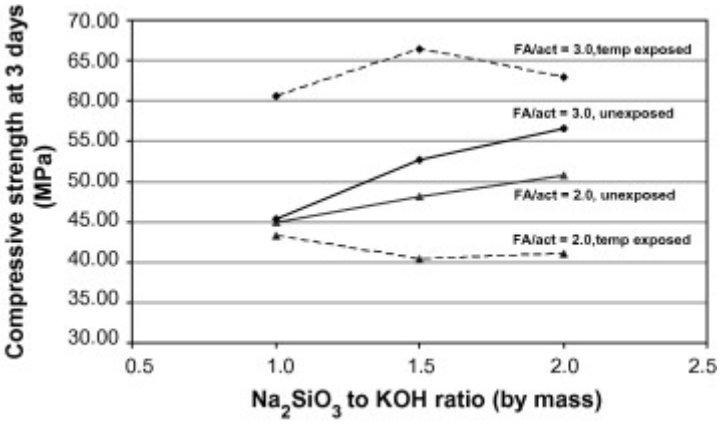

Fig. 2.31 Effect of fly ash-to-activator ratio on compressive strength.[63]

In order to compare the strength performance, a study was conducted using different fly ash-to-activator ratios, which aimed to replicate the concept of water-to-cement ratio commonly used to assess compressive strength in Ordinary Portland Cement (OPC). The liquid activators consisted of a combination of Na2SiO3 and KOH liquids, and the total mass of these activators was considered. The findings, depicted in Fig. 2.31, revealed a general decrease in strength as the amount of activator introduced into the system was increased, resulting in a reduction of the fly ash-to-activator ratio from 3.0 to 2.0.

(3) Curing temperature and time

Another factor that significantly affects the strength of geopolymer concrete (GPC) is the temperature during the concrete curing process. Along with temperature, curing time also has an impact on the strength of geopolymer concrete. Table 2.8 provides a summary of the impact of curing time (in hours) and curing temperature (in °C) on the compressive strength of geopolymer concrete (GPC)[54].

Table 2.8. Effect of curing time and curing Temperature on compressive strength of GPC.[54]

GPC Type	Curing Time (hours)	Curing Temperature (°C)	Compressive Strength (MPa)
50FA/50GGBS	12	80	38.71
	24	80	50.22
	12	90	67.91
	24	90	66.91
	12	100	57.21
	24	100	47.24
100FA	24	60	43
	24	70	53
	24	80	49
	24	90	48
100FA	48	50	25
	48	70	48
	48	90	45
100FA	48	60	28

The compressive strength results presented in Fig. 2.32 challenge the claim made by Hardjito et al. [66]in their study on fly ash-based geopolymer concrete, which stated that higher curing temperatures lead to higher compressive strengths. The test results indicate that increasing the curing temperature from 60°C to 70°C actually enhances the compressive strength of the concrete. However, when the curing temperature is further increased beyond 70°C, the compressive strength of self-compacting geopolymer concrete decreases[67].

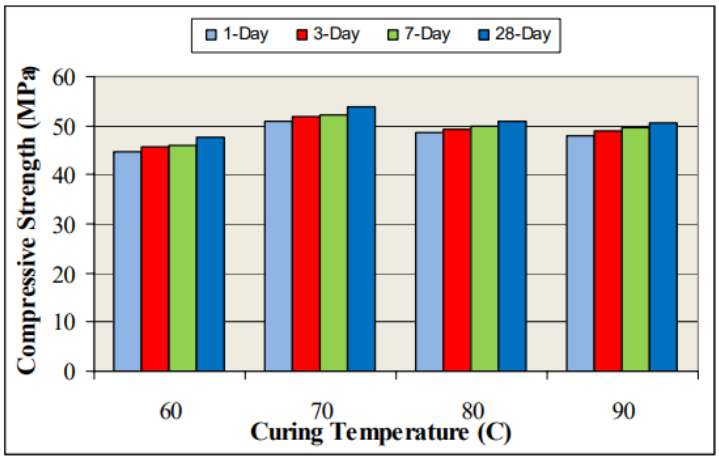

Fig. 2.32 Effect of Curing Temperature on Compressive Strength[66]

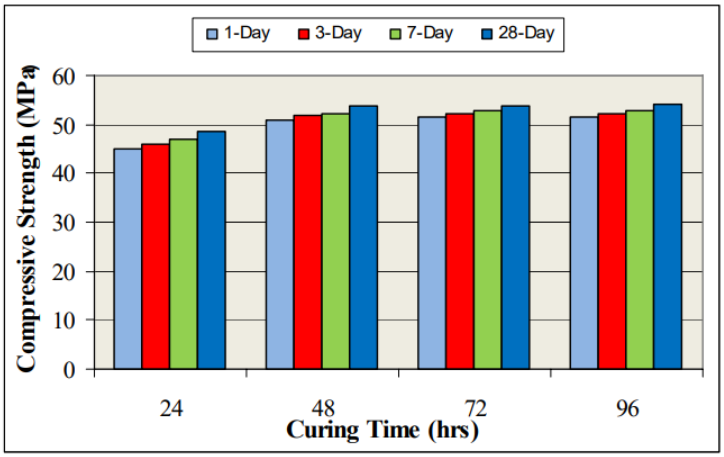

Fig. 2.33 Effect of Curing Time on Compressive Strength[66]

Fig. 2.33 illustrates the impact of curing time on the compressive strength of self-compacting geopolymer concrete. The test specimens were cured in an oven at a temperature of 70°C, with curing times ranging from 24 hours to 96 hours (4 days). It is believed that a longer curing time enhances the geopolymerization process, resulting in higher compressive strength.

The test results depicted in Figure 1 indicate a positive correlation between curing time and compressive strength. As the curing time increases, the compressive strength of the geopolymer concrete also increases. Among all the curing periods, the specimens cured at 70°C for 96 hours exhibited the highest compressive strength at all ages. The rate of strength gain is rapid within the first 48 hours of curing time. However, beyond this point, the increase in strength becomes less significant.

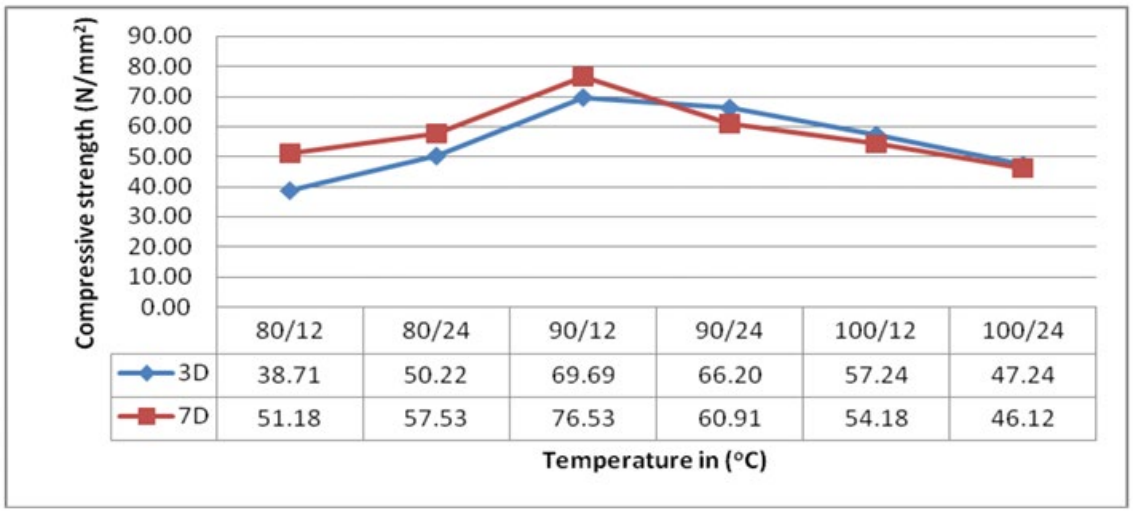

Fig. 2.34 Spread compression strength for all combinations of curing temperatures and curing time.[68]

Fig. 2.34 illustrates that the compressive strength of geopolymer concrete (GPC) increases as the temperature and curing hours rise, specifically from 80ºC to 90ºC with a 12-hour curing period on the 3rd and 7th day of testing. The experimental results indicate that the maximum strength was achieved on the 7th day with curing at 90ºC for 12 hours. This temperature can be considered the optimum for further study. However, it was observed that when the curing period exceeded 12 hours, the compressive strength of geopolymer concrete decreased. This decrease in strength can be attributed to the continuous evaporation of moisture from the specimens. As geopolymer concrete has a low water content, the exposure to high temperatures causes moisture loss from the surface, leading to the development of surface cracks. Consequently, the strength of geopolymer concrete is compromised[68].

Tensile strength refers to the maximum stress a material or structural element can withstand before fracturing under a tensile load. Concrete is typically considered a compression material with high compressive strength. However, it also exhibits some tensile characteristics that are crucial for designing concrete structural members. This is because structural members, under normal conditions, may experience various types of loads, including compressive loads, tensile loads, bending loads, and more. Geopolymer Concrete (GPC) is generally known to possess superior tensile characteristics compared to Ordinary Portland Cement Concrete (OPCC)[50].However, the composition of GPC can greatly impact these tensile properties. An increase in the sand-to-binder ratio may lead to a decrease in the tensile strength of GPC, as illustrated in Fig. 2.35[69]. However, this reduction in tensile strength can be mitigated by incorporating GGBS, which has demonstrated its effectiveness in enhancing the tensile properties of GPC[70].

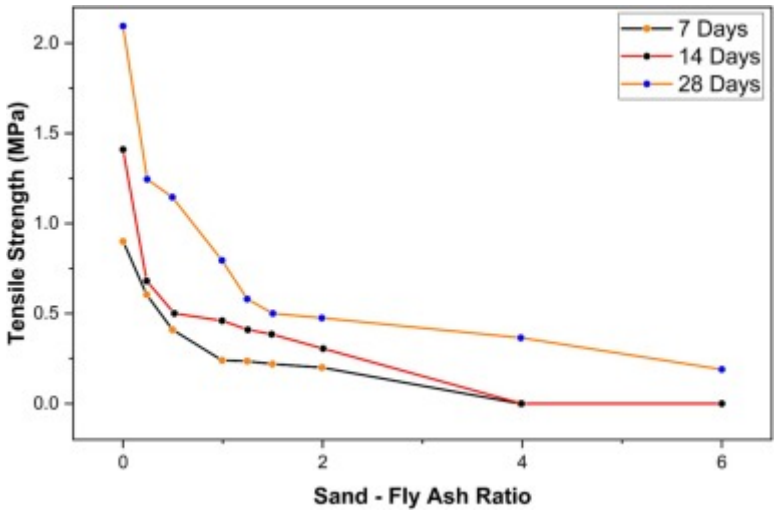

Fig. 2.35 Effect of Sand-FA ratio on the Tensile Strength of GPC.[69]

The direct tensile strength of geopolymer mixes was evaluated with varying GGBS content (10-40% wt. of the total binder) and cured under ambient temperature. The results, depicted in Fig. 2.36, revealed that increasing the GGBS content positively influenced the tensile strength at both 7 and 28 curing days. Specifically, the specimens containing 40% GGBS exhibited the highest direct tensile strength, reaching approximately 3 MPa at 28 days. It is worth noting that there is a scarcity of published studies in the literature that have conducted similar tests on geopolymer samples to determine their direct tensile strength. Furthermore, only a limited number of studies have presented results on the splitting tensile strength of geopolymer concrete.

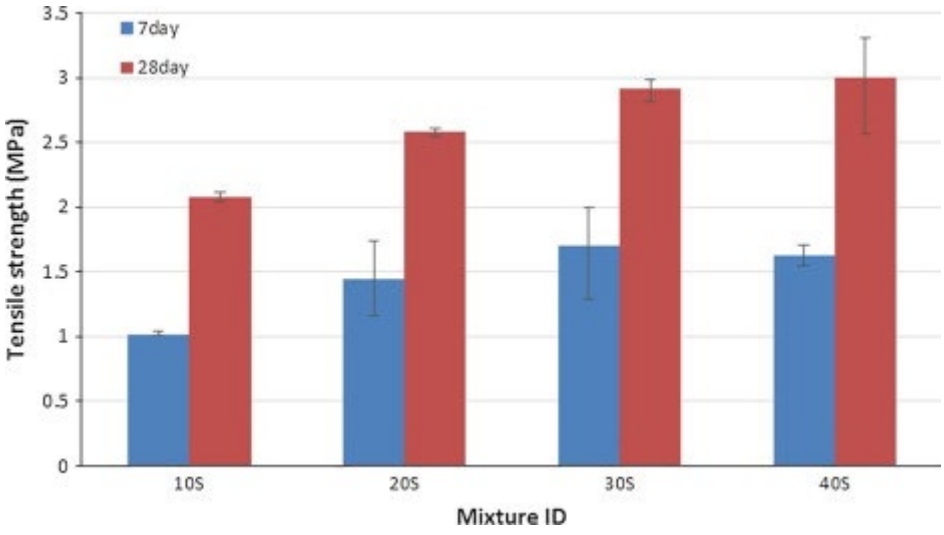

Fig. 2.36. Effect of slag content on the tensile strength of geopolymer mortar samples cured at ambient temperature.[69]

The results of the tensile strength tests on Geopolymer mortar (GM), ordinary Portland cement mortar (CM), and polymer-modified cement mortar (PMCM) specimens, both at ambient temperature and after exposure to 100, 300, 500, and 700 °C, are illustrated in Fig. 2.37. It shows that the tensile strength of GM increases at 100 °C and then experiences a rapid decline in the 300-700 °C

temperature range. Across the temperature range of 25-700 °C, GM specimens demonstrate higher tensile strength compared to CM specimens. However, the disparity in tensile strength between GM and CM diminishes as the temperature increases. Specifically, at ambient temperature, the tensile strength of GM is 1.85 times greater than that of CM, while after exposure to 300 °C, the tensile strength of GM is only 1.38 times higher than that of CM. Comparing GM with PMCM, GM exhibits higher tensile strength at 25 and 100 °C but lower tensile strength at 300 °C. This suggests a higher rate of tensile strength degradation in GM than in CM and PMCM between the temperature range of 100 and 300 °C. This decline in tensile strength in geopolymer mortar can be attributed to significant microstructural pore changes that occur in geopolymers at high temperatures[71]. Notably, at 500 °C, significant strength degradation is also observed in PMCM.

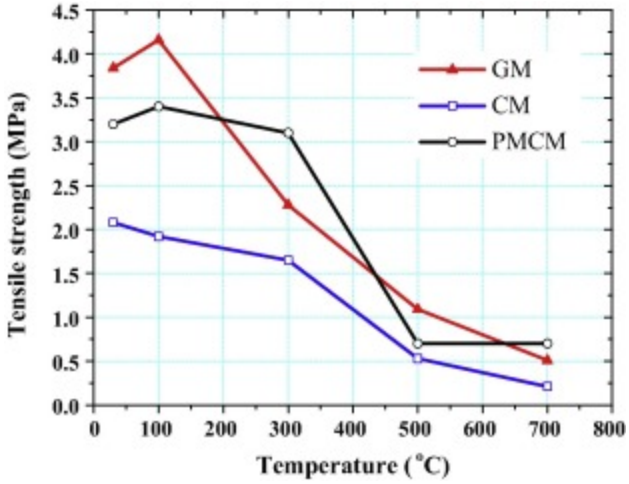

Fig. 2.37 Tensile strength of GM, CM and PMCM.[70]

2.3.2 Durability of GPC

1. Chemical resistant

The durability of materials plays a crucial role in designing their lifespan, ensuring safety, and determining their mechanical behavior. The durability issues commonly associated with OPC are often attributed to the presence of calcium oxide in the concrete gel. However, the behavior of GPC in the face of chemical attacks differs significantly due to its low calcium content in the matrix[72].

In Fig. 2.38 , it can be observed that all specimens immersed in sodium chloride and sodium sulphate + magnesium sulphate solutions did not exhibit any visual signs of deterioration. However, in Fig. 2.39(a), OPC concrete specimens exposed to sodium sulphate did not show any visual signs of deterioration, whereas geopolymer concrete specimens developed a white layer of sodium carbonate on their surfaces after being dried. The thickness of this layer gradually increased over time, reaching a maximum thickness of 1 mm for cylinders and 5 mm for prisms, as depicted in Fig. 2.39(b). It is important to note that all specimens were air-dried after being removed from their respective solutions, and the white layer developed upon exposure to air. Similar results have been observed in previous studies, such as those reported by Singh et al.[73]. Additionally, Bakharev [74] highlighted that sodium hydroxide migrates from geopolymer specimens when exposed to solutions containing Na_2SO_4. Therefore, it can be inferred that the formation of this white layer is a result of the reaction between

leached sodium hydroxide and atmospheric carbon dioxide (CO_2), leading to the formation of a white layer of sodium carbonate (Na_2CO_3). Over time, specimens immersed in sulfuric acid solutions exhibited gradual deterioration, to the extent that the coarse aggregates of the OPC concrete became visibly apparent[75].

(a) Fly ash (b) GLSS (c) OPC

Fig. 2.38 Specimens immersed in sodium sulphate + magnesium sulphate for nine months.

(a) OPC, GLSS and fly ash cylinders (b) GLSS prism

Fig. 2.39 Specimens immersed in sodium sulphate for nine months.

2. Resistance of seawater attack and sulphate attack

According to Johansen[76], the internal structure of the aluminosilicate gel components plays a significant role in determining the durability of fly ash-based geopolymer concrete in harsh environments such as a 5% Na_2SO_4 solution and 5% $MgSO_4$ solution. As depicted in Fig. 2.40, the compressive strength of GPC and OPC concrete exposed to 5% Na_2SO_4 and $MgSO_4$ displays some fluctuations, which may be attributed to the transition of alkaline components from the geopolymer into the solution. Comparative analysis of GPC prepared with sodium hydroxide (NaOH) and sodium-silicate activator indicates that the former exhibits a more crystalline structure. Additionally, the geopolymer concrete activated with NaOH solution outperforms OPC concrete in terms of strength and durability[76].Furthermore, Criado et al. [77][78] reported that the strength and durability of GPC improve over time, regardless of the chemical solution in which the samples were immersed.

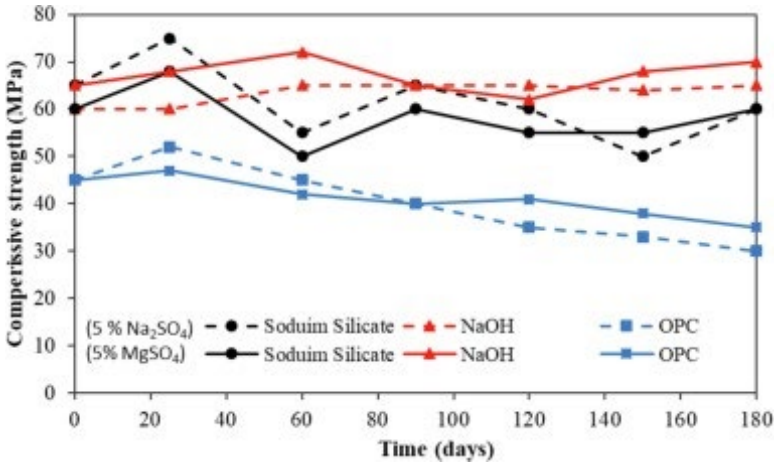

Fig. 2.40 Compressive strength of fly ash activated with sodium silicate solution and NaOH, and OPC specimens, exposed to 5% of Na2SO4 and $MgSO_4$ (Johansen, 2011).

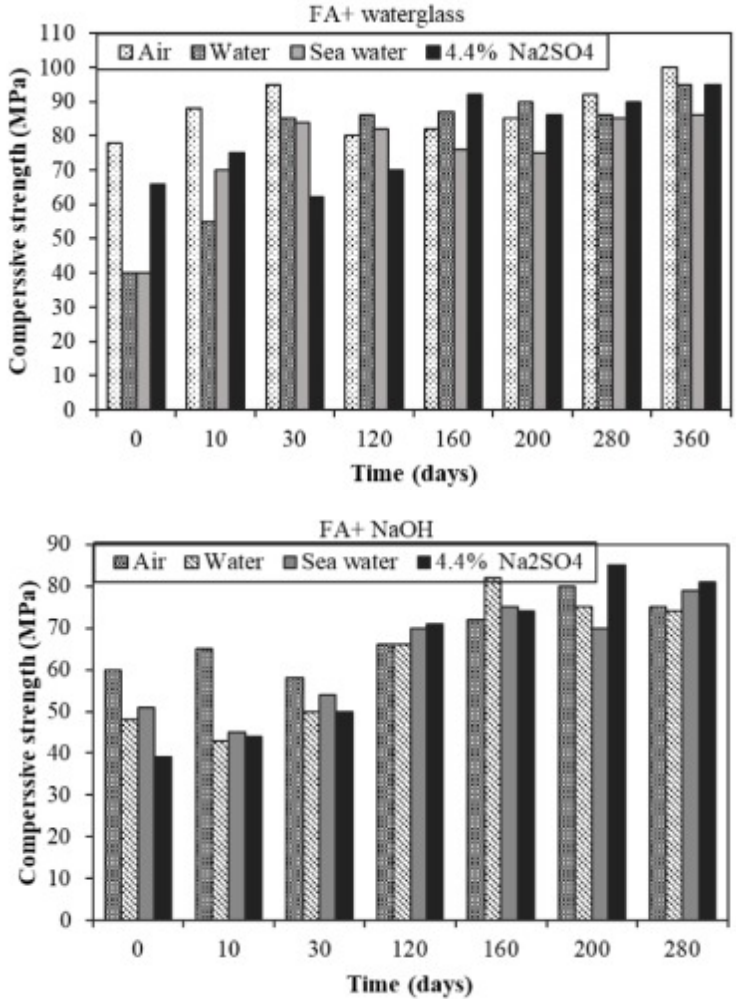

Fig.2.41 Mechanical strength of fly ash mortars NaOH-activated, and water glass-activated [77][78].

2.3.3 Workability

All the geopolymer concrete and mortar mixtures were formulated using only alkaline solution as the liquid component, without the addition of extra water or superplasticizer. Consequently, the alkaline solutions and the moisture present in the aggregate (which was used in a saturated surface dry condition) served as the sole sources of water in the mixture. Most of the mixtures contained a combination of sodium hydroxide and sodium silicate solutions, which constituted 40% of the total binder. The high viscosity of sodium silicate resulted in a sticky mixture when combined with the alkaline solution. In the absence of a significant amount of additional water or superplasticizer, this solution typically formed a thick and cohesive paste with the fly ash. As a result, the mixture of aggregates and geopolymer paste exhibited a high degree of cohesion. The consistency of the mixture could be quite stiff when the liquid content was relatively low. The fresh mixture demonstrated a viscous behavior and had a tendency to flow under the influence of gravity. However, these properties varied depending on the alkaline liquid content, as discussed further. Furthermore, when GGBS was added to the mixture, the concrete mixture typically appeared stiffer compared to mixtures containing only fly ash.

The rheology of a geopolymer mixture differs from that of an OPC mixture, leading to variations in the results of conventional slump and flow tests. While these tests may not directly correspond to the same level of workability as in OPC mixtures, they still offer useful indications of the flow ability or workability of geopolymer mixtures. The slump and flow values presented in the following sections serve to highlight the impact of different parameters on the workability of the mixtures. It should be noted that in order to enhance workability, additional water or superplasticizer can be added; however, this may have an effect on the mechanical properties of the hardened concrete.

The mixtures 2 (S10), 3 (S20), and 4 (S30) were designed to investigate the impact of incorporating increasing amounts of GGBFS (Ground Granulated Blast Furnace Slag) in fly ash-based geopolymer. These mixtures were compared to the control geopolymer mixture 1 (S00), which contained fly ash alone as the binder. Fig. 2.42 illustrates the influence of slag inclusion on the workability, setting time, and compressive strength development of the geopolymer mixtures[79].

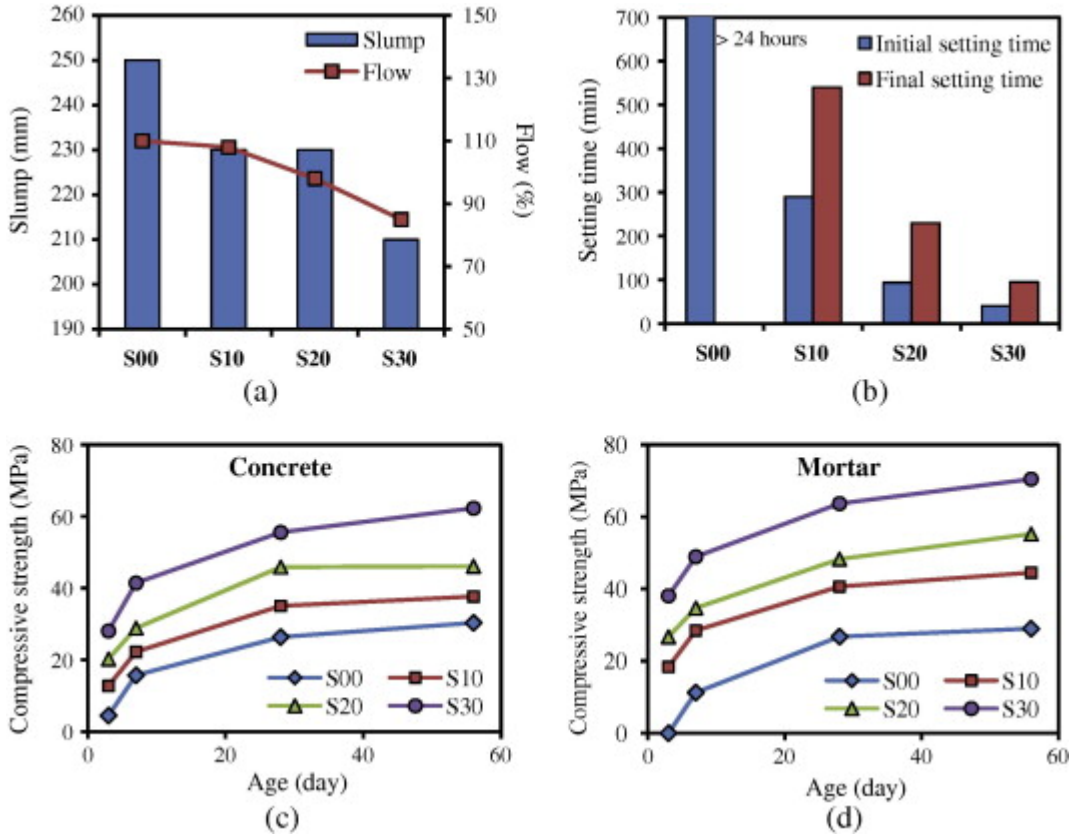

Fig. 2.42 Effect of different percentage of GGBFS on the workability (a), setting time (b) and compressive strength development of the geopolymer concretes (c) and mortars (d). [79]

The workability of the geopolymer mortar was influenced by the concentration of NaOH and the ratio of sodium silicate to NaOH, as indicated in Table 5. For the 10 M NaOH series, the flow of the geopolymer mortar decreased as the sodium silicate to NaOH ratio increased. The flows of the mortar with ratios of 0.67, 1.00, and 1.50 were 135 ± 5%, 125 ± 5%, and 110 ± 5%, respectively. However, when the ratio was increased to 3.00, the flow dropped below 110 ± 5%. To achieve a flow of 110 ± 5%, additional water at a rate of 2.3% by weight of fly ash was required. Alternatively, the addition of 3% of superplasticizer (SP) also yielded a mortar with a flow of 110 ± 5%. Thus, an increase in sodium silicate concentration resulted in a reduction in the flow of the geopolymer mortar.

For the 15 M NaOH mortar, it exhibited a thicker consistency compared to the 10 M NaOH mortar. Slightly more water was needed to achieve a similar flow pattern. To obtain a similar flow as the 10 M NaOH series, additional water at rates of 3.4% by weight of fly ash for ratios of 0.67, 1.00, and 1.50, and 4.5% for the 3.00 ratio, was required. Alternatively, the addition of 3%, 4%, 5%, and 6% of SP was necessary to obtain a flow pattern similar to that of the 10 M NaOH mixes.

For the 20 M NaOH mortar, it exhibited a significantly thicker consistency compared to the 10 M and 15 M NaOH mortars. To achieve a similar flow to the other series, additional water at rates of 6.8% by weight of fly ash for ratios of 0.67, 1.00, and 1.50, and 7.9% water for the 3.00 ratio, was required. Additionally, the use of 12%, 8%, 10%, and 10% of SP, respectively, produced a similar flow pattern, as shown in Table 5. Increasing the NaOH concentration resulted in a decrease in the flow of the geopolymer mortar.

In general, an increase in NaOH concentration and the amount of sodium silicate solution reduced the workability of the mixes. The higher NaOH concentration increased the viscosity of the solution, resulting in a reduced flow of the mortar. Similarly, the sodium silicate solution itself has a high viscosity, and an increase in the amount further reduced the flow of the mortar. To achieve mixes with suitable flow, additional water or SP was necessary. [79]

Table 2.9 Extra water, SP and flow of geopolymer mortar[79]

Sodium silicate to NaOH ratio	NaOH (M)	Flow (%)	Water (% of fly ash)	or SP (% of fly ash)
0.67	10	135±5	0	0
1	10	125±5	0	0
1.5	10	110±5	0	0
3	10	110±5	2.3	3
0.67	15	135±5	3.4	3
1	15	125±5	3.4	4
1.5	15	110±5	3.4	5
3	15	110±5	4.5	6
0.67	20	135±5	6.8	12
1	20	125±5	6.8	8
1.5	20	110±5	6.8	10
3	20	110±5	7.9	10

Reference

[1] Gholampour, A.; Zheng, J.; Ozbakkaloglu, T. Development of waste-based concretes containing foundry sand, recycled fine aggregate, ground granulated blast furnace slag and fly ash. Constr. Build. Mater. **2021**, 267, 121004.

[2] Kirthika, S. K., & Singh, S. K. (2020). Durability studies on recycled fine aggregate concrete. *Construction and Building Materials*, *250*, 118850.

[3] Verian, K. P. (2012). *Using recycled concrete as coarse aggregate in pavement concrete* (Doctoral dissertation, Purdue University).

[4] Wang, B., Yan, L., Fu, Q., & Kasal, B. (2021). A comprehensive review on recycled aggregate and recycled aggregate concrete. *Resources, Conservation and Recycling*, *171*, 105565.

[5] Dhir, R. K., Limbachiya, M. C., Leelawat, T., BS 5328, & BS 882. (1999). SUITABILITY OF RECYCLED CONCRETE AGGREGATE FOR USE IN BS 5328 DESIGNATED MIXES. *Proceedings of the Institution of Civil Engineers-Structures and buildings*, *134*(3), 257-274.

[6] Cachim, P. B. (2009). Mechanical properties of brick aggregate concrete. *Construction and Building Materials*, *23*(3), 1292-1297.

[7] He, Z. H., Hu, H. B., Casanova, I., Liang, C. F., & Du, S. G. (2020). Effect of shrinkage reducing admixture on creep of recycled aggregate concrete. *Construction and Building Materials*, *254*, 119312.

[8] Matias, D., de Brito, J., Rosa, A., & Pedro, D. (2014). Durability of concrete with recycled coarse aggregates: influence of superplasticizers. *Journal of materials in civil engineering*, *26*(7), 06014011.

[9] Tam, V. W., & Tam, C. M. (2007). Assessment of durability of recycled aggregate concrete produced by two-stage mixing approach. *Journal of Materials Science*, *42*, 3592-3602.

[10] Domingo-Cabo, A., Lázaro, C., López-Gayarre, F., Serrano-López, M. A., Serna, P., & Castaño-Tabares, J. O. (2009). Creep and shrinkage of recycled aggregate concrete. *Construction and building materials*, *23*(7), 2545-2553.

[11] Kou, S. C., & Poon, C. S. (2012). Enhancing the durability properties of concrete prepared with coarse recycled aggregate. *Construction and building materials*, *35*, 69-76.

[12] Vieira, T., Alves, A., De Brito, J., Correia, J. R., & Silva, R. V. (2016). Durability-related performance of concrete containing fine recycled aggregates from crushed bricks and sanitary ware. *Materials & design*, *90*, 767-776.

[13] Bai, G., Zhu, C., Liu, C., & Liu, B. (2020). An evaluation of the recycled aggregate characteristics and the recycled aggregate concrete mechanical properties. *Construction and building materials*, *240*, 117978.

[14] Etxeberria, M., Vázquez, E., Marí, A., & Barra, M. (2007). Influence of amount of recycled coarse aggregates and production process on properties of recycled aggregate concrete. *Cement and concrete research*, *37*(5), 735-742.

[15] Fonseca, N., De Brito, J., & Evangelista, L. (2011). The influence of curing conditions on the mechanical performance of concrete made with recycled concrete waste. *Cement and Concrete*

Composites, *33*(6), 637-643.

[16] Thomas, C., Setién, J., Polanco, J., Alaejos, P., & De Juan, M. S. (2013). Durability of recycled aggregate concrete. *Construction and building materials*, *40*, 1054-1065.

[17] Sosa, M. E., & Zega, C. J. (2023). Experimental and Estimated Evaluation of Drying Shrinkage of Concrete Made with Fine Recycled Aggregates. *Sustainability*, *15*(9), 7666.

[18] Yu, Y., Wang, P., Yu, Z., Yue, G., Wang, L., Guo, Y., & Li, Q. (2021). Study on the effect of recycled coarse aggregate on the shrinkage performance of green recycled concrete. *Sustainability*, *13*(23), 13200.

[19] Katar, I., Ibrahim, Y., Abdul Malik, M., & Khahro, S. H. (2021). Mechanical properties of concrete with recycled concrete aggregate and fly ash. *Recycling*, *6*(2), 23.

[20] Lv, Z., Liu, C., Zhu, C., Bai, G., & Qi, H. (2019). Experimental study on a prediction model of the shrinkage and creep of recycled aggregate concrete. *Applied Sciences*, *9*(20), 4322.

[21] De Brito, J., Ferreira, J., Pacheco, J., Soares, D., & Guerreiro, M. (2016). Structural, material, mechanical and durability properties and behaviour of recycled aggregates concrete. *Journal of Building Engineering*, *6*, 1-16.

[22] Lei, B., & Xiao, J. Z. (2008). Research on carbonation resistance of recycled aggregate concrete. *Journal of Building Materials*, *11*(5), 605-611.

[23] Silva, R. V., Neves, R., De Brito, J., & Dhir, R. K. (2015). Carbonation behaviour of recycled aggregate concrete. *Cement and Concrete Composites*, *62*, 22-32.

[24] Kou, S. C., & Poon, C. S. (2013). Long-term mechanical and durability properties of recycled aggregate concrete prepared with the incorporation of fly ash. *Cement and Concrete Composites*, *37*, 12-19.

[25] Amorim, P., De Brito, J., & Evangelista, L. (2012). Concrete made with coarse concrete aggregate: influence of curing on durability. *ACI Materials Journal*, *109*(2), 195-204.

[26] Yang, K. H., Chung, H. S., & Ashour, A. F. (2008). Influence of Type and Replacement Level of Recycled Aggregates on Concrete Properties.

[27] Harison A, Srivastava V, Herbert A. Effect of fly ash on compressive strength of Portland pozzolona cement concrete[J]. journal of academia and industrial research (JAIR), 2014, 2(8): 476-479.

[28] Padhye R D, Deo N S. Cement replacement by fly ash in concrete[J]. International Journal of Engineering Research, 2016, 5(1): 60-62

[29] Oner A, Akyuz S, Yildiz R. An experimental study on strength development of concrete containing fly ash and optimum usage of fly ash in concrete[J]. Cement and Concrete Research, 2005, 35(6): 1165-1171.

[30] Dinakar P, Reddy M K, Sharma M. Behaviour of self compacting concrete using Portland pozzolana cement with different levels of fly ash[J]. Materials & Design, 2013, 46: 609-616.

[31] De Maeijer, P. K., Craeye, B., Snellings, R., Kazemi-Kamyab, H., Loots, M., Janssens, K., & Nuyts, G. (2020). Effect of ultra-fine fly ash on concrete performance and durability. Construction and Building Materials, 263, 120493.

[32] Chindaprasirt, P., Jaturapitakkul, C., & Sinsiri, T. (2005). Effect of fly ash fineness on compressive strength and pore size of blended cement paste. Cement and concrete composites, 27(4), 425-428.

[33] Saha, A. K. (2018). Effect of class F fly ash on the durability properties of concrete. Sustainable environment research, 28(1), 25-31.

[34] Moffatt, E. G., Thomas, M. D., & Fahim, A. (2017). Performance of high-volume fly ash concrete in marine environment. Cement and Concrete Research, 102, 127-135.

[35] A.D. Ross, Some problems in concrete construction, Mag. Concr. Res. 12 (34) (1960) 27–34.

[36] P. Bamforth, In situ measurement of the effect of partial Portland cement replacement using either fly ash or ground granulated blast-furnace slag on the performance of mass concrete, Proc, Inst. Civ. Eng. 69 (3) (1980) 777–800.

[37] R. Lohtia, B. Nautiyal, O. Jain, Creep of fly ash concrete, ACI J. 73 (39) (1976) 469–472.

[38] S.A. Kristiawan, M.T.M. Aditya, Effect of high volume fly ash on shrinkage of selfcompacting concrete, Procedia Eng. 125 (2015) 705–712.

[39] A.M. Neville, Properties of Concrete, Vol. 4, Longman, London, 1995.

[40] Siddique R, Bennacer R. Use of iron and steel industry by-product (GGBS) in cement paste and mortar[J]. Resources, Conservation and recycling, 2012, 69: 29-34.

[41] Gupta S. Effect of content and fineness of slag as high volume cement replacement on strength and durability of ultra-high performance mortar[J]. Journal of Building Materials and Structures, 2016, 3(2): 43-54.

[42] Dai J, Wang Q, Xie C, et al. The effect of fineness on the hydration activity index of ground granulated blast furnace slag[J]. Materials, 2019, 12(18): 2984.

[43] Ganesh P, Murthy A R. Tensile behaviour and durability aspects of sustainable ultra-high-performance concrete incorporated with GGBS as cementitious material[J]. Construction and Building Materials, 2019, 197: 667-68

[44] H. El-Chabib, A. Syed, Properties of self-consolidating concrete made with high volumes of supplementary cementitious materials, J. Mater. Civ. Eng. 25 (11) (2013) 1579–1586.

[45] A. Darquennes, E. Rozi`ere, M.I.A. Khokhar, P. Turcry, A. Loukili, F. Grondin, Longterm deformations and cracking risk of concrete with high content of mineral additions, Mater. Struct. 45 (11) (2012) 1705–1716.

[46] J.J. Brooks, P.J. Wainwright, M. Boukendakji, Influence of slag type and replacement level on strength elasticity, shrinkage and creep of concrete, Special Publication 132 (1992) 1325–1342.

[47] J.-H. Lee, Y.-S. Yoon, The effects of cementitious materials on the mechanical and durability performance of high-strength concrete, KSCE J. Civ. Eng. 19 (5) (2015) 1396–1404.

[48] R.P. Khatri, V. Sirivivatnanon, W. Gross, Effect of different supplementary cementitious materials on mechanical properties of high performance concrete, Cem. Concr. Res. 25 (1) (1995) 209–220.

[49] Waqas, Rana Muhammad, et al. "A comprehensive study on the factors affecting the workability and mechanical properties of ambient cured fly ash and slag based geopolymer concrete." *Applied Sciences* 11.18 (2021): 8722.

[50] Asghar, Raheel, et al. "Promoting the green construction: Scientometric review on the mechanical and structural performance of geopolymer concrete." *Construction and Building Materials* 368 (2023): 130502.

[51] Assi, Lateef N., et al. "Review of availability of source materials for geopolymer/sustainable concrete." *Journal of Cleaner Production* 263 (2020): 121477.

[52] Dafedar, J. B., and Y. M. Desai. "Stability of composite and sandwich struts by mixed formulation." *Journal of engineering mechanics* 130.7 (2004): 762-770.

[53] Joseph, Benny, and George Mathew. "Interface shear strength of fly ash based geopolymer concrete." *Annals of the Faculty of Engineering Hunedoara* 11.3 (2013): 105.

[54] Paruthi, Sagar, et al. "A review on material mix proportion and strength influence parameters of geopolymer concrete: Application of ANN model for GPC strength prediction." *Construction and Building Materials* 356 (2022): 129253.

[55] Alekhya, Pateel, and S. Aravindan. "Experimental investigations on geopolymer concrete." *Int J Civ Eng Technol (IJCIET)* 5.4 (2014): 01-09.

[56] Rajamane, N. P., et al. "Sulphate resistance and eco-friendliness of geopolymer concretes." *Indian Concrete Journal* 86.1 (2012): 13.

[57] Laskar, Sulaem Musaddiq, and Sudip Talukdar. "Preparation and tests for workability, compressive and bond strength of ultra-fine slag based geopolymer as concrete repairing agent." *Construction and building materials* 154 (2017): 176-190.

[58] Venu, M., and TD Gunneswara Rao. "Tie-confinement aspects of fly ash-GGBS based geopolymer concrete short columns." *Construction and Building Materials* 151 (2017): 28-35.

[59] Cheah, Chee Ban, et al. "The use of high calcium wood ash in the preparation of Ground Granulated Blast Furnace Slag and Pulverized Fly Ash geopolymers: A complete microstructural and mechanical characterization." *Journal of Cleaner Production* 156 (2017): 114-123.

[60] Moradikhou, Amir Bahador, Alireza Esparham, and Mohammad Jamshidi Avanaki. "Physical & mechanical properties of fiber reinforced metakaolin-based geopolymer concrete." *Construction and Building Materials* 251 (2020): 118965.

[61] Jones, Michael A. "Metakaolin production and enhancement of industrial minerals." U.S. Patent No. 9,108,884. 18 Aug. 2015.

[62] Kong, Daniel LY, and Jay G. Sanjayan. "Damage behavior of geopolymer composites exposed to elevated temperatures." *Cement and Concrete Composites* 30.10 (2008): 986-991.

[63] Bakharev, T. "Geopolymeric materials prepared using Class F fly ash and elevated temperature curing." *Cement and concrete research* 35.6 (2005): 1224-1232.

[64] Short, N. R., J. A. Purkiss, and S. E. Guise. "Assessment of fire damaged concrete using colour image analysis." *Construction and building materials* 15.1 (2001): 9-15.

[65] Bakharev, T. "Geopolymeric materials prepared using Class F fly ash and elevated temperature curing." *Cement and concrete research* 35.6 (2005): 1224-1232.

[66] D. Hardjito, S. E. Wallah, D. M. J. Sumajouw, and B. V. Rangan, “Flyash-based geopolymer concrete”, Australian Journal of StructuralEngineering, Vol 6, No.1, 2005, pp. 1-9.

[67] Nagral, Mohammed Rabbani, Tejas Ostwal, and Manojkumar V. Chitawadagi. "Effect of curing temperature and curing hours on the properties of geo-polymer concrete." *Int. J. Comput. Eng. Res* 4.9 (2014): 1-11.

[68] Memon, Fareed Ahmed, et al. "Effect of curing conditions on strength of fly ash-based self-compacting geopolymer concrete." *International Journal of Civil and Environmental Engineering* 5.8 (2011): 342-345.

[69] Lee, Bokyeong, et al. "Strength development properties of geopolymer paste and mortar with respect to amorphous Si/Al ratio of fly ash." *Construction and Building Materials* 151 (2017):

512-519.

[70] Shahmansouri, Amir Ali, Mahdi Nematzadeh, and Ali Behnood. "Mechanical properties of GGBFS-based geopolymer concrete incorporating natural zeolite and silica fume with an optimum design using response surface method." *Journal of Building Engineering* 36 (2021): 102138.

[71] Zhang, Hai Yan, et al. "Comparative thermal and mechanical performance of geopolymers derived from metakaolin and fly ash." *Journal of Materials in Civil Engineering* 28.2 (2016): 04015092.

[72] Hassan, Amer, Mohammed Arif, and Mohd Shariq. "Use of geopolymer concrete for a cleaner and sustainable environment–A review of mechanical properties and microstructure." *Journal of cleaner production* 223 (2019): 704-728.

[73] Singh, Neetu, et al. "Effect of aggressive chemical environment on durability of green geopolymer concrete." *International Journal of Engineering and Innovative Technology (IJEIT)* 3.4 (2013): 277-284.

[74] Bakharev, T. "Durability of geopolymer materials in sodium and magnesium sulfate solutions." *Cement and concrete research* 35.6 (2005): 1233-1246.

[75] Albitar, M., et al. "Durability evaluation of geopolymer and conventional concretes." *Construction and Building Materials* 136 (2017): 374-385.

[76] Hanrahan, Eamon T. *The Geotechnics of Real Materials: The εgεk Method*. Elsevier, 2013.

[77] Criado, María, Ana Fernández-Jiménez, and A. Palomo. "Alkali activation of fly ash: Effect of the SiO_2/Na_2O ratio: Part I: FTIR study." *Microporous and mesoporous materials* 106.1-3 (2007): 180-191.

[78] Criado, María, et al. "An XRD study of the effect of the SiO_2/Na_2O ratio on the alkali activation of fly ash." *Cement and concrete research* 37.5 (2007): 671-679.

[79] Nath, Pradip, and Prabir Kumar Sarker. "Effect of GGBFS on setting, workability and early strength properties of fly ash geopolymer concrete cured in ambient condition." *Construction and Building materials* 66 (2014): 163-171.

Chapter 3

A STUDY ON ENGINEERING PROPERTIES AND ENVIRONMENTAL IMPACT OF SUSTAINABLE CONCRETE WITH FLY ASH OR GGBS

3.1 Introduction

With the rapid worldwide development of urbanization in recent years, concrete, one of the most widely used materials in the construction industry, is consumed in large quantities every year. Ordinary Portland cement (OPC) is used as the main cementitious material in concrete. Cement consumption is expected to rise from its present annual value of roughly 4.2 billion tons to around 5.2 billion tons by 2050, according to current projections [1]. For each ton of clinker produced, an average of 850 kg of CO2 is released into the environment using current cement production techniques [2]. Therefore, new materials need to be found to replace cement in order to reduce the negative impact of concrete production on the environment. The rapid development of the construction industry has also created a large demand for river sand as fine aggregate in the production of concrete, which leads to the depletion of river sand, another urgent problem that needs to be solved [3].

From the perspective of sustainable development, replacing cement or fine aggregate with supplementary cementitious materials, such as fly ash and ground granulated blast furnace slag (GGBS), is an effective and feasible method. It has been reported that the global annual output of fly ash exceeds 900 million tons [4], of which the annual output of China is about 580 million tons [5], India is 169.25 million tons [6], the United States is 43.5 million tons [7], and Australia is 14 million tons [8]. However, the effective utilization rate of fly ash currently accounts for only about 53.5% of the total [4]. This leads to a series of problems related to waste disposal, and the ashes are either disposed of in landfill or in the ocean. In addition, the global annual output of blast furnace slag is about 530 million tons, but only about 65% of the total is recycled [9].

In recent years, a lot of research has been conducted on the application of mineral admixtures in concrete. Because the pozzolanic reaction of fly ash is usually a relatively slow process, the improvements it gives to the microstructure and strength of concrete is mainly reflected at later ages, such that the early strength of concrete containing fly ash is lower [10]. In addition, some studies have shown that the use of fly ash in concrete can improve the workability and durability of concrete. De Maeijer, P. K. et al. reported that replacing cement with fly ash can improve resistivity, the chloride migration coefficient, and alkali-silicon reactions, but reduces the carbonization resistance of concrete [11]. Chindaprasirt et al. found that replacing OPC with fly ash can increase the porosity but decrease the average pore size. Furthermore, as the fly ash content increases, the gel pore volume (5.7–10 nm) increases [12]. Saha studied concrete incorporating fly ash, and the results showed that drying shrinkage decreases with increasing fly ash content. The incorporation of fly ash reduced the porosity of concrete, resulting in concrete with better water sorptivity and chloride permeability [13]. Moffatt and others found that resistance to chloride-ion penetration was considerably enhanced when high replacement amounts of fly ash were used [14]. Hussain et al. reported that using the same water-to-binder ratio, fly ash concrete showed better mechanical properties compared with plain concrete, and the carbonation resistance of high-strength concrete including fly ash as a partial replacement for cement was comparable to that of plain cement concrete [15]. Early concrete strength is reduced when fly ash is used as a partial replacement for cement, but at the ages of 56–180 days, there was a considerable increase in concrete strength, and after exposure to high temperatures, the use of fly ash greatly improved concrete strength [16]. Sun et al. reported that because of the diluting impact of fly ash, the compressive strength of high volume fly ash concrete was much lower than that of control

concrete at 3 and 7 days (early age). However, because of the pozzolanic reaction of fly ash, the compressive strength developed more quickly compared with control concrete, and concrete with a 40% fly ash substitution had a 180-day compressive strength comparable to that of control concrete [17]. Zhang et al. reported that concrete using fly ash to replace sand has a higher early compressive strength compared with ordinary concrete, and concrete using fly ash as fine aggregate has higher carbonation resistance [18]. Siddique found that the incorporation of fly ash as part of the fine aggregate significantly promotes the mechanical properties (compressive strength, splitting tensile strength, flexural strength, and modulus of elasticity), and the abrasion resistance of concrete increases as the percentage of sand replaced by fly ash increases [19], [20]. The replacement of fine aggregate with fly ash can improve the freeze–thaw resistance of concrete when compared to conventional concrete [21]. Özbay et al. reviewed the application of GGBS in concrete and found that the utilization of GGBS in concrete improves the long-term compressive strength and flexural strength, and slightly promotes the elastic modulus. In addition, the utilization of GGBS can modify the durability of concrete, for example by reducing creep and drying shrinkage, improving abrasion resistance, reducing water, gas, and chloride ion permeability, and significantly improving sulfate and alkali–silica reactions [22]. It has been reported that the inclusion of GGBS can reduce the porosity of concrete due to the greater surface area of GGBS [23]. It has also been reported that regardless of the substitution rate, the pore structure of concrete will be denser and more solid [24], [25]. Another study reported that, GGBS-based concrete continues to develop strength over 10–12 years until it reaches twice its 28-day strength [26]. Li et al. analyzed the pore structure of cement-based materials with and without 70% GGBS and found that GGBS substantially reduced the pores, increased the specific surface area and fractal dimension, and decreased the pore distribution from 10 to 100 nm to <10 nm [27]. It has also been reported that self-compacting concrete containing GGBS has a higher level of strength [28], [29]. In summary, many researchers have conducted in-depth research on concrete with supplementary cementitious materials (fly ash, GGBS) as part of cement, but research on such concrete as a part of fine aggregate remains insufficient.

Concrete creep refers to the characteristic that the strain of concrete increases continuously over time under long-term stress. Drying shrinkage refers to the shrinkage caused by the evaporation of water in capillary pores [10]. Creep and drying shrinkage are important factors to consider when evaluating losses in prestressed concrete structures such as bridge girders. It has been reported that concrete with fly ash replacing 25% of the cement has a 15% lower creep compared with conventional concrete [30]. Bamforth reported that concrete containing 30% fly ash replacing cement exhibited 50% reduced creep strain compared with concrete without fly ash [31]. Lohtia et al. studied the creep of concrete containing 0%–25% fly ash replacing cement and found an increase in creep for concrete with replacement of more than 15% fly ash compared with conventional concrete [32]. It has also been reported that self-compacting concrete with a higher fly ash content in place of cement tends to reduce both drying and autogenous shrinkage [33]. Saha also reported that drying shrinkage decreases with increasing fly ash content [13]. However, one study reported that shrinkage increases with percentage of fly ash content [10]. Zhao et al. found that, compared with cement-only high-performance concrete, the total shrinkage of high-performance concrete using both fly ash and GGBS was reduced by 15%–25%. In contrast, the autogenous shrinkage of high-performance concrete rose by 66%–106% when both fly ash and GGBS were added [34]. It has been reported that in self-consolidating concrete made

with high volumes of GGBS, replacing up to 70% of the cement with GGBS reduces the shrinkage of concrete by more than 45% compared with conventional concrete [35]. Darquennes et al. studied the free shrinkage of concrete incorporating 75% GGBS and found that for a GGBS concentration of ≤50% of the volume of the binder, the overall shrinkage evolution rate and amplitude were lower over time than those for conventional concrete [36]. Brooks et al. found that GGBS concrete exhibited equivalent or greater long-term strength and shrinkage, relatively less basic creep, and comparable or less total creep compared with ordinary concrete [37]. It has also been reported that at an early age, the creep of GGBS-blended concrete is less than that of ordinary concrete. However, creep was higher in the long term compared with ordinary concrete [38]. Khatri et al. reported the opposite result, indicating that concrete with less slag in its binder has less creep [39]. In the above of literature, contradictory results are presented regarding the effects of GGBS and fly ash on the creep and drying shrinkage of concrete.

In addition, ACI Committee 209 showed that the effect of supplementary cementitious materials has not been considered in many existing prediction models of concrete creep and drying shrinkage, such as the ACI 209 model [40], CEB-FIP 1990 model [41], Gardner and Lockman (GL-2000) [42], AIJ Model [43], JSCE model [44], and CEB MC90-99 model [40]. It is critical to predict delayed strain in concrete structures in order to assess their durability and serviceability. Deformation of concrete often leads to cracks in the concrete, and early-stage cracks may hasten the deterioration of the concrete, leading to the corrosion of the embedded reinforcement by facilitating the passage of contaminants and moisture. The load-carrying capacity of a structure is reduced as a result of such damage that develops over time. This review of the literature shows that further research is needed to analyze the effect of supplementary cementitious materials on concrete creep and drying shrinkage.

This study carried out experiments on concrete containing mineral admixture (fly ash, GGBS) as part of the cement or fine aggregate. The experimental data were compared with predicted values from the existing prediction models, and the applicability of each prediction model to concrete containing mineral admixtures was analyzed, and the results indicated which predictive model is the most accurate. Therefore, we analyzed the engineering properties of concrete containing some portion of fly ash or GGBS as fine aggregate and introduced a parameter to capture the effect of fly ash content in the model showing the highest accuracy for ordinary concrete.

3.2. Materials and experimental program

3.2.1 Materials properties

Locally available sea sand was used as the fine aggregate, and locally available crushed stone aggregate was used as the coarse aggregate. The physical properties of the fine and coarse aggregates are shown in Table 3.1. The particle size distribution diagram of fine aggregate and binder are shown in Fig. 3.1 (a) and (b).

Table 3.1 properties of the fine and coarse aggregates

Property	Coarse aggregate	Fine aggregate
Oven-dried density (g/cm^3)	2.69	2.59
Fineness modulus	6.9	2.58
Water absorption (%)	1.14	1.04
Solid content (%)	62.1	60.9

OPC as defined according to JIS R 5210 [45] was used in the experiments. Fly ash corresponding to Class II in JIS A 6201 [46] and GGBS as defined in JIS A 6206 [47] were used as mineral admixture. Table 2 shows the properties of the cement, fly ash, and GGBS.

Table 3.2 the properties of the cement, fly ash, and GGBS

	FA	GGBS	Cement
SiO_2 (%)	53.8	32.7	21.5
Al_2O_3 (%)	13.5	13.4	5.4
Fe_2O_3 (%)	13	0.5	3.0
CaO (%)	8.99	41.6	64.9
SO_3 (%)	0.489	6.9	1.4
MgO (%)	1.48	0.3	2.1
Loss on ignition (%)	2.1	0.6	0.8
Density (g/cm^3)	2.2	2.91	3.16
Blaine specific area (cm^2/g)	3270	4100	3000

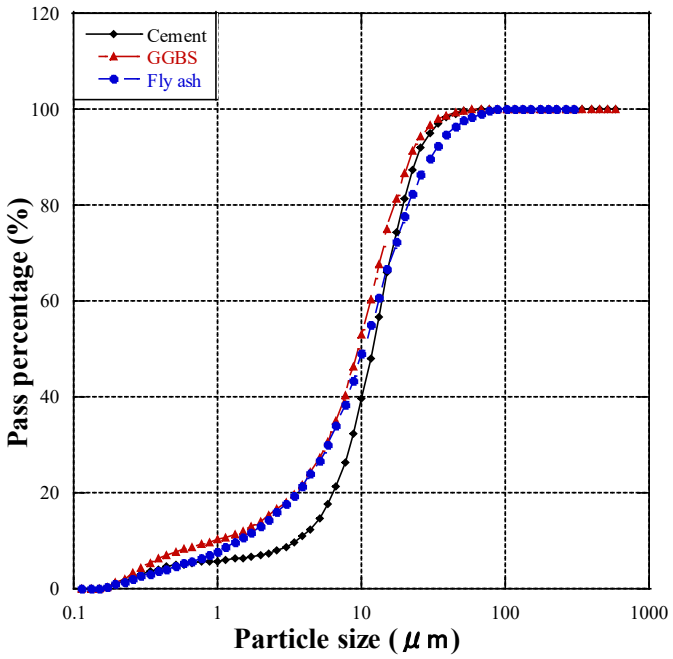

Fig. 3.1 (a) The particle size distribution of binder

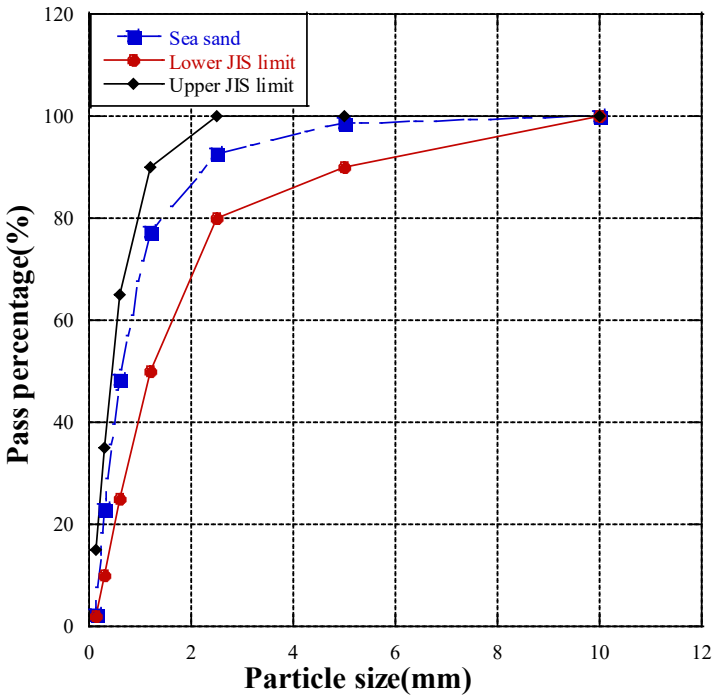

Fig. 3.1 (b) The particle size distribution of fine aggregate

3.2.2 Mix proportion

A total of 13 mixes of concrete were prepared: the control concrete, three mixes including cement replaced with fly ash (10%, 20%, and 30% by weight), three mixes including fine aggregate replaced with fly ash (10%, 20%, and 30% by volume), three mixes including cement replaced with GGBS (10%, 20%, and 30% by weight), and three mixes including fine aggregate replaced with GGBS (10%, 20%, and 30% by volume). The unit water amount was 180 kg/m^3, the unit coarse aggregate amount was 945 kg/m^3. The mix proportions are shown in Table 3.3. In the table, symbols indicate replacement of cement by weight and fine aggregate by volume, the type of mineral admixture used, and the replacement ratio. The target air volume of fresh concrete was set to 4.5 ± 1.0%.

3.2.3 Experiment method

Compressive strength tests were conducted according to JIS A 1108 [48], and cylinder specimens (diameter 100 mm × height 200 mm) were prepared. The cylinders were cast in a mold and kept in a chamber at 20 °C and 60% relative humidity for 24 hours until demolded, then cured in water at 20 °C. The ages of the tested specimens were 7, 28, and 91 days. Load was applied at a uniform rate to avoid subjecting the specimens to impact loading, with the loading rate such that the compressive stress increased by 0.6 ± 0.4 N/mm^2 per second. During each test, specimens were stored at the temperature and humidity specified for that test

Table 3.3 Mix proportions.

Type	W/B	Unit mass(kg/m³)					
		Water	Cement	FA	GGBS	Fine aggregate	Coarse aggregate
N	0.50	180	360	0	0	805	945
IFA-10	0.50	180	324	36	0	791	945
IFA-20	0.50	180	288	72	0	778	945
IFA-30	0.50	180	252	108	0	764	945
IBS-10	0.50	180	324	0	36	802	945
IBS-20	0.50	180	288	0	72	799	945
IBS-30	0.50	180	252	0	108	797	945
OFA-10	0.47	180	360	67	0	724	945
OFA-20	0.44	180	360	134	0	644	945
OFA-30	0.41	180	360	201	0	536	945
OBS-10	0.46	180	360	0	89	724	945
OBS-20	0.42	180	360	0	179	644	945
OBS-30	0.39	180	360	0	268	536	945

The drying shrinkage test was conducted according to the “Method of measurement for length change of mortar and concrete” outlined in JIS A 1129-2 [49], and 100 × 100 × 400 mm prismatic specimens were produced. After casting, the specimens were demolded at 1 day of age and cured in water at 20 °C until the age of 7 days. Specimens were taken out of the water at the age of 7 days, stainless steel chips were attached to both end faces of the specimens, and both end faces were sealed to measure the base length. The specimens for measuring the drying shrinkage were cured in a temperature- and humidity-controlled room (temperature, 20 ± 1.0 °C; relative humidity, 60 ± 5%).

In the creep test, the strain was measured according to JIS A 1157 [50], and diameter 100 × height 200 mm cylinders were produced. After casting, the specimens were demolded at 1 day of age and then cured in water at 20 °C until the age of 7 days. Then the specimens were cured in a temperature- and humidity-controlled room (temperature, 20 ± 1.0 °C; relative humidity, 60 ± 5%) until the age of 28 days. The creep test uses a loading device with a separate hydraulic jack. Three test specimens were stacked vertically. The loading load was set to 1/3 of the maximum load of compressive strength at 28 days, and loading started from 28 days. Strain gauges were attached at three positions in the center of each test specimen, and the average of the values obtained by the three strain gauges was taken as the total measured strain for each specimen. The average of the total measured strain for three test specimens was taken as the total strain of the mix proportion. To calculate the creep strain, the drying shrinkage strain was measured in two prepared no-load specimens of diameter 100 × 200 mm in each mix proportion. Measurements were performed similarly to the creep test strain gauges were attached, samples were stored in the same temperature-controlled room where the creep test was performed, and the measurements were performed using a data logger simultaneously with the creep strain measurements. Fig. 3.2 shows the changes over time in the temperature and humidity of the

homeothermic chamber. In the homeothermic chamber where the creep test was conducted, the humidity could not be strictly controlled, so the creep test could not be performed at a constant humidity.

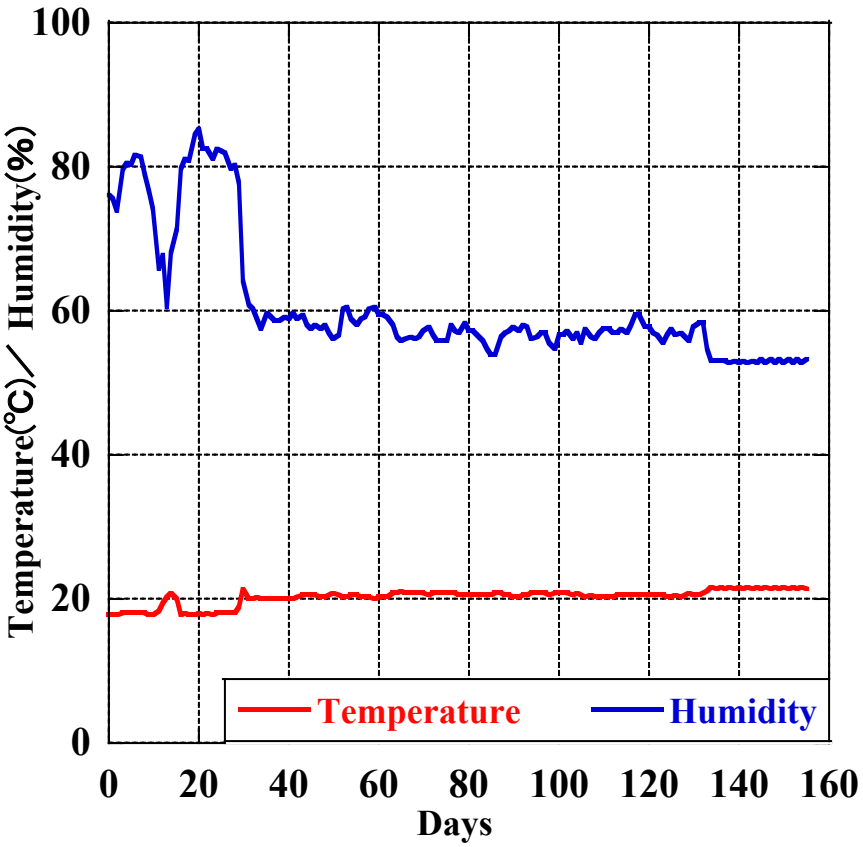

Fig. 3.2 The changes over time in the temperature and humidity

3.3. Results and discussion

3.3.1 Compressive strength

Fig. 3.3(a)-(d) show the compressive strength of concrete including cement replaced with fly ash, sand replaced with fly ash, cement replaced with GGBS, and sand replaced with GGBS, respectively. Fig. 3.3(a) shows the effect of the percentage of cement replaced by fly ash on the compressive strength of the concrete. As shown in the figure, the 7-day and 28-day compressive strength of concrete decreased as the fly ash content increased. The lime content in fly ash is low, so the compressive strength decreases with the increase of fly ash content [51,52]. However, the trends in the 91-day compressive strength differed from the early compressive strength (7 and 28 days), with the 91-day compressive strength of the concrete first rising and then decreasing with increasing fly ash content. Due to the pozzolanic reaction of fly ash, Al2O3 and SiO2 in fly ash react with cement hydration product calcium hydroxide to produce hydrated gel. Because the gel produced by the pozzolanic reaction can fill the capillaries of the concrete, the strength of the concrete is effectively improved [53]. The compressive strength was the largest at a fly ash content of 20%. Compared with conventional concrete, the 7-day

compressive strengths of IFA10, IFA20, and IFA30 mixes were reduced by 1.7%, 14.8%, and 24.5%, and the 28-day compressive strengths are reduced by 10%, 9.8%, and 19%, respectively. For the 91-day compressive strength, the IFA10 and IFA20 mixes increased by 2.5% and 1.9%, respectively, but the IFA30 mix decreased by 4.5%.

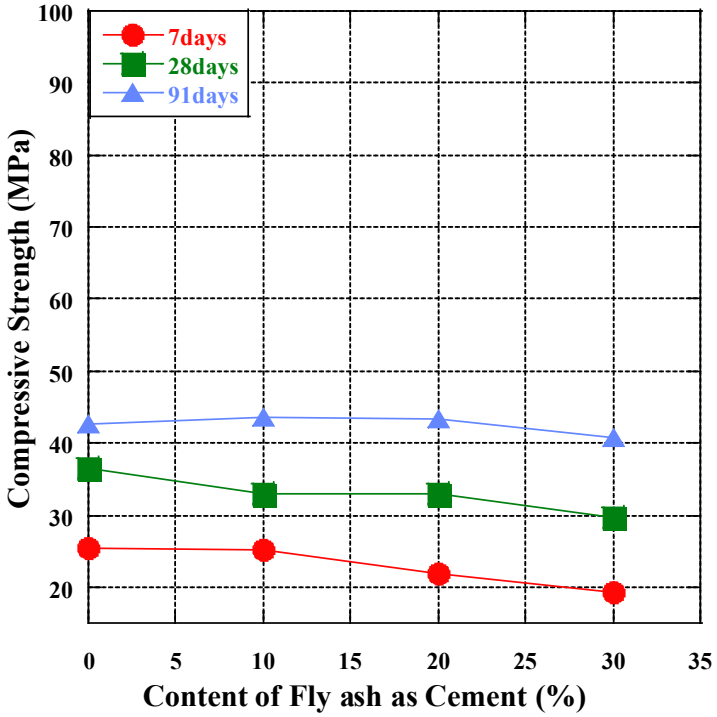

(a) Cement replaced with fly ash

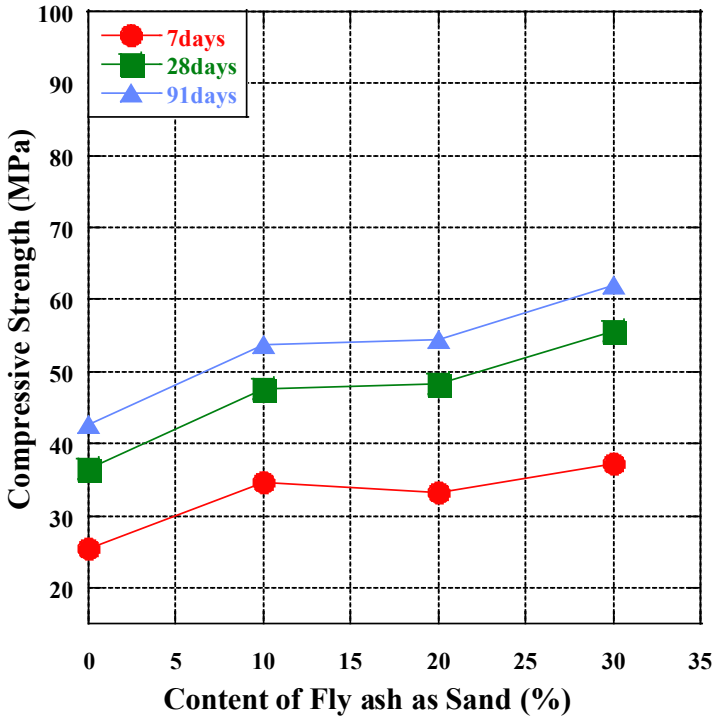

(b) Sand replaced with fly ash

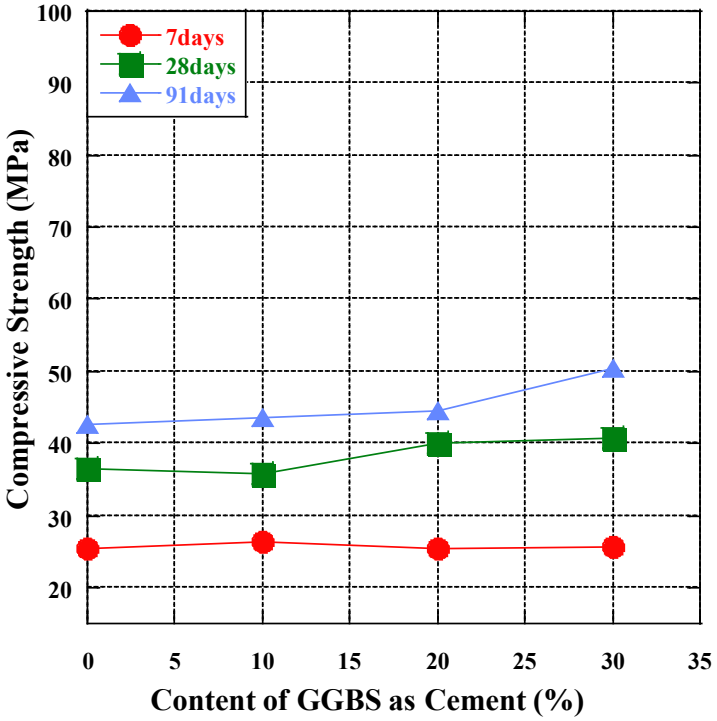

(c) Cement replaced with GGBS

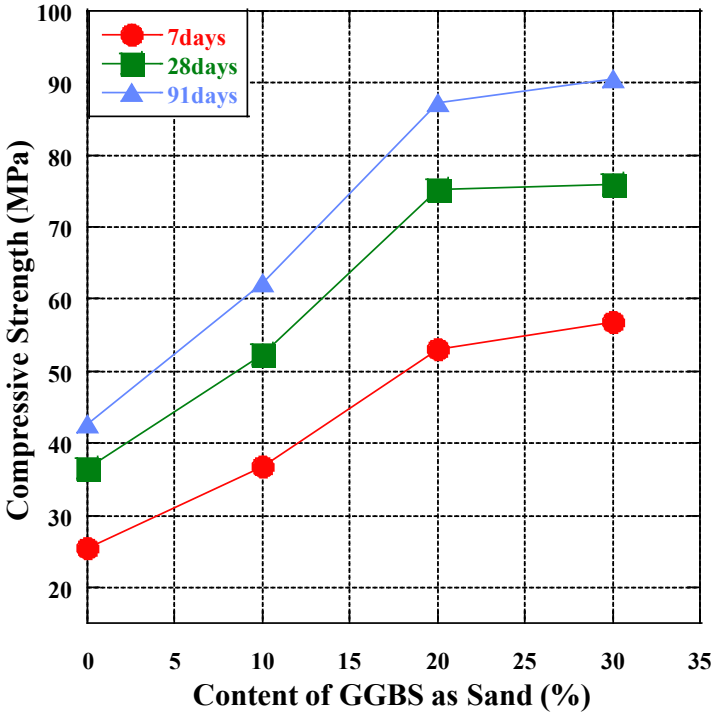

(d) Sand replaced with GGBS

Fig. 3.3. Compressive strength of concrete with fly ash or GGBS

Fig. 3.3(b) shows the effect of the percentage of sand replaced by fly ash on the compressive strength of the concrete. Regardless of the early compressive strength (7 and 28 days) and long-term compressive strength (91 days), increased fly ash content led to increased compressive strength. OFA10, OFA20, and OFA30 mixes exhibited 35%, 31%, and 46% higher 7-day compressive strength, 30%, 32%, and 52% higher 28-day compressive strength, and 26%, 28%, and 45% higher 91-day compressive strength, respectively, compared with conventional concrete. Ravina reported that concrete incorporating fly ash as partial fine aggregate replacement has a similar or a little higher early compressive strength (1, 7days), and the compressive strength of 28 days is higher, compared with control concrete [54]. Siddique reported that concrete with part fine aggregate replaced by fly ash has a significantly higher compressive strength at all ages, and the improvement of strength is more significant after 28 days [19].

Fig. 3.3(c) shows the effect of the percentage of cement replaced by GGBS on the compressive strength of the concrete. Compared with ordinary concrete, adding blast furnace slag to concrete had no obvious effect on the 7-day compressive strength of the concrete. However, the 28-day and 91-day compressive strengths increased as the GGBS content increased. There was no obvious change in the 28-day compressive strength of IBS10, while IBS20 and IBS30 exhibited 9.7% and 11.8% higher 28-day compressive strength, respectively. IBS10, IBS20, and IBS30 mixes exhibited 26%, 28%, and 45% higher 91-compressive strength, respectively. Johari et al. reported that concrete containing GGBS has the largest increase in compressive strength during the age of 28 to 91 days [55]. According to Vejmelkova et al. reported, XRD analysis showed that the content of $Ca(OH)_2$ in concrete containing GGBS decreased significantly with age, and calcium silicate hydrate (C-S-H) was formed to fill part of the pores, making the internal structure of concrete more compact [56].

Fig. 3.3(d) shows the effect of the percentage of sand replaced by GGBS on the compressive strength of the concrete. It can be seen that, regardless of the age of the concrete, the compressive strength of concrete with GGBS replacing sand is increased compared with conventional concrete, and the compressive strength increased as the GGBS content increased. In addition, analysis of the change in compressive strength with increasing GGBS content showed that increasing the GGBS content from 10% to 20% caused a sharp improvement in compressive strength. Compared with conventional concrete, the 7-day compressive strength of OBS10, OBS20, and OBS30 mixes was increased by 44%, 108%, and 122%, the 28-day compressive strength was increased by 43%, 106%, and 108%, and the 91-day compressive strength was increased by 46%, 105%, and 112%, respectively. This is due to the replacement of sand with GGBS, which leads to a decrease in the water-binder ratio and an increase in strength [57].

Focusing on replacement of cement by fly ash, when the content of fly ash was less than 20%, the early compressive strength of concrete decreased but the 91-day compressive strength increased. Replacing cement with GGBS had no obvious effect on early compressive strength, but caused an improvement in 28-day and 91-day compressive strength. Replacement of sand with fly ash or GGBS increased the compressive strength of concrete, with the concrete containing GGBS found to have a higher compressive strength at the same sand replacement content. The concrete with 30% GGBS replacement of sand exhibited the highest compressive strength. These results show that replacing sand with fly ash or GGBS can produce high-performance concrete.

3.3.2 Drying shrinkage

The results of drying shrinkage development with time are shown in Fig. 3.4a-d. Fig. 3.4a and Fig. .4b show the drying shrinkage of concrete with fly ash as part of the cement or sand. Compared with ordinary concrete, the concrete containing fly ash as part of the cement or sand exhibited lower drying shrinkage. Fly ash as sand replacement decrease the water-binder ratio, the water-binder ratio reflects the content of evaporable water in the concrete and the rate of water movement to the surface of the sample, drying shrinkage decreases with the decrease of water-binder ratio [10]. Because the content of lime in fly ash is too low, the replacement of cement with fly ash leads to a decrease in the content of lime in the concrete, which in turn leads to a decrease in the hydration rate, so the concrete with fly ash as cement replacement has a lower drying shrinkage [52], [58]. In addition, for both concrete with fly ash as part of the cement and sand, the drying shrinkage was confirmed to increase with increasing fly ash content, with concrete with 10% fly ash having the lowest drying shrinkage. Saha studied concrete with 10–40% fly ash replacing cement, the results showed that drying shrinkage decreases with increasing fly ash content, and concrete with 40% exhibited the lowest drying shrinkage about 75% of control concrete drying shrinkage [13]. Fig. 3.4c and Fig. 3.4d show the drying shrinkage of concrete with GGBS as part of the cement or sand. In both concrete with GGBS as part of the cement and sand, the drying shrinkage tended to decrease with increasing GGBS content, and concrete with 30% GGBS as sand was found to have the lowest shrinkage in this experiment, at about 20% less than the control concrete.

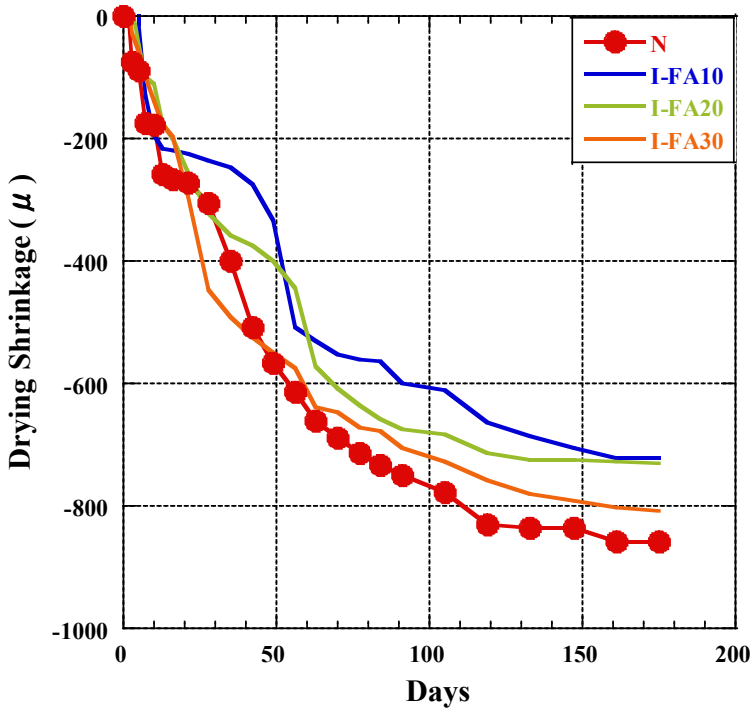

(a) Cement replaced with fly ash

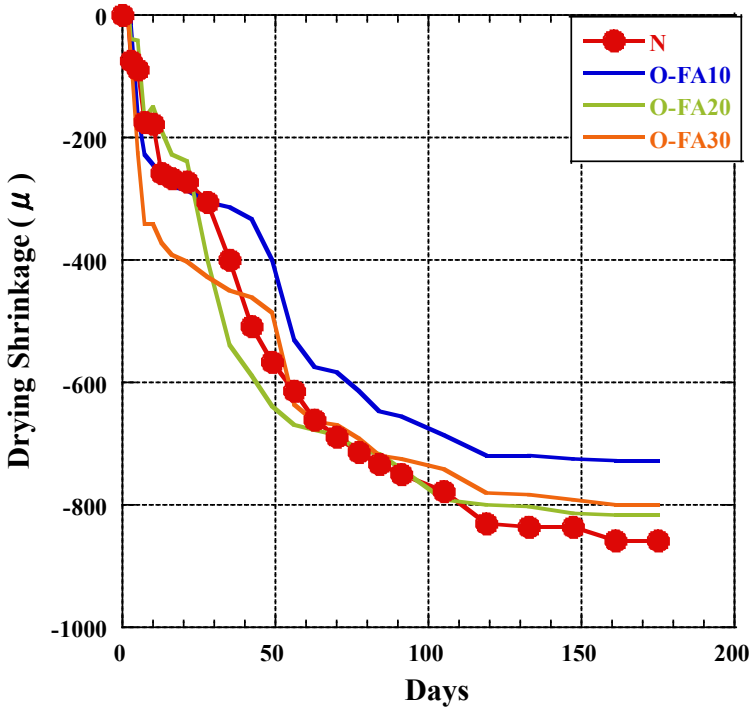

(b) Sand replaced with fly ash

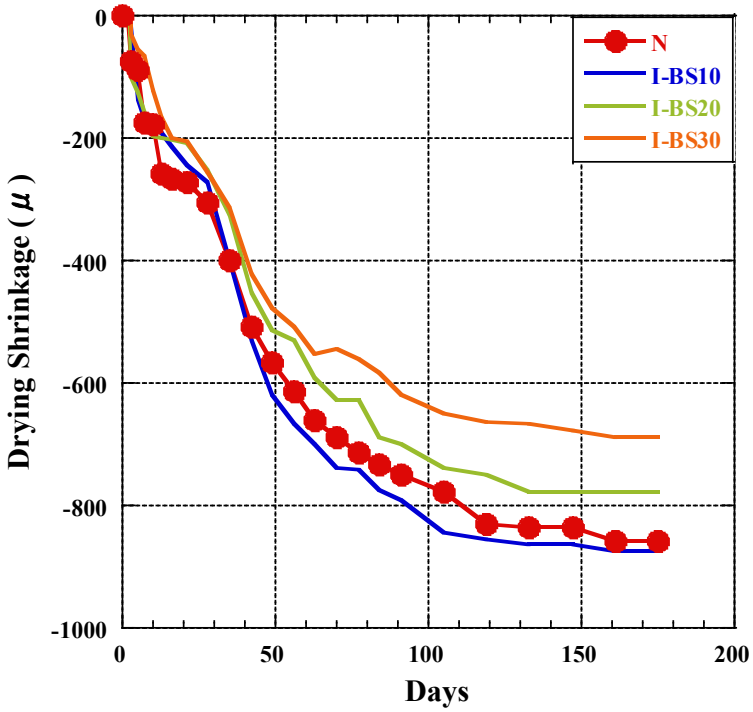

(c) Cement replaced with GGBS

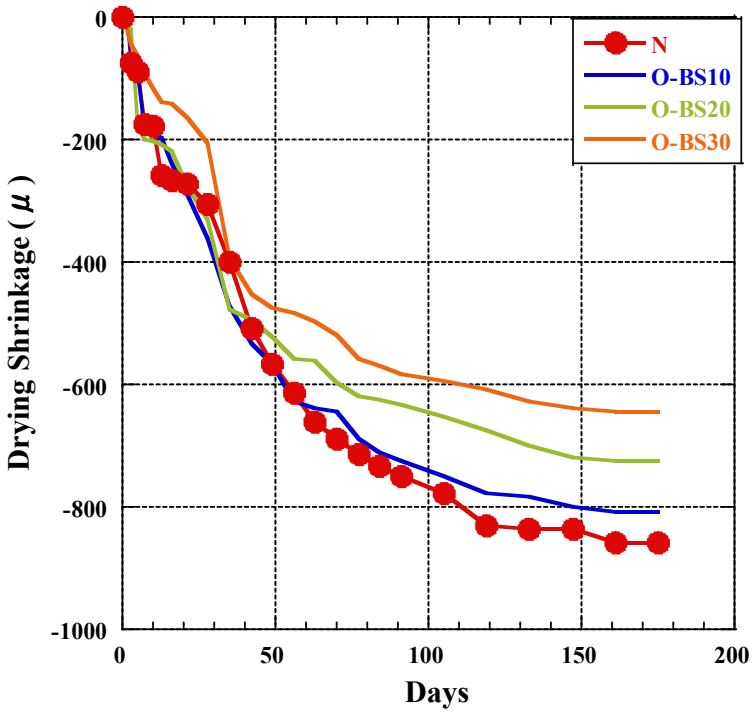

(d) Sand replaced with fly ash

Fig. 3.4. Drying shrinkage of concrete with fly ash or GGBS

Fig. 3.5 shows the relationship between drying shrinkage (147 days) and the content of the mineral admixture (fly ash and GGBS) used as cement or sand. As the figure shows, regardless of whether the concrete contained fly ash as part of the cement or sand, the concrete that contained fly ash had a lower drying shrinkage than did the control concrete, and concrete with 10% fly ash exhibited the lowest drying shrinkage, with the drying shrinkage increasing with increasing fly ash content. For concrete with fly ash as sand replacement, the increase in drying shrinkage with the increase of fly ash content may be due to the decrease in sand content, which leads to a decrease in the inhibitory effect of aggregate on shrinkage [10]. For concrete with GGBS as part of the cement and sand, the concrete containing GGBS as sand or cement exhibited a significant reduction in drying shrinkage, with the exception of the IBS10 mix, and the drying shrinkage decreased with increasing GGBS content. Yuan et al. reported similar result, compared with ordinary concrete, concrete containing GGBS has lower drying shrinkage [59]. Li et al. also got similar results, high performance concrete with GGBS has a lower drying shrinkage than normal concrete [60]. It is also observed that GGBS as sand had a more obvious inhibitory effect on drying shrinkage than did GGBS as cement.

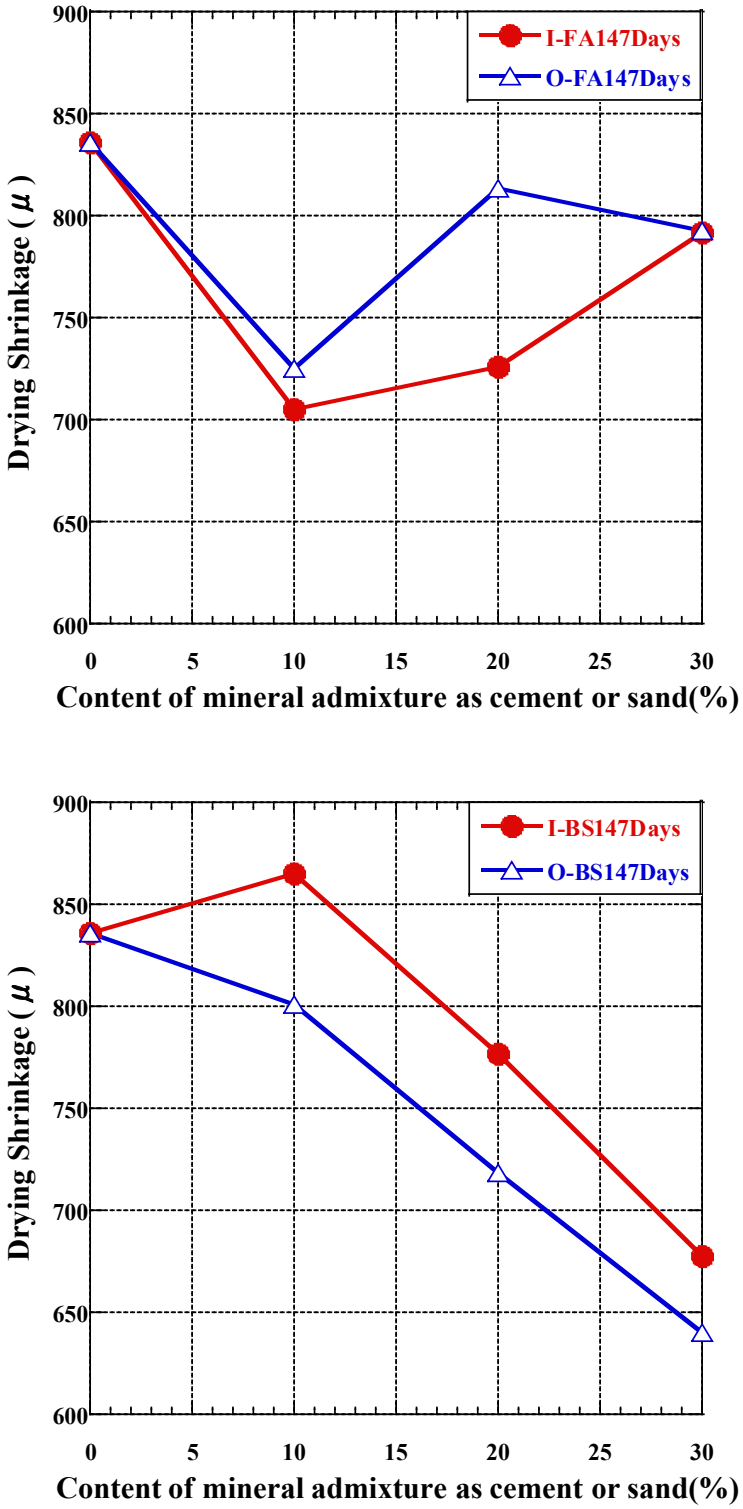

Fig. 3.5 The effect of mineral admixture on drying shrinkage

3.3.3 Creep

Fig. 3.6(a,b) shows the time development of creep strain under compression for concrete containing fly ash. The creep strain is calculated as the total strain minus the sum of elastic strain at loading and shrinkage strain. In this experiment, the creep strain was suppressed when fly ash was used both as part of the cement and as sand compared with the control concrete. For the fly ash as part of the cement, the concrete with 20% fly ash was found to have the lowest creep strain, which was about 40% lower than that of the control concrete. In addition, it was confirmed that the creep strain increased as the fly ash content increased when the content was more than 20%. IFA10, IFA20, and IFA30 exhibited creep strains that were 31.1%, 47.3%, and 43.6% lower, respectively, compared with the control concrete at 175 days. When the fly ash was used as part of the sand, the creep strain exhibited a decreasing trend as the fly ash content increased. At 175 days, the OFA10 and OFA30 mixes exhibited a 38% and 50.1% lower creep strain, respectively, compared with the control concrete.

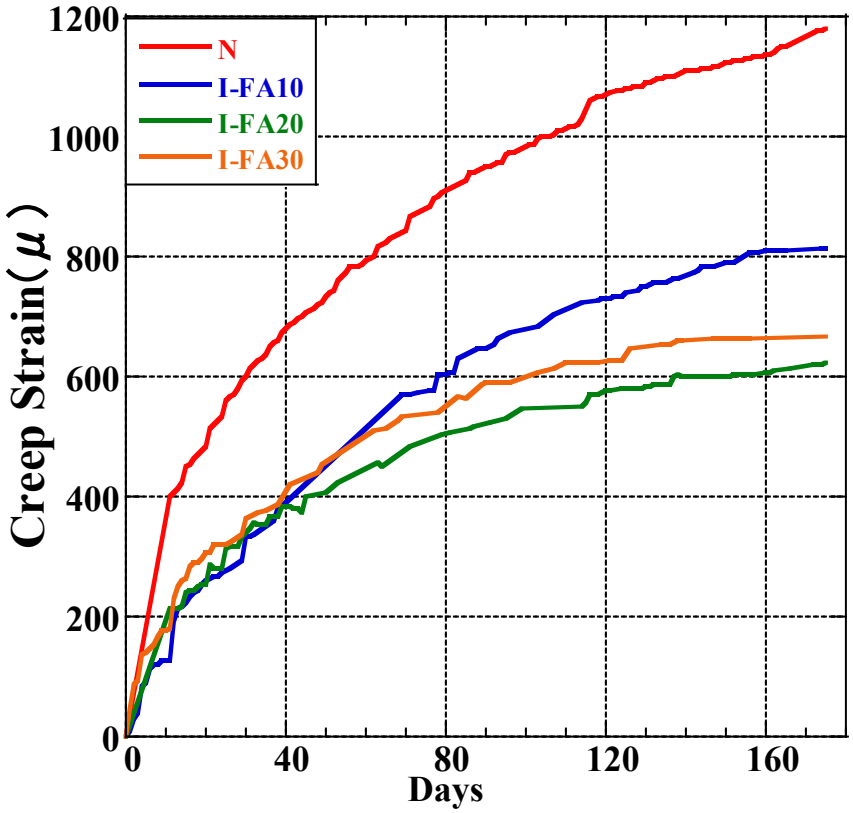

Fig. 3.6 Creep strain of concrete with fly ash(a)

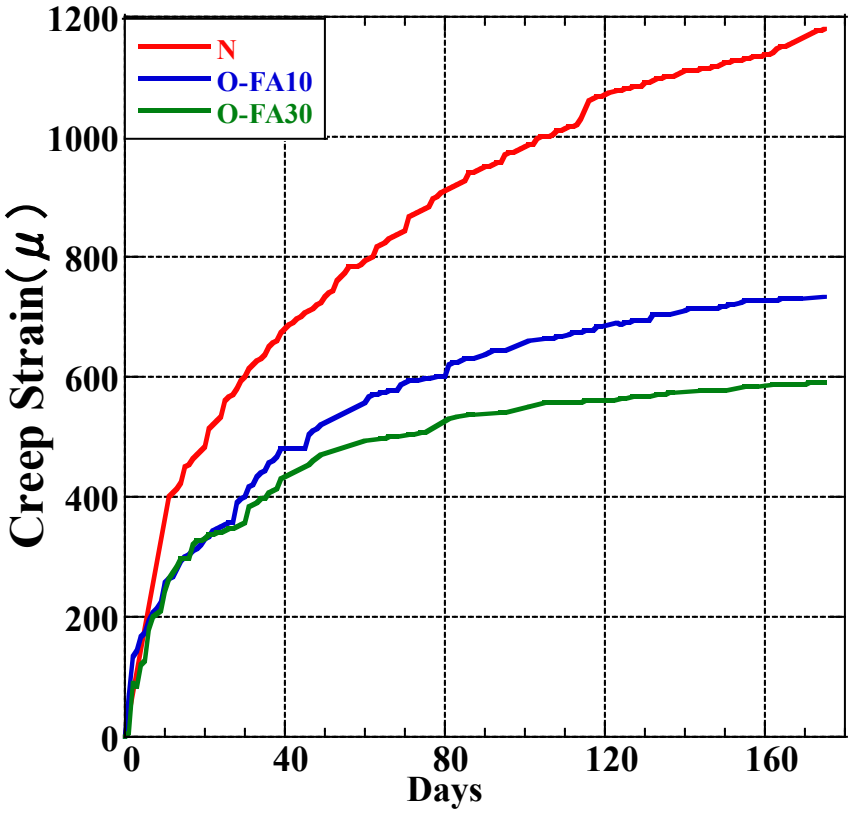

Fig. 3.6 Creep strain of concrete with fly ash(b)

Ghosh et al. also reported, adding fly ash into concrete can significantly reduce the creep of concrete [61]. Kristiawan et al. studied self-compacting concrete with 30%, 55%, 65% fly ash replacing cement, the results showed that the concrete containing 55–65% fly ash exhibited 50–60% lower creep coefficient than concrete with 35% fly ash [62]. It has been reported that concrete with 25% fly ash replacing cement has a 15% lower creep strain, concrete with 30% fly ash replacing cement has a 50% lower creep strain, compared to ordinary concrete [30], [31]. Lohtia et al. studied the concrete with 0–25% fly ash replacing cement, results showed that concrete containing more than 15% of fly ash exhibited a higher creep strain than ordinary concrete [32]. According to Dhir et al. reported, the lower creep strain of fly ash concrete is due to the increase in compressive strength after the load is applied [63]. Due to the greater increase in the compressive strength of fly ash concrete in the later stage, the stress/strength ratio during creep test is lower than that of ordinary concrete. The lower creep strain of fly ash concrete can be attributed to the lower stress/strength ratio during the creep test [64].

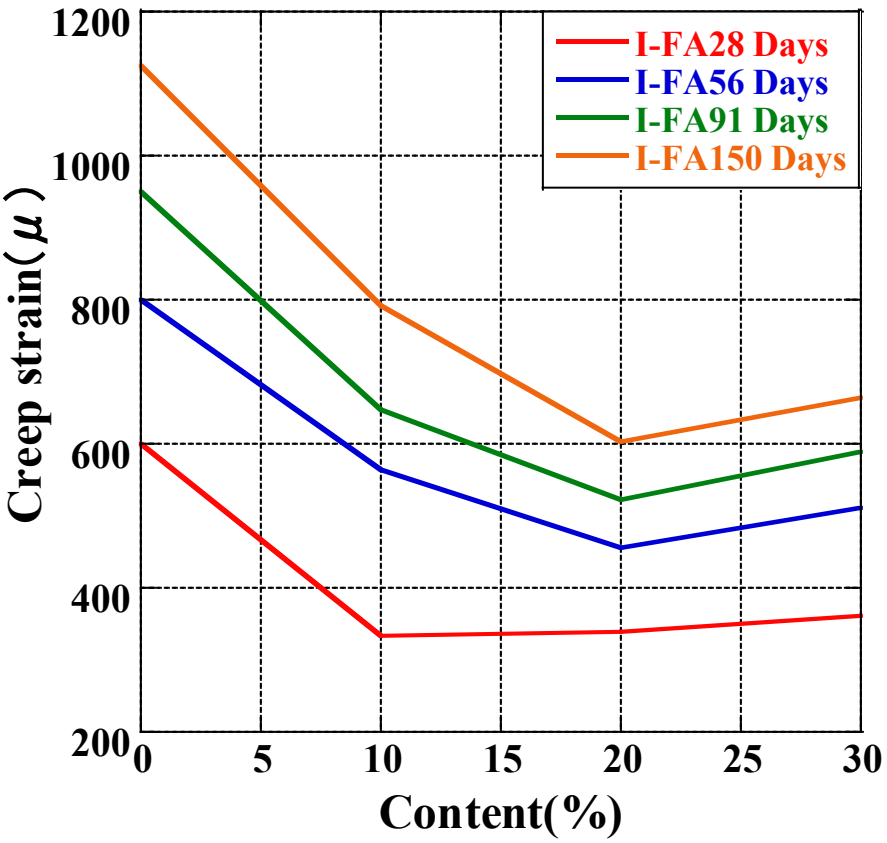

Fig. 3.7 The effect of fly ash content on creep strain.

Fig. 3.7 shows the relationship between the creep strain at different ages and the fly ash content of the cement. It was confirmed that the inhibitory effect on creep strain in concrete containing 20% fly ash increased as the material aged. It was also confirmed that when the fly ash content was more than 30%, the creep strain increased.

Fig. 3.8 shows the time development of specific creep strain under compression for concrete containing fly ash. It can be seen that the specific creep of concrete with fly ash as part of the cement was similar to the creep strain, with concrete containing 20% fly ash having the lowest specific creep. However, over time, the concrete containing 10% fly ash and the control concrete showed similar specific creep. Concrete with fly ash as part of the sand exhibited a greater difference in specific creep compared with the control concrete and lower specific creep compared with concrete with fly ash as part of the cement. In all mixes, concrete with 30% fly ash replacing sand had the lowest specific creep. Fig. 3.9 shows the relationship between specific creep at different ages and the amount of cement replaced by fly ash.

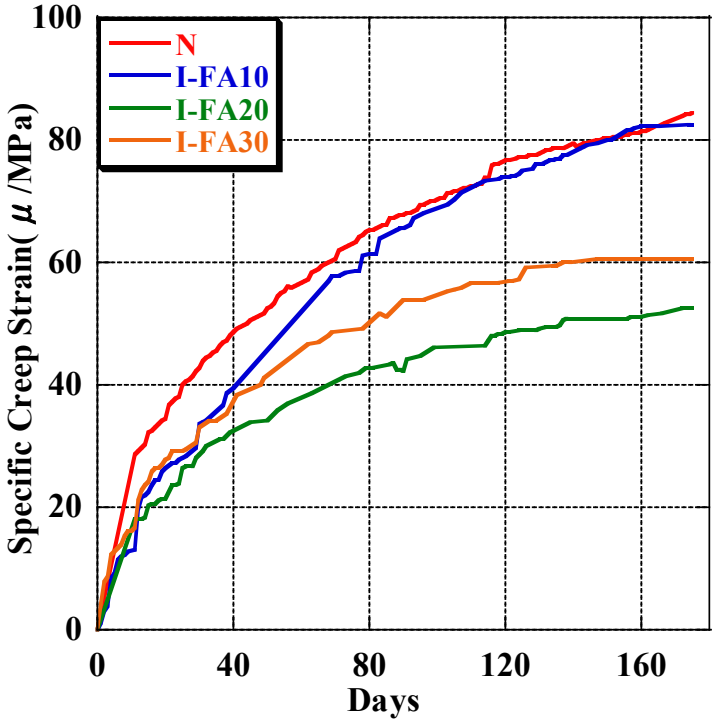

Fig. 3.8. Specific creep strain of concrete with fly ash (a)

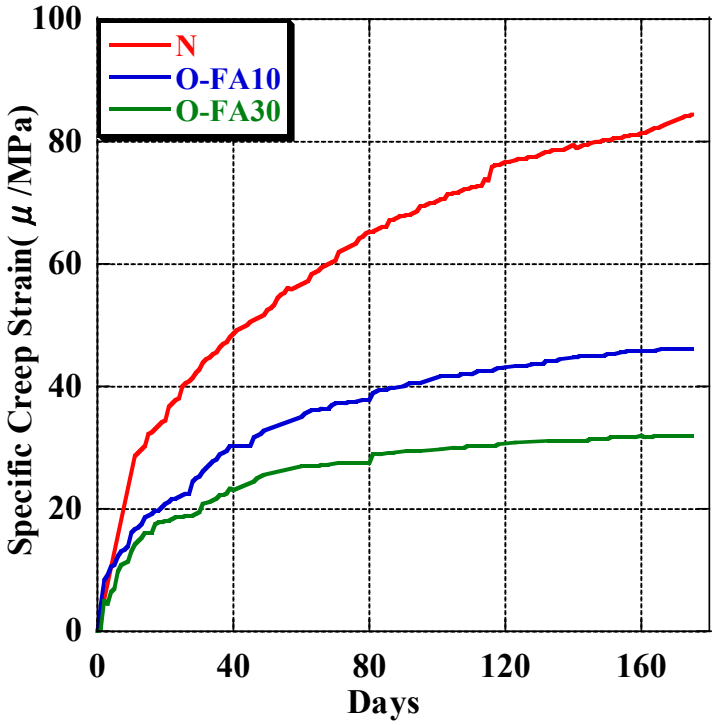

Fig. 3.8. Specific creep strain of concrete with fly ash (b)

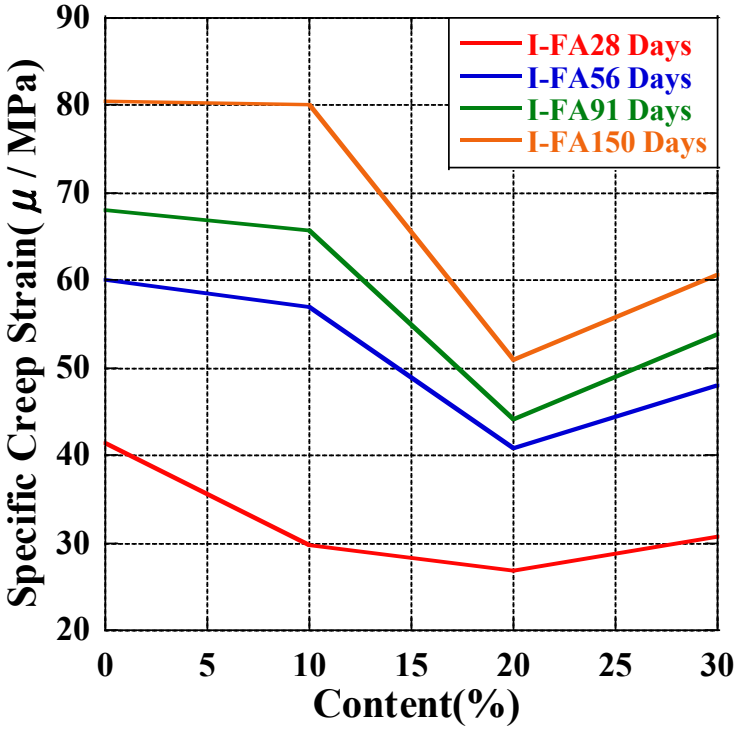

Fig. 3.9 The effect of fly ash content on specific creep strain

It was confirmed that the difference in the specific creep strain between the control concrete and the concrete with 10% cement replaced by fly ash became smaller as the material aged. Similar to the creep strain results, the inhibitory effect on creep strain in concrete containing 20% fly ash increased as the material aged. It was also confirmed that when the fly ash content was more than 30%, the creep strain increased.

3.3.4 Analysis on carbonation dioxide emission per unit volume

The CO_2 emissions of each mix were calculated from the Recommendation on Environmental Performance Verification for Concrete Structures (draft) [65]. Table 3.4 shows the CO_2 emission intensities of the materials. The CO_2 emission per unit volume of cement production is large, and it has been proven that the environmental impact can be reduced by replacing cement with fly ash or GGBS [66].

Fig. 3.10 shows the calculation results for the CO_2 emissions of all mix proportions. For concrete with fly ash or GGBS as part of the cement, the emissions of CO_2 decreased as the replacement rate increased. Fig. 3.11 shows the CO_2 emissions per unit compressive strength, where smaller values represent a smaller impact on the environment. This shows that the emissions decreased as the replacement rate increased in all series at the age of 28 days, and that at the age of 91 days the emissions of CO_2 decreased as the replacement rate increased in all series. In addition, it was confirmed that concrete with GGBS could reduce the CO_2 emissions more than concrete with fly ash. It was also shown that the CO_2 emissions of the OBS30 mix were about half that of the control concrete.

Table 3.4. The emission intensities of materials

Materials	Emission of CO2
Tap Water	0.27 kg/m3
Portland Cement	771.7 kg/ton
Fly Ash	23.0 kg/ton
GGBS	40.36 kg/ton
Sea Sand	3.7 kg/ton
Rubble	3.9 kg/ton
AE Water Reducer	121 kg/ton
Superplasticizers	350 kg/ton

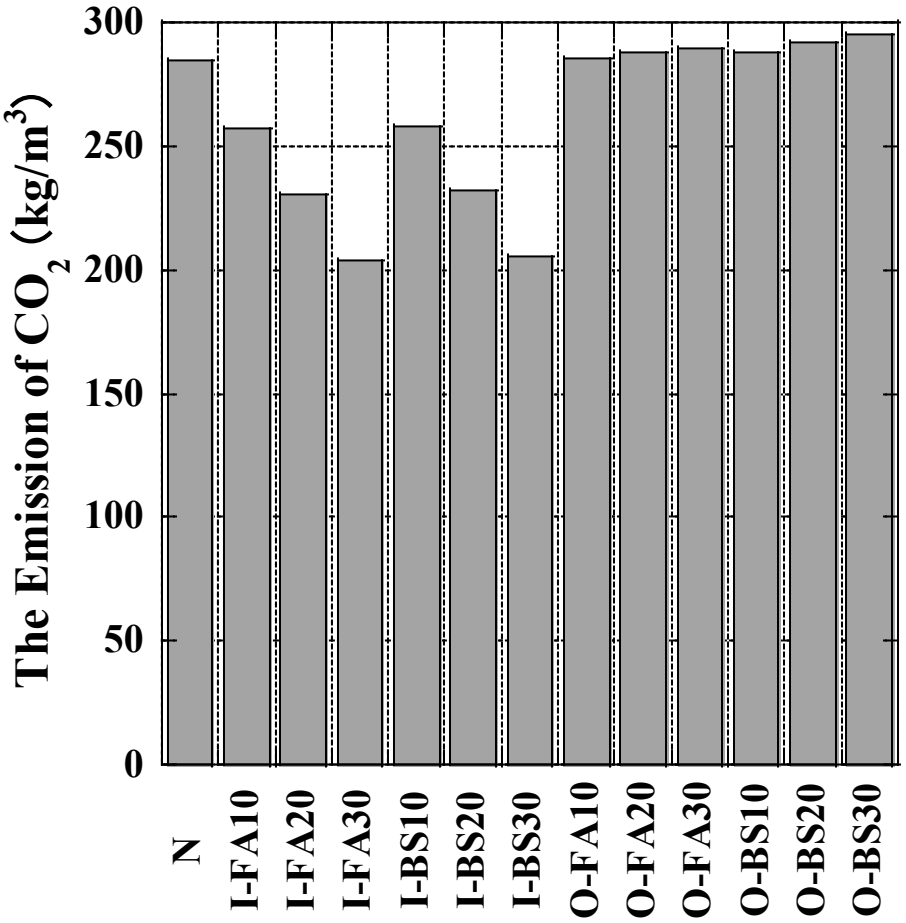

Fig. 3.10 CO_2 emissions of each mix proportions

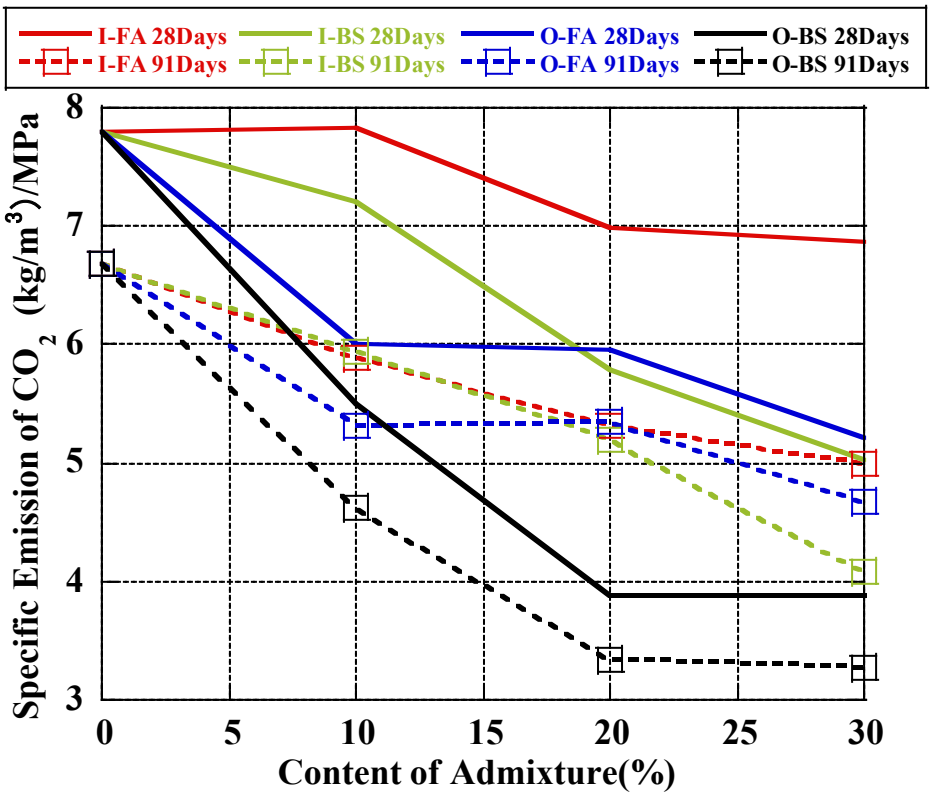

Fig 3.11 CO_2 emissions per unit compressive strength

3.3.5 Comparative study of creep strain

In the following, prediction models were used as templates for comparing the prediction values of concrete creep strain with the experimental data in this paper. These prediction models are widely recognized by the engineering and academic communities.

AIJ Model is presented in Equation (1) [43]

$$C(t,t_0) = CR \cdot log_e(t - t_0 + 1)$$

$$CR = (6.8X - 0.12G + 17.5)(t_0)^{-0.33}(1 - \frac{h}{100})^{0.36}(V/S)^{-0.43} \quad (1)$$

Where $C(t,t_0)$ is specific creep strain(×10-6/(N/mm2), t is the age of concrete (day), t_0 is age of concrete at beginning of load (day), G is specific coarse aggregate amount (kg/m^3), X is water binder ratio (%), h is relative humidity, V/S is volume surface area ratio .

JSCE Model is presented in Equation (2) [44]

$$C_r(t,t_0) = \frac{4W(1-h)+350}{12+f_c(t_0)} log_e(t - t_0 + 1) \quad (2)$$

Where $C_r(t,t')$ is specific creep strain(×10-6/(N/mm2), t is the age of concrete (day), t_0 is age of concrete at beginning of load (day), h is relative humidity, W is specific water amount (kg/m3), $f_c(t_0)$ is compressive strength of age at the start of loading.

ACI209 Model is presented in Equation (3) [40]

$$\varphi(t,t_0) = \frac{(t-t_0)^{\psi}}{d+(t-t_0)^{\psi}}\varphi_u \quad (3)$$

where $\varphi(t,t_0)$ is the creep coefficient; d (in days) and ψ are considered constants for a given member shape and size that define the time-ratio part; t is the age of concrete (day), t_0 is the age of load applied (day), and φ_u is the ultimate creep coefficient. For the standard conditions, φ_u is 2.35, ACI-209R-92 recommends, an average value of 10 and 0.6 for d and ψ, respectively.

CEB MC90-99 is presented in Equation (4) [40]

$$\varphi_{28}(t,t_0) = \varphi_0\beta_c(t-t_0)$$
$$\varphi_0 = \varphi_{RH}(h)\beta(f_{cm28})\beta(t_0)$$
$$\varphi_{RH} = \left[1 + \frac{1-h/h_0}{\sqrt[3]{0.1[(V/S)/(V/S)_0]}}\alpha_1\right]\alpha_2$$
$$\beta(f_{cm28}) = \frac{5.3}{\sqrt{f_{cm28}/f_{cmo}}}$$
$$\beta(t_0) = \frac{1}{0.1 + (t_0/t_1)^{0.2}}$$
$$\beta_c(t-t_0) = \left[\frac{(t-t_0)/t_1}{\beta_H + (t-t_0)/t_1}\right]^{0.3}$$
$$\beta_H = 150[1 + (1.2\cdot h/h_0)^{18}](V/S)/(V/S)_0 + 250\alpha_3$$
$$\alpha_1 = \left[\frac{3.5f_{cmo}}{f_{cm28}}\right]^{0.7} \quad \alpha_2 = \left[\frac{3.5f_{cmo}}{f_{cm28}}\right]^{0.2} \quad \alpha_3 = \left[\frac{3.5f_{cmo}}{f_{cm28}}\right]^{0.5} \quad (4)$$

where t is the age of concrete(day), t_0 is the age of concrete at beginning of load (day), f_{cm28} is compressive strength at the age of 28 days (MPa), f_{cmo} is 10 MPa, V/S is the volume surface ratio, $(V/S)_0$ is 50mm, h is the relative humidity, ho = 1, t_1 is 1 day.

GL200 Model is presented in Equation (5) [42]

$$\varphi_{28}(t,t_0) = \Phi(t_c)\left[2\frac{(t-t_0)^{0.3}}{(t-t_0)^{0.3}+14} + \left(\frac{7}{t_0}\right)^{0.5}\left(\frac{(t-t_0)}{(t-t_0)+7}\right)^{0.5} + 2.5(1-1.086h^2)\left(\frac{(t-t_0)}{(t-t_0)+0.12(V/S)^2}\right)^{0.5}\right]$$

$$\Phi(t_c) = \left[1 - \left(\frac{(t_0-t_c)}{(t_0-t_c)+0.12(V/S)^2}\right)^{0.5}\right]^{0.5} \quad (5)$$

Where t is the age of concrete, t_0 is the age of concrete at beginning of load (day), t_c is the age of concrete at beginning of drying, V/S is the volume surface ratio, h is the relative humidity.

CEB-FIP 1990 Model is presented in Equation (6) [41]

$$\varphi(t,t_0) = \varphi_0\beta_c(t-t_0)$$
$$\varphi_0 = \varphi_{RH}(h)\beta(f_{cm28})\beta(t_0)$$
$$\varphi_{RH} = 1 + \frac{\text{1-RH/RH}_0}{\sqrt[3]{0.46[h/h_0]}}$$
$$\beta(f_{cm28}) = \frac{5.3}{\sqrt{f_{cm28}/f_{cmo}}}$$
$$\beta(t_0) = \frac{1}{0.1 + (t_0/t_1)^{0.2}}$$

$$\beta_c(t-t_0) = \left[\frac{(t-t_0)/t_1}{\beta_H + (t-t_0)/t_1}\right]^{0.3}$$

$$\beta_H = 150 \times [1 + \{1.2 \cdot h/h_0\}^{18}] \times \frac{h}{h_0} + 250$$

$$h = 2A_C/u \qquad (6)$$

where t is the age of concrete(day), t_0 is the age of concrete at beginning of load (day), f_{cm28} is compressive strength at the age of 28 days (MPa), f_{cmo} is 10 MPa, V/S is the volume surface ratio, A_C is the cross-section and u is the perimeter of the member in contact with the atmosphere, h_0 is 100mm, RH is the relative humidity, RH0 = 1, t_1 is 1 day.

Many of the prediction formulas proposed to date do not take into account the effects of admixtures. Even the prediction formulas used in this study do not take the influence of the admixture into consideration in all the formulas. This study analyses the corresponding relationship between the predicted value of specific creep strain obtained from the above prediction models and the experimental measurement value. However, because humidity was unstable in the compression creep test, the average humidity of the homeothermic chamber throughout the measurement period was used for the prediction models.

In the AIJ model, the coefficient depending on the mix proportion was based on the unit coarse aggregate amount and the water binder ratio.

In the JSCE model, the coefficient depending on the mix proportion was based only on the unit water amount. The unit water amount was kept constant at 180 kg/m³ in the mix proportions used in this experiment, and the experimental value of the 28-day compressive strength was used for the compressive strength of the loading start material age.

In the CEB-FIP 1990 and CEB MC90-99 models, the creep coefficient was calculated by the prediction models, multiplied by the elastic strain during loading, and divided by the loading stress, and the value of the unit creep strain was calculated and compared. Moreover, because the humidity was not stablein this experiment, the predicted value was not stable until around 30 days.

In the ACI 209 and GL2000 models, the creep coefficient was calculated using the material constants and age of the material, and the coefficient depending on the mix proportion was not defined. Therefore, in this experiment, the predicted values were the same for all mixes.

In addition, we also evaluated the prediction accuracy by the root mean square error (RMSE) value, which indicates how much the predicted values obtained from these prediction models deviate from the experimental values. The RMSE value is calculated from Equation (7).

$$RMSE = \sqrt{\frac{1}{N}\sum_{i=1}^{N}(y_i - \hat{y}_i)^2} \quad (7)$$

Where: N is the number of all prediction values; $y_i$is the experimental data; $\hat{y}_i$is the prediction value.

Fig. 12(a)-(f) show the experimental value of creep strain and the predicted value from each prediction model for each mix. For the control concrete, the values predicted by the AIJ model was closest to the experimental value. The value predicted by the CEB-FIP 1990 model was too large, and that by the other prediction models was too small. For the IFA10 mix, the difference between the experimental value and the value predicted by the AIJ model gradually decreased with increasing age. It was also found that the value predicted by the CEB-FIP 1990 model and CEB MC90-99 model was too large,

and that by the JSCE model was too small. Since the early temperature in this experiment was not stable, the early prediction value was not stable.

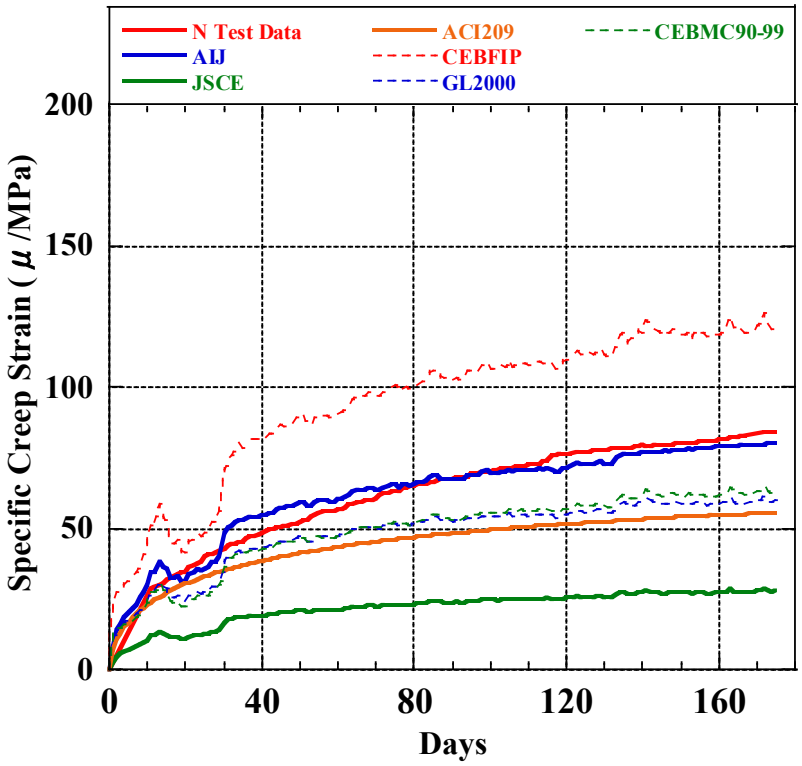

(a)

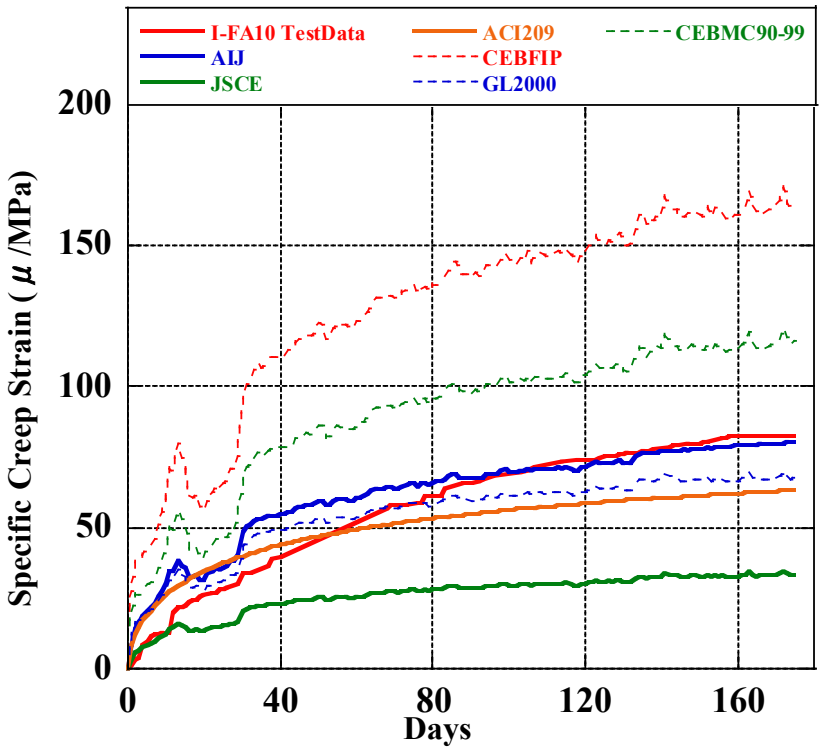

(b)

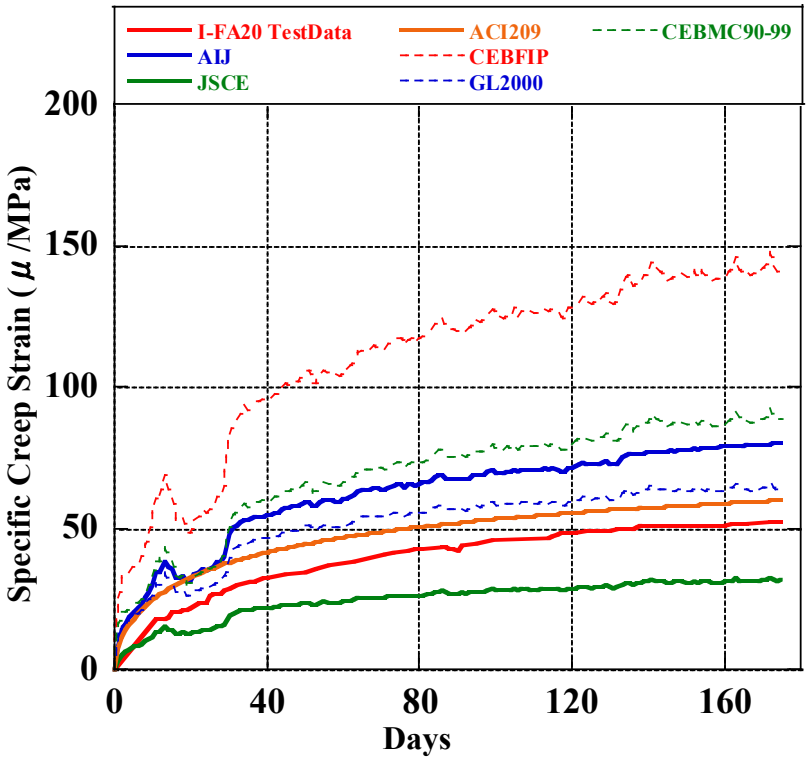
I-FA20 TestData
ACI209
CEBMC90-99
AIJ
CEBFIP
JSCE
GL2000
Specific Creep Strain (μ /MPa)
200
150
100
50
0
0
40
80
120
160
Days

(c)

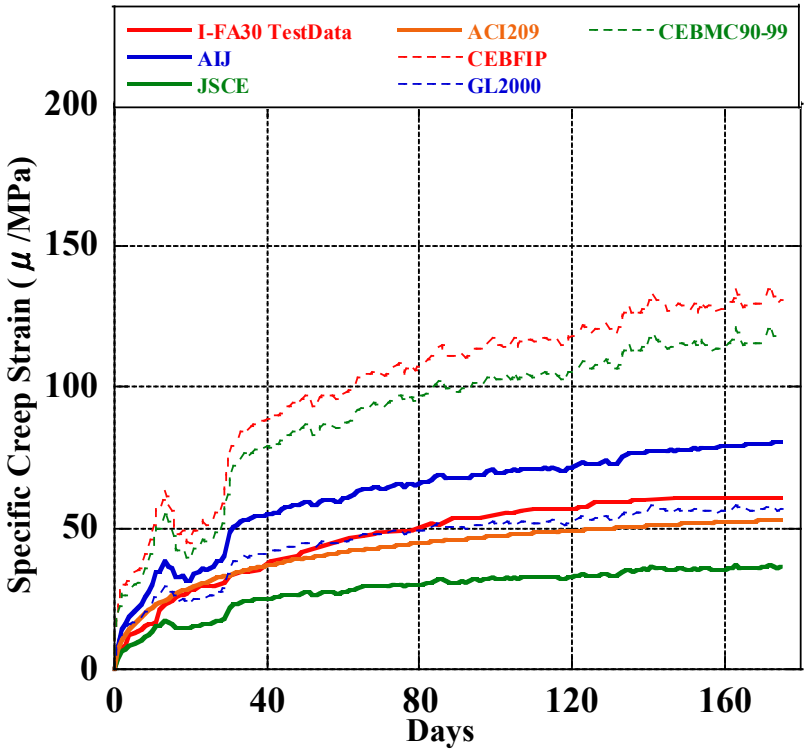
I-FA30 TestData
ACI209
CEBMC90-99
AIJ
CEBFIP
JSCE
GL2000
Specific Creep Strain (μ /MPa)
200
150
100
50
0
0
40
80
120
160
Days

(d)

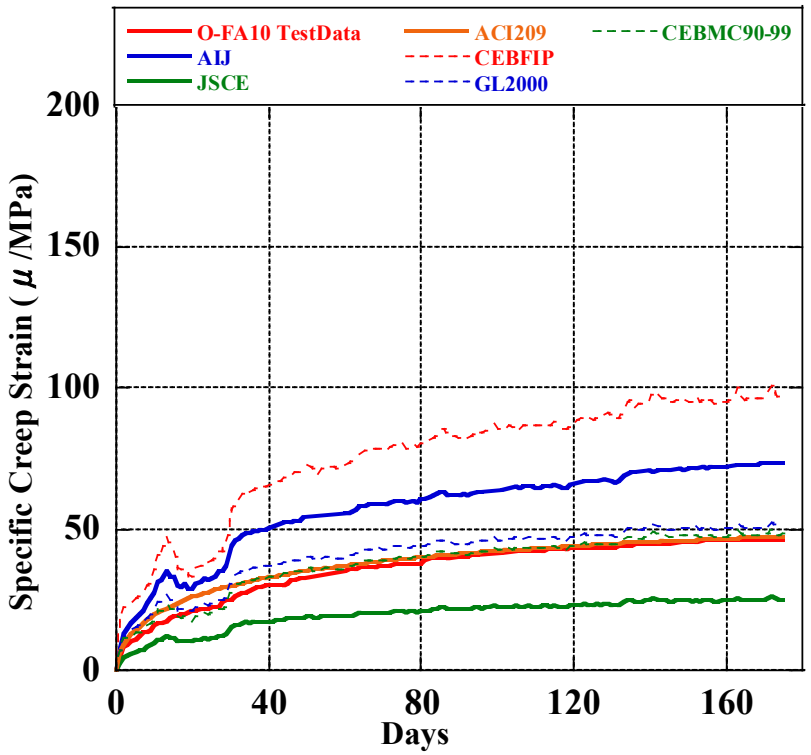

(e)

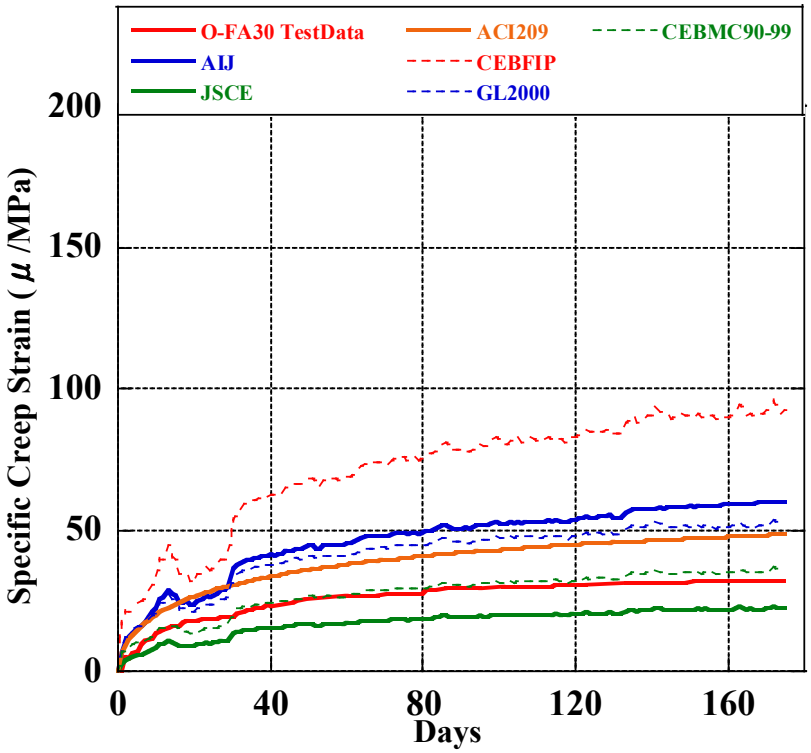

(f)

Fig. 3.12 Comparison of experimental value and predicted value for each mix proportions

Therefore, it is thought that the AIJ model was the most suitable for the creep strain of general concrete or concrete with low fly ash content. However, for IFA20 and IFA30, the values predicted by the GL-2000 and ACI209 models were more suitable, while those predicted by the AIJ, CEB MC90-99, and CEB-FIP 1990 models were too small or large. Fig. 3.12(e) and (f) show the results for concrete with fly ash as part of the sand. For OFA10, the ACI209, GL2000, and CEBMC90-99 models were suitable. The value predicted by the AIJ and CEB-FIP 1990 models was too large, and that by the JSCE model was too small. For OFA30, the CEBMC90-99 model was the most suitable, the prediction by the JSCE model was too small, and that by the other models was too large.

Fig. 3.13. shows the RMSE between experimental and prediction values. It was found that the control concrete had the lowest RMSE with the AIJ model. Concrete with fly ash as part of the cement had a lower RMSE with the ACI209 model and the RMSE decreased as the fly ash content increased, and concrete with fly ash as part of the sand had the lowest RMSE with CEBMC90-99. This confirms that the AIJ model was suitable for normal concrete or concrete with only a small fly ash content as part of the cement, that the ACI model was suitable for concrete with fly ash as part of the cement, with the error between the predicted and experimental values decreasing with increasing fly ash content, and that the CEBMC90-99 model was suitable for concrete with fly ash as part of the sand.

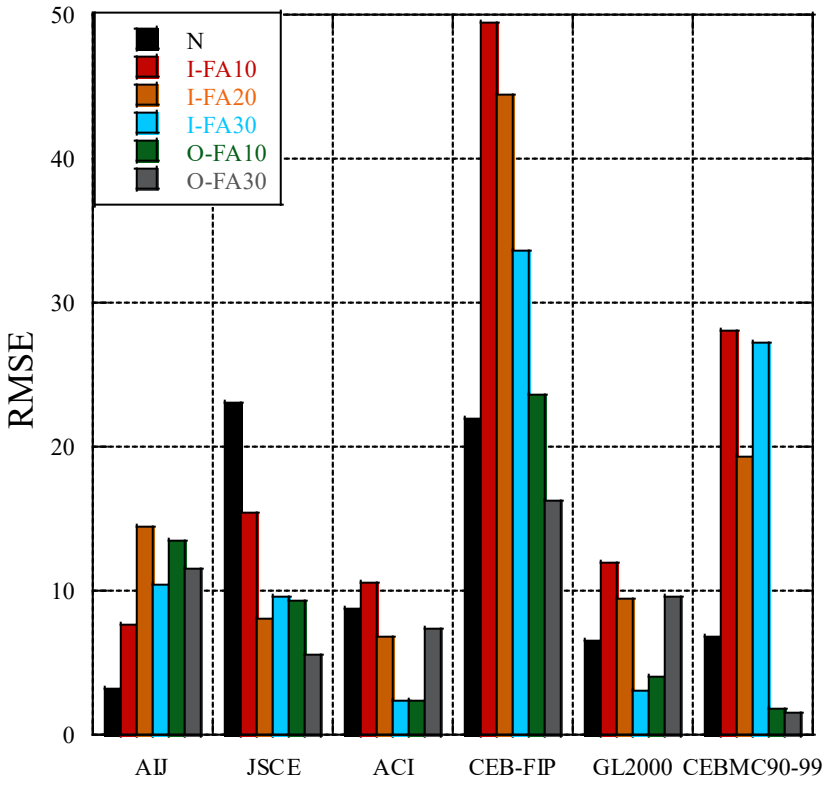

Fig. 3.13. The RMSE between experimental and prediction values

3.3.6 Creep strain prediction model for concrete containing fly ash

Due to the AIJ Model has the highest accuracy for ordinary concrete and concrete that contained a low amount of fly ash, we consider introducing a parameter K_L to capture the effect of fly ash content to make the AIJ Model more suitable for concrete containing fly ash. Therefore, a regression analysis has performed on the experimental data. It shows that the regression curve and regression equation of concrete with fly ash as part of cement which is shown in Fig 3.14. Through the regression analysis of the experimental data, it is concluded that the parameter of concrete with fly ash as part of the cement is presented in Equation (8).

$$K_L = 0.919 - 0.76x \qquad (8)$$

Where, x is the ratio of fly ash replacing cement.

In addition, the creep test data of concrete with fly ash as part of fine aggregate was fitted, found that the content of fly ash has no obvious effect on the parameter. It is concluded that the parameter of concrete with fly ash as part of sand is a constant, $K_L = 0.6$.

Fig 3.15. shows the RMSE of the AIJ Model with and without fly ash effect parameter, the results show that the introduction of fly ash effect parameter can effectively improve the accuracy of AIJ Model. Therefore, it is recommended to introduce the parameter obtained above into the concrete with fly ash content not higher than 30%. The specific creep strain can be calculated from Equation (9).

$$C(t,t_0) = CR \cdot log_e(t - t_0 + 1)$$

$$CR = (6.8X - 0.12G + 17.5)(t_0)^{-0.33}(1 - \frac{h}{100})^{0.36}(V/S)^{-0.43} \cdot K_L \qquad (9)$$

Where $C(t,t_0)$ is specific creep strain($\times 10^{-6}$/(N/mm^2), t is the age of concrete (day), t_0 is age of concrete at beginning of load (day), G is specific coarse aggregate amount (kg/m^3), X is water binder ratio (%), h is relative humidity, V/S is volume surface area ratio, K_L is the parameter to capture the effect of fly ash, for fly ash as part of cement $K_L = 0.919 - 0.76x$ and x is the ratio of fly ash replacing cement, fly ash as part of sand $K_L = 0.6$.

In the future, it is necessary to further study the creep prediction model of high-volume fly ash concrete. In addition, the effect of other mineral admixtures needs to be further studied in the creep prediction model.

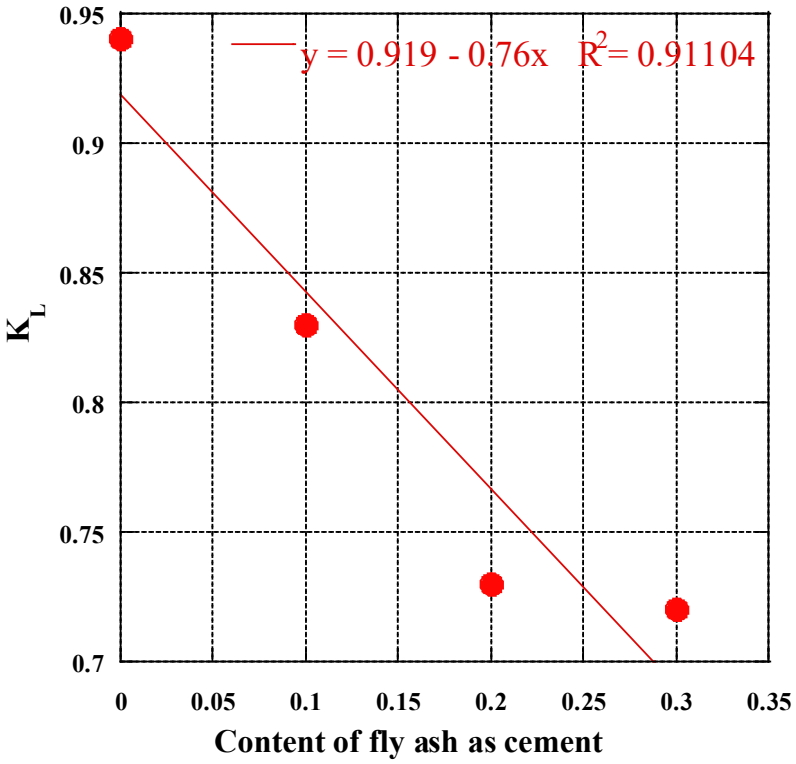

Fig. 3.14 The regression curve of concrete with fly ash as part of cement

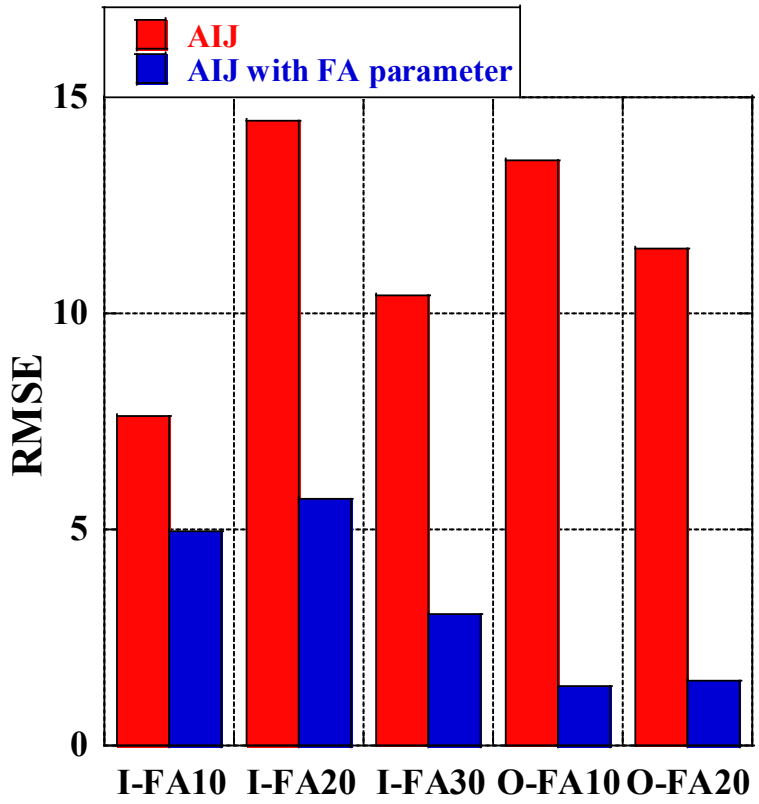

Fig. 3.15 The RMSE of AIJ Model with and without fly ash effect parameter

3.4 Conclusion

1. Replacement of sand with fly ash or GGBS significantly increased the compressive strength of the concrete. Compared with ordinary concrete, concrete in which fly ash replaced 30% of the sand exhibited 45% higher compressive strength, with 30% GGBS replacement of sand exhibiting a 112% higher compressive strength. These results indicate that replacing sand with fly ash or GGBS can produce high-performance concrete.

2. Regardless of whether the concrete contained fly ash as a replacement for part of the cement or sand, concrete with 10% fly ash exhibited the lowest drying shrinkage, and the drying shrinkage increased with increasing fly ash content. Concrete containing GGBS as a replacement for sand or cement exhibited a significant reduction in drying shrinkage compared with ordinary concrete, and concrete with 30% GGBS as a replacement for cement or sand exhibited 20% lower drying shrinkage.

3. When fly ash was used as a replacement for cement, the 20% fly ash concrete was found to have the lowest creep strain, which was about 40% lower than that of the control concrete. In addition, it was confirmed that the creep strain increased as the fly ash content increased when the content was >20%. And concrete with 30% fly ash as a replacement for sand exhibited 50% lower creep strain.

4. For the ratio of CO2 emissions to compressive strength, concrete containing GGBS as a replacement for sand exhibited lower CO2 emissions, and concrete with 30% GGBS as a replacement for sand exhibited around half of the CO2 emissions compared with the control concrete.

5. Creep prediction models that are widely recognized by the engineering and academic communities were analyzed, and we introduced a parameter KL to capture the effect of fly ash content in the AIJ Model, which has the highest accuracy for ordinary concrete. A low RMSE obtained between the experimental and predicted values by using the developed model indicated the effectiveness of the introduced parameter for concrete containing fly ash.

Reference

[1] Ecra (European Cement Research Academy). Calcined Clay: A Supplementary Cementitious Material with a Future. Available online: https://ecra-online.org/fileadmin/ecra/newsletter/ECRA_Newsletter_3_2019.pdf
(Accessed on 02 October 2021)
[2] Colaço, R. Reduce the Environmental Impact of Cement (Portuguese). Constr. Mag. 2019, 90, 12–14.
[3] Gholampour, A., Ozbakkaloglu, T., Etemadi, E., & Vincent, T. (2020). Sustainable mortars containing fly ash, glass powder and blast-furnace and lead-smelter slag. Magazine of Concrete Research, 72(9), 447-459.
[4] Heidrich, C., Feuerborn, H. J., & Weir, A. (2013, April). Coal combustion products: a global perspective. In World of coal ash conference (pp. 22-25).
[5] NDRC, Annual Report on Comprehensive Utilization of Resources in China (2014), China, National Development and Reform Commission, 201
[6] CEA, Fly ash generation at coal/lignite based thermal power stations and its utilization in the country for the year 2015-16, New Delhi, Central Electricity Authority, 2016
[7] ACAA, 2016 Coal Combustion Product (CCP) Production and Use Survey Report, Farmington Hills, American Coal Ash Association, 2016.
[8] ADAA, Annual Membership Survey Results, in H. G. P. Ltd, ed. Ash Development Association of Australia, 2016
[9] Gholampour, A., & Ozbakkaloglu, T. (2017). Performance of sustainable concretes containing very high volume Class-F fly ash and ground granulated blast furnace slag. Journal of Cleaner Production, 162, 1407-1417.
[10] Neville, Adam M. Properties of concrete. Vol. 4. London: Longman, 1995.
[11] De Maeijer, P. K., Craeye, B., Snellings, R., Kazemi-Kamyab, H., Loots, M., Janssens, K., & Nuyts, G. (2020). Effect of ultra-fine fly ash on concrete performance and durability. Construction and Building Materials, 263, 120493.
[12] Chindaprasirt, P., Jaturapitakkul, C., & Sinsiri, T. (2005). Effect of fly ash fineness on compressive strength and pore size of blended cement paste. Cement and concrete composites, 27(4), 425-428.
[13] Saha, A. K. (2018). Effect of class F fly ash on the durability properties of concrete. Sustainable environment research, 28(1), 25-31.
[14] Moffatt, E. G., Thomas, M. D., & Fahim, A. (2017). Performance of high-volume fly ash concrete in marine environment. Cement and Concrete Research, 102, 127-135.
[15] Hussain, S., Bhunia, D., & Singh, S. B. (2017). Comparative study of accelerated carbonation of plain cement and fly-ash concrete. Journal of Building Engineering, 10, 26-31.
[16] Hefni, Y., Abd El Zaher, Y., & Wahab, M. A. (2018). Influence of activation of fly ash on the mechanical properties of concrete. Construction and Building Materials, 172, 728-734.
[17] Sun, J., Shen, X., Tan, G., & Tanner, J. E. (2019). Compressive strength and hydration characteristics of high-volume fly ash concrete prepared from fly ash. Journal of Thermal Analysis

and Calorimetry, 136(2), 565-580.
[18] Zhang, D., Yang, Q., Mao, M., & Li, J. (2020). Carbonation performance of concrete with fly ash as fine aggregate after stress damage and high temperature exposure. Construction and Building Materials, 242, 118125.
[19] Siddique, R. (2003). Effect of fine aggregate replacement with Class F fly ash on the mechanical properties of concrete. Cement and Concrete research, 33(4), 539-547.
[20] Siddique, R. (2003). Effect of fine aggregate replacement with Class F fly ash on the abrasion resistance of concrete. Cement and concrete research, 33(11), 1877-1881.
[21] Zhang, D., Mao, M., Zhang, S., & Yang, Q. (2019). Influence of stress damage and high temperature on the freeze–thaw resistance of concrete with fly ash as fine aggregate. Construction and Building Materials, 229, 116845.
[22] Özbay, E., Erdemir, M., & Durmuş, H. İ. (2016). Utilization and efficiency of ground granulated blast furnace slag on concrete properties–A review. Construction and Building Materials, 105, 423-434.
[23] Łukowski, P., & Salih, A. (2015). Durability of mortars containing ground granulated blast-furnace slag in acid and sulphate environment. Procedia Engineering, 108, 47-54.
[24] Luo, R., Cai, Y., Wang, C., & Huang, X. (2003). Study of chloride binding and diffusion in GGBS concrete. Cement and Concrete Research, 33(1), 1-7.
[25] Garg, E. K., & Kapoor, E. K. (2016). A review on ground granulated blast-furnace slag as a cement replacing material. International Journal of Engineering Research and Management (IJERM), 3(07), 214-217.
[26] R. Sapuay, Ground Granulated Blast Furnace Slag, Saudi Readymix, 2016, 4.
[27] Li, K., Zeng, Q., Luo, M., & Pang, X. (2014). Effect of self-desiccation on the pore structure of paste and mortar incorporating 70% GGBS. Construction and Building Materials, 51, 329-337.
[28] Mohan, A., & Mini, K. M. (2018). Strength and durability studies of SCC incorporating silica fume and ultra fine GGBS. Construction and Building Materials, 171, 919-928.
[29] Mohan, A., & Mini, K. M. (2018). Strength studies of SCC incorporating silica fume and ultra fine GGBS. Materials Today: Proceedings, 5(11), 23752-23758.
[30] A. Ross, Some problems in concrete construction, Mag. Concr. Res. 12(34) (1960) 27–34.
[31] P. Bamforth, In situ measurement of the effect of partial Portlandcement replacement using either fly ash or ground granulated blast-furnace slag on the performance of mass concrete, Proc., Inst. Civ. Eng. 69(3) (1980) 777–800.
[32] R. Lohtia, B. Nautiyal, O. Jain, Creep of fly ash concrete, ACI J. 73(39) (1976) 469–472.
[33] Kristiawan, S. A., & Aditya, M. T. M. (2015). Effect of high volume fly ash on shrinkage of self-compacting concrete. Procedia Engineering, 125, 705-712.
[34] Zhao, Y., Gong, J., & Zhao, S. (2017). Experimental study on shrinkage of HPC containing fly ash and ground granulated blast-furnace slag. Construction and Building Materials, 155, 145-153.
[35] El-Chabib, H., & Syed, A. (2013). Properties of self-consolidating concrete made with high volumes of supplementary cementitious materials. Journal of materials in civil engineering, 25(11), 1579-1586.
[36] Darquennes, A., Roziere, E., Khokhar, M. I. A., Turcry, P., Loukili, A., & Grondin, F. (2012). Long-term deformations and cracking risk of concrete with high content of mineral additions.

Materials and structures, 45(11), 1705-1716.
[37] Brooks, J. J., Wainwright, P. J., & Boukendakji, M. (1992). Influence of slag type and replacement level on strength elasticity, shrinkage and creep of concrete. Special Publication, 132, 1325-1342.
[38] Lee, J. H., & Yoon, Y. S. (2015). The effects of cementitious materials on the mechanical and durability performance of high-strength concrete. KSCE Journal of Civil Engineering, 19(5), 1396-1404.
[39] Khatri, R. P., Sirivivatnanon, V., & Gross, W. (1995). Effect of different supplementary cementitious materials on mechanical properties of high performance concrete. Cement and Concrete research, 25(1), 209-220.
[40] ACI Committee. ACI 209.2 R-08: guide for modeling and calculating shrinkage and creep in hardened concrete. American Concrete Institute Committee, 2008.
[41] COMITE EURO-INTERNATIONAL DU BETON: CEB-FIP Model Code 90, Thomas Telford 1990
[42] Gardner, N. J., & Lockman, M. J. (2001). Design provisions for drying shrinkage and creep of normal-strength concrete. Materials journal, 98(2), 159-167.
[43] Sato, Y., et al. "Study on the prediction formula for time-dependent strain of concrete: Prediction formula of total creep strain" Journal of Structural and Construction Engineering (Transactions of AIJ) 71.599 (2006): 9-15. (In Japanese)
[44] Standard specifications for concrete structures-2007, Japan Society of Civil Engineers (JSCE)
[45] JIS R 5210: Portland cement (2009)
[46] JIS A 6201: Fly ash for use in concrete (1999)
[47] JIS A 6206: Ground granulated blast-furnace slag for concrete (2013)
[48] JIS A 1108: Method of test for compressive strength of concrete (2006)
[49] JIS A 1129-2: Method of measurement for length change of mortar and concrete-Part 2: Method with contact-type strain gauge
[50] JIS A 1157: Method of test for compressive creep of concrete (2010)
[51] Sumer, M. (2012). Compressive strength and sulfate resistance properties of concretes containing Class F and Class C fly ashes. Construction and Building Materials, 34, 531-536.
[52] Siddique, R. (2004). Performance characteristics of high-volume Class F fly ash concrete. Cement and Concrete Research, 34(3), 487-493.
[53] Uysal, M., & Akyuncu, V. (2012). Durability performance of concrete incorporating Class F and Class C fly ashes. Construction and Building Materials, 34, 170-178.
[54] Ravina, D. (1998). Mechanical properties of structural concrete incorporating a high volume of class F fly ash as partial fine sand replacement. Materials and structures, 31(2), 84-90.
[55] Johari, M. M., Brooks, J. J., Kabir, S., & Rivard, P. (2011). Influence of supplementary cementitious materials on engineering properties of high strength concrete. Construction and Building Materials, 25(5), 2639-2648.
[56] Vejmelková, E., Pavlíková, M., Keršner, Z., Rovnaníková, P., Ondráček, M., Sedlmajer, M., & Černý, R. (2009). High performance concrete containing lower slag amount: a complex view of mechanical and durability properties. Construction and Building Materials, 23(6), 2237-2245.
[57] ElNemr, A. (2020). Generating water/binder ratio-to-strength curves for cement mortar used in Masnory walls. Construction and Building Materials, 233, 117249.

[58] Saha, A. K., & Sarker, P. K. (2017). Sustainable use of ferronickel slag fine aggregate and fly ash in structural concrete: Mechanical properties and leaching study. Journal of Cleaner Production, 162, 438-448.
[59] Yuan, J., Lindquist, W. D., Darwin, D., & Browning, J. (2015). Effect of slag cement on drying shrinkage of concrete. American Concrete Institute.
[60] Li, J., & Yao, Y. (2001). A study on creep and drying shrinkage of high performance concrete. Cement and Concrete Research, 31(8), 1203-1206.
[61] Ghosh, R. S., & Timusk, J. (1981, September). Creep of fly ash concrete. In Journal Proceedings (Vol. 78, No. 5, pp. 351-357).
[62] Kristiawan, S. A., & Nugroho, A. P. (2017). Creep behaviour of self-compacting concrete incorporating high volume fly ash and its effect on the long-term deflection of reinforced concrete beam. Procedia engineering, 171, 715-724.
[63] Dhir, R. K., MUNDAY, J. L., & Ong, L. T. (1986). Investigations of the engineering properties of OPC/pulverised-fuel ash concrete: Deformation properties.
[64] Kou, S. C., Poon, C. S., & Chan, D. (2007). Influence of fly ash as cement replacement on the properties of recycled aggregate concrete. Journal of materials in civil engineering, 19(9), 709-717.
[65] JSCE, “Recommendation on Environmental Performance Verification for Concrete Structures (draft)” Concrete library, 125 (2005): 14-16 (in Japanese)
[66] Flower, D. J., & Sanjayan, J. G. (2007). Green house gas emissions due to concrete manufacture. The international Journal of life cycle assessment, 12(5), 282-288.

Chapter 4

THE EFFECT OF BIOMASS FLY ASH AND LIMESTONE POWDER ON THE PROPERTIES OF CONCRETE

4.1 Introduction

In recent years, the construction industry has witnessed rapid growth due to urbanization and industrialization. However, this development has come at a cost, as the production of cement used in construction leads to significant CO_2 emissions [6]. Recognizing the need for sustainable development, many researchers have turned their attention to improving the durability of concrete. Two approaches gaining traction in this area are the addition of limestone powder [2,3] and the utilization of biomass fly ash [4,5]. Specifically, the combination of biomass fly ash and limestone powder in concrete has emerged as a promising method for concrete recycling. Despite its potential, the existing research on concrete incorporating biomass fly ash or limestone powder remains insufficient.

To address this research gap, this paper conducts a series of experiments to investigate the properties of concrete containing different components. The experiments focus on evaluating the compressive strength, drying shrinkage, porosity, and accelerated carbonation resistance of concrete mixed with wood biomass fly ash (WFA), blend fly ash (BFA) mixed with coal and wood, and limestone powder (LSP). Additionally, the study examines the relationship between the volume of pores with varying diameters and the concrete's compressive strength, drying shrinkage, and carbonation velocity coefficient. In conclusion, this research aims to contribute to the understanding of concrete characteristics when incorporating biomass fly ash and limestone powder. By exploring the effects of these components on various concrete properties, we can advance the knowledge in the field of sustainable concrete development.

In this study, the researchers investigated the effects of replacing cement with either biomass fly ash or wood-coal mixed fly ash by weight and replacing sand with limestone powder by volume in concrete mixes. They cast a total of 13 concrete mixes, including a control mix, and tested compressive strength, drying shrinkage, carbonation resistance, and pore structure. The study found that adding limestone powder to biomass fly ash or wood-coal mixed fly ash concrete improved the 91-day compressive strength but increased drying shrinkage and decreased carbonation resistance. The use of biomass fly ash or wood-coal mixed fly ash reduced early compressive strength, increased drying shrinkage, and decreased carbonation resistance. However, adding biomass cementitious materials to concrete improved the micropore structure. The compressive strength and pore structure were tested at 7, 28, and 91 days, drying shrinkage was tested until 182 days, and carbonation resistance was tested until 91 days. The researchers also analyzed the correlation between the pore structure and concrete properties.

4.2 Experimental outline

Table 4.1 shows the physical properties of aggregates used in this experiment. Sea sand as fine aggregate and crushed stone as coarse aggregate was used. As binders, blend biomass fly ash and woody biomass fly ash which is modified by flotation method, and limestone powder was used. The properties of cement, WFA, BFA, LSP are shown in Table 4.2.

Table 4.1 Properties of aggregates

Property	Coarse aggregate	Fine aggregate
Oven-dried density (g/cm^3)	2.69	2.59
Fineness modulus	6.9	2.41
Water absorption (%)	1.41	1.04
Solid content (%)	56.7	61.2

Table 4.2 Properties of supplementary cementitious material and cement

Composites	WFA	BFA	LSP	Cement
SiO_2 (%)	50.50	63	0.53	21.5
Al_2O_3 (%)	12.30	18.1	0.20	5.4
Fe_2O_3 (%)	10.70	7.14	0.08	3.0
CaO (%)	14.10	3.9	46.37	64.9
SO_3 (%)	0.49	_	_	1.4
MgO (%)	2.96	1.66	8.20	2.1
Loss on ignition (%)	1.59	4.33	44.57	0.8
Density (g/cm^3)	2.41	2.19	2.76	3.16
Blaine specific area (cm^2/g)	5830	4038	3469	3000

Table 4.3 shows the mix proportion. The unit water amount is 180kg/m^3, the unit coarse aggregate amount is 945 kg/m^3. In addition, replacing cement with admixture in the same mass, with a total of 12 mix proportions including normal concrete. The symbols indicate replacement of cement, the type of admixture used, and the substitution rate. The target air volume was set to 4.5± 1.0%

Measurement items are compressive strength, drying shrinkage, carbonation and porosity. The compressive strength test was conducted according to JIS A 1108, the drying shrinkage test was conducted according to “Method of measurement for length change of mortar and concrete” of JIS A1129-2, and 100 × 100 × 400 mm prismatic specimens were produced. After casting, they were demolded at 1 day of age, and cured in water at 20 ° C for 7 days. Specimens were taken out of the water at 7 days of age, and a stainless-steel chip was attached to both end faces of the specimens, and then both end faces were sealed to measure the base length. The specimens for measuring the drying shrinkage were cured in a constant temperature and humidity room with a temperature of 20 ± 1.0 ° C and a relative humidity of 60 ± 5%. For porosity measurement, a specimen (φ100×200mm) that had been cured in water to the target material age was crushed, and a sieve was used to make a particle group of 2.5 to 5.0mm, and then the hydration reaction was stopped by immersion in acetone, and vacuum drying for 72 hours, then the sample was used. The measurement was performed with a mercury intrusion porosimetry (MIP). The accelerated carbonation test was carried out according to JIS A1153, and 100 × 100 × 400 mm prismatic specimens were produced.

Table 4.3 Mix proportions

Type	W/B	Unit mass(kg/m³)						
		W	C	BFA	WFA	LSP	S	RS
N	0.5	180	360	0	0	0	802	945
BFA10	0.5	180	324	36	0	0	792	945
BFA20	0.5	180	288	72	0	0	781	945
BFA30	0.5	180	252	108	0	0	770	945
WFA10	0.5	180	324	0	36	0	795	945
WFA20	0.5	180	288	0	72	0	787	945
WFA30	0.5	180	252	0	108	0	779	945
BSP10	0.5	180	252	108	0	85	690	945
BSP20	0.5	180	252	108	0	171	610	945
BSP30	0.5	180	252	108	0	256	530	945
WSP10	0.5	180	252	0	108	85	699	945
WSP20	0.5	180	252	0	108	171	619	945
WSP30	0.5	180	252	0	108	256	539	945

4.3 Result and discussion

4.3.1 Compressive strength

Fig. 4.1 shows the compressive strength of concrete containing biomass fly ash or limestone powder. About the concrete with only biomass fly ash (BFA and WFA). At 7 days, the proportion of WBFA added is inversely proportional to the early strength, while the addition of BFA is proportional to the early strength, and at 91 days, the strength of the concrete increases with the proportion of BFA or WFA added within a certain range, and only BFA30 exceeded expectations above ordinary concrete. This may be because the addition of biomass fly ash in the early stage slows down the hydration process of concrete, and the sufficient reaction of biomass fly ash in the later stage reduces the porosity of concrete [1]. Although the strength is still smaller than that of ordinary concrete, the strength of concrete within a certain range increase with the WFA content increase. And due to the BFA particles are finer, so that BFA can improve the particle size distribution, the concrete strength increases with the addition of BFA within a certain range at all ages. The strength of BFA30 is greater than that of ordinary concrete at 28 days and 91 days, which may also be due to the addition of BFA in the early stage delays the hydration reaction of concrete, and the strength develops rapidly in the later stage [1]. About effect of limestone powder on concrete containing 30% BFA or 30% WFA. For concrete with 30% WFA and various content of limestone powder, it can be seen that the addition of limestone powder greatly improves the early compressive strength of concrete. At 7 days, the compressive strength of WSP10, 20, and 30 is 29.9%, 24.7%, and 38.3% higher than that of WFA30, maybe it's due to the nucleation effect of limestone powder. And at 28 days and 91 days, the compressive strength of WSP10, 20, 30 is also significantly improved compared to WFA30, probably due to the filling effect of limestone powder since the nucleation effect is most pronounced in the early stage and vanishes with time as hydration proceeds.

Due to its finer particle size, limestone powder can fill the interstices (pores) between cement particles, leading to a denser packing and refinement of pore structure with higher strength [2]. For concrete with 30% BFA and various content of limestone powder, according to the previous studies which the addition of limestone powder will increase the compressive strength of concrete, some studies also reported similar results [7]. And the general trend between BSP10, 20, 30 also reflects this, the compressive strength increases with the increase of limestone powder content, but due to the performance of BFA30 excessive strength data makes this not obvious.

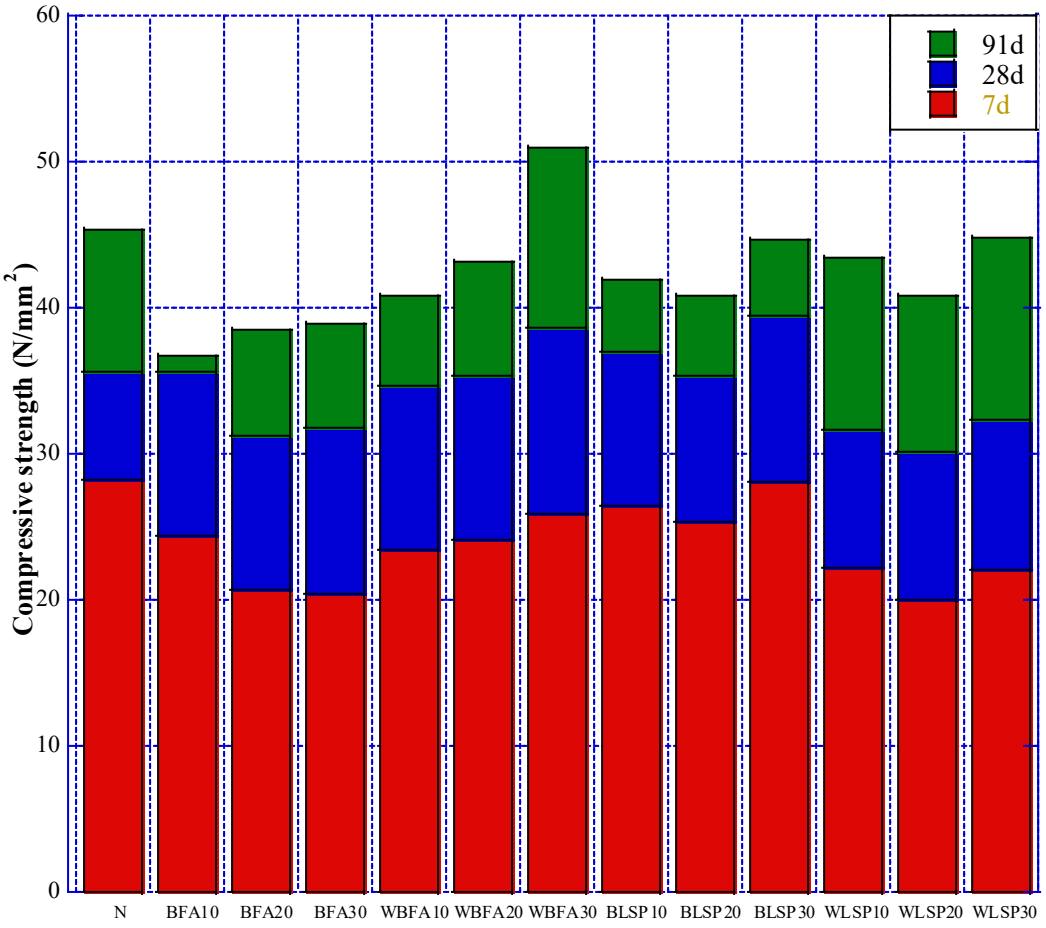

Fig. 4.1 The compressive strength of concrete containing biomass fly ash or limestone powder.

4.3.2 Drying shrinkage

The effects of biomass fly ash on drying shrinkage are shown in Fig 4.2. The results showed that the drying shrinkage of WFA and BFA developed rapidly and differed from N production after about ten days. Compared with N, the drying shrinkage of concrete with 30% WFA and 30% BFA increased by 41.4% and 31.6% at 126 days. And with the increase of the content of WFA and BFA, the drying shrinkage also increased gradually. Fig 4.3. showed the drying shrinkage of concrete with 30% biomass fly ash and various content limestone powder. As shown in Fig 4.3, the drying shrinkage of limestone powder group developed rapidly, and the gap with N was opened in about a week. And at 126 days, the drying shrinkage of concrete with limestone powder was larger than that of concrete with only 30% WFA or BFA. And with the increase of limestone powder content, the

drying shrinkage also increases. This shows that the addition of limestone powder increases the drying shrinkage of concrete. Some studied [2,3] also reported that the drying shrinkage of concrete increases with the increase of limestone powder content.

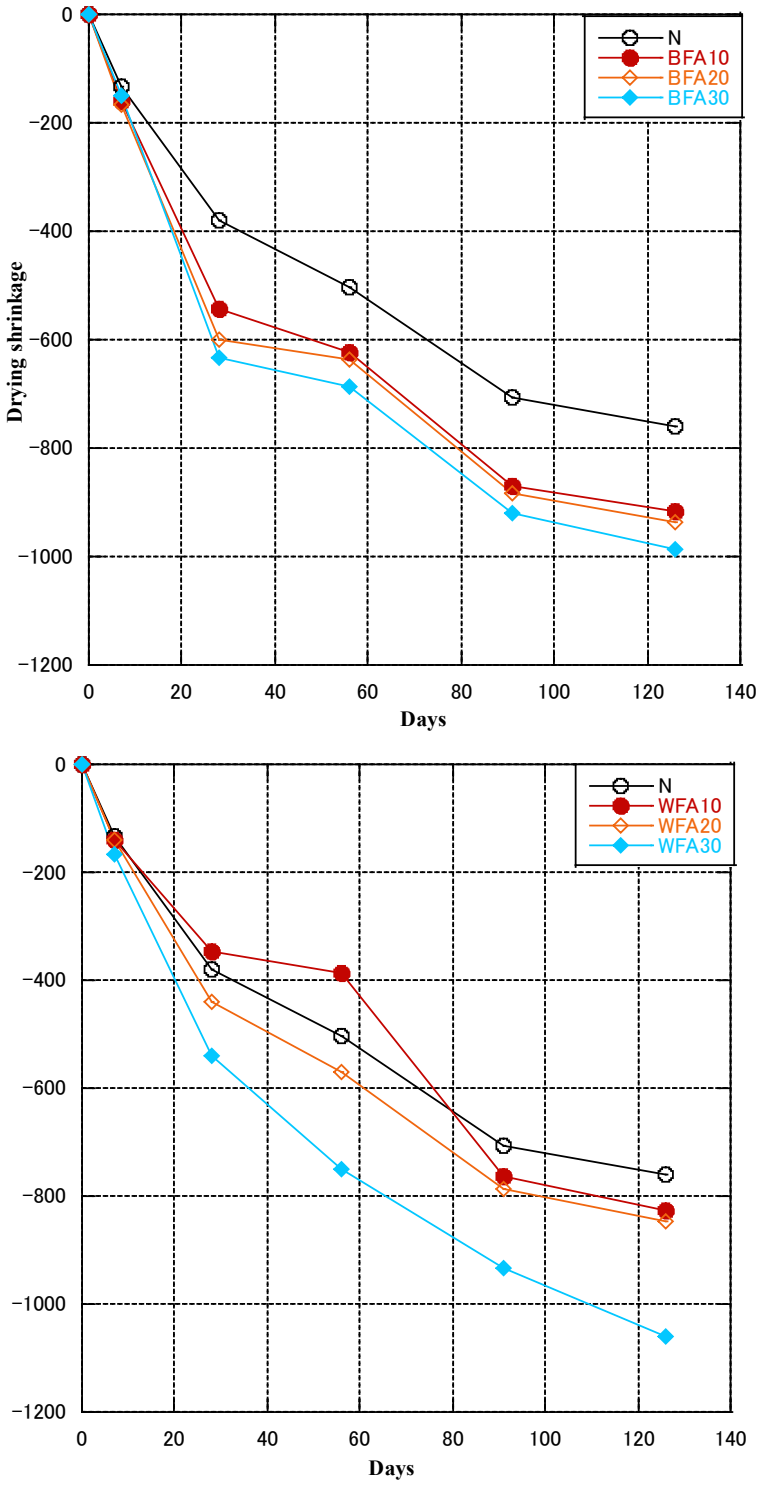

Fig. 4.2 The effect of biomass fly ash on drying shrinkage.

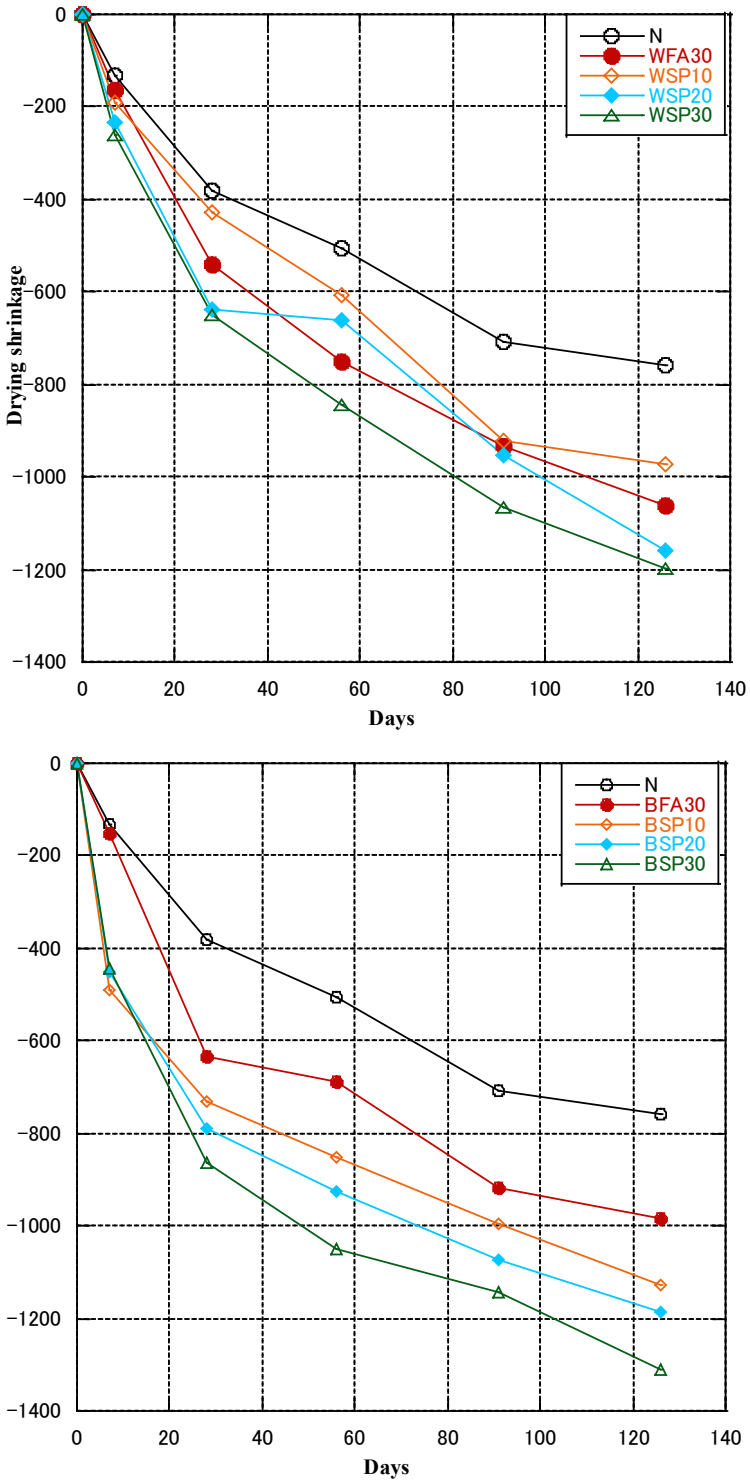

Fig 4.3 The effect of limestone powder on drying shrinkage.

4.3.3 Carbonation depth

The accelerated carbonation test results are given in Fig. 4.4. The increase in carbonation depth of WFA30 and BFA30 was about 41% and 27.6% to WFA10 and BFA10 at 56 days probably due to that pozzolanic reaction of biomass fly ash consumes Ca(OH)2 in concrete. As the increase of WFA or BFA in the mixture decreases the content of amorphous silica minerals that react with calcium hydroxide, enabling the formation of hydrated compounds and decreasing the carbonation resistance. So that contenting biomass fly ash led to a lower resistance of carbonation. For concrete containing 30% BFA or WFA with various content of limestone powder, as shown in Figure 4, it is clear that the carbonation depth of concrete with limestone powder is much higher than that of WFA30 and BFA30. The carbonization depth of WSP10, WSP20, WSP30 were 18.4%, 31.7%, and 30.2% higher than that of WFA30, respectively. The carbonization depths of BSP10, BSP20, and BSP30 were 26.1%, 53.1%, and 54.8% higher than that of BFA30, respectively.

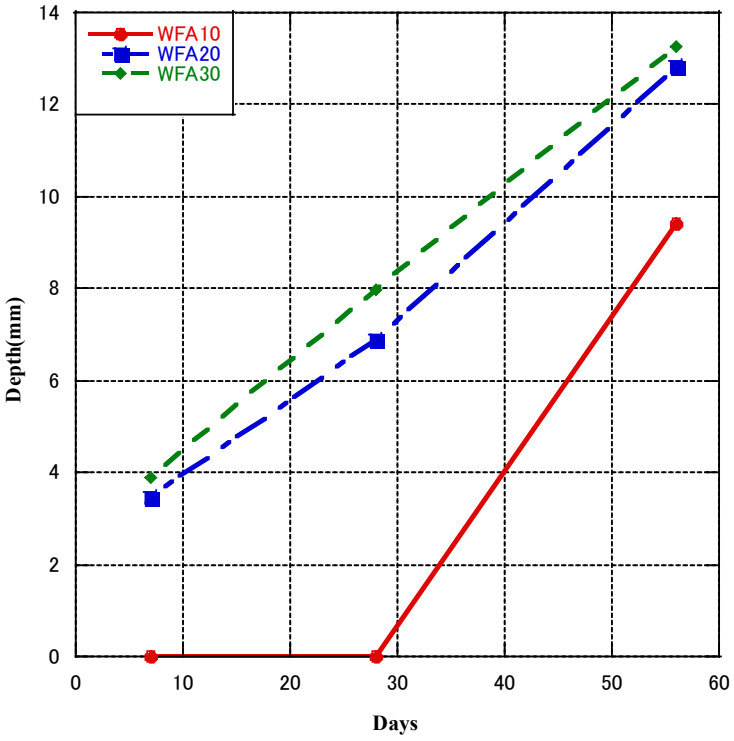

(a)

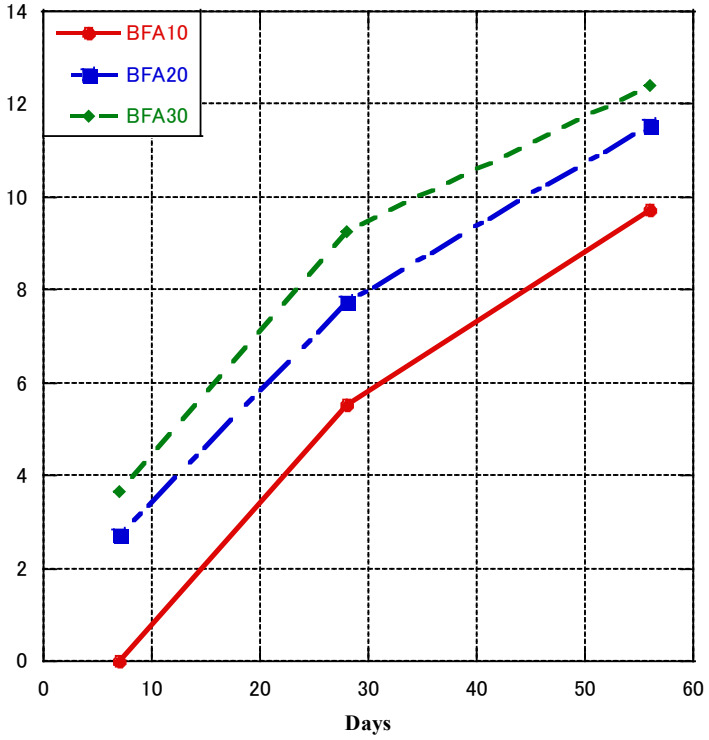
BFA10
BFA20
BFA30
14
12
10
8
6
4
2
0
0
10
20
30
40
50
60
Days

(b)

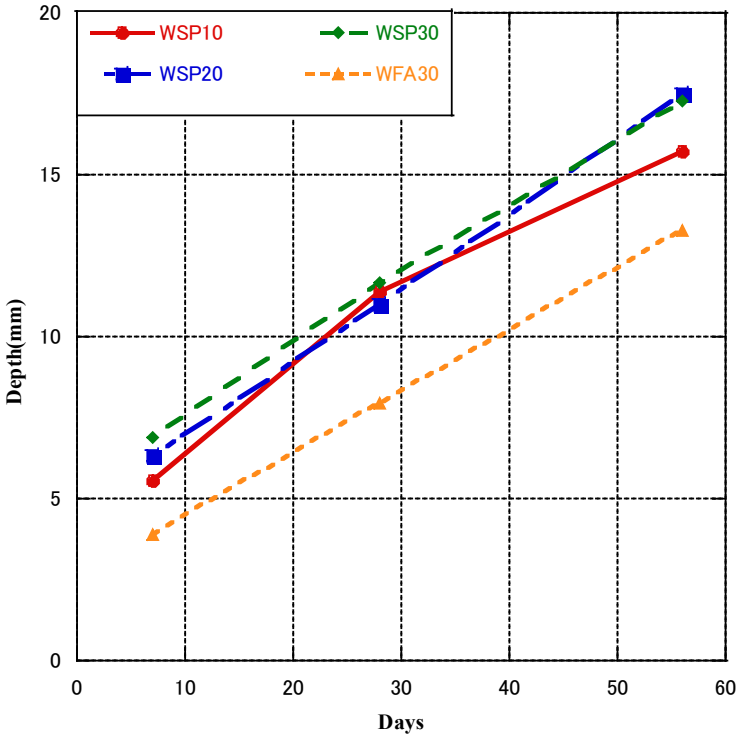
WSP10
WSP20
WSP30
WFA30
20
15
10
5
0
Depth(mm)
0
10
20
30
40
50
60
Days

(c)

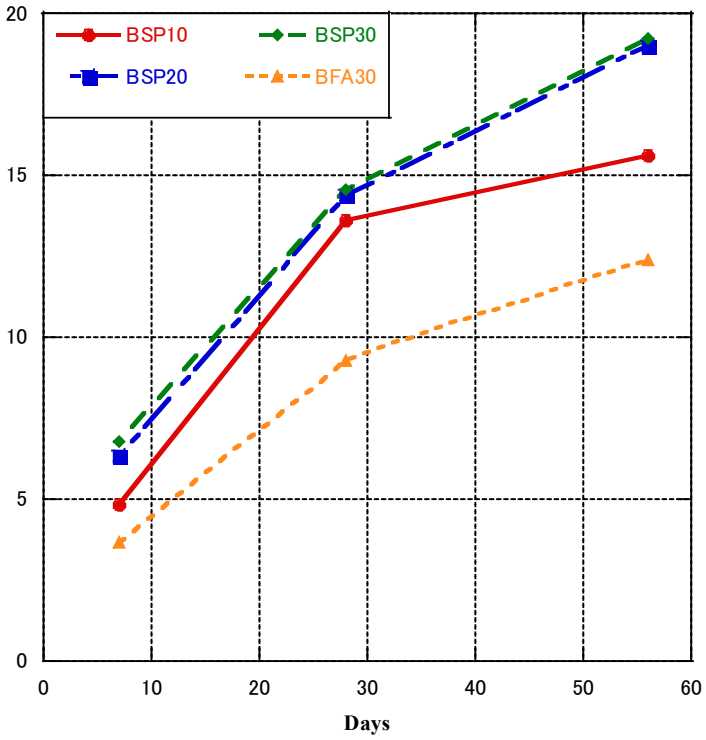

(d)

Fig. 4.4 Carbonation depth of concrete(a-d)

4.3.4 Pore structure of concrete

Fig. 4.5 shows the pore structure of concrete cured in water. The three columns for each mix ratio are 7, 28, 91 days from left to right. The pore volume of all concretes generally decreases with time. It can be seen from the figure that the addition of BFA or WFA to the concrete increases the pore volume of the concrete in each diameter range at 7 days. The total pore volume increases with the increase of BFA or WFA content, but the volume of pores greater than 0.05 decreases with the increase of BFA or WFA content, and the volume of pores less than 0.05 increases with the increase of BFA or WFA content. This may be due to that the pozzolanic reaction proceeds with the age of concrete, thereby modifying the pore structure of concrete. The limestone powder group also showed the similar results with BFA and WFA group, the volume of pore larger than 0.05 decreased and smaller than 0.05 increased. The reason is that the pore structure of the concrete is modified due to the filling effect of the limestone powder.

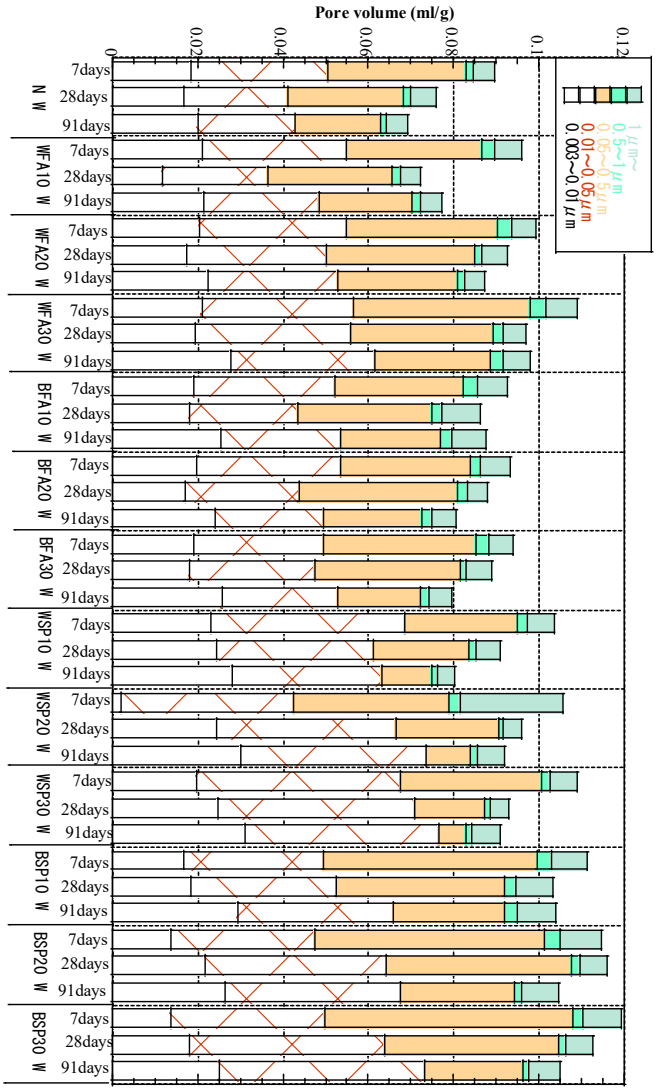

Fig. 4.5 The pore structure of concrete cured in water.

Fig. 4.6 shows the pore structure of concrete cured in air. Compared with the samples cured in water, the pore structure of the control group did not change significantly, but the pore structure of the other groups changed significantly. For concrete containing biomass fly ash or limestone powder, there is no major change in the total pore volume compared to curing in water, but the volume of pores with diameters less than 0.05μm decreases and the volume of pores with larger diameters increases.

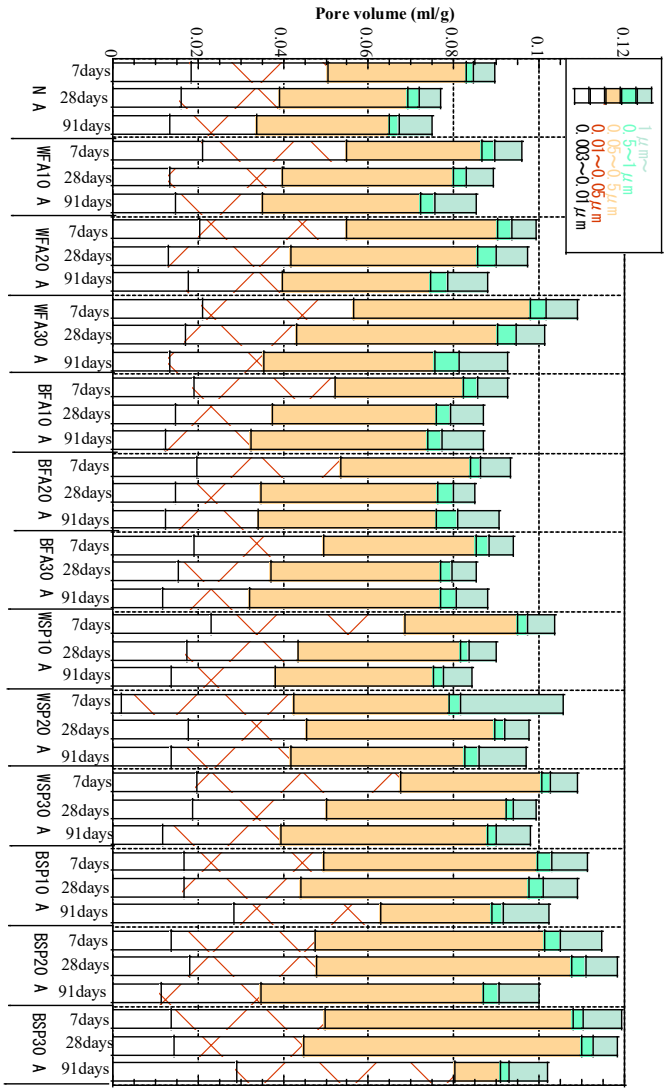

Fig. 4.6 The pore structure of concrete cured in air.

According to the variation trend of concrete pore structure, the correlation between drying shrinkage or compressive strength and pore structure was analyzed. Fig. 4.7 shows the relationship between 0.05 μm-36μm pore volume, total pore volume and compressive strength. The pore volume of pores with diameters ranging from 0.05μm to 36μm has the highest correlation with compressive strength, The largest correlation coefficient (R^2) reached 0.96. Because the fluctuation of the carbonization coefficient of concrete is too large, its correlation with the pore volume is not large, so we study the correlation between the carbonization coefficient of each mix and the pore volume. Fig. 4.8 shows the relationship between 0.003μm-0.05μm pore volume, total pore volume and concrete drying shrinkage. The pore volume of pores with diameters from 0.003μm to 0.05μm has the highest correlation with drying shrinkage, and the correlation coefficient (R^2) is 0.89.

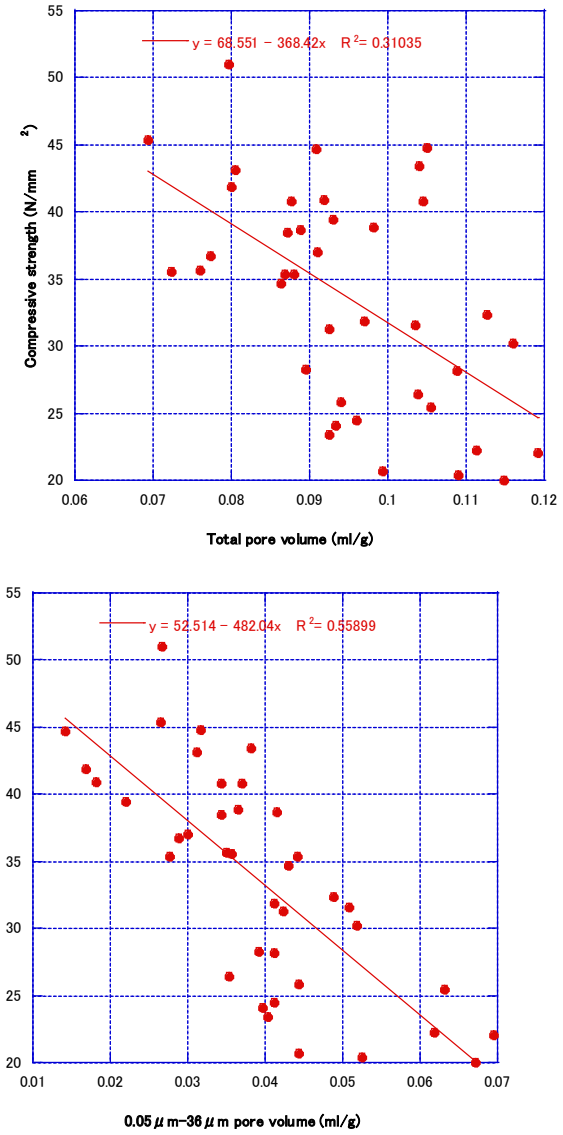

Fig. 4.7 Correlation between porosity and compressive strength

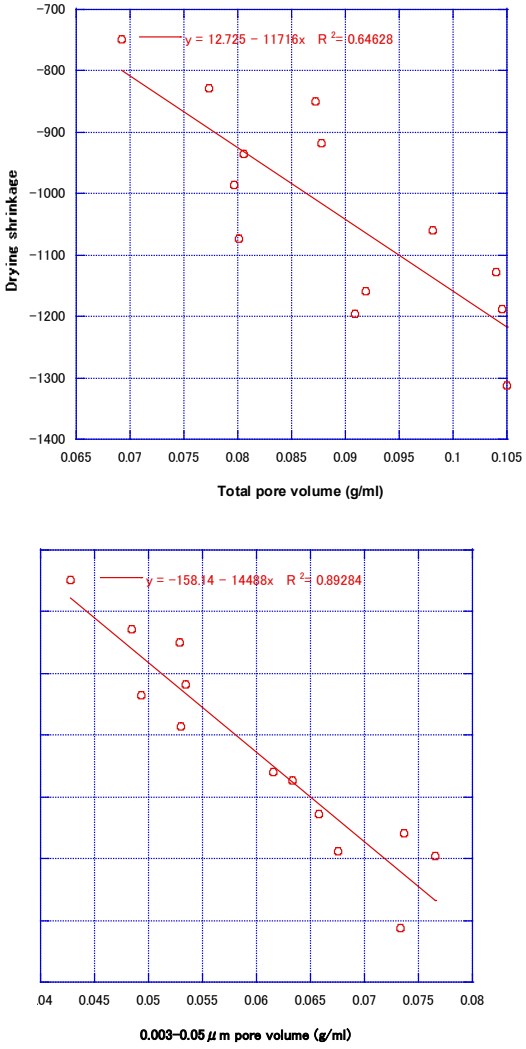

Fig. 4.8 Correlation between porosity and drying shrinkage.

4.4 Conclusion

Adding limestone powder to wood biomass fly ash concrete or blend biomass fly ash concrete increases the compressive strength of concrete in all ages. In addition, the drying shrinkage and carbonization depth increase with the limestone powder content increases. The using of wood biomass fly ash or blend biomass fly ash alone also increases the compressive strength within a certain range, but it is still smaller than the original concrete, and also increases the drying shrinkage and carbonization depth. Regarding porosity, adding blend biomass fly ash or wood biomass fly ash to concrete increases the total pore volume of concrete, and adding limestone powder increases the total pore volume but reduces the pore volume of pores with large diameter. Under water curing, the decrease of pore volume with larger pore volume is more obvious. The compressive strength of concrete has a higher correlation with the volume of 0.05~36μm pores and the drying shrinkage has a higher correlation with the volume of 0.003~0.05μm pores.

Reference

[1] Wang, S., Miller, A., Llamazos, E., Fonseca, F., & Baxter, L. (2008). Biomass fly ash in concrete: Mixture proportioning and mechanical properties. *Fuel*, *87*(3), 365-371.

[2] Wang, D., Shi, C., Farzadnia, N., Shi, Z., & Jia, H. (2018). A review on effects of limestone powder on the properties of concrete. *Construction and building materials*, *192*, 153-166.

[3] Menadi, B., Kenai, S., Khatib, J., & Aït-Mokhtar, A. (2009). Strength and durability of concrete incorporating crushed limestone sand. *Construction and Building Materials*, *23*(2), 625-633.

[4] Llorente, M. F., & García, J. C. (2006). Concentration of elements in woody and herbaceous biomass as a function of the dry ashing temperature. *Fuel*, *85*(9), 1273-1279.

[5] Martirena, F., Middendorf, B., Day, R. L., Gehrke, M., Roque, P., Martínez, L., & Betancourt, S. (2006). Rudimentary, low tech incinerators as a means to produce reactive pozzolan out of sugar cane straw. *Cement and Concrete Research*, *36*(6), 1056-1061.

[6] Benhelal, E., Zahedi, G., Shamsaei, E., & Bahadori, A. (2013). Global strategies and potentials to curb CO2 emissions in cement industry. *Journal of cleaner production*, *51*, 142-161.

[7] Joudi-Bahri, I., Lecomte, A., Ouezdou, M. B., & Achour, T. (2012). Use of limestone sands and fillers in concrete without superplasticizer. *Cement and Concrete Composites*, *34*(6), 771-780.

Chapter 5

THE EFFECT OF CEMENTITIOUS MATERIALS ON THE ENGINEERING PROPERTIES AND PORE STRUCTURE OF CONCRETE WITH RECYCLED FINE AGGREGATE

5.1 Introduction

Since the beginning of the 21st century, concrete has been a widely used building material, with yearly production estimated at 10 billion m3 [1]. Aggregate includes coarse aggregate (gravel) and fine aggregate (sand), accounting for about 60–80% of the total volume of concrete [2]. Because of the extensive use of concrete, the demand for aggregates has greatly increased [3], and the production of fine aggregates by crushing gravel has a high energy cost and causes problems with fresh concrete because of high angularity [4,5]. However, the demolition of old buildings generates a large amount of construction waste, at 850 to 880 Mt/year in the European Union [6,7], 317 Mt/year in the US, and 77 Mt/year in Japan [8]. Therefore, the rational use of recycled aggregate produced from waste concrete can simultaneously solve problems with building material supply and disposal. The building industry has previously approved the use of recycled coarse aggregates in concrete, with some limits, and in some countries, full substitution is permitted in certain circumstances. However, practically all existing standards and regulations prohibit the use of recycled fine aggregate (RFA) in the manufacturing of concrete and mortar [9]. Several studies have been conducted on the properties of RFA concrete. Gholampour et al. [10] studied concrete containing 25, 50, and 100% RFA, and their results showed that the compressive strength of the concrete decreased as the replacement rate of RFA increased, although the strength of concrete containing 25% RFA was slightly increased. Kirthik et al. [11] showed that increasing the content of RFA in concrete decreased its durability, and the best RFA content was 30%, which decreased shrinkage and porosity by 14% and 25%, respectively, and increased resistance to chlorine penetration by 21%. Khatib et al. [12] studied concrete containing 0, 25, 50, and 100% RFA, and showed that concrete containing 100% and 25% RFA had 30% and 15% lower compressive strength, respectively, compared with normal concrete, and increasing the RFA content increased shrinkage. The chloride permeability of concrete increases with the RFA content, whereas incorporating fly ash decreases chloride permeability [13–17]. Lovato et al. [18] reported that the carbonation depth of concrete increased with the content of RFA. Evangelista et al. [19] showed that in concrete containing 30% and 100% RFA, the carbonation depth increased by 40% and 100%, respectively, compared with normal concrete. Bu et al. [20] reviewed the literature on the durability of concrete containing RFA and found that the durability of concrete decreased as the replacement rate of RFA increased; for concrete containing 100% RFA, the drying shrinkage of was twice that of ordinary concrete and the carbonation depth increased by about 110%. The density and mechanical properties of concrete decreases as the RFA content increases [21,22]. In summary, exceeding an RFA content in concrete of 30% has several negative effects, including increased shrinkage, decreased compressive strength, decreased carbonation resistance, and increased water absorption. This has greatly limited the application of RFA in concrete, so finding a method that can modify the properties of RFA concrete should expand its applications in practical engineering. On the other hand, some studies have shown that the application of cementitious materials in concrete can improve durability, reduce long-term deformation, and modify the pore structure. It has been reported that cementitious materials enhance the workability, improve the performance of concrete at high temperatures, and inhibit the alkali-aggregate reaction [23]. Fly ash can be used instead of OPC to decrease porosity and reduce average pore size. Additionally, the volume of the gel's pores (less than 0.01 μm) increases with the fly ash content [24]. The fly ash content in concrete is about 20%, and its compressive strength is the largest [25]. Adding fly ash to concrete reduces porosity and changes water absorptivity and

chloride permeability [26]. High replacement volumes of fly ash increase resistance to chloride penetration substantially [27]. A fly ash content of 50% in concrete mixes offers benefits such as high resistance to chloride and sulfate attack, reduced alkali-silica expansion, and low heat generation [28]. The addition of fly ash to concrete can also reduce the creep [29,30] and drying shrinkage of concrete [26,31]. Özbay et al. [32] found that using GGBS in concrete increases the long-term mechanical properties of concrete. Additionally, using GGBS improves the deformation of concrete and increases the durability of concrete. Adding GGBS to concrete can reduce the porosity and modify the pore structure of the concrete [33]. Concrete containing GGBS tends to have lower shrinkage and creep than ordinary concrete [34–37]. In addition, some scholars have studied the use of cementitious materials in recycled aggregate concrete (fine and coarse). Qureshi et al. [38] studied recycled coarse aggregate concrete containing 20% fly ash and 30% GGBS, and their results showed that the concrete containing 20% fly ash and 30% GGBS had 2–10% and 5–12% higher compressive strength, respectively. Ahmad et al. [39] reported that the addition of GGBS to recycled coarse aggregate concrete can significantly increase its slump and strength. Kurad et al. [40] analyzed the effect of fly ash on concrete containing recycled fine and coarse aggregate and showed that the concrete had lower initial strength, but fly ash had little effect on its the strength. Ali et al. [41] showed that recycled coarse aggregate concrete containing 20–40% fly ash had a higher compressive strength at 180 days than control concrete. It has also been reported that fly ash improves mechanical properties and significantly reduces water absorption and chloride penetration of recycled coarse aggregate concrete [42]. Kou et al. [43] reported that GGBS and FA had great contributions to the performance of recycled coarse aggregate concrete. Anastasiou et al. [44] studied RFA concrete containing fly ash and showed that fly ash improves long-term strength and decreases water penetration under pressure, and chloride ion penetration. In conclusion, using cementitious materials such as fly ash or GGBS in concrete can improve durability, reduce long-term deformation, and modify pore structure. However, most researchers paid attention to recycled coarse aggregate. Research on the effect of cementitious materials on RFA concrete is still insufficient and requires further investigation. In addition, studies on the effect of GGBS and fly ash have mainly focused on mechanical properties and durability, and little research has been done on microscopic pore structure. The purpose of this study was to enhance the compressive strength and durability performance of RFA concrete by adding cementitious materials, and to analyze the influence of microstructure on the mechanical properties and durability of RFA concrete. The optimal addition rate of fly ash or GGBS in RFA concrete was obtained. After adding supplementary cementitious materials, RFA concrete had higher strength and lower drying shrinkage than ordinary concrete. In addition, the influence of pore volume of different pore diameters on the compressive strength and durability of RFA concrete was analyzed. The micropores in RFA concrete were divided into harmful pores, small harmful pores, and harmless pores according to diameter. The results of this study will provide a basis for the application of RFA in practical engineering.

5.2 Materials and experimental program

5.2.1 Materials properties

Sea sand (S) and M standard RFA conforming to JIS A 5022 [45] were used as fine aggregate. RFA was made from waste concrete after crushing, grinding and classifying. Crushed stone aggregate was used for coarse aggregate (G). Table 5.1 shows the physical properties of the fine and coarse aggregates.

Table 5.1. Properties of the fine and coarse aggregates.

Property	Coarse aggregate	Sea sand	RFA	JIS A5022 (M)
Oven-dried density (g/cm^3)	2.69	2.59	2.37	> 2.2
Fineness modulus	6.9	2.41	2.58	_
Water absorption (%)	1.41	1.04	6.86	< 7.0
Void content (%)	43.3	38.8	32.6	_

Table 5.2. The properties of the cement, FA, MFA, and GGBS

	FA	MFA	GGBS	Cement
SiO_2 (%)	53.8	62.4	32.7	21.5
Al_2O_3 (%)	13.5	17.6	13.4	5.4
Fe_2O_3 (%)	13	8.7	0.5	3.0
CaO (%)	8.99	2.3	41.6	64.9
SO_3 (%)	0.49	_	6.9	1.4
MgO (%)	1.48	1.32	0.3	2.1
Loss on ignition (%)	2.1	1.2	0.6	0.8
Density (g/cm^3)	2.31	2.18	2.91	3.16
Blaine specific area (cm^2/g)	3270	5480	4100	3000

OPC as defined in JIS R 5210 [46], supplementary cementitious materials were fly ash (FA) conforming to Class II in JIS A 6201 [47], fly ash with a higher carbon content from a local power plant that had its carbon content reduced by the floatation method (modified fly ash [MFA]), and GGBS as defined in JIS A 6206 [48]. The properties of cement, FA, MFA, and GGBS are shown in Table 5.2.

5.2.2 Mix proportions

The mix proportions of the concrete cast in this experiment are shown in Table 5.3. The design strength of concrete was 27 MPa, according to JASS 5 [49], water-binder ratio was set to 0.55, and the unit water volume was 180 kg/m^3, the unit coarse aggregate amount was 945 kg/m^3. A total of 12 concrete mixes were prepared: the control concrete, concrete containing sea sand replaced with RFA (50% by volume), four mixes containing cement replaced with FA or MFA (10% and 15% by weight), two mixes containing cement re-placed with GGBS (30% and 45% by weight), and four mixes with cement replaced (30% and 45% by weight) by FA and GGBS using ternary binders (the ratio of FA to GGBS is 1 or 0.5). In the process of concrete production, the aggregates were all surface dry.

5.2.3 Experiment method

Table 5.3. Mix proportions.

Type	W/B	Unit mass(kg/m³)							
		W	C	FA	MFA	GGBS	S	RFA	G
N	0.55	180	327	0	0	0	832	0	945
M50	0.55	180	327	0	0	0	416	379	945
M50FA10	0.55	180	294	33	0	0	411	375	945
M50FA15	0.55	180	278	49	0	0	409	372	945
M50MFA10	0.55	180	294	0	33	0	411	375	945
M50MFA15	0.55	180	278	0	49	0	409	372	945
M50BS30	0.55	180	229	0	0	98	413	376	945
M50BS45	0.55	180	180	0	0	147	411	375	945
M50FA10BS20	0.55	180	229	33	0	65	409	373	945
M50FA15BS15	0.55	180	229	49	0	49	407	371	945
M50FA15BS30	0.55	180	180	49	0	98	405	369	945
M50FA22.5BS22.5	0.55	180	180	74	0	74	402	367	945

According to JIS A 1108 [50], testing for compressive strength was performed on cylindrical specimens that were 100 mm in diameter and 200 mm in height. The specimens were cast in a mold and kept for 24 h in a room at 20 °C and 60% RH before demolding. The specimens were then cured in water at 20 °C until the age required for the test. The compressive strength was tested at 7, 28, and 91 days. In order to avoid impact loads on concrete specimens, the loading rate was set at 0.6 ± 0.4 MPa per second. Three specimens were tested for each group, and the average value was taken.

The “Method of measurement for length change of mortar and concrete” described in JIS A 1129-2 [51] was used to conduct the drying shrinkage test, and prismatic specimens measuring 100 × 100 × 400 mm were cast. The specimens were demolded 1 day after casting, and then cured in water at 20 °C until 7 days. At the age of 7 days, a stainless-steel chip was attached to both ends of the specimens, and length of the specimen was measured as the base length. The specimens were then cured in a constant humidity and temperature chamber (20 ± 1.0 °C; RH, 60 ± 5%) and tested until 182 days.

The accelerated carbonation experiment was conducted according to JIS A1153 [52] using 40 × 40 × 160 mm test specimens. The specimens were cured in water at 20 °C for 4 weeks, and then placed in a thermo-hygrostat at 20 °C and 60% relative humidity for 4 weeks. After curing, the specimens were placed in a carbonation chamber at a CO2 concentration of 2.0%, 20 °C, and RH of 65% for 7, 28, 56, and 91 days. The depth of carbonation was tested at a specified age by splitting the specimen at right angles to the length di-rection, and immediately spraying the split surface with 1% phenolphthalein solution to measure the depth-stained red purple. The carbonation depth of was measured at 5 points on each side (total of 10 points), and the average was taken as the carbonation

depth. The carbonation depth can be modelled by Equation (1):

$$Xc = K\sqrt{t} \quad (1)$$

where Xc is carbonation depth (mm), t is carbonation age (weeks), and K is the carbona-tion coefficient (mm/weeks $^{0.5}$).

Porosity was measured by mercury intrusion porosimetry (MIP). The samples were prepared by crushing a specimen (φ100 × 200 mm) that had been cured in water at 20 °C to the specific material age and sieving the powder to obtain particles of 2.5 to 5.0 mm. The hydration reaction was stopped by immersion in acetone, and then the powder was dried under vacuum for 72 h before use. The porosity was tested at 7, 28, and 91 days to investigate the development of the pore structure of concrete.

5.3 Results and discussion

5.3.1 Compressive strength

Figure 5.1 a,b shows the compressive strength of RFA concrete containing only FA or MFA. The concrete containing 50% RFA had lower compressive strength than the control concrete. Compared with the control concrete, the compressive strength at 7, 28, and 91 days decreased by 2.8, 8.9, and 17.6%, respectively. Khatib [12] reported that when sand was substituted with RFA, the long-term strength was systematically decreased. At a replacement level of 100%, this reduction might approach 30%. A reduction of only 15% resulted from a replacement level of 25%. This was attributable to RFA's porous structure and higher water absorption [24]. The FA specimens, consisting of RFA concrete containing FA, had a lower compressive strength than the M50 concrete at 7 and 28 days, and the MFA specimens showed similar results. The compressive strength of the concrete containing 15% FA was lower than that of the concrete containing 10% FA at 7 and 28 days. However, the decrease of compressive strength at 91 days was not significant. These decreases can be attributed to fly ash's diluting effect and early-stage poor reactivity [53–57]. The results are in good agreement with the results of some previous studies, which showed that the long-term mechanical characteristics of fly ash concrete had clearly improved [54,58–60]. The RFA concrete specimens containing MFA had a higher 91-day compressive strength than the M50 concrete. Compared with M50 concrete, the compressive strength of MFA10 and MFA15 concrete at 91 days increased by 10.93% and 14.04%, respectively. Therefore, the removal of unburned carbon from fly ash by flotation is an effective method for using fly ash with high carbon content in concrete. As shown in Table 5.2, MFA had a larger specific surface area than ordinary fly ash, which may be an important reason for the better performance of MFA than ordinary fly ash. In addition, the 91-day compressive strength of M50FA10 concrete was 4.8% lower than that of M50 concrete, whereas that of M50FA15 concrete was similar. According to previous studies, the results showed that the reaction degree of fly ash varied depending on the fly ash properties, from less than 4% at 3 days to 9–23% at 28 days to 26–33% at 180 days [53,61–64]. The pozzolanic reaction between fly ash and $Ca(OH)_2$ might result in abundant CSH, resulting in modified pore structure and improved long-term strength, which is ultimately responsible for the improvement in the mechanical performance [56,63,65]. The results of pore structure in this experiment also indicated the pozzolanic reaction. Figure 5.1c shows the compressive strength of RFA

concrete containing only GGBS. The compressive strengths of M50BS30 and M50BS45 were lower than that of the M50 and control concrete at 7 days. The 28-day compressive strengths of M50BS30 and M50BS45 were higher than that of M50, but lower than that of the control concrete. Both M50BS30 and M50BS45 had a higher 91-day compressive strength than M50, and M50BS45 had a higher 91-day compressive strength than the control concrete. Therefore, using GGBS in RFA concrete decreased the 7-day compressive strength, but did not affect the 28-day compressive strength. In addition, GGBS increased the 91-day compressive strength, and the compressive strength increased with the GGBS content. Some studies also reported similar results [37,66,67]; the early strength of GGBS concrete was lower, and with the increase of curing time, the compressive strength of GGBS concrete increased faster than that of the normal concrete. The compressive strength increases of GGBS concrete took longer due to the slow pozzolanic reaction [66,68]. As shown in Table 2, GGBS has a larger specific surface area and higher CaO content than fly ash. The GGBS group exhibited higher compressive strength than the fly ash group due to the higher CaO content and larger specific surface a rea of GGBS, which resulted in a better pozzolanic reaction rate in GGBS-based concrete. Figure 5.1d shows that the compressive strength of RFA concrete containing 30% blended cementitious materials was lower at 7 and 28 days than M50 concrete. The compressive strengths of M50BS30, M50FA10BS20, and M50FA15BS15 concrete were around 23% lower than that of M50 concrete at 7 days, although at 28 days those of M50FA10BS20 and M50FA15BS15 concrete were 2.6% and 7.9% lower, respectively, and that of M50BS30 was similar. However, at 91 days, RFA concrete containing 30% blended cementitious materials had a higher compressive strength than M50 concrete. Compared with M50 concrete, the compressive strengths of M50BS30, M50FA10BS20, and M50FA15BS15 concrete increased by 9.8, 10.2, and 17.5%, respectively. Figure 5.1e shows that the concrete containing 45% blended cementitious materials. In addition, M50BS45 concrete had a 7-day compressive strength 24.1% lower than that of M50, a 28-day compressive strength 5.7% higher than that of M50 and similar to that of N, and a 91-day compressive strength 31.6% higher than M50 and 8.5% higher than N.M50BS45 was the only specimen that had a higher compressive strength than N at 91 days, and had the highest compressive strength at 91 days in this experiment. Compared with M50, the 7-day compressive strengths of M50FA15BS30 and M50FA22.5BS22.5 were 32.9% and 39.8% lower, and the 28-day compressive strengths were 9.8% and 18.4% lower, respectively. The compressive strength of every mixture proportion was higher than that of M50 at 91 days; M50BS45, M50FA15BS30, and M50FA22.5BS22.5 concrete were 31.6, 12.6, and 4.0% higher, respectively. Zhao et al. [69] researched concrete containing 30, 40, and 50% cementitious materials (fly ash and GGBS) and showed that the compressive strength of concrete decreased with the increase of cementitious materials content. In addition, the 28-day compressive strength increased with the increase of fly ash content at the same content of cementitious materials content. Geso ˘glu et al. [70] found that concrete incorporating 10% fly ash and 10% GGBS had the highest compressive strength. Experimental results showed that adding cementitious materials to recycled aggregate concrete helps to increase its strength; especially M50BS45 and M50FA15BS15 exhibited higher and similar compressive strength than normal concrete, respectively. Therefore, it can be said that adding GGBS and fly ash can increase the compressive strength of RFA concrete, but the mixing ratio of GGBS and fly ash needs further study. Figure 5.1f shows the compressive strength of RFA concrete with constant FA content (10% and 15%). In RFA concrete containing 10–15% FA, adding 15–30% GGBS resulted

in the 7-day compressive strength being similar, the 28-day compressive strength increased by about 20%, and the 91-day compressive strength increased by about 15% compared with M50FA10, M50FA15 specimens. Therefore, adding GGBS to concrete containing FA can address the problem of low 28-day compressive strength of FA concrete and increase the 91-day compressive strength.

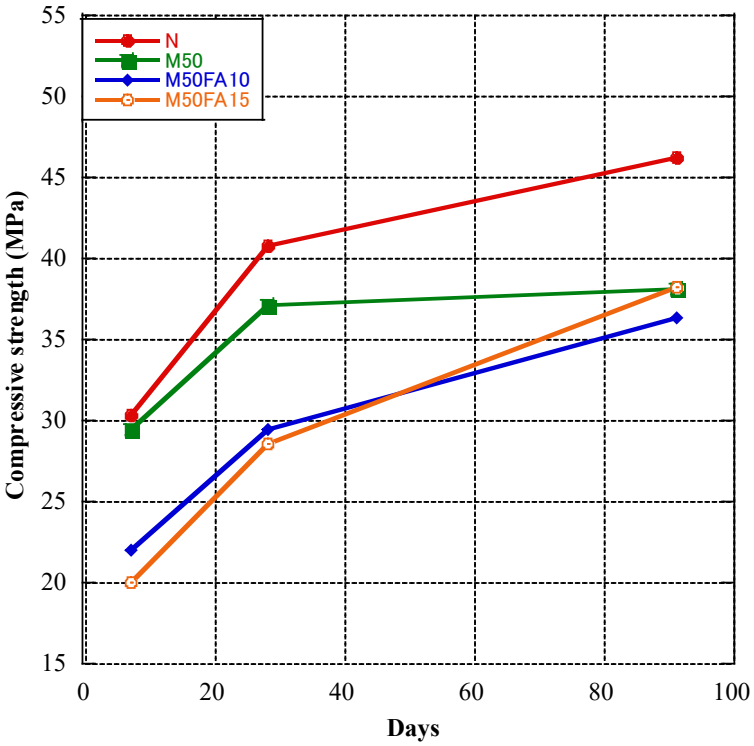

(a)

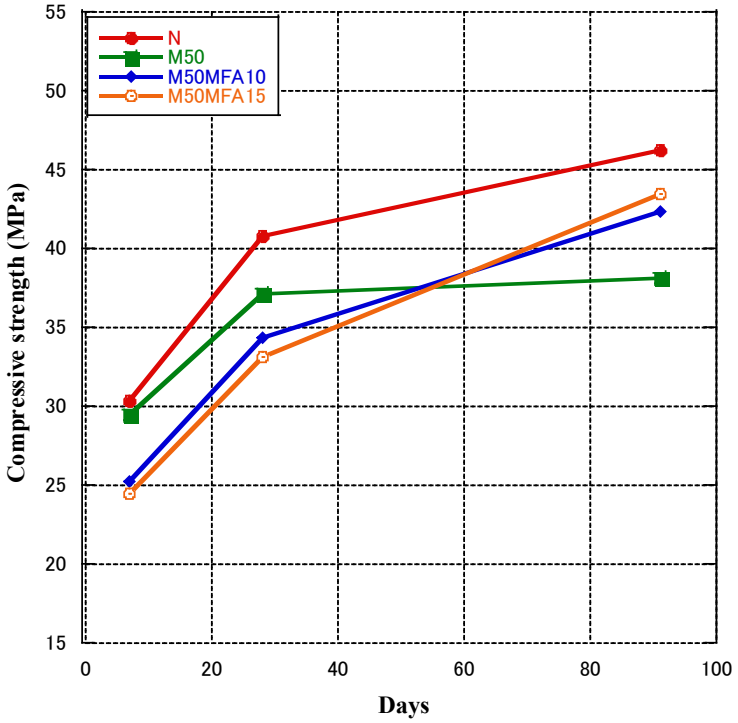

(b)

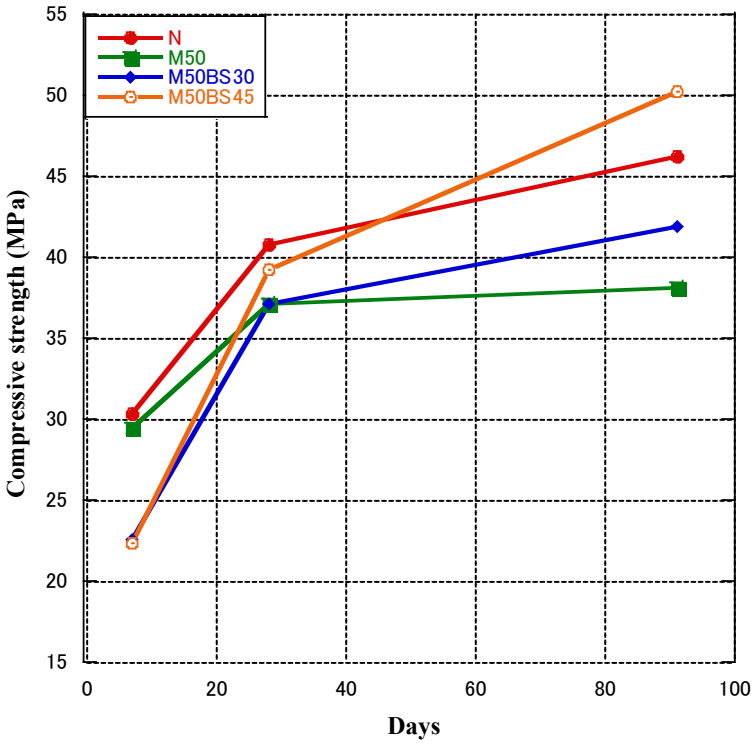
N
M50
M50BS30
M50BS45
Compressive strength (MPa)
Days
55
50
45
40
35
30
25
20
15
0
20
40
60
80
100

(c)

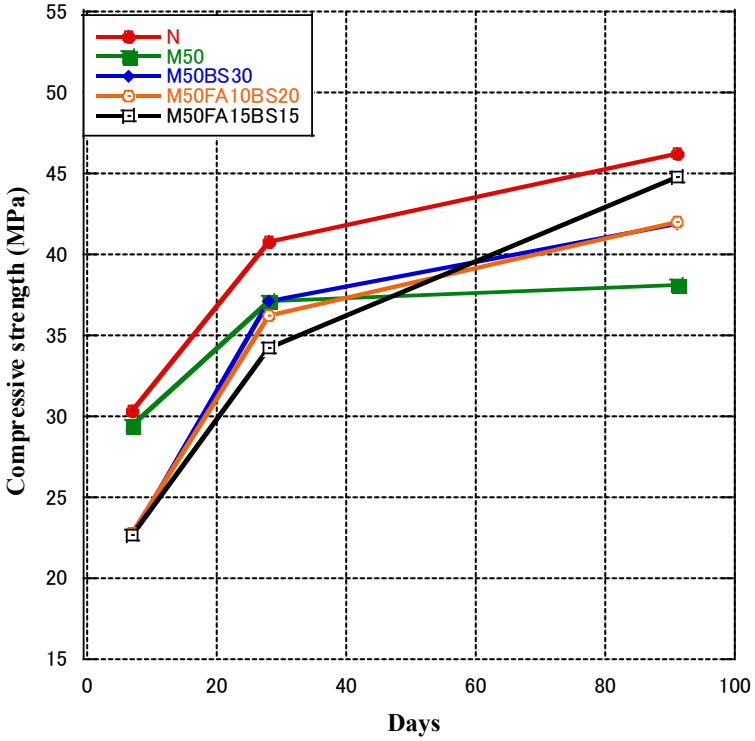
N
M50
M50BS30
M50FA10BS20
M50FA15BS15
Compressive strength (MPa)
Days
55
50
45
40
35
30
25
20
15
0
20
40
60
80
100

(d)

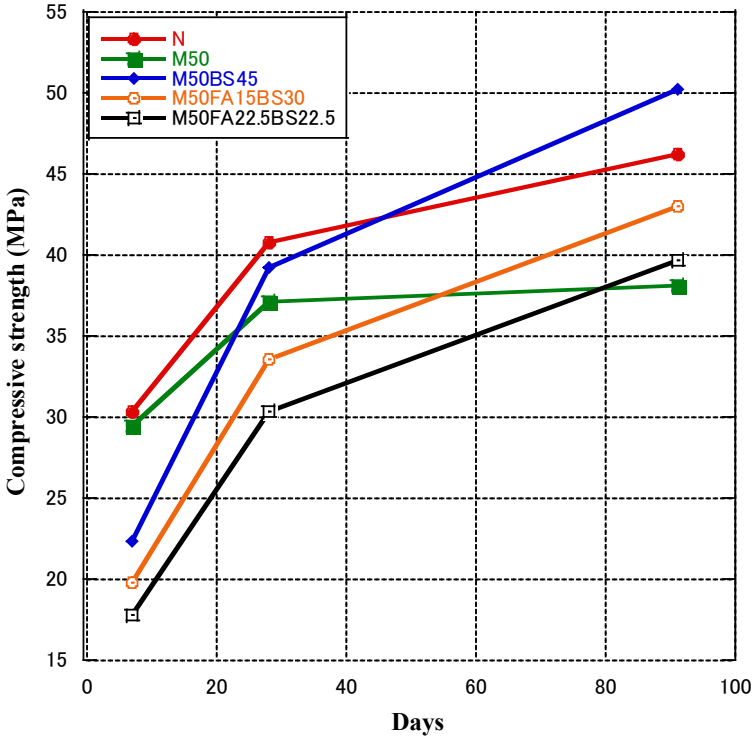

(e)

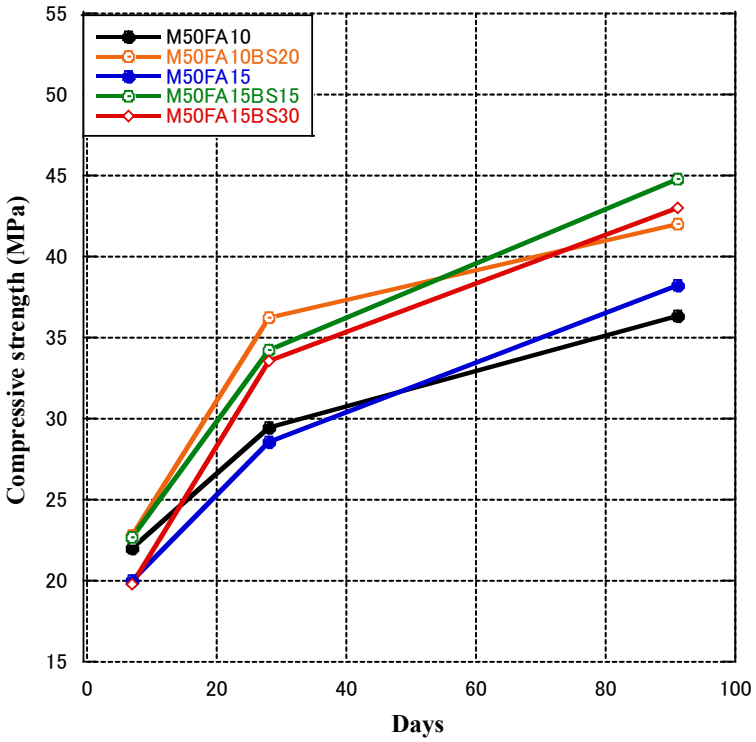

(f)

Fig. 1. Compressive strength of concrete with cementitious materials

5.3.2 Drying shrinkage

Figure 5.2a shows the drying shrinkage of the FA specimens. The drying shrinkage of M50 developed quickly, diverged from the control concrete after 1 week, and was 10.85% higher after 182 days, Kirthika et al. [11] reported the similar results. It is common knowledge that the greatest cause of drying shrinkage is the water content of the concrete mixture [71]. The higher drying shrinkage of RFA concrete was due, in part, to RFA's higher water absorption, and because a large amount of fines in the pores and gaps of coarse particles of RFA increased the paste volume of the concrete [2]. The drying shrinkage of RFA concrete containing FA was suppressed compared with M50; the drying shrinkages of M50FA10 and M50FA15 were 2.3% and 7.1% lower after 182 days, respectively. Thus, adding FA to RFA concrete decreased the drying shrinkage and the decrease was greater as the FA content increased. Figure 5.2b shows the drying shrinkage of the MFA specimens. Both M50MFA10 and M50MFA15 concrete had lower drying shrinkages than M50, which were similar to that of the control concrete. Compared with M50, the drying shrinkages of M50MFA10 and M50MFA15 were 9.5% and 9.3% lower at 182 days, respectively. Saha et al. [26], and Wang et al. [72] also reported similar results in that the drying shrinkage decreased with increasing fly ash content. Adding fly ash to concrete lowered the cement concentration and delayed the development of shrinkage, which caused a modest reduction in early drying shrinkage [31,73]. The results of pore structure in this experiment showed that fly ash modified the pore structure of concrete, which inhibited evaporation of water and reduced drying shrinkage.

Figure 5.2c shows the drying shrinkage of the GGBS specimens. GGBS reduced the drying shrinkage considerably. The drying shrinkage of M50BS30 at 182 days was 8.6% lower than that of M50 and was similar to that of the control concrete. Furthermore, at 182 days, the drying shrinkage of M50BS45 was the lowest, was 24% lower than that of M50 and 15.8% lower than that of the control concrete. Some studies also reported similar results [37,74,75], adding GGBS inhibited the development of drying shrinkage of concrete. Adding GGBS to concrete reduced the porosity and modified the pore structure of the concrete [33,76]. On the one hand, GGBS had a larger specific surface area than fly ash, and on the other hand, GGBS had a higher CaO content than fly ash, so the activity of GGBS was higher, and the inhibition effect on drying shrinkage was greater. Figure 5.2d shows the drying shrinkage of the 30% blended cementitious materials specimens. The cementitious materials reduced the drying shrinkage, and the mixture of GGBS and FA had a greater effect. The drying shrinkage of M50FA10BS20 and M50FA15BS15 at 182 days was 14.8% and 24.7% lower than that of M50, and 5.6% and 16.5% lower than that of the control concrete, respectively. Figure 5.2e shows the drying shrinkage results of 45% blended cementitious material specimens. In contrast to the 30% blended cementitious material specimens, M50FA15BS30 had a similar 182-day drying shrinkage compared to M50BS45, whereas the 182-day shrinkage value of M50FA22.5BS22.5 was 16.2% higher than that of M50BS45. Therefore, for a cementitious materials content of 30–45%, the reduction in drying shrinkage was higher for GGBS mixed with FA, although FA contents higher than 15% increased the drying shrinkage. Zhao et al. [69] reported that comparing concrete with the simultaneous addition of fly ash and GGBS to cement-only concrete, shrinkage was reduced by 15%. Weng et al. [77] studied concrete with binary cementitious materials (FA, GGBS) and showed that drying shrinkage of concrete was less with binary FA and GGBS than with GGBS alone. Due to

GGBS's fineness and hydration activity, which aid in the formation of a compact microstructure and stop water evaporating from the concrete, drying shrinkage of concrete is significantly reduced [77]. Adding fly ash or GGBS to concrete promoted the hydration of cement and modified the microstructure of concrete, lowing permeability of free water, so that drying shrinkage decreased significantly [69].

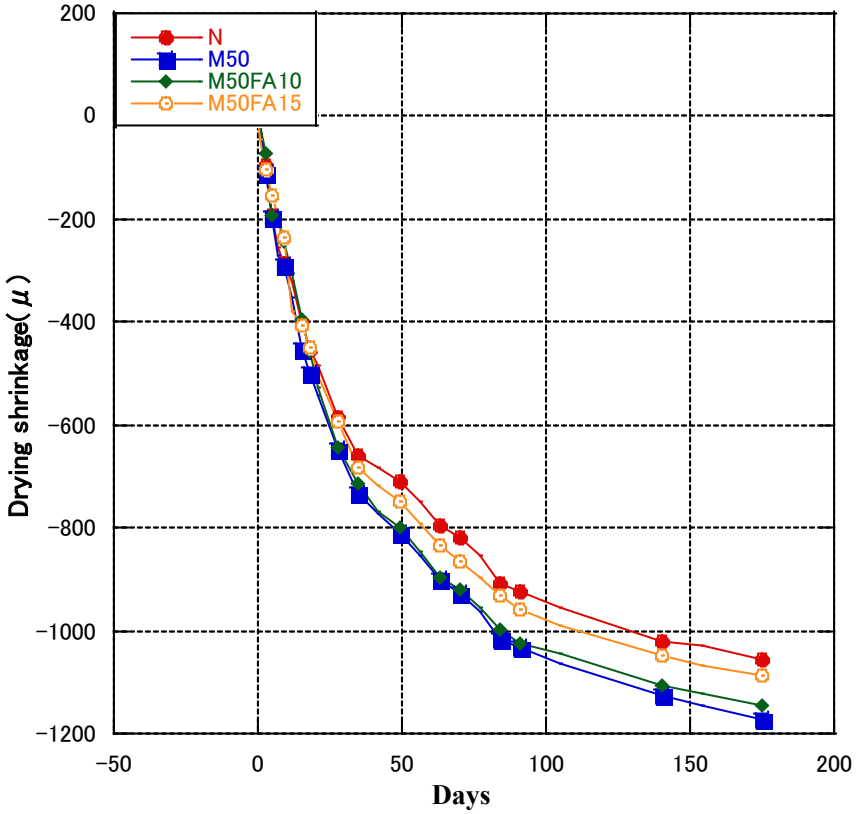

(a)

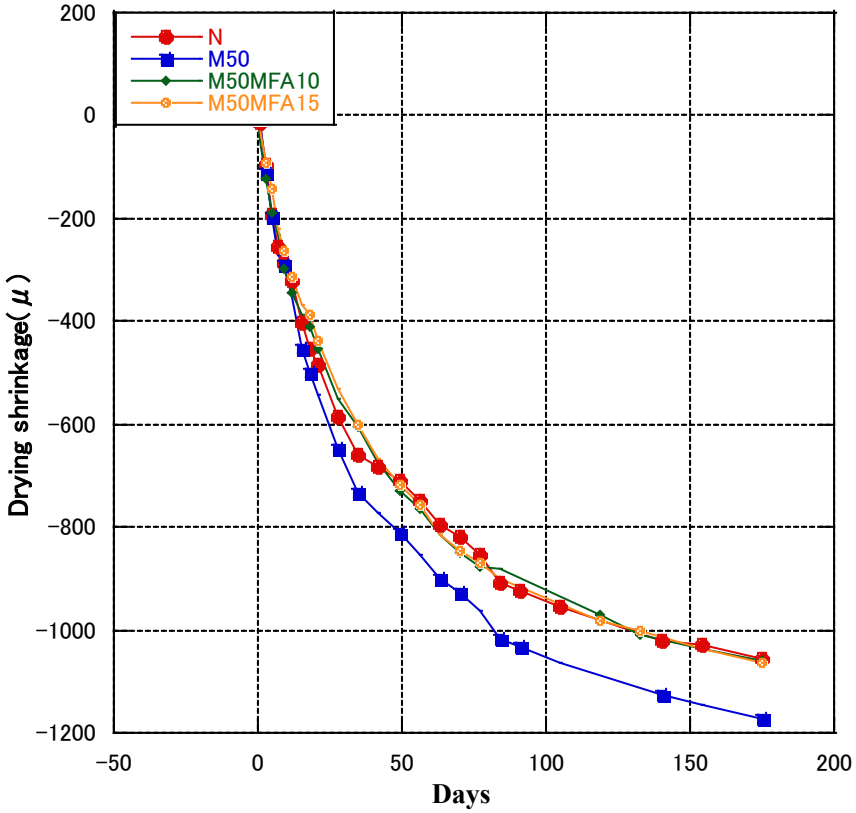
N
M50
M50MFA10
M50MFA15
Drying shrinkage(μ)
Days
200
0
-200
-400
-600
-800
-1000
-1200
-50
0
50
100
150
200

(b)

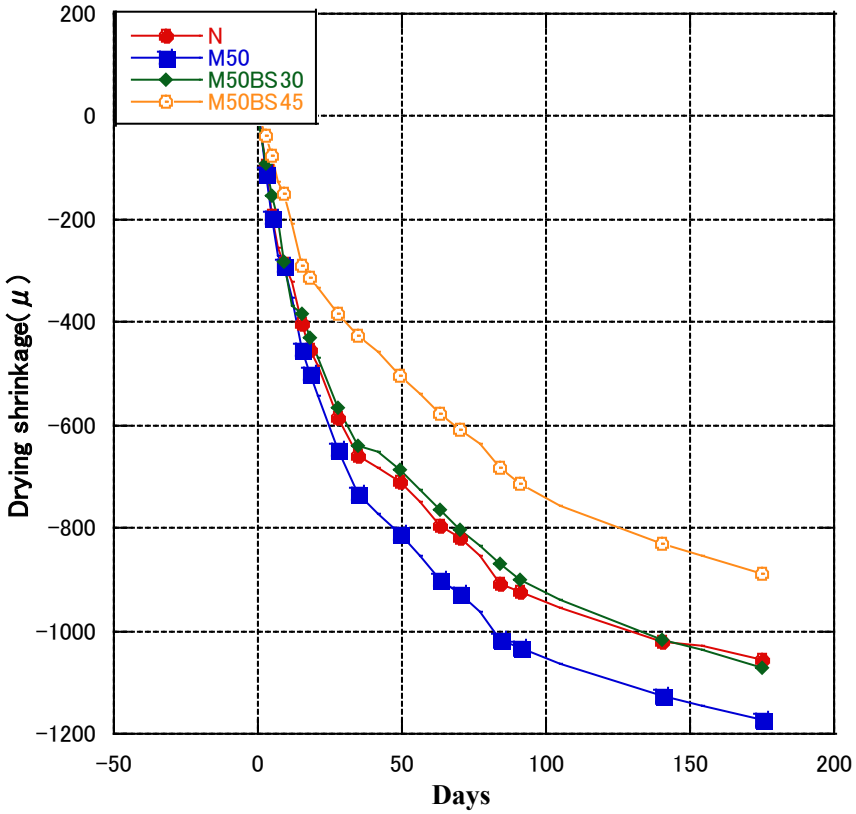
N
M50
M50BS30
M50BS45
Drying shrinkage(μ)
Days
200
0
-200
-400
-600
-800
-1000
-1200
-50
0
50
100
150
200

(c)

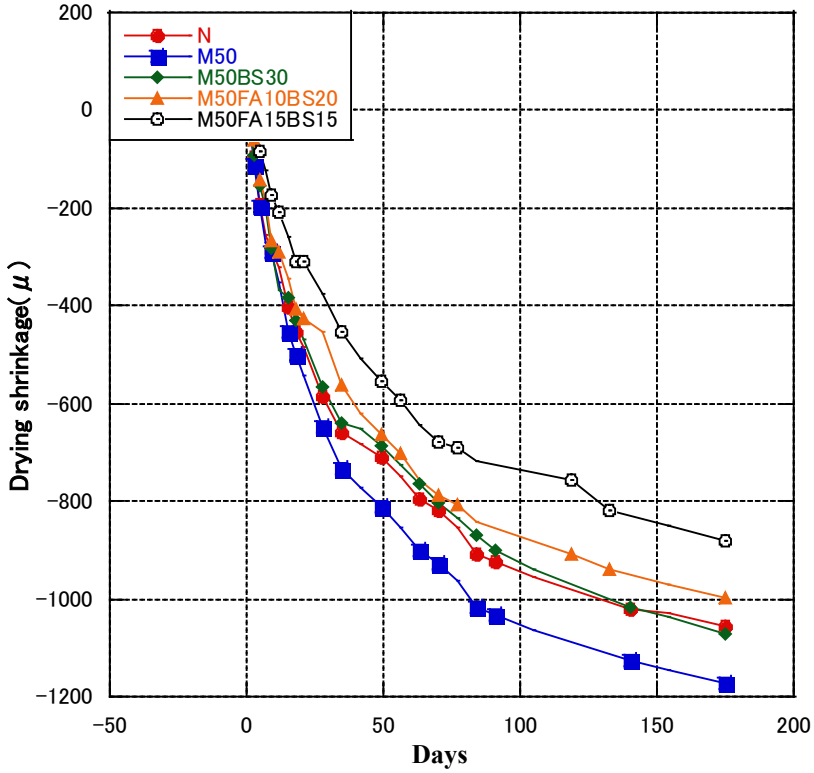

(d)

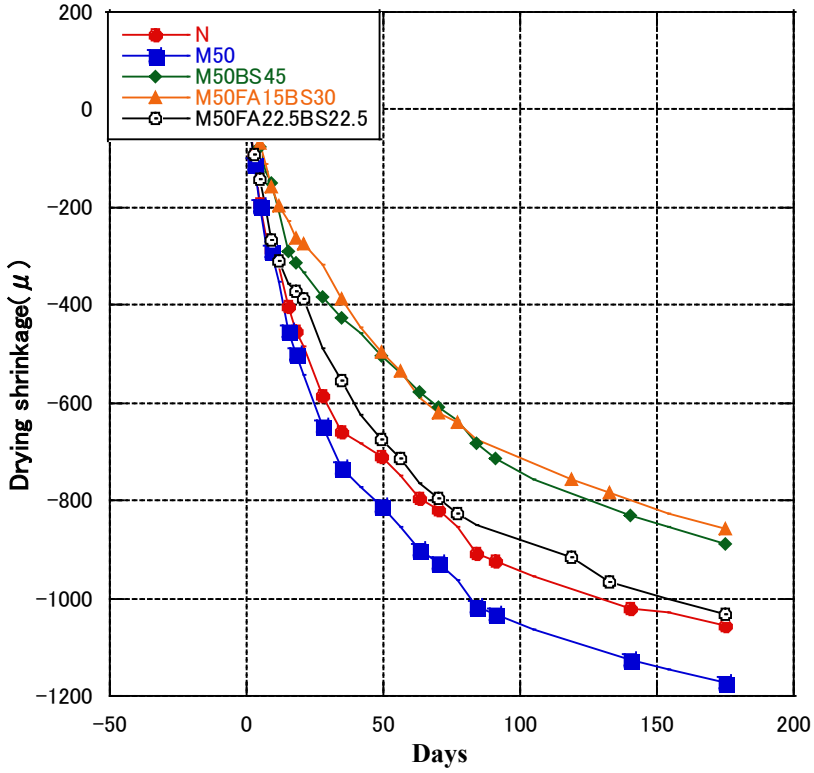

(e)

Fig. 5.2. Drying shrinkage of concrete with cementitious materials

5.3.3 Accelerated carbonation

The accelerated carbonation experiment results are shown in Figure 5.3a–e. The carbonation depth of M50 was about 27.8% greater than that of the normal concrete at 91 days, probably due to the higher porosity of the concrete. Therefore, RFA decreased the carbonation resistance. Some studies reported that the carbonation depth of RFA concrete likewise rises with the recycled aggregate replacement level [18,19] because concrete with RFA has higher porosity than normal concrete, which makes it easier for atmospheric CO_2 to diffuse into concrete. Figure 5.3a,b shows the results of the FA and MFA groups. Increasing the FA content increased the carbonation depth at 91 days, regardless of whether it was MFA or class II FA. Compared with the M50 concrete, the carbonation depths of M50FA10, M50FA15, M50MFA10, and M50MFA15 were 19.8, 22.9, 1.65, and 4.92% higher, respectively. Some research reported similar results and showed that the depth of carbonation increased as FA quantity increased [78–80]. This was due to the lower content of available $Ca(OH)_2$ in fly ash concrete compared to normal concrete [81,82], which resulted in faster carbonation of the C-S-H bond [83]. Figure 5.3c show the results of GGBS group. The results were similar to concrete containing FA. Increasing the GGBS content increased the carbonation depth at 91 days. Compared with the M50 concrete, the carbonation depths of M50BS30 and M50BS45 were 14.2% and 31.6% higher, respectively. It was reported that with up to 20% GGBS content, the carbonation of GGBS concrete was similar to that of normal concrete, while with a GGBS content over 20%, carbonation depth increased with the increase of GGBS content [84]. Sulapha et al. [85] also reported that concrete with GGBS exhibited lower resistance to carbonation than conventional concrete. Figure 5.3d,e shows the results of the blended admixture (FA, GGBS) group. Increasing the blended admixture content (FA and GGBS) increased the carbonation depth at 91 days. In concrete containing 30% and 45% blend admixtures, increasing the FA content increased the carbonation depth, and M50FA22.5BS22.5 had the highest carbonation depth. Therefore, FA had a greater effect on carbonation than GGBS, although after 7 days, specimens containing FA had a smaller carbonation depth. Jones et al. [86] studied concrete containing ternary binders, and showed that compared to regular concrete, concrete incorporating GGBS and fly ash showed noticeably greater rates of rapid carbonation. On average, carbonation depths for the concrete made with GGBS and fly ash mixes were 2.5 times greater than those for regular concrete, and as the cement replacement level was raised, carbonation rates increased [86]. Figure 5.4 shows the carbonation velocity coefficients. The incorporation of FA, GGBS, and RFA increased the carbonation velocity coefficient. In the RFA concrete containing 30% and 45% blended admixtures, the carbonation depth increased with the FA content. Generally, increasing the content of mineral admixture increases the carbonation depth of concrete. This is mainly because the pozzolanic reaction consumes a large amount of Ca(OH)2, resulting in a decrease in the pH of the concrete [87]. When the FA content was constant, adding GGBS to the concrete increased the carbonization velocity coefficient. When the total FA and GGBS content was constant, increasing the FA content increased the carbonation velocity coefficient.

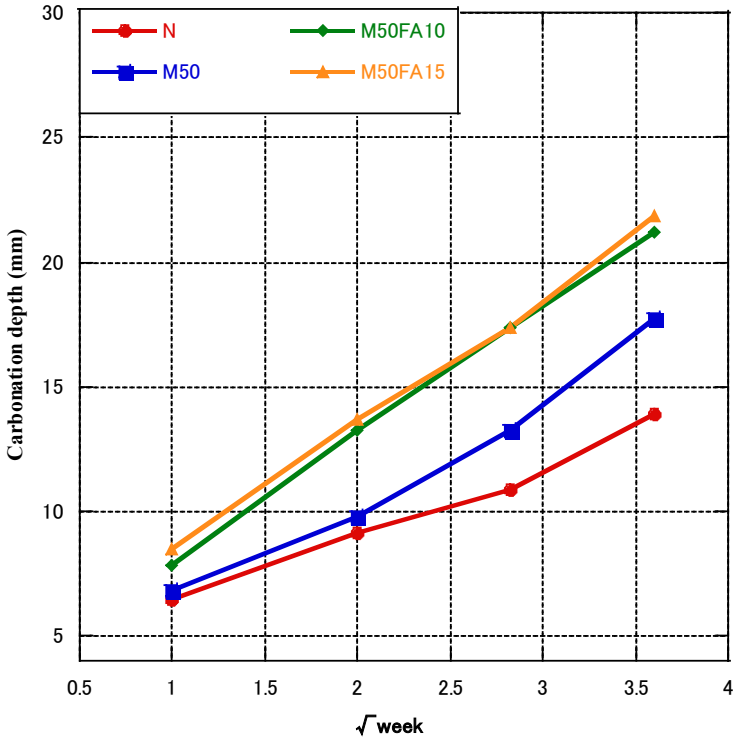
N
M50
M50FA10
M50FA15
Carbonation depth (mm)
30
25
20
15
10
5
0.5
1
1.5
2
2.5
3
3.5
4
√week

(a)

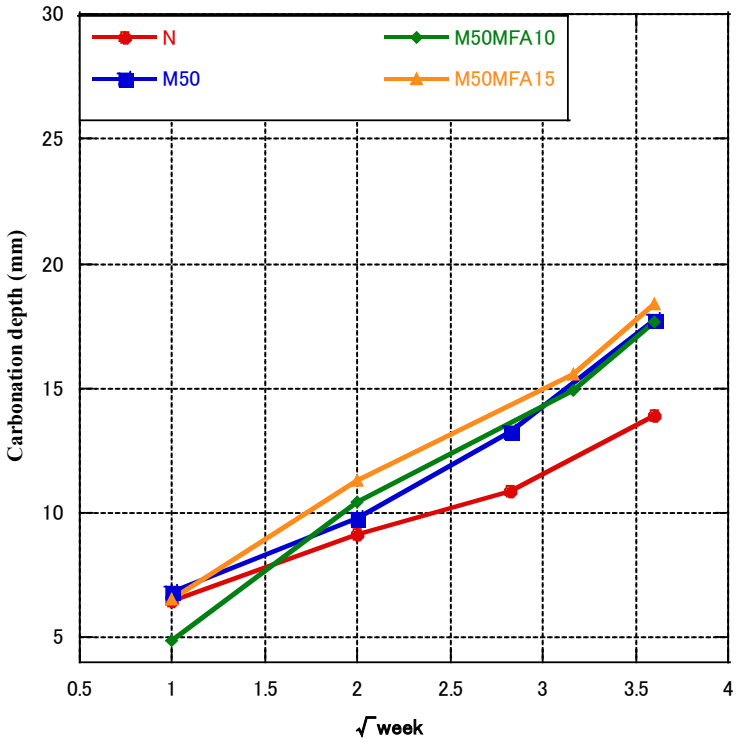
N
M50
M50MFA10
M50MFA15
Carbonation depth (mm)
30
25
20
15
10
5
0.5
1
1.5
2
2.5
3
3.5
4
√week

(b)

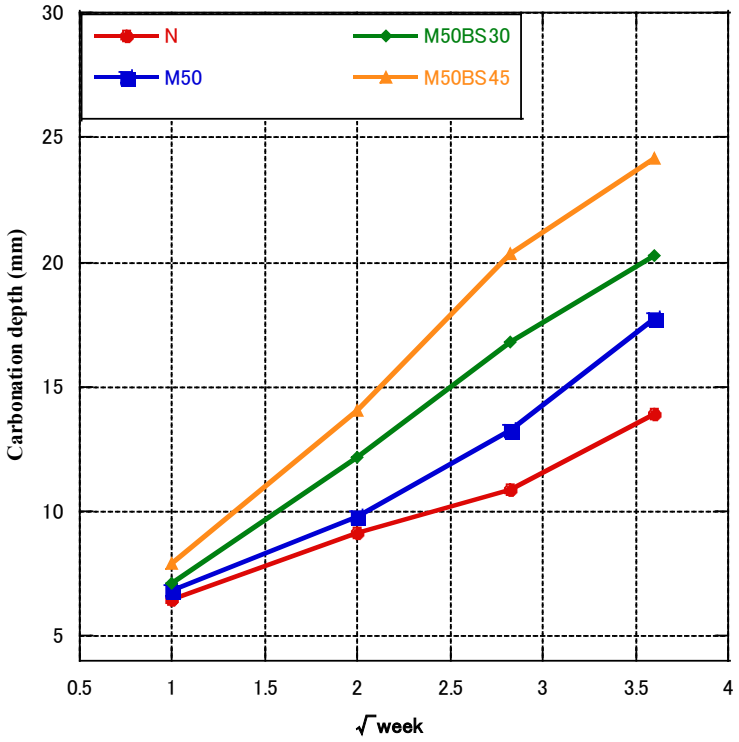
N
M50
M50BS30
M50BS45
Carbonation depth (mm)
30
25
20
15
10
5
0.5
1
1.5
2
2.5
3
3.5
4
√week

(c)

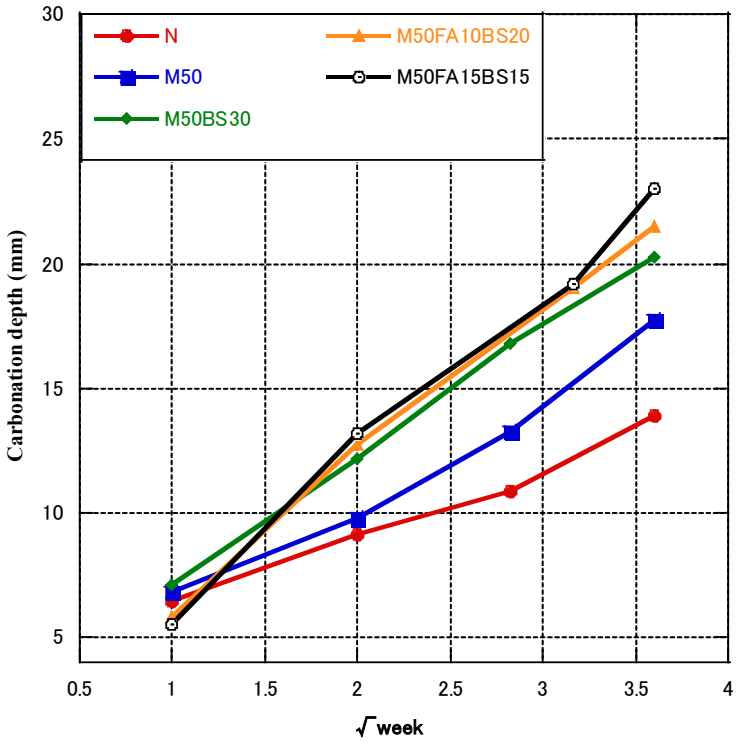
N
M50
M50BS30
M50FA10BS20
M50FA15BS15
Carbonation depth (mm)
30
25
20
15
10
5
0.5
1
1.5
2
2.5
3
3.5
4
√week

(d)

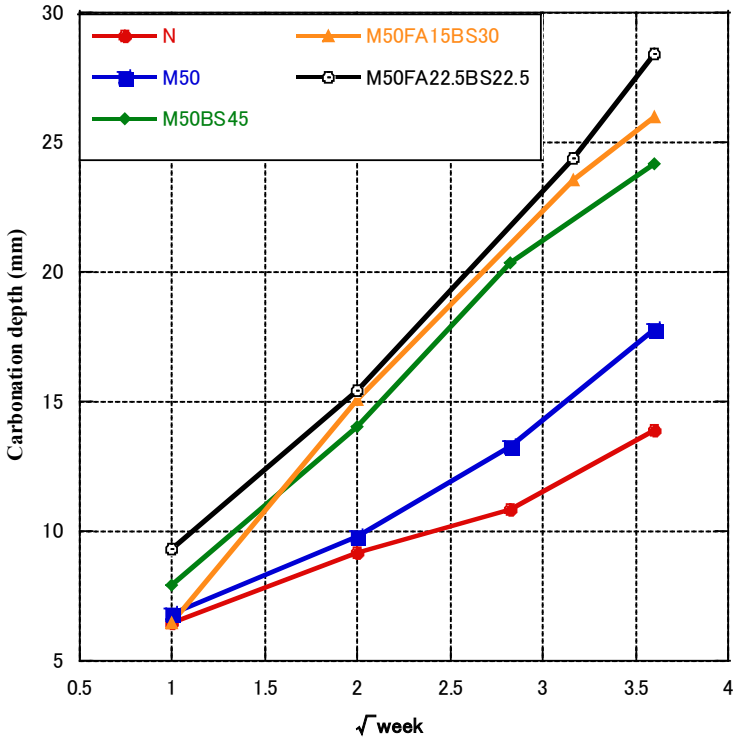

(e)

Fig. 5.3. Carbonation depth of concrete with cementitious material

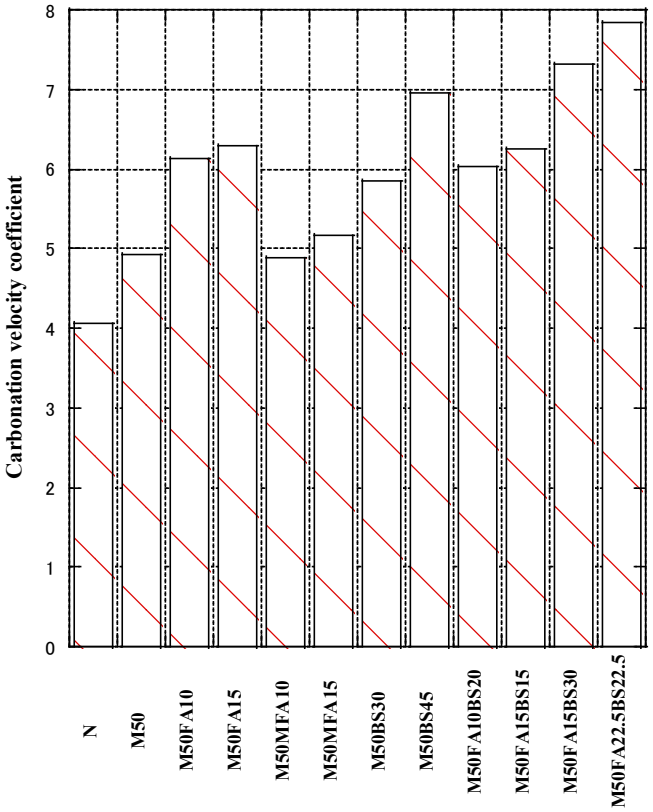

Fig. 5.4. The results of carbonation velocity coefficient

5.3.4 Pore structure

Figure 5.5 shows the cumulative pore volume at 7 days. The concrete containing RFA had a higher pore volume, especially for pore diameters of 0.05–2 μm. The concrete containing class II FA had a higher pore volume than M50 concrete, whereas the concrete containing MFA had a lower pore volume. Thus, the properties of FA strongly affect the pore volume of concrete. The concrete containing GGBS had a higher pore volume than M50 concrete, and the pore volume increased with the GGBS content. The concrete containing the blended admixtures had a lower pore volume when the admixture content was 30% compared with concrete containing only GGBS, and the ratio of FA to GGBS of 1:2 was better than 1:1. Figure 5.6 shows the cumulative pore volume at 28 days. The effect of RFA on the pore volume of concrete was similar to the effect at 7 days, and the concrete containing RFA had a higher pore volume than the control concrete. The pore volume at 28 days was much lower than that at 7 days due to the hydration of the cement and cementitious materials. The concrete containing fly ash had different results; that containing class II FA had a higher volume than the control concrete, whereas that containing MFA had a lower pore volume. For concrete containing GGBS, the change in cumulative pore volume was negligible, but the pore volume between 0.05 and 2 μm was considerably lower. For concrete containing the blended admixture, concrete containing FA and GGBS had a higher pore volume than concrete containing only GGBS, especially for pore diameters of 0.01–0.05 μm. When the cementitious materials content was constant, the pore volume increased with the FA content. Figure 5.7 shows the cumulative pore volume at 91 days. The pore volume of M50 was higher than that in the control concrete. The pore volume of RFA concrete containing FA was larger than that in the M50 concrete, but the volume of pores between 0.05 and 2 μm did not change much, mainly due to the increase in the volume of pores less than 0.05 μm, regardless of whether the FA was class II FA or MFA. This may be due to the pozzolanic reaction and the tiny aggregate effect of FA [71]. Poon et al. [88] also reported that replacing cement with fly ash increased porosity but decreased average pore size of the pastes. Other studies reported similar results [89,90]. The total pore volume of concrete containing GGBS was larger than that of M50 concrete, but the 0.05–2 μm pore volume was smaller than that of M50 concrete, mainly due to the increase in the volume of pores less than 0.05 μm.

The pore volume of concrete containing 30% cementitious materials did not change substantially, whereas that containing 45% cementitious materials was different. The total pore volume of concrete containing the blended admixture was larger than that containing only GGBS; while the volume of the pores at 0.05–2 μm did not change much, the volume of the pores at 0.01–0.05 μm increased. The experimental results prove that the activity of pozzolanic reaction of GGBS is greater than that of fly ash, so the pore volume of concrete mixed with GGBS only had a higher pore volume at pore diameters of less than 0.01 μm. Furthermore, we found that the incorporation of GGBS decreased the volume of pores with a diameter greater than 0.01, and the incorporation of fly ash had little effect on the volume of pores. with a diameter of 0.05–2μm but increased the volume of pores with a diameter of 0.01–0.05μm.

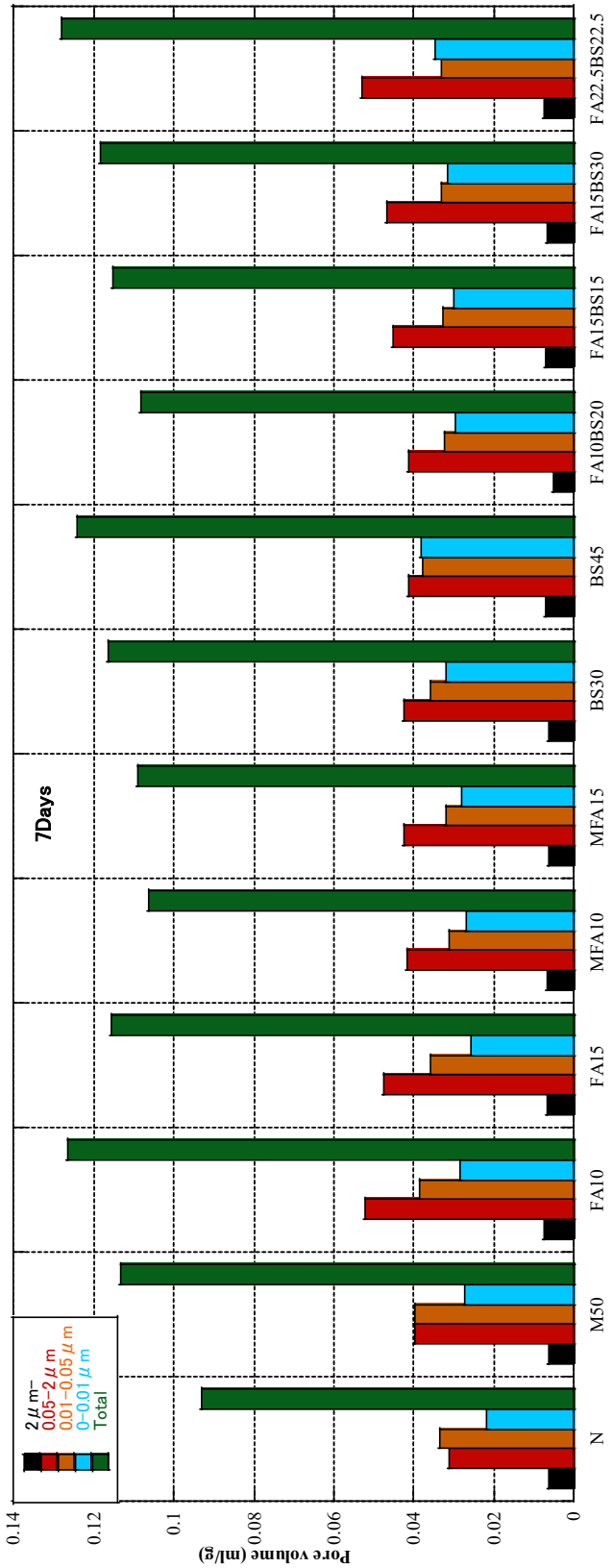

Fig. 5.5. Pore structure at 7 days

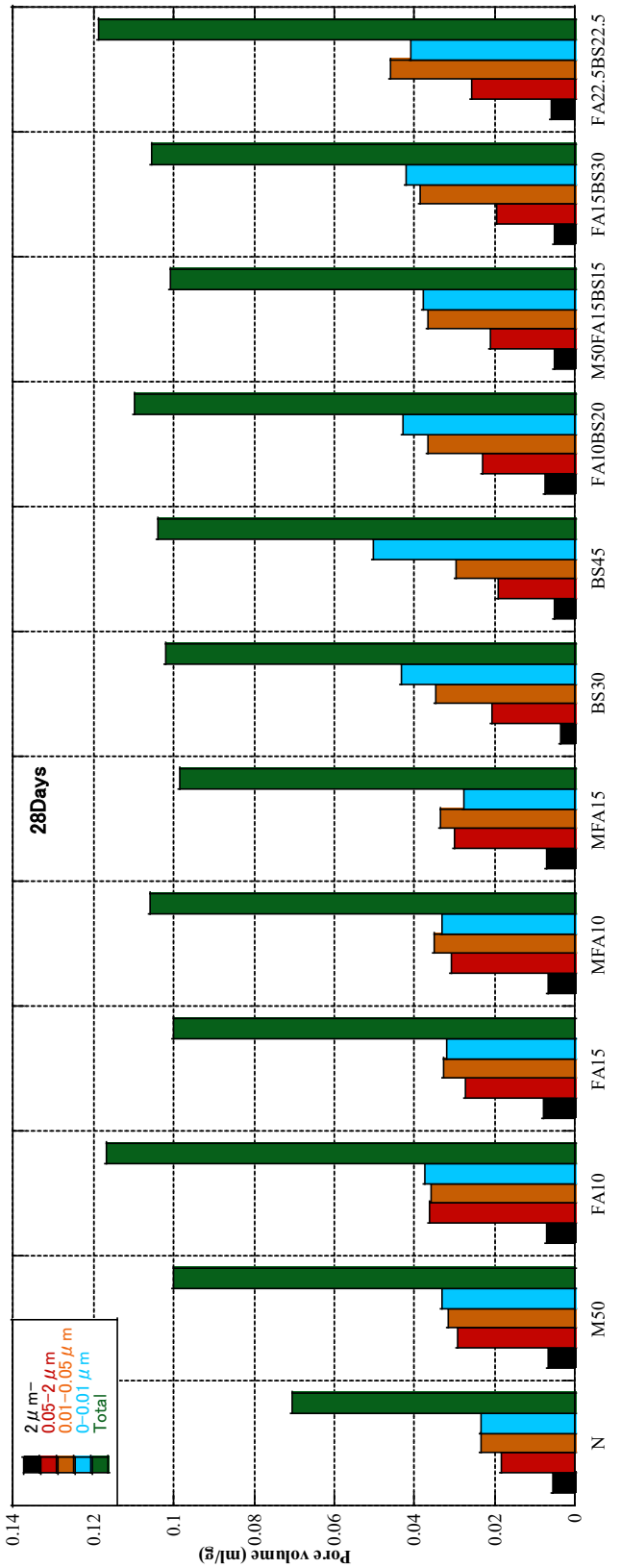

Fig. 5.6. Pore structure at 28 days

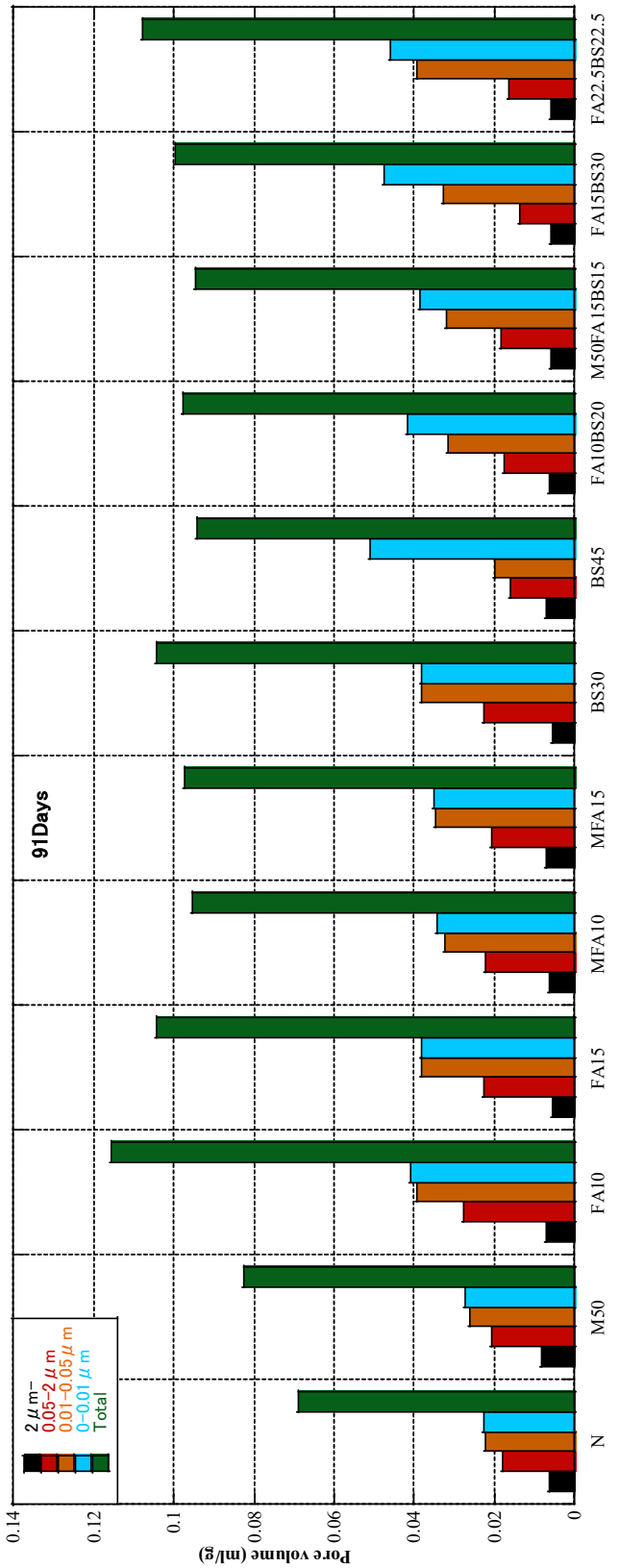

Fig. 5.7. Pore structure at 91 days

Based on MIP-determined trials, Mindess et al. [91] defined capillary pores as being greater than 0.01 μm, and gel pores as being less than 0.01 μm. PK Mehta [92] analyzed pore size in four ranges: less than 4.5 nm, 4.5–50 nm, 50–100 nm, and greater than 100 nm. Wu and Lian [93] examined four ranges of pores: pores under 20 nm, between 20 and 50 nm, 50 and 200 nm and those over 200 nm. It was reported that the strength of mortar was mainly affected by capillary pores, and the durability was mainly affected by gel pores [94].

Based on the relationship between pore volume and pore diameter, we analyzed the correlation between the compressive strength of concrete at each age and the total pore volumes, pore volumes of 0.01–36, 0.05–36, 0.003–2, 0.01–2, and 0.05–2 μm. Fig. 5.8 shows the relationship between compressive strength and cumulative pore volume at each age (all mix proportions). In all pore size ranges, the compressive strength tended to increase as the pore volume decreased. For the 28- and 91-day compressive strength, the correlation coefficients (R2) for the 0.01–36 μm pore volume were the highest. However, the 7-day compressive strength had a good correlation with the 0.05–2 μm pore volume.

In Fig. 5.9, regardless of the age and mix proportions of the specimens, all the compressive strength and cumulative pore volumes obtained were fitted. The compressive strength has a low correlation with the total pore volume and the pore volume of 0.003-2μm. Furthermore, compressive strength was linearly related to the pore volumes larger than 0.01 or 0.05 μm. This proved that pores with a diameter of less than 0.01 μm had no effect on the compressive strength of concrete, pores with a diameter of 0.01-0.05 μm had weak effect on the compressive strength of concrete, and pores with a diameter greater than 0.05 μm had a greater effect on the strength of concrete. The correlation coefficient between the 0.05–2 μm pore volume and the compressive strength was the largest R2 of 0.87. Therefore, for the compressive strength, we can call the pores with a diameter greater than 0.05μm as harmful pores, 0.01-0.05μm as small harmful pores, and less than 0.01μm as harmless pores.

Fig. 5.10 shows the correlation between carbonation velocity coefficient and cumulative pore volume obtained from the MIP tests at 91 days (total pore volumes, pore volumes of 0.003–0.1, 0.003–0.05, and 0.003–0.01 μm), respectively. The correlation between cumulative pore volume and carbonation velocity coefficient increases gradually with the de-crease of pore diameter. Besides, the correlation between the carbonation velocity coefficient and 0.003–0.01 μm pore volume was the highest, with R2 of 0.83. Thus, the carbona-tion velocity coefficient of concrete was linearly related to the volume of pores with diameter less than 0.01 μm.

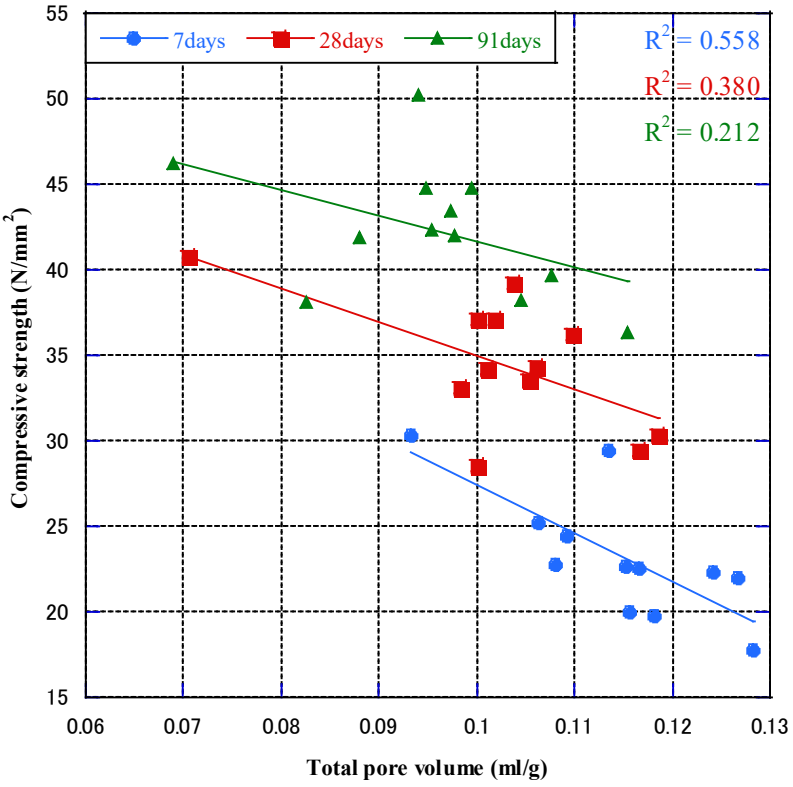
7days
28days
91days
R2= 0.558
R2= 0.380
R2= 0.212
Compressive strength (N/mm2)
Total pore volume (ml/g)
55
50
45
40
35
30
25
20
15
0.06
0.07
0.08
0.09
0.1
0.11
0.12
0.13

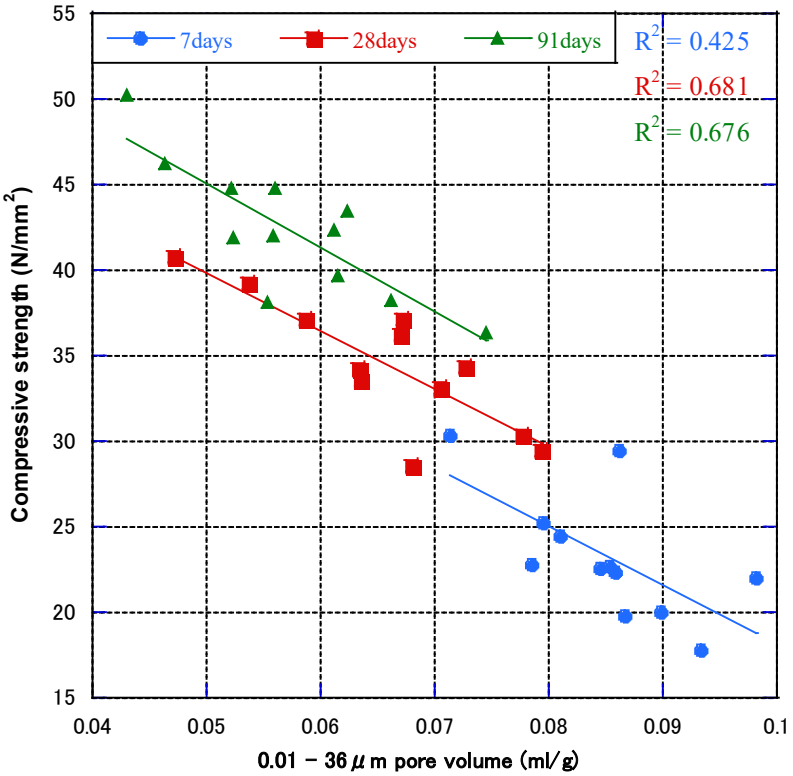
7days
28days
91days
R2= 0.425
R2= 0.681
R2= 0.676
Compressive strength (N/mm2)
0.01 – 36μm pore volume (ml/g)
55
50
45
40
35
30
25
20
15
0.04
0.05
0.06
0.07
0.08
0.09
0.1

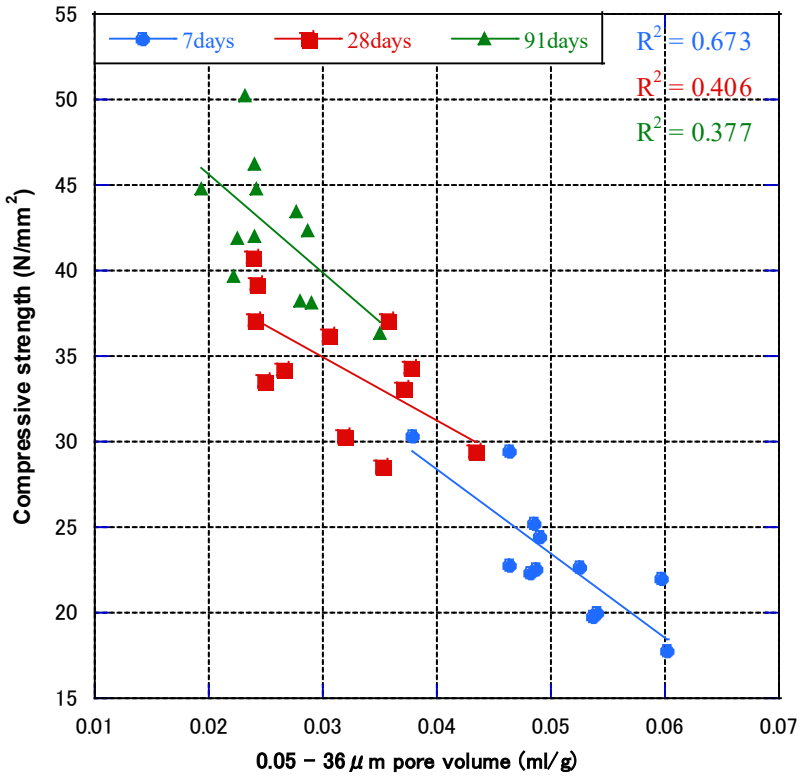
7days
28days
91days
R2= 0.673
R2= 0.406
R2= 0.377
Compressive strength (N/mm2)
55
50
45
40
35
30
25
20
15
0.01
0.02
0.03
0.04
0.05
0.06
0.07
0.05 – 36μm pore volume (ml/g)

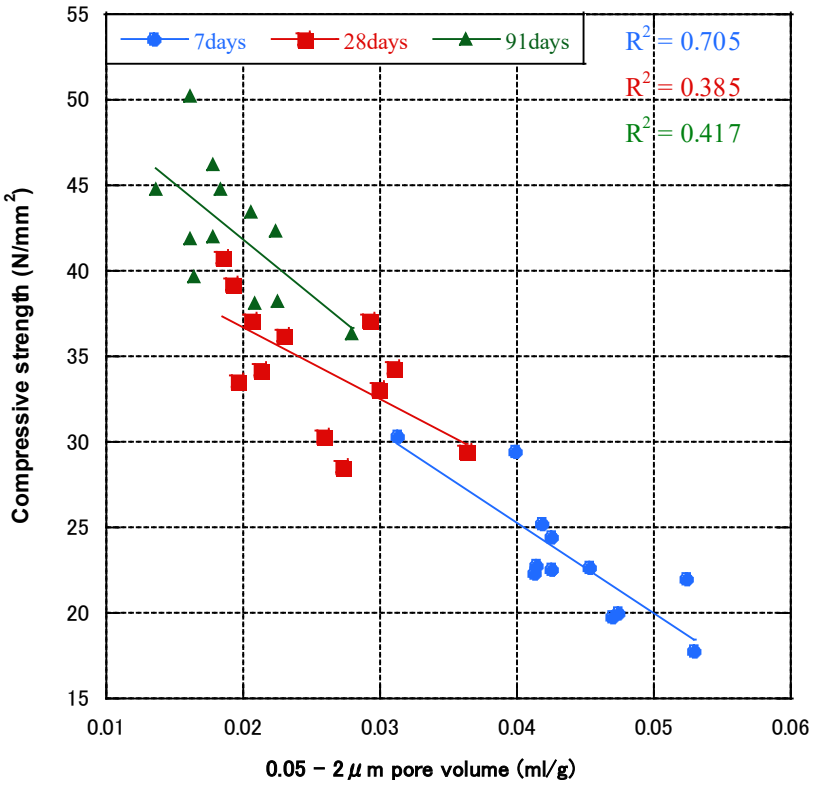
7days
28days
91days
R2= 0.705
R2= 0.385
R2= 0.417
Compressive strength (N/mm2)
55
50
45
40
35
30
25
20
15
0.01
0.02
0.03
0.04
0.05
0.06
0.05 – 2μm pore volume (ml/g)

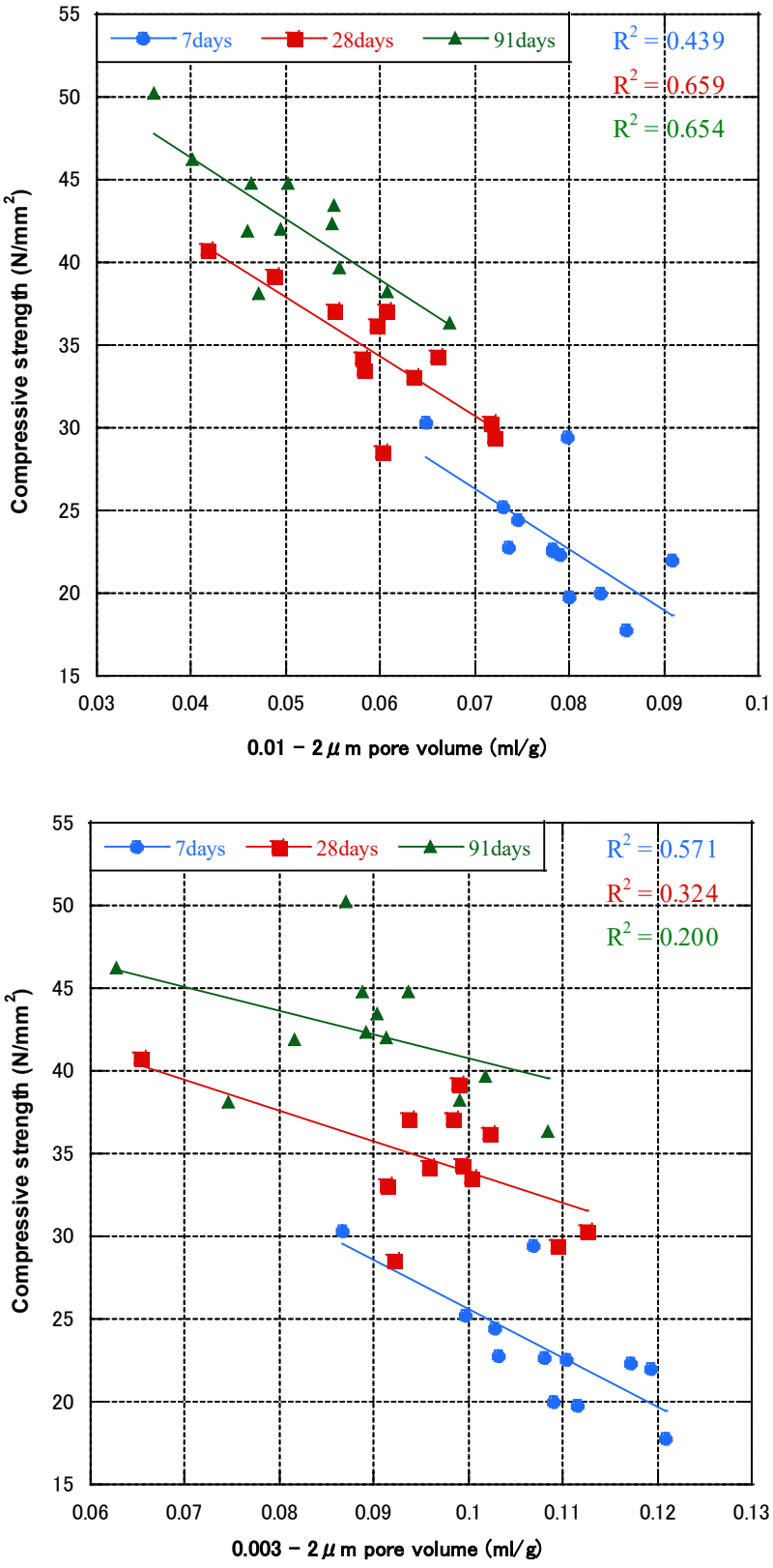

Fig. 5.8 Relationship between pore volume and compressive strength at each age

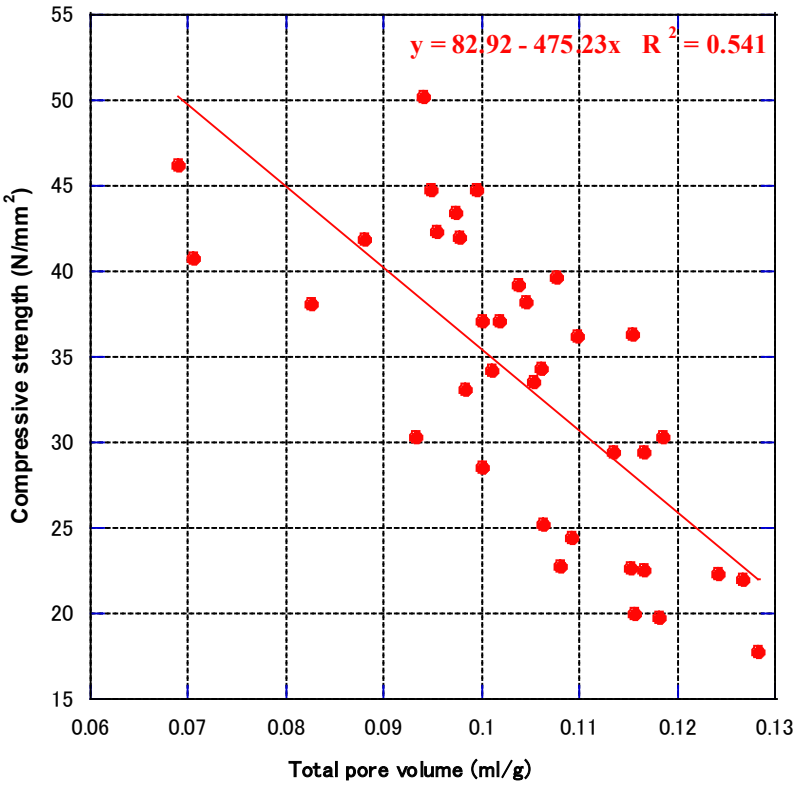
y = 82.92 - 475.23x R 2 = 0.541
Compressive strength (N/mm 2)
Total pore volume (ml/g)
55
50
45
40
35
30
25
20
15
0.06
0.07
0.08
0.09
0.1
0.11
0.12
0.13

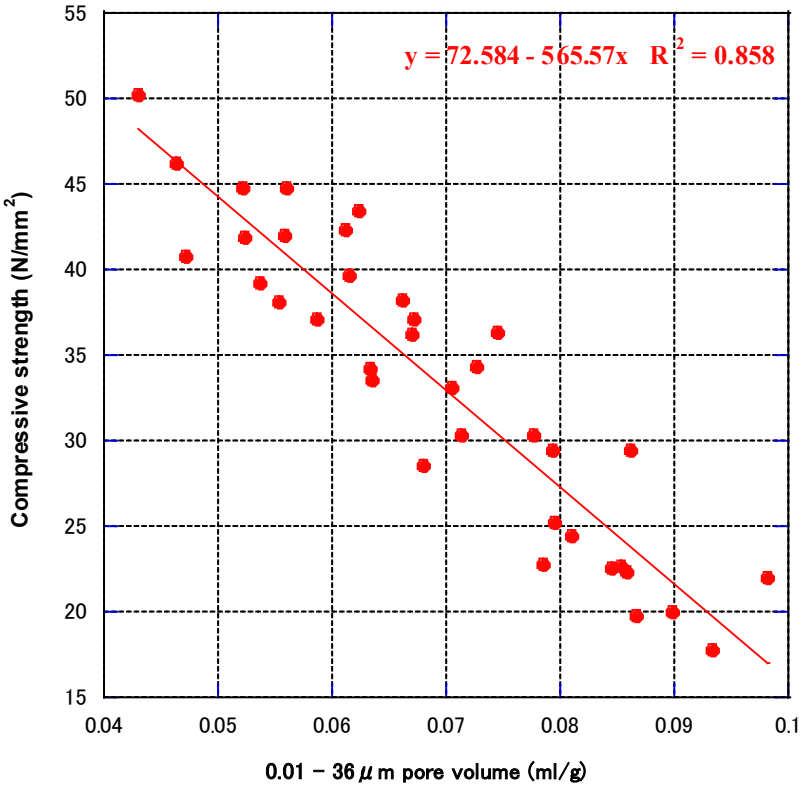
y = 72.584 - 565.57x R 2 = 0.858
Compressive strength (N/mm 2)
0.01 – 36 μm pore volume (ml/g)
55
50
45
40
35
30
25
20
15
0.04
0.05
0.06
0.07
0.08
0.09
0.1

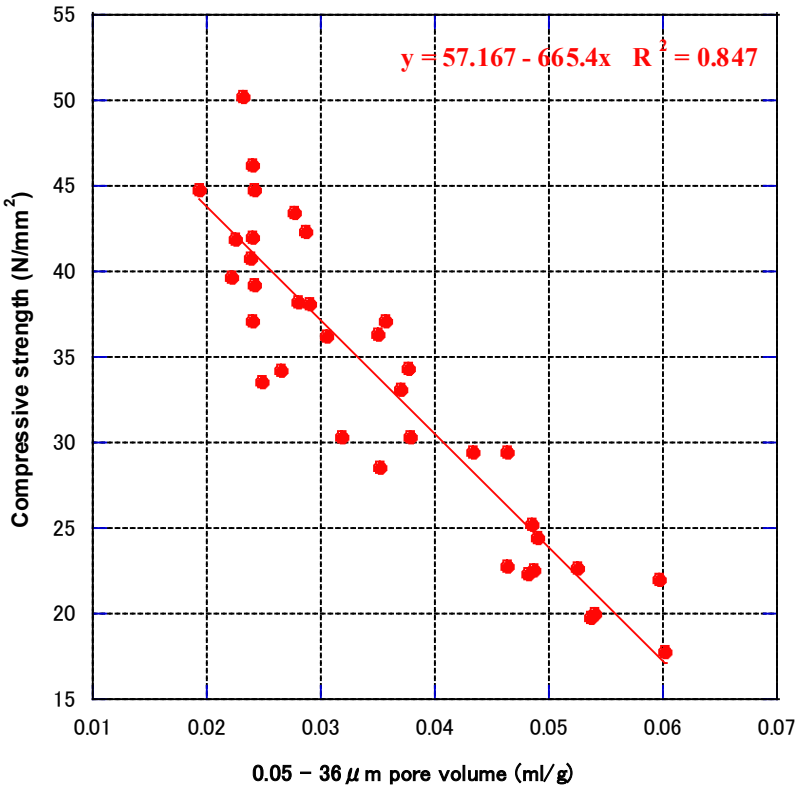
y = 57.167 - 665.4x R 2 = 0.847
Compressive strength (N/mm2)
55
50
45
40
35
30
25
20
15
0.01
0.02
0.03
0.04
0.05
0.06
0.07
0.05 − 36μm pore volume (ml/g)

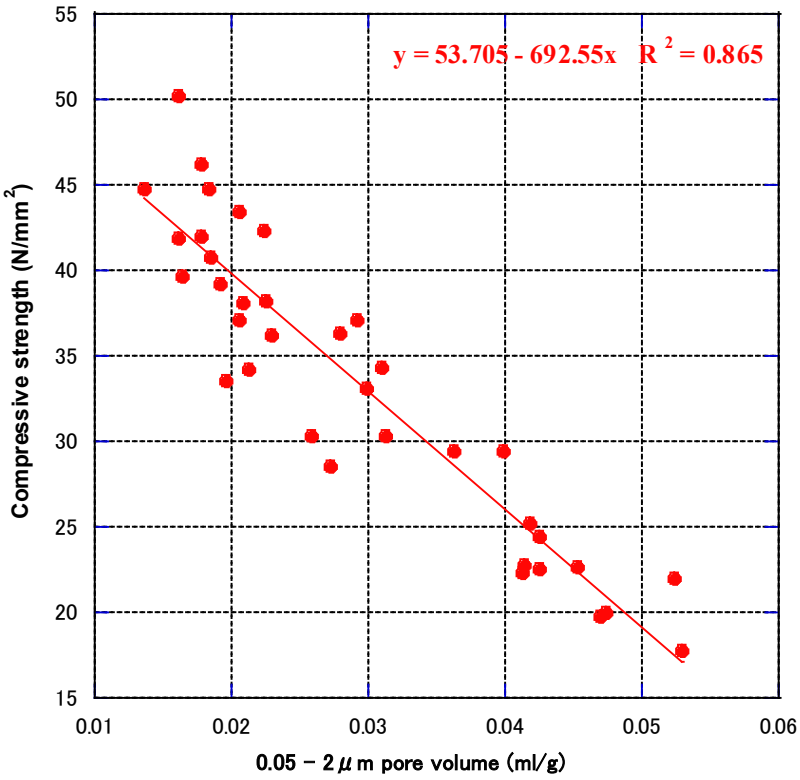
y = 53.705 - 692.55x R 2 = 0.865
Compressive strength (N/mm2)
55
50
45
40
35
30
25
20
15
0.01
0.02
0.03
0.04
0.05
0.06
0.05 − 2μm pore volume (ml/g)

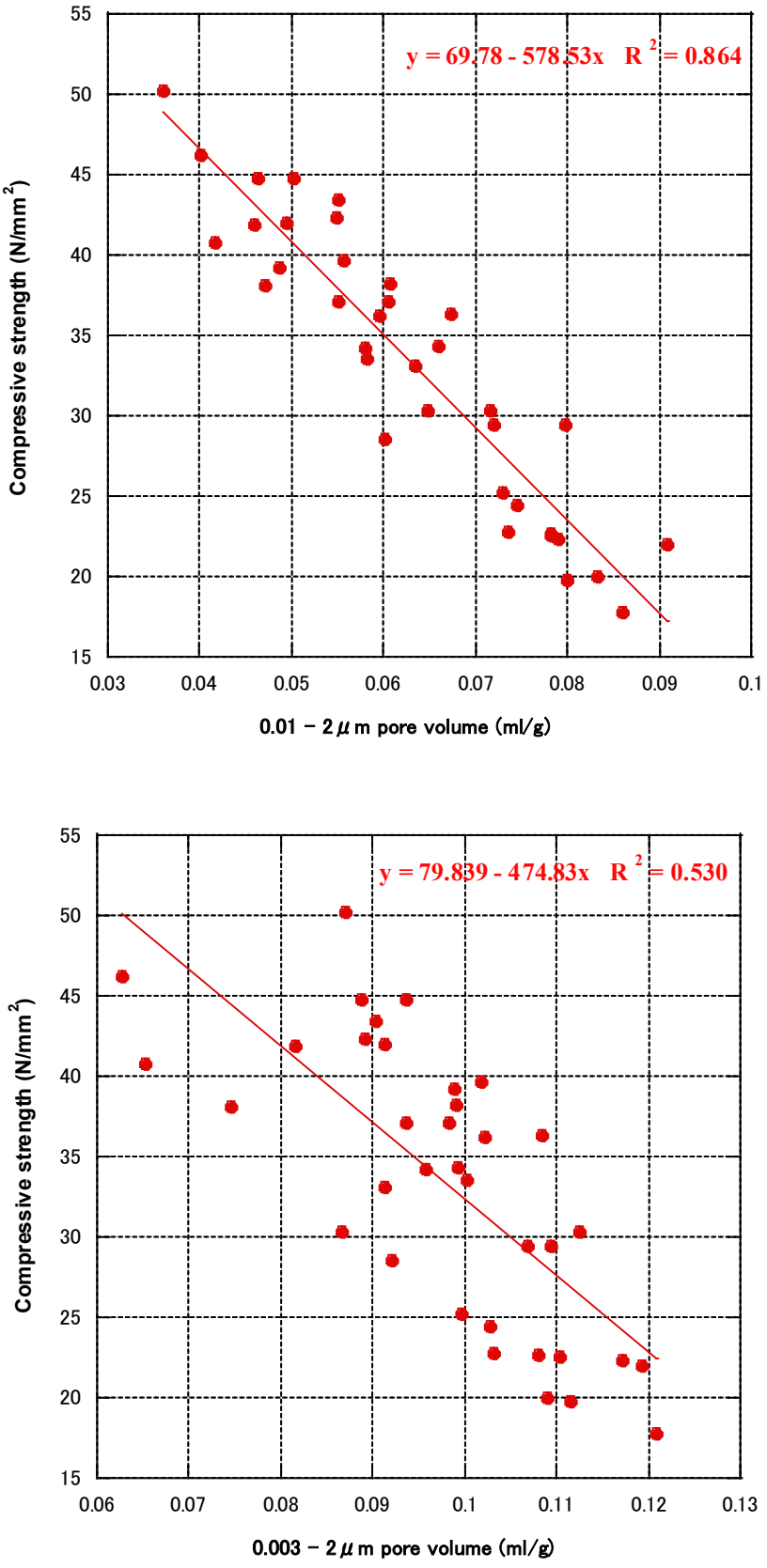

Fig. 5.9 Relationship between pore volume and compressive strength (all mixes and ages)

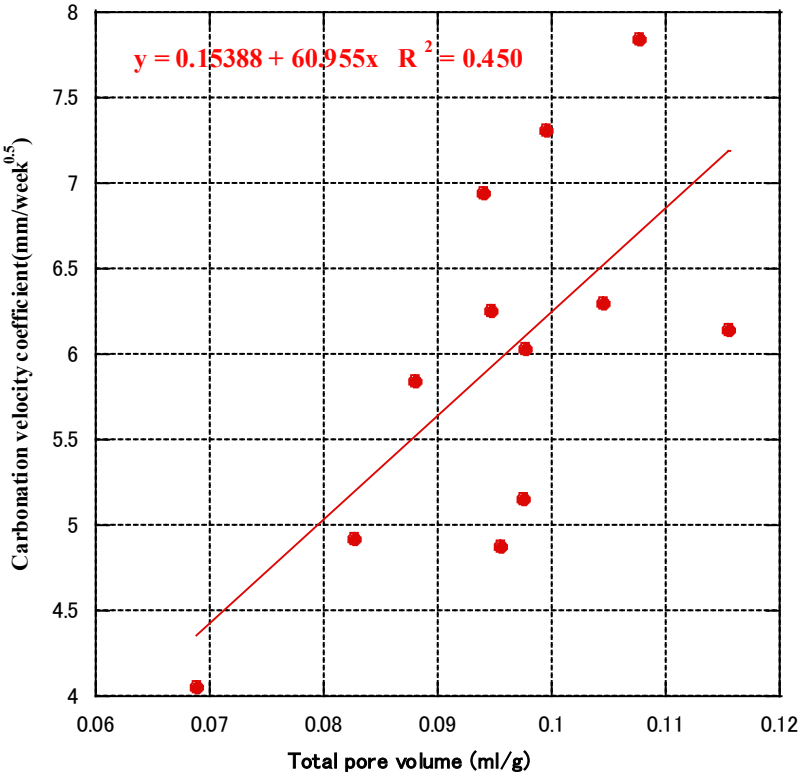
y = 0.15388 + 60.955x R 2 = 0.450
Carbonation velocity coefficient(mm/week0.5)
Total pore volume (ml/g)
8
7.5
7
6.5
6
5.5
5
4.5
4
0.06
0.07
0.08
0.09
0.1
0.11
0.12

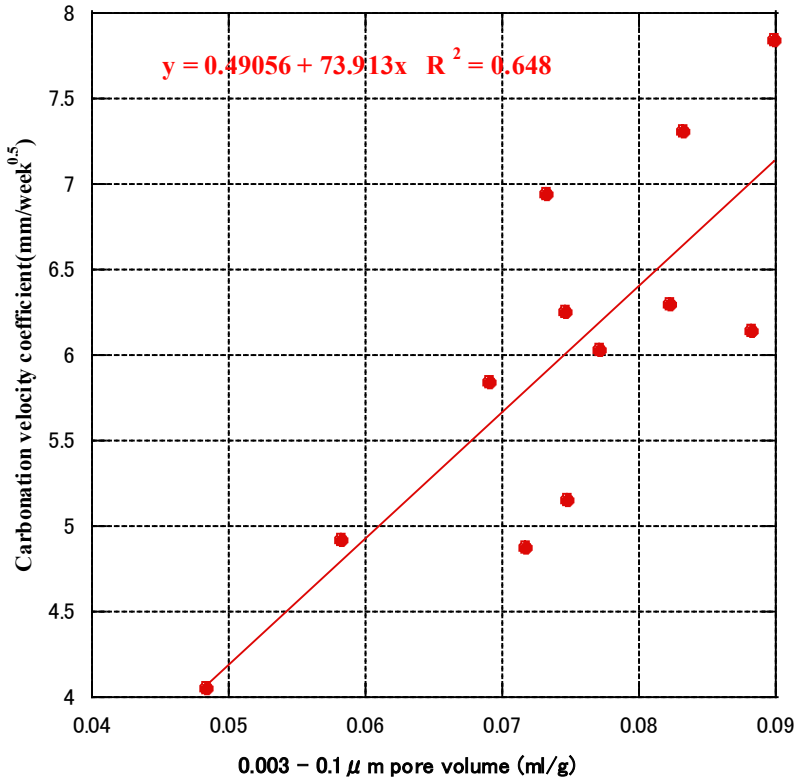
y = 0.49056 + 73.913x R 2 = 0.648
Carbonation velocity coefficient(mm/week0.5)
0.003 − 0.1 μ m pore volume (ml/g)
8
7.5
7
6.5
6
5.5
5
4.5
4
0.04
0.05
0.06
0.07
0.08
0.09

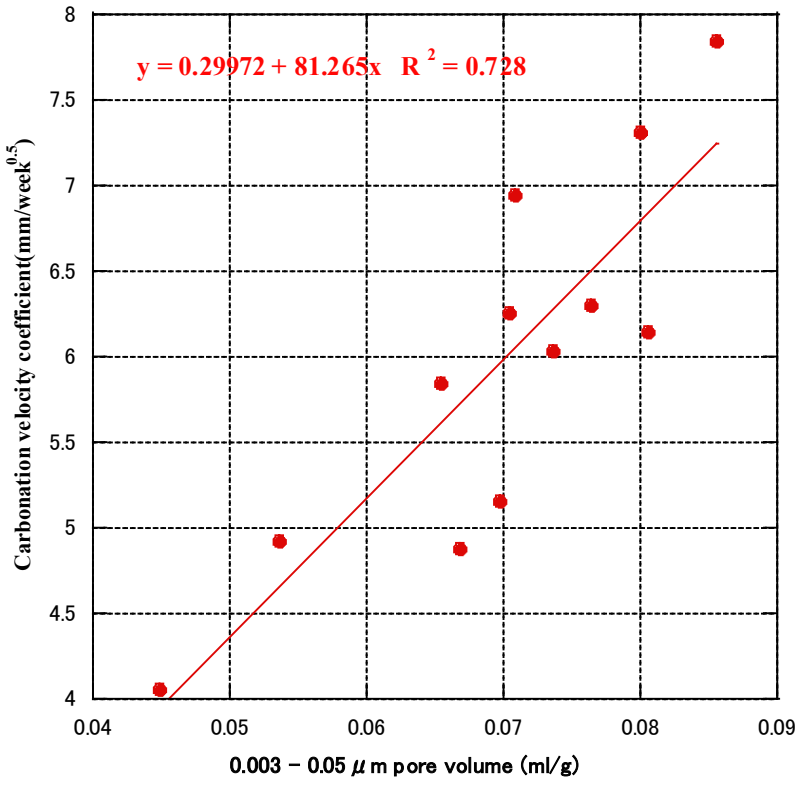

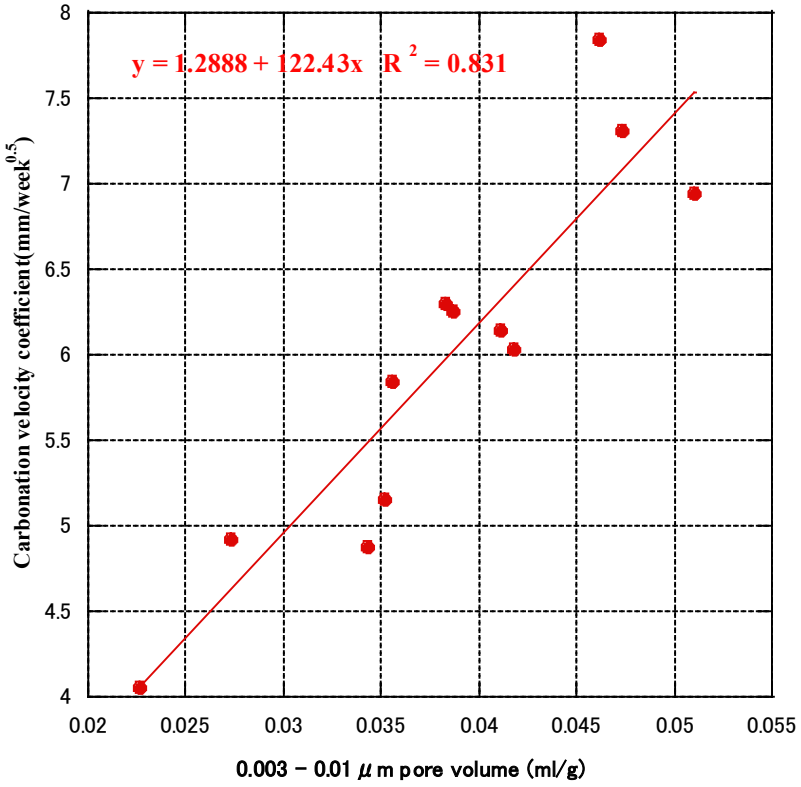

Fig. 5.10 Relationship between cumulative pore volume and carbonation velocity coefficient

5.4 Conclusion

1. Adding fly ash and GGBS to RFA concrete increased its compressive strength. M50BS45 and M50FA15BS15 exhibited similar 91-day compressive strengths with normal concrete. Therefore, the compressive strength of RFA concrete can be effectively improved by the use of cementitious materials.

2. Replacement of cement with fly ash or GGBS significantly decreased the drying shrinkage of the RFA concrete. The drying shrinkage of all specimens in this experiment reach the level of ordinary concrete, even lower than that of ordinary concrete. Besides, M50FA15BS15 showed 16.5% lower drying shrinkage, M50BS45 and M50FA15BS30 showed around 25% lower drying shrinkage than normal concrete.

3. Increasing the cementitious (fly ash and GGBS) materials content decreased the carbon-ation resistance of RFA concrete. Besides, fly ash had a greater effect on carbonation than GGBS.

4. Incorporating FA or GGBS into concrete modified the pore structure of concrete, reduced the volume of capillaries larger than 0.05μm. In addition, the compressive strength was mainly affected by the capillary pores (greater than 0.01μm or 0.05μm), and the carbona-tion was mainly affected by the gel pores (less than 0.01μm).

5. For compressive, the pores with a diameter greater than 0.05μm are considered harmful pores, 0.01-0.05μm are considered small harmful pores, and less than 0.01μm are consid-ered harmless pores.

Reference

[1] Meyer, C. The greening of the concrete industry. Cem. Concr. Compos. 2009, 31, 601–605.

[2] Evangelista, L.; Guedes, M.; de Brito, J.; Ferro, A.; Pereira, M. Physical, chemical and mineralogical properties of fine recycled aggregates made from concrete waste. Construct. Build. Mater. 2015, 86, 178–188.

[3] Kumar, G.S. Influence of fluidity on mechanical and permeation performances of recycled aggregate mortar. Constr. Build. Mater. 2019, 213, 404–412.

[4] Elavenil, S.; Vijaya, B. Manufactured sand, a solution and an alternative to river sand and in concrete manufacturing. J. Eng. Comput. Appl. Sci. 2013, 2, 20–24.

[5] Villalobos, S.; Lange, D.A.; Roesler, J.R. Evaluation, Testing and Comparison between Crushed Manufactured Sand and Nat-ural Sand; Technical Note, 2005, 15.

[6] Fischer, C.; Werge, M. EU as a recycling society. European Topic Centre on Resource Waste Management, Working Paper 2/2009, 2009.

[7] Sáez, P.V.; Merino, M.; Del, R.; Porras-Amores, C. Managing construction and demolition (C&D) waste—A European per-spective. In International Conference on Petroleum and Sustainable Development; IPCBEE: Dubai, UAE, 2011; pp. 27–31.

[8] CSI. The Cement Sustainability Initiative. Recycling Concrete: Executive Summary; CSI: Genève, Switzerland, 2009.

[9] Gonçalves, P.; de Brito, J. Recycled aggregate concrete (RAC)—Comparative analysis of existing specifications. Mag. Concr. Res. 2010, 62, 339–346.

[10] Gholampour, A.; Zheng, J.; Ozbakkaloglu, T. Development of waste-based concretes containing foundry sand, recycled fine aggregate, ground granulated blast furnace slag and fly ash. Constr. Build. Mater. 2021, 267, 121004.

[11] Kirthika, S.K.; Singh, S.K. Durability studies on recycled fine aggregate concrete. Constr. Build. Mater. 2020, 250, 118850.

[12] Khatib, J.M. Properties of concrete incorporating fine recycled aggregate. Cem. Concr. Res. 2005, 35, 763–769.

[13] Abbas, A.; Fathifazl, G.; Isgor, O.B.; Razaqpur, A.G.; Fournier, B.; Foo, S. Durability of recycled aggregate concrete designed with equivalent mortar volume method. Cem. Concr. Compos. 2009, 31, 555–563.

[14] Corinaldesi, V.; Moriconi, G. Influence of mineral additions on the performance of 100% recycled aggregate concrete. Constr. Build. Mater. 2009, 23, 2869–2876.

[15] Xiao, J.; Li, W.; Fan, Y.; Huang, X. An overview of study on recycled aggregate concrete in China (1996–2011). Constr. Build. Mater. 2012, 31, 364–383.

[16] Somna, R.; Jaturapitakkul, C.; Amde, A.M. Effect of ground fly ash and ground bagasse ash on the durability of recycled ag-gregate concrete. Cem. Concr. Compos. 2012, 34, 848–854.

[17] Ann, K.Y.; Moon, H.Y.; Kim, Y.B.; Ryou, J. Durability of recycled aggregate concrete using pozzolanic materials. Waste Manag. 2008, 28, 993–999.

[18] Lovato, P.S.; Possan, E.; Dal Molin D.C.C.; Masuero Â.B.; Ribeiro J.L.D. Modeling of mechanical properties and durability of recycled aggregate concretes. Constr. Build. Mater. 2012,

26, 437–447.

[19] Evangelista, L.; De Brito, J.M.C.L. Durability performance of concrete made with fine recycled concrete aggregates. Cem. Concr. Compos. 2010, 32, 9–14.

[20] Bu, C.; Liu, L.; Lu, X.; Zhu, D.; Sun, Y.; Yu, L.; OuYang, Y.; Cao, X.; Wei, Q.; et al. The Durability of recycled fine aggregate Concrete: A Review. Materials 2022, 15, 1110.

[21] Martínez-García, R.; de Rojas, M.S.; Jagadesh, P.; López-Gayarre, F.; Morán-del-Pozo, J.M.; Juan-Valdes, A. Effect of pores on the mechanical and durability properties on high strength recycled fine aggregate mortar. Case Stud. Constr. Mater. 2022, 16, e01050.

[22] Martínez-García, R.; Rojas, M.I.S.D.; Pozo, J.M.M.D.; Fraile-Fernández, F.J.; Juan-Valdés, A. Evaluation of mechanical charac-teristics of cement mortar with fine recycled concrete aggregates (FRCA). Sustainability 2021, 13, 414.

[23] Jiang, X.; Xiao, R.; Bai, Y.; Huang, B.; Ma, Y. Influence of waste glass powder as a supplementary cementitious material (SCM) on physical and mechanical properties of cement paste under high temperatures. J. Clean. Prod. 2022, 340, 130778.

[24] Chindaprasirt, P.; Jaturapitakkul, C.; Sinsiri, T. Effect of fly ash fineness on compressive strength and pore size of blended cement paste. Cem. Concr. Compos. 2005, 27, 425–428.

[25] Moradi, N.; Tavana, M.H.; Habibi, M.R.; Amiri, M.; Moradi, M.J.; Farhangi, V. Predicting the Compressive Strength of Concrete Containing Binary Supplementary Cementitious Material Using Machine Learning Approach. Materials 2022, 15, 5336.

[26] Saha, A.K. Effect of class F fly ash on the durability properties of concrete. Sustain. Environ. Res. 2018, 28, 25–31.

[27] Moffatt, E.G.; Thomas, M.D.; Fahim, A. Performance of high-volume fly ash concrete in marine environment. Cem. Concr. Res. 2017, 102, 127–135.

[28] De Maeijer, P.K.; Craeye, B.; Snellings, R.; Kazemi-Kamyab, H.; Loots, M.; Janssens, K.; Nuyts, G. Effect of ultra-fine fly ash on concrete performance and durability. Constr. Build. Mater. 2020, 263, 120493.29.

[29] Ross, A.D. Some problems in concrete construction. Mag. Concr. Res. 1960, 12, 27–34.

[30] Bamforth, P. In situ measurement of the effect of partial Portland cement replacement using either fly ash or ground granulated blast-furnace slag on the performance of mass concrete. Proc. Inst. Civ. Eng. 1980, 69, 777–800.

[31] Kristiawan, S.A.; Aditya, M.T.M. Effect of high volume fly ash on shrinkage of self-compacting concrete. Procedia Eng. 2015, 125, 705–712.

[32] Özbay, E.; Erdemir, M., Durmuş, H.İ. Utilization and efficiency of ground granulated blast furnace slag on concrete properties–A review. Constr. Build. Mater. 2016, 105, 423–434.

[33] Li, K.; Zeng, Q.; Luo, M.; Pang, X. Effect of self-desiccation on the pore structure of paste and mortar incorporating 70% GGBS. Constr. Build. Mater. 2014, 51, 329–337.

[34] El-Chabib, H.; Syed, A. Properties of Self-Consolidating Concrete Made with High Volumes of Supplementary Cementitious Materials. J. Mater. Civ. Eng. 2013, 25, 1579–1586.

[35] Darquennes, A.; Rozière, E.; Khokhar, M.I.A.; Turcry, P.; Loukili, A.; Grondin, F. Long-term deformations and cracking risk of concrete with high content of mineral additions. Mater. Struct. 2012, 45, 1705–1716.

[36] Brooks, J.J.; Wainwright, P.J.; Boukendakji, M. Influence of Slag Type and Replacement Level

on Strength Elasticity, Shrinkage and Creep of Concrete. Spec. Publ. 1992, 132, 1325–1342.

[37] Liu, Z.; Takasu, K.; Koyamada, H.; Suyama, H. A study on engineering properties and environmental impact of sustainable concrete with fly ash or GGBS. Constr. Build. Mater. 2022, 316, 125776.

[38] Qureshi, L.A.; Ali, B.; Ali, A. Combined effects of supplementary cementitious materials (silica fume, GGBS, fly ash and rice husk ash) and steel fiber on the hardened properties of recycled aggregate concrete. Constr. Build. Mater. 2020, 263, 120636.

[39] Ahmad, J.; Martínez-García, R.; Szelag, M.; De-Prado-Gil, J.; Marzouki, R.; Alqurashi, M.; Hussein, E.E. Effects of Steel Fibers (SF) and Ground Granulated Blast Furnace Slag (GGBS) on Recycled Aggregate Concrete. Materials 2021, 14, 7497.

[40] Kurad, R.; Silvestre, J.D.; de Brito, J.; Ahmed, H. Effect of incorporation of high volume of recycled concrete aggregates and fly ash on the strength and global warming potential of concrete. J. Clean. Prod. 2017, 166, 485–502.

[41] Ali, B.; Qureshi, L.A.; Nawaz, M.A.; Aslam, H.M.U. Combined influence of fly ash and recycled coarse aggregates on strength and economic performance of concrete. Civ. Eng. J. 2019, 5, 832–844.

[42] Ali, B.; Qureshi, L.A.; Shah SH, A.; Rehman, S.U.; Hussain, I.; Iqbal, M. A step towards durable, ductile and sustainable concrete: Simultaneous incorporation of recycled aggregates, glass fiber and fly ash. Constr. Build. Mater. 2020, 251, 118980.

[43] Kou, S.C.; Poon, C.S.; Agrela, F. Comparisons of natural and recycled aggregate concretes prepared with the addition of dif-ferent mineral admixtures. Cem. Concr. Compos. 2011, 33, 788–795.

[44] Anastasiou, E.; Filikas, K.G.; Stefanidou, M. Utilization of fine recycled aggregates in concrete with fly ash and steel slag. Constr. Build. Mater. 2014, 50, 154-161.

[45] JIS A 5022; Recycled Aggregate Concrete-Class M. Japanese Industrial Standard Committee, Japan. 2018. Available online: www.jisc.go.jp/app/jis/general/GnrJISSearch.html (accessed on 25 December 2022).

[46] JIS R 5210; Portland Cement. Japanese Industrial Standard Committee, Japan. 2019. Available online: www.jisc.go.jp/app/jis/general/GnrJISSearch.html (accessed on 25 December 2022).

[47] JIS A 6201; Fly Ash for Use in Concrete. Japanese Industrial Standard Committee, Japan. 2015. Available online: www.jisc.go.jp/app/jis/general/GnrJISSearch.html (accessed on 25 December 2022).

[48] JIS A 6206; Ground Granulated Blast-Furnace Slag for Concrete. Japanese Industrial Standard Committee, Japan. 2013. Available online: www.jisc.go.jp/app/jis/general/GnrJISSearch.html (accessed on 25 December 2022).

[49] Japanese Architectural Standard Specification JASS 5 Reinforced Concrete Work, Japan. Available online: www.aij.or.jp/jpn/databox/2020/public_jass5-01.pdf (accessed on 25 December 2022).

[50] JIS A 1108; Method of Test for Compressive Strength of Concrete. Japanese Industrial Standard Committee, Japan. 2018. Available online: www.jisc.go.jp/app/jis/general/GnrJISSearch.html (accessed on 25 December 2022).

[51] JIS A 1129-2; Method of Measurement for Length Change of Mortar and Concrete- Part 2:

Method with Contact-Type Strain Gauge. Japanese Industrial Standard Committee, Japan. 2010. Available online: www.jisc.go.jp/app/jis/general/GnrJISSearch.html (accessed on 25 December 2022).

[52] JIS A 1153: Method of Accelerated Carbonation Test for Concrete. Japanese Industrial Standard Committee, Japan. 2022. Available online: www.jisc.go.jp/app/jis/general/GnrJISSearch.html (accessed on 25 December 2022).

[53] Termkhajornkit, P.; Nawa, T.; Nakai, M.; Saito, T. Effect of fly ash on autogenous shrinkage. Cem. Concr. Res. 2005, 35, 473–482.

[54] Hu, X.; Shi, Z.G.; Shi, C.J.; Wu, Z.M.; Tong, B.H.; Ou, Z.H.; de Schutter, G. Drying shrinkage and cracking resistance of concrete made with ternary cementitious components. Constr. Build. Mater. 2017, 149, 406–415.

[55] Atis, C.D. Heat evolution of high-volume fly ash concrete. Cem. Concr. Res. 2002, 32, 751–756.

[56] Wang, L.; Yang, H.Q.; Zhou, S.H.; Chen, E.; Tang, S.W. Mechanical properties, long-term hydration heat, shrinkage behavior and crack resistance of dam concrete designed with low heat Portland (LHP) cement and fly ash. Constr. Build. Mater. 2018, 187, 1073–1091.

[57] Yin, B.; Kang, T.; Kang, J.; Chen, Y.; Wu, L.; Du, M. Investigation of the hydration kinetics and microstructure formation mechanism of fresh fly ash cemented filling materials based on hydration heat and volume resistivity characteristics. Appl. Clay Sci. 2018, 166, 146–158.

[58] Yoon, Y.S.; Won, J.P.; Woo, S.K. Enhanced durability performance of fly ash concrete for concrete-faced rockfill dam application. Cem. Concr. Res. 2002, 32, 23–30.

[59] Bouzoubaâ, N.; Zhang, M.H.; Malhotra, V.M. Mechanical properties and durability of concrete made with high-volume fly ash blended cements using a coarse fly ash. Cem. Concr. Res. 2001, 31, 1393–1402.

[60] De Matos, P.R.; Foiato, M.; Prudencio, L.R., Jr. Studies of the physical properties of hardened Portland cement paste—Part 8. The freezing of water in hardened Portland cement paste. Constr. Build. Mater. 2019, 203, 282–293.

[61] Termkhajornkit, P.; Nawa, T.; Kurumisawa, K. Effect of water curing conditions on the hydration degree and compressive strengths of fly ash–cement paste. Cem. Concr. Compos. 2006, 28, 781–789.

[62] Jiang, D.B.; Li, X.G.; Lv, Y.; Zhou, M.K.; Li, C.J. Utilization of limestone powder and fly ash in blended cement: Rheology, strength and hydration characteristics. Constr. Build. Mater. 2020, 232, 117228.

[63] Poon, C.S.; Lam, L.; Wong, Y.L. A study on high strength concrete prepared with large volumes of low calcium fly ash. Cem. Concr. Res. 2000, 30, 447–455.

[64] Sakai, E.; Miyahara, S.; Ohsawa, S.; Lee, S.H.; Daimon, M. Hydration of fly ash cement. Cem. Concr. Res. 2005, 35, 1135–1140.

[65] Oner, A.; Akyuz, S.; Yildiz, R. An experimental study on strength development of concrete containing fly ash and optimum usage of fly ash in concrete. Cem. Concr. Res. 2005, 35, 1165–1171.

[66] Oner, A.; Akyuz, S. An experimental study on optimum usage of GGBS for the compressive strength of concrete. Cem. Concr. Compos. 2007, 29, 505–514.

[67] Shariq, M.; Prasad, J.; Masood, A. Effect of GGBFS on time dependent compressive strength of

concrete. Constr. Build. Mater. 2010, 24, 1469–1478.

[68] Brooks, J.J.; Al-Kaisi, A.F. Early strength development of Portland and slag cement concretes cured at elevated temperatures. Mater. J. 1990, 87, 503–507.

[69] Zhao, Y.; Gong, J.; Zhao, S. Experimental study on shrinkage of HPC containing fly ash and ground granulated blast-furnace slag. Constr. Build. Mater. 2017, 155, 145–153.

[70] Gesoğlu, M.; Güneyisi, E.; Özbay, E. Properties of self-compacting concretes made with binary, ternary, and quaternary ce-mentitious blends of fly ash, blast furnace slag, and silica fume. Constr. Build. Mater. 2009, 23, 1847–1854.

[71] Neville, A.M. Properties of Concrete; Longman: London, UK; Volume 4, 1995.

[72] Wang, L.; Yu, Z.; Liu, B.; Zhao, F.; Tang, S.; Jin, M. Effects of fly ash dosage on shrinkage, crack resistance and fractal charac-teristics of face slab concrete. Fractal Fract. 2022, 6, 335.

[73] Altoubat, S.; Talha Junaid, M.; Leblouba, M.; Badran, D. Effectiveness of fly ash on the restrained shrinkage cracking resistance of self-compacting concrete. Cem. Concr. Compos. 2017, 79, 9–20.

[74] Yuan, J.; Lindquist, W.; Darwin, D.; Browning, J. Effect of slag cement on drying shrinkage of concrete. ACI Mater. J. 2015, 112, 267–276

[75] Li, J.; Yao, Y. A study on creep and drying shrinkage of high performance concrete. Cem. Concr. Res. 2001, 31, 1203–1206.

[76] Yang, J.; Huang, J.; He, X.; Su, Y.; Tan, H.; Chen, W.; Wang, X.; Strnadel, B. Segmented fractal pore structure covering nano- and micro-ranges in cementing composites produced with GGBS. Constr. Build. Mater. 2019, 225, 1170–1182.

[77] Weng, J.R.; Liao, W.C. Microstructure and shrinkage behavior of high-performance concrete containing supplementary ce-mentitious materials. Constr. Build. Mater. 2021, 308, 125045.

[78] Ignjatovic, I.; Carevic, V.; Sas, Z.; Dragas, J. In Proceedings Macedonian Association of Structural Engineers of the 17th Int. Symp. High volume fly ash concrete: Part 2: Durability and radiological properties. 4–7 October 2017, Ohrid, Macedonia; pp. 700–709.

[79] Ashraf, W. Carbonation of cement-based materials: Challenges and opportunities. Constr. Build. Mater. 2016, 120, 558–570.

[80] Lu, C.F.; Wang, W.; Li, Q.T.; Hao, M.; Xu, Y. Effects of micro-environmental climate on the carbonation depth and the pH value in fly ash concrete. J. Clean. Prod. 2018, 181, 309–317.

[81] Liu, J.; Qiu, Q.; Chen, X.; Wang, X.; Xing, F.; Han, N.; He, Y. Degradation of fly ash concrete under the coupled effect of car-bonation and chloride aerosol ingress. Corros. Sci. 2016, 112, 364–372.

[82] Younsi, A.; Turcry, P.; Aït-Mokhtar, A.; Staquet, S. Accelerated carbonation of concrete with high content of mineral additions: Effect of interactions between hydration and drying. Cem. Concr. Res. 2013, 43, 25–33.

[83] Castellote, M.; Fernandez, L.; Andrade, C.; Alonso, C. Chemical changes and phase analysis of OPC pastes carbonated at dif-ferent CO2 concentrations. Mater. Struct. 2009, 42, 515–525.

[84] Lye, C.-Q.; Dhir, R.K.; Ghataora, G.S. Carbonation resistance of GGBS concrete. Mag. Concr. Res. 2016, 68, 936–969.

[85] Sulapha, P.; Wong, S.F.; Wee, T.H.; Swaddiwudhipong, S. Carbonation of concrete containing cementitious materials. J. Mater. Civ. Eng. 2003, 15, 134–143.

[86] Jones, M.; Dhir, R.; Magee, B. Concrete containing ternary blended binders: Resistance to chloride ingress and carbonation. Cem. Concr. Res. 1997, 27, 825–831.

[87] Kurda, R.; de Brito, J.; Silvestre, J.D. Carbonation of concrete made with high amount of fly ash and recycled concrete aggregates for utilization of CO2. J. CO2 Util. 2019, 29, 12–19.

[88] Poon, C.S.; Lam, L.; Wong, Y.L. Effects of Fly Ash and Silica Fume on Interfacial Porosity of Concrete. J. Mater. Civ. Eng. 1999, 11, 197–205.

[89] Yu, Z.; Ma, J.; Ye, G.; van Breugel, K.; Shen, X. Effect of fly ash on the pore structure of cement paste under a curing period of 3 years. Constr. Build. Mater. 2017, 144, 493–501.

[90] Yu, Z.; Ni, C.; Tang, M.; Shen, X. Relationship between water permeability and pore structure of Portland cement paste blended with fly ash. Constr. Build. Mater. 2018, 175, 458–466.

[91] Mindess, S.; Young, F.; Darwin, D. Concrete 2nd Editio, Technical Documents; Prentice Hall, Upper Saddle River, U.S.A. 2003.

[92] Mehta, P.; Monteiro, P. Concrete Microstructure, Properties and Materials; McGraw-Hill Education, New York City, U.S.A., 2014.

[93] Wu, Z.; Lian, H. High Performance Concrete; China Railway Publication House: Beijing, China, 1999.

[94] Ho, H.-L.; Huang, R.; Lin, W.-T.; Cheng, A. Pore-structures and durability of concrete containing pre-coated fine recycled mixed aggregates using pozzolan and polyvinyl alcohol materials. Constr. Build. Mater. 2018, 160, 278–292.

Chapter 6

THE EFFECT OF FLY ASH AND GARBAGE MOLTEN SLAG FINE AGGREGATE ON THE CREEP OF CONCRETE

6.1 Introduction

As reported, the world produces about 900 million tons of fly ash every year, of which only about 53.5% is effectively utilized [8]. The utilization of by-product powders that emit less CO_2 as a replacement for a portion of cement in concrete has gained significant attention as a strategy for achieving a low-carbon society. Fly ash (FA) is one such powder that is recognized as a high-performance concrete admixture, but its utilization rate remains low. One of the reasons for this is the presence of unburned carbon in FA, which affects the stability of the finished concrete. Developing technologies to remove unburned carbon from FA can promote its increased use as a concrete admixture. Flotation methods are being developed and studied to improve and stabilize the quality of FA [1]. However, there is a lack of research on the use of flotation-modified FA as an admixture, warranting further investigation Many scholars have studied the properties of fly ash concrete, pointing out that the application of fly ash can improve the working performance of concrete, improve durability, reduce shrinkage, and improve the microscopic pore structure [9-13]. Moreover, when FA is used as an admixture in concrete structures, significant deflections, and deformations due to creep and drying shrinkage are observed. In this study, the compression creep properties of concrete containing 20% FA were examined.

In addition, with the rapid development of industrialization and urbanization, concrete was widely used in the construction industry, around 10 billion cubic meter of concrete was used every year [5], aggregate accounts for about 60% to 80% of the concrete volume [6]. As a result, a large amount of natural aggregate is consumed [7]. In 2012, the amount of direct incineration of general waste in Japan was 33.99 million tons per year, of which 12.35 million tons, or 36%, was melted to produce 790,000 tons of molten slag. The manufactured molten slag is used as road aggregate, concrete aggregate, ground improvement material, and the like. The garbage molten slag (GMS) generated from the melting facility for general waste is being effectively used from the viewpoint of recycling and quality stability, but the utilization rate as an aggregate for concrete is currently low. Therefore, with the aim of increasing the amount of molten slag used, it is necessary to consider a formulation that exhibits the same performance as when using natural aggregate. However, the research on the properties of concrete containing GMS and the effect of fly ash on concrete containing GMS is not enough. Therefore, in this study, we evaluated the durability of concrete with different mixing ratios of garbage molten slag and fly ash.

In summary, our findings underscore the considerable potential benefits of utilizing fly ash and garbage molten slag fine aggregate in concrete mixtures. These advantages include improved long-term strength and reduced shrinkage, which are of utmost importance in the construction industry. We recommend further research in this area to explore additional properties and fine-tune the utilization of these alternative materials in concrete production, contributing to a more sustainable and resilient construction sector.

6.2 Creep of fly ash concrete

6.2.1 Experiment outline

In this experiment, various materials were used, and their physical properties are summarized in Table 6.1. Ash A and Ash B are fly ashes obtained from thermal power generation, and they were modified to have an ignition loss of ≤1.0%. Ash C is a Japanese Industrial Standard (JIS)-certified product.

Table 6.1. Materials properties

Item	Type	Physical properties	Symbol
Cement	Ordinary Portland cement	Density 3.16[g/cm³]	C
Water	Tap water	-	W
Fine aggregate	Sea sand	Absolute dry density 2.59[g/cm³] Water absorption 0.76% Coarse grain rate 2.4 Actual rate 61.2%	S
Coarse aggregate	Crushed stone	Absolute dry density 2.69[g/cm³] Water absorption 1.41% Coarse grain rate 6.9 Actual rate 56.7%	G
Agent	AE water reducer	Alkyl ether type anionic surfactant	
Admixture	Modified fly ash(A)	Density 2.25[g/cm³] Ignition loss0.42% Plain specific surface area 3480 [cm²/g] BET specific surface area 1.54[m²/g]	FA
	Modified fly ash(B)	Density 2.29[g/cm³] Ignition loss0.92% Plain specific surface area 3690 [cm²/g] BET specific surface area 5.23[m²/g]	
	Fly ash(C) (Adapted to JIS II)	Density 2.36[g/cm³] Ignition loss1.32% Plain specific surface area 4900 [cm²/g] BET specific surface area 2.17[m²/g]	

The mix proportions used in the experiment are presented in Table 6.2. The mixing procedure involved a unit water volume of 180 kg/m^3 and a water-to-binder ratio of 50%. Four formulations were tested in total: one without fly ash (FA-free concrete) for comparison, and three with 20% of the cement replaced by fly ash, each using a different type of fly ash.

Table 6.2. Mix proportions.

Symbol	W/C	W/B	Unit mass(kg/m³)				
			W	C	FA	S	G
N	50	50	180	360	0	805	945
A,B,C	63			288	72	794	

In order to measure the strain, a creep test was conducted following the guidelines of JIS A 1157, a method for testing the compressive creep of concrete. The test specimens were demolded after 1 day of aging, cured in water at 20°C for 7 days, and then transferred to a constant temperature room at 20°C for air curing, where the creep test was conducted. However, it is important to note that the humidity in this room could not be strictly controlled, and during the loading, the humidity fluctuated between 40% and 63%.

For the creep test, a loading device utilizing a separation-type hydraulic jack was used. Three test pieces with dimensions of φ100 × 200 mm were vertically stacked. The applied load was set to one-third of the compressive strength of a 28-day-old test piece, and the loading was initiated at 28 days. Three strain gauges were affixed to three different locations at the center of each test piece, and the average value of the strain measured by these gauges was considered as the total strain of that particular test piece. The average value of the strain from the three test pieces was then calculated as the total strain for that specific preparation.

To determine the applied load, three specimens with dimensions of φ100 × 200 mm were prepared for the compressive strength test. The specimens were cured in the constant temperature room where the creep test was conducted. The compressive strength was measured following the guidelines of JIS A1108, a method for testing the compressive strength of concrete.

To calculate the creep strain, two unloaded specimens with the same size as those used in the creep test (φ100 × 200 mm) were prepared to test the drying shrinkage. Strain gauges were attached to these specimens, which were then stored in the constant temperature room until the measurements were performed using a data logger. Both the creep test and the drying shrinkage test were conducted simultaneously.

The pore structure of the concrete was evaluated since voids with a diameter of ≥3 nm are known to significantly affect properties such as strength, elastic modulus, creep, and shrinkage[2]. The pore diameter was measured using the mercury intrusion method. After the creep specimens were removed from the loading device, each unloaded specimen was crushed and filtered through a sieve to collect grains with a diameter of 2.5–5.0 mm, which were used as samples. These samples were immersed in acetone for 2 hours to halt hydration, then vacuum-dried using a vacuum pump for 72 hours until there was no further change in mass. The samples were finally cured, and the pore diameter measurement was performed twice for each sample, with the average value calculated.

6.2.2 Compressive strengths

Fig. 6.1 illustrates the compressive strength of the test specimens at different stages: before loading at 28 days, after loading at 273 days, and without loading at 273 days. The results indicate that the difference in compressive strength between normal concrete at 28 days and 273 days was small. This suggests that the continued loading did not have a significant impact on the strength of the normal concrete specimens.

At 273 days, it was observed that Ash A had the lowest compressive strength among the three types of fly ash formulations. On the other hand, Ash B exhibited increased strength both before and after loading compared to the strength at 28 days. This increase in strength can be attributed to the pozzolanic reaction, which is a chemical reaction between the fly ash and calcium hydroxide in the concrete matrix. Ash C also showed a slight increase in strength, but Ash B had the highest compressive strength among the three types of formulations containing fly ash. Furthermore, when

fly ash was added to the mixture, the compressive strength after loading tended to be slightly higher than that without loading. This suggests that the presence of fly ash in the concrete contributed to maintaining or enhancing the compressive strength, even under the applied loading conditions.

Overall, the results indicate that incorporating fly ash into the concrete mixture can have a positive impact on the compressive strength, with Ash B demonstrating the most significant improvement among the tested formulations.

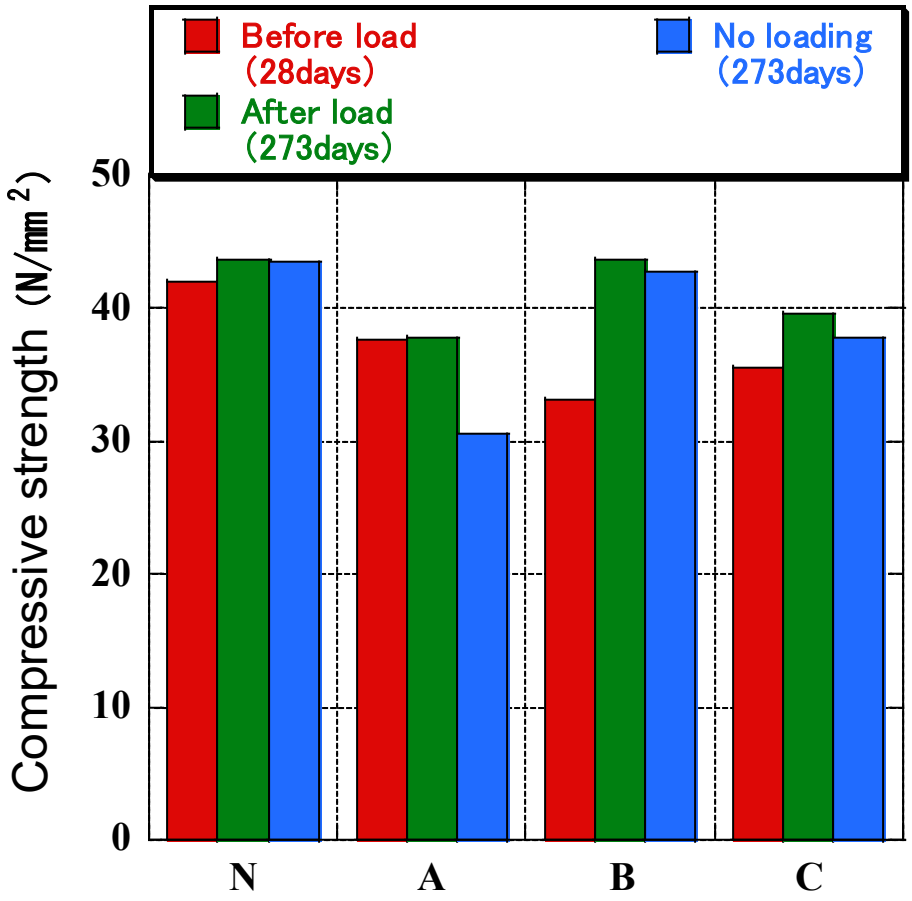

Fig 6.1. Compressive strength

6.2.3 Drying shrinkage

Fig. 6.2 shows the results of drying shrinkage with time. The results show that there is no relationship with the type of fly ash, and concrete with three different types of fly ash with 20% content shows similar drying shrinkage values to normal concrete. In the literature review section of Chapter 2 of this paper, it is shown that fly ash replacing a portion of cement tends to reduce the drying shrinkage of concrete. However, in this experiment, in order to maintain the same conditions as the creep experiment, the concrete specimens were first cured in water for 7 days and then in air until the age of the material was 28 days. This is different from the experimental method used in most other studies. Therefore, it is possible that the difference between fly ash concrete and normal concrete drying shrinkage is mainly concentrated before 28 days.

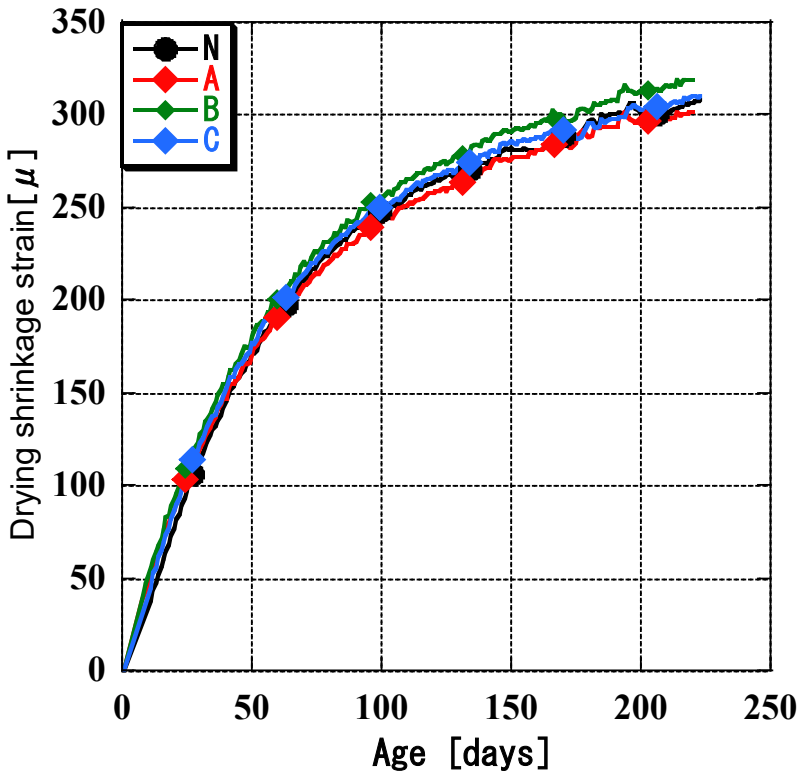

Fig. 6.2 Drying shrinkage strain

6.2.4 Creep

Fig. 6.3 displays the development of creep strain over time. The findings indicate that the addition of fly ash (FA) led to a reduction in creep strain by approximately 30% to 50% compared to the scenario where no FA was added. This suggests that incorporating FA at a replacement ratio of 20% effectively mitigated creep strain in the concrete.

Furthermore, the findings suggest that the specific type of FA used had a notable impact on the extent of creep strain reduction. Different types of FA exhibited varying levels of effectiveness in reducing creep strain. When compared to ordinary concrete, the concrete samples containing 20% of Ash A, Ash B, and Ash C fly ash experienced reductions in creep strain of approximately 28.8%, 37.8%, and 45.8% respectively over a period of 182 days. These results underscore the importance of considering the distinct properties and characteristics of the FA being utilized.

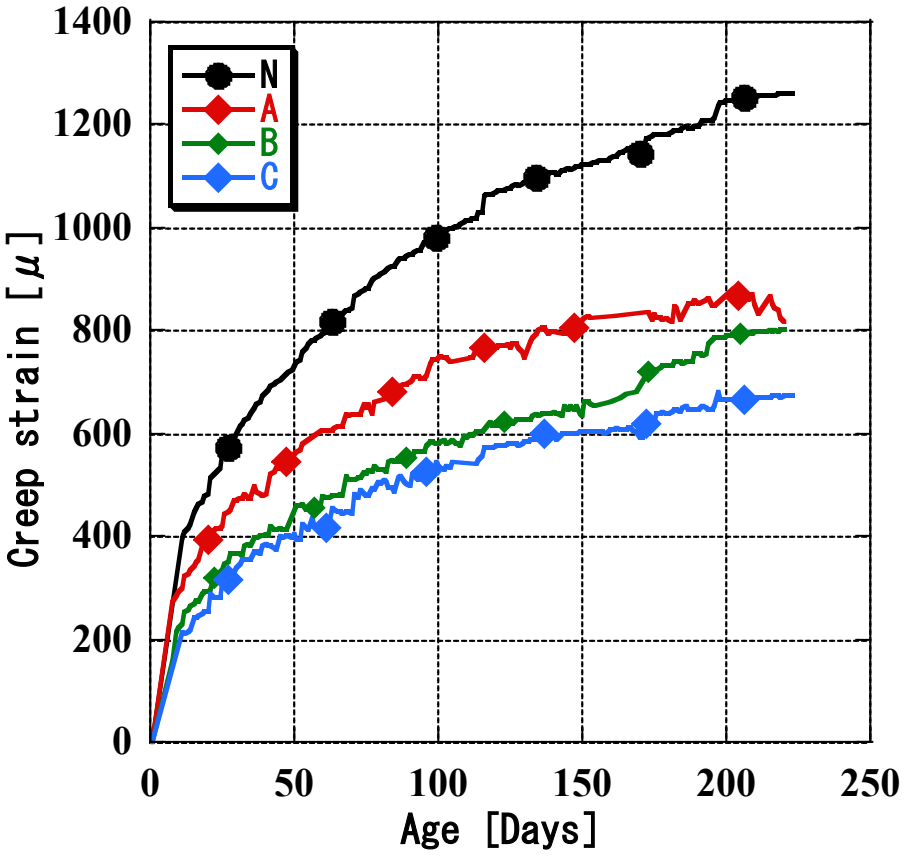

Fig. 6.3 Creep strain

The correspondence between the experimental results of the specific creep strain obtained from the experiments and the predicted values obtained from the AIJ equation[3] was examined.

$$C(t,t_0) = CR \cdot \log_e(t - t_0 + 1) \tag{1}$$

$$CR = (6.8 \cdot x - 0.12 \cdot G + 17.5) \cdot (t_0)^{-0.33} \cdot \left(1 - \frac{h}{100}\right)^{0.36} \cdot (V/S)^{-0.43}$$

C(t,t₀)： Specific creep strain (×10-6/(N/mm²))

CR： Coefficient determined by regression analysis (×10-6/(N/mm²))

t： AGE(days)　　t₀： Loading age (days)　　h： Relative humidity (%)

G： Unit coarse aggregate (kg/m³)　　V / S： Volume surface area ratio

Fig. 6.4 illustrates the relationship between the predicted values obtained from equation (1) and the specific creep strain as measured for each specimen. The predicted values closely align with the measured values of normal concrete creep strain. However, it is important to note that the AIJ (Architectural Institute of Japan) formula, represented by equation (1), does not consider variables related to admixtures, including fly ash. As a result, the formula does not account for the effects of admixtures on creep strain. To address this limitation, in this study, since fly ash was added as an admixture, the accuracy of the numerical predictions was evaluated using the root mean square error (RMSE). The RMSE indicates the deviation between the predicted values and the actually measured values. Consequently, a correction coefficient was employed to adjust the predicted values to align with the measured values.

Table 6.3 presents the calculated correction coefficients for the different types of fly ash used in the study: Ash A, Ash B, and Ash C. The correction coefficients were determined as follows: Ash A is 0.79, Ash B is 0.76, and Ash C is 0.64, with an average coefficient of 0.73. Based on these

findings, it was determined that the appropriate correction coefficient for incorporating 20% fly ash into the concrete mixture is approximately 0.73. In summary, the numerical predictions based on the AIJ formula were adjusted using a correction coefficient to better align with the actually measured creep strain values.

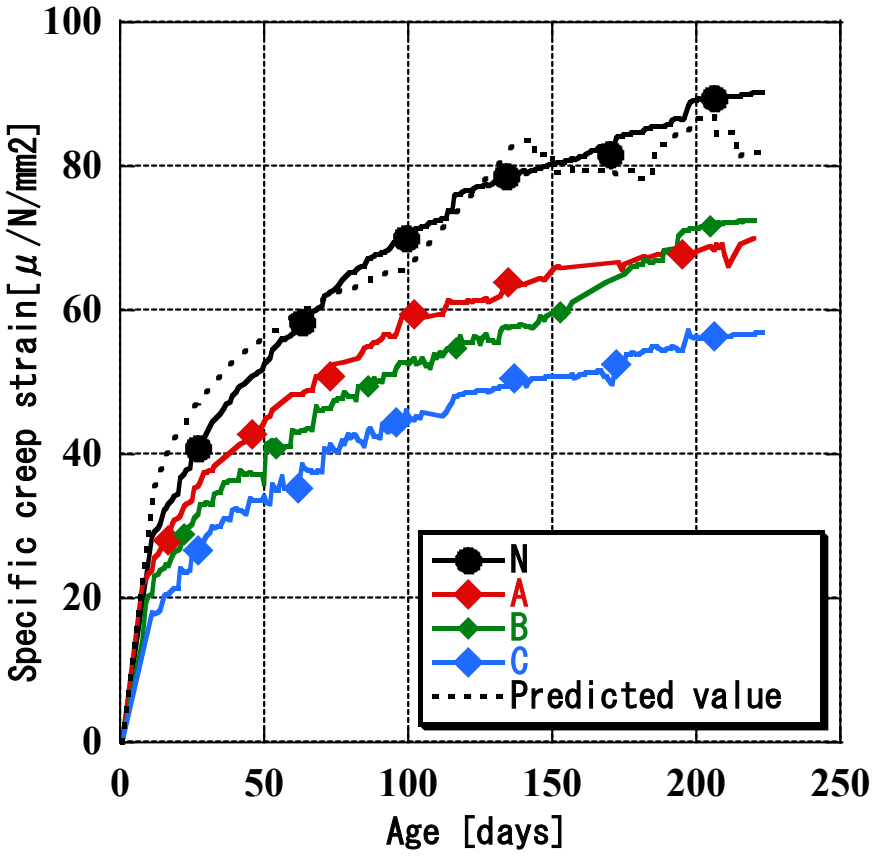

Fig. 6.4 Specific creep strain

Table 6.3 Correction factor

	A	B	C
Correction factor	0.79	0.76	0.64
Average	0.73		

6.2.5 Pore structure

Fig. 6.5 presents the total pore volume for each formulation. It can be observed that Ash B exhibited lower pore volume values compared to the other formulations, both after loading and without loading. This indicates that the concrete containing Ash B had smaller voids in comparison to the other formulations. The smaller total pore volume in Ash B is believed to be a contributing factor to its higher compressive strength when compared to the other formulations that included fly ash (FA). A lower pore volume generally corresponds to a more compact and denser concrete structure, which can lead to improved compressive strength. Therefore, based on the results, it can be inferred that the relatively small total pore volume in Ash B, resulting in a more compact concrete

matrix, played a role in its superior compressive strength among the formulations that incorporated fly ash.

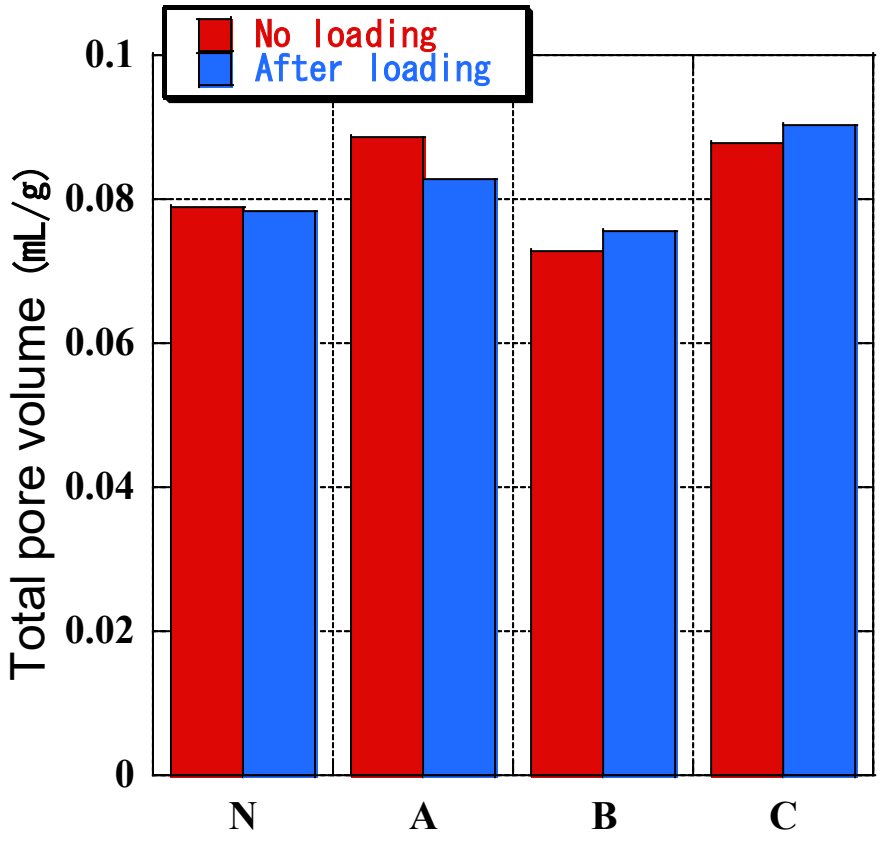

Fig 6.5 Total pore volume

Fig 6.6 depicts the distribution of pore sizes after loading, while Fig. 6.7 illustrates the distribution of pore sizes without loading. In both cases, Ash B exhibited the lowest pore volumes for voids with a diameter of ≥0.1 μm. Previous research [4] has indicated that the pozzolanic reaction of fly ash (FA) leads to a decrease in pore volumes for pores >0.1 μm and an increase in pores ≤0.1 μm, resulting in increased strength of pores ≤0.1 μm. This suggests that the lower pore volumes for ≥0.1 μm in Ash B may be attributed to the pozzolanic reaction. Subsequently, the pore volumes were classified into different size ranges, including ≤50 nm, ≤100 nm, ≤200 nm, ≤500 nm, and ≤2000 nm, to examine their relationship with specific creep strain. Figure 8 demonstrates the correlation between the pore volume in each size range and the specific creep strain. Moreover, a regression analysis was conducted to determine the coefficient of determination (R^2). Notably, the regression line for pores with a diameter of ≤500 nm exhibited a high determination coefficient ($R^2 \geq 0.95$), indicating a strong correlation. In contrast, the regression line for pores with a diameter of ≤2000 nm had a lower determination coefficient ($R^2 = 0.79$). Consequently, regardless of the presence or absence of fly ash (FA), the relationship between the number of pores with a diameter of ≤500 nm in the concrete and the specific creep strain could be approximated by a straight line. This suggests that as the number of pores with a diameter of ≤500 nm increases, the specific creep strain tends to decrease.

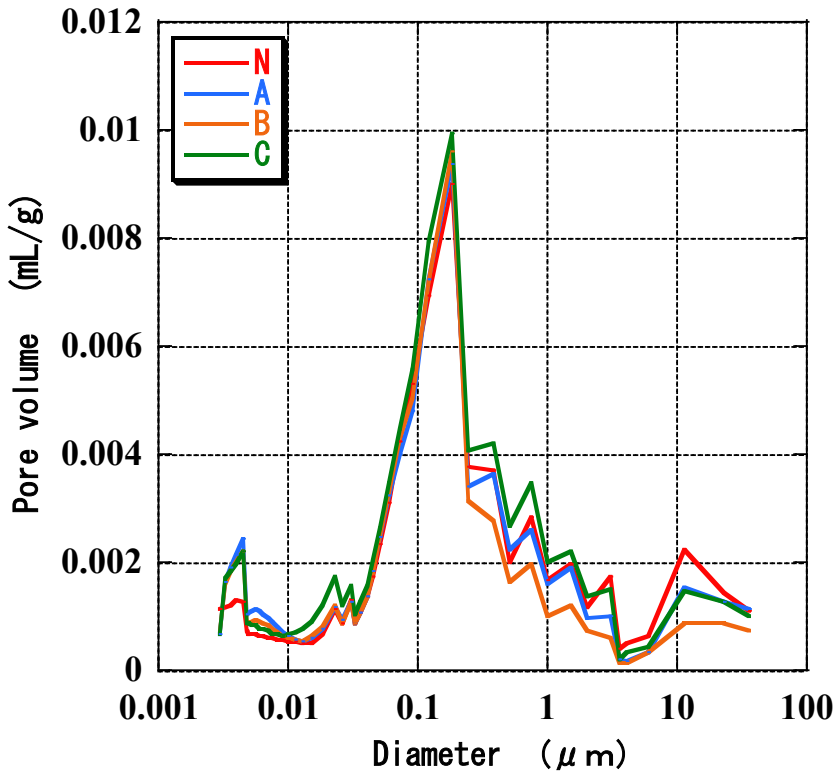

Fig. 6.6 Distribution of pore volume after loading

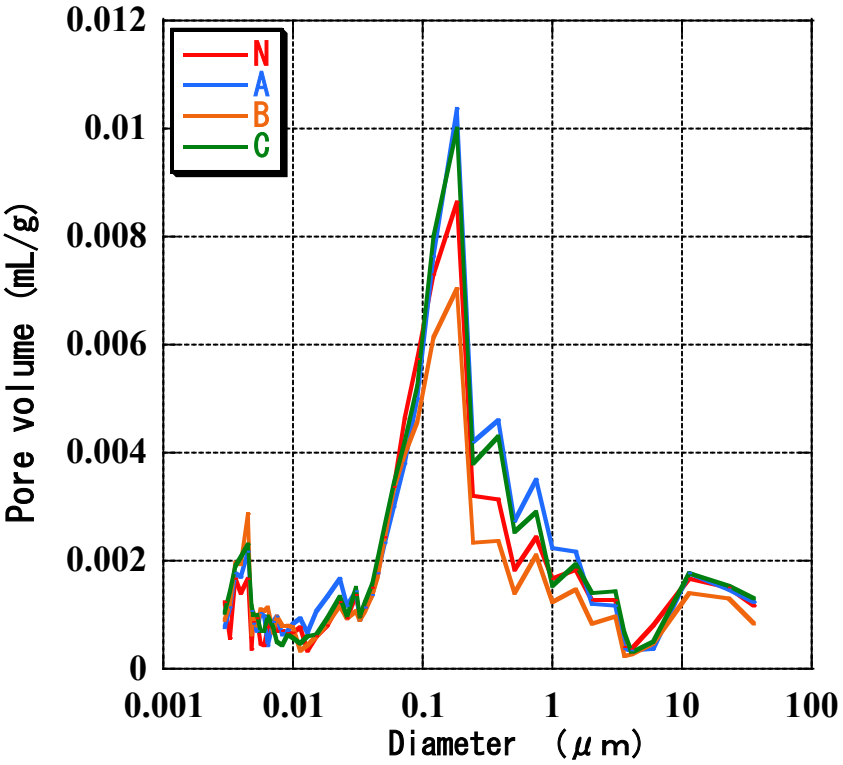

Fig. 6.7 Unloaded pore volume distribution

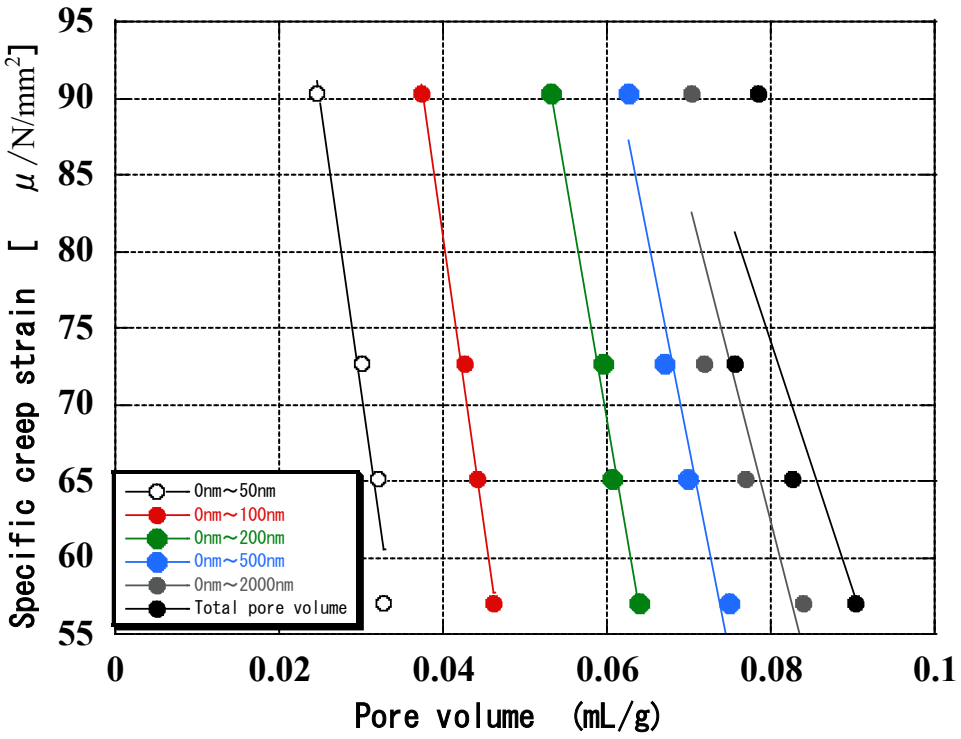

Fig. 6.8 Interval pore volume and specific creep strain

6.3 Properties of Fly Ash and Garbage Molten Slag Fine Aggregate Concrete

6.3.1 Experiment outline

Table 1 and 2shows the physical properties of the materials used in this experiment. As the cement, ordinary Portland cement was used, sea sand and garbage molten slag (GMS) were used as fine aggregate, and crushed stone was used as coarse aggregate. Fly ash (FA) corresponding to Class II in JIS A 6201.

Table 6.4 Properties of the fine and coarse aggregates

Property	Coarse aggregate	Sea sand	GMS	JIS A5022 (M)
Oven-dried density (g/cm^3)	2.69	2.63	2.79	> 2.2
Fineness modulus	6.9	2.41	2.75	_
Water absorption (%)	1.41	0.94	0.81	< 7.0
Void content (%)	43.3	38.8	40.3	_

Table 6.5 The properties of the cement and fly ash

Composites	FA	Cement
SiO_2 (%)	53.8	21.5
Al_2O_3 (%)	13.5	5.4
Fe_2O_3 (%)	13	3.0
CaO (%)	8.99	64.9
SO_3 (%)	0.49	1.4
MgO (%)	1.48	2.1
Loss on ignition (%)	2.1	0.8
Density (g/cm^3)	2.31	3.16
Blaine specific area (cm^2/g)	3270	3000

Table 3 shows the mix proportions, and the unit water volume was 170 kg / m^{3,} the water-binder ratio was 45.5% for the control concrete, and 52.3% for the concrete with fly ash. Keep the compressive strength of concrete at 28d remain the same as the control group, cement replaced with fly ash (30% by strength contribution rate). In addition, the unit coarse aggregate bulk volume was set to 0.5 m^3 / m^3 to make it a high-fluidity concrete, target air volume is 5.0 ± 1%.

Table 6.6 Mix proportions

Type	W/B	Unit mass(kg/m³)					
		W	C	FA	S	RFA	G
FA0-0	0.455	170	374	0	952	0	945
FA30-0	0.366	170	325	139	828	0	945
FA30-25	0.366	170	325	139	621	220	945
FA30-50	0.366	170	325	139	414	439	945

Measurement items are compressive strength, drying shrinkage and creep properties. The compressive strength test was conducted according to JIS A 1108, the drying shrinkage test was conducted according to "Method of measurement for length change of mortar and concrete" of JIS A1129-2, and 100 × 100 ×400mm prismatic specimens were produced. After casting, they were demolded at 1 day of age, then cured in water at 20 ° C for 7 days or in a constant temperature room with a temperature of 20 ° C and a humidity of 60%. Specimens were taken out of the water at 7 days of age, and a stainless-steel chip was attached to both end faces of the specimens, and then both end faces were sealed to measure the base length. The specimens for measuring the drying shrinkage were cured in a constant temperature and humidity room with a temperature of 20 ± 1.0 ° C and a relative humidity of 60 ± 5%. In the creep test, the strain was measured according to JIS A 1157 "Method of test for compressive creep of concrete". This constant temperature room could not strictly control the initial one-month humidity. The creep test uses a loading device of a separate type of hydraulic jack. Three test specimens were stacked vertically. The loading load was set to 1/3 of the maximum load of compressive strength at 28 days, and loading started from 28 days. Three strain gauges were attached to three places in the center of the test specimen, and the average value of the three strain gauges was taken as the total measured strain of the test specimen. And the average value of three test specimens was taken as the total strain of the mix proportion. In order to calculate the creep strain, measuring the no-load strain by preparing two pieces no-load specimen of Φ100 x 200 mm in each mix proportion similar to the creep test, attaching the strain gauges, and storing in a constant temperature room where the creep test is performed, and the measurement was performed with a data logger simultaneously with creep strain.

6.3.2 Compressive strength

Figure 1 illustrates the results of compressive strength testing. At 7 days of age in a water curing environment, there is a tendency for the compressive strength to decrease as the substitution rate of both fly ash (FA) and garbage molten slag increases. However, at 28 days of age in water curing, the compressive strength values of the FA0-0, FA30-0, and FA30-25 mixes show similar results. This suggests that a 30% strength contribution rate through the incorporation of fly ash is an appropriate choice. Notably, the FA30-0 mix exhibits the highest increase in strength after 28 days of age, indicating the influence of the pozzolanic reaction. While the FA30-25 and FA30-50 mixes also expected to undergo pozzolanic reaction due to the presence of fly ash, the increase in strength is not as significant as in the FA30-0 mix. This implies that the addition of garbage molten slag in concrete is harmful to the increase of compressive strength beyond 28 days of age. In terms of curing methods, it is observed that for concrete containing fly ash, the compressive strength increase is more pronounced during air curing up to 28 days of age, while water curing tends to enhance strength between 28 and 91 days of age. This suggests that water curing has a greater effect on enhancing the pozzolanic reaction facilitated by fly ash compared to air curing.

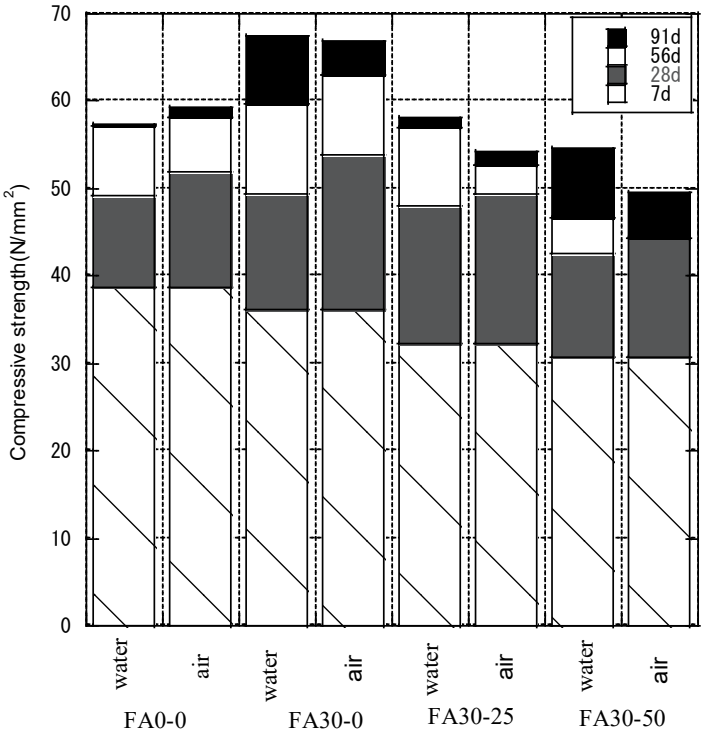

Fig. 6.9 The compressive strength of concrete

6.3.3 Drying shrinkage

Figure 2 presents the time-dependent development of drying shrinkage. A comparison between FA0-0 and FA30-0 reveals a tendency for reduced drying shrinkage when fly ash is incorporated. Furthermore, FA30-25 exhibits a larger strain, while FA30-50 demonstrates a smaller strain compared to FA30-0. In comparison to normal concrete (FA0-0), the drying shrinkage strain of FA30-0, FA30-25, and FA30-50 in 98 days is reduced by approximately 13.5%, 9.6%, and 18.7%, respectively. These results indicate that incorporating fly ash in the concrete mix has a beneficial effect in reducing the drying shrinkage strain over time. Furthermore, the inclusion of garbage molten slag fine aggregate in the concrete mix did not show a significant impact on the drying shrinkage.

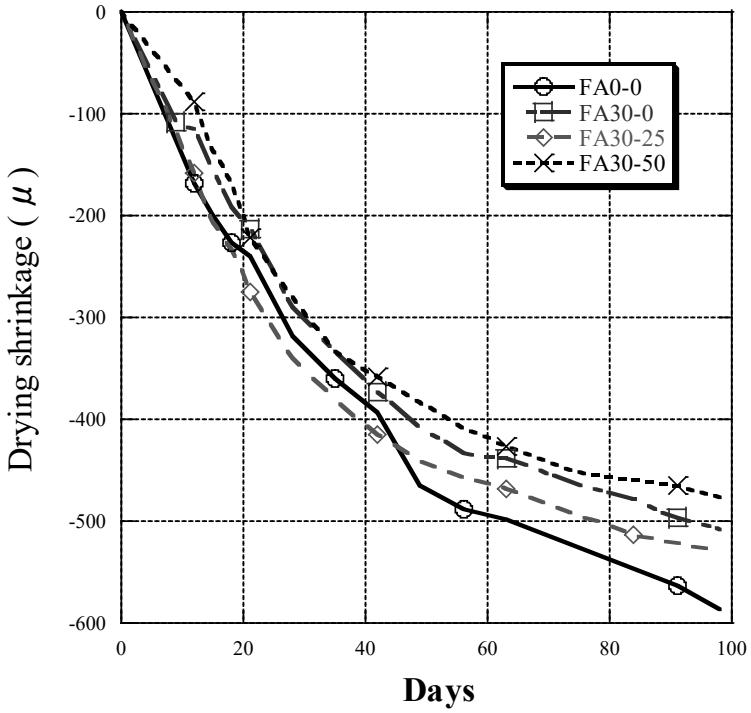

Fig. 6.10 The development over time in drying shrinkage.

6.3.4 Creep

Figure 4 illustrates the variation of unit creep strain over time. It can be observed that FA30-0 and FA30-25 exhibit lower creep strain values compared to FA0-0. This confirms that incorporating fly ash in the concrete mix has a beneficial effect in mitigating creep strain. However, FA30-50 shows a higher strain value than FA0-0. This indicates that when the replacement rate of molten slag reaches 50%, the impact on strain becomes more prominent, leading to an increase in creep strain. In this study, we aimed to assess the accuracy of the creep strain prediction formula by comparing it with the experimental results obtained in our experiments. The AIJ formula (proposed by the Architectural Institute of Japan) is known for its high adaptability to ordinary concrete [10], so we focused on analyzing this formula exclusively. However, it was observed that the predicted values of FA0-0, FA30-0, and FA30-25 tended to be overestimated compared to the experimental values. On the other hand, the predicted value for FA30-50 was closer to the experimental value. It should be noted that while the AIJ formula is commonly applied to ordinary concrete, the specimens used in our study were designed as high-strength concrete with a water-binder ratio of approximately 40%. As a result, the experimental values deviated significantly from the predictions based on the formula. To address this discrepancy, we conducted regression analysis to determine correction factors that would align the predicted values with the experimental values. Table 3 presents the analyzed correction coefficients, which were found to be 0.52 for FA0-0, 0.56 for FA30-0, 0.60 for FA30-25, and 0.95 for FA30-50.

In light of these findings, when applying the AIJ formula to calculate predicted values for high-strength concrete, it is recommended to utilize the respective correction coefficients mentioned above, which is 0.56 on average for low aggregate replacement rate. This adjustment will lead to

more accurate predictions aligned with the experimental data. However, the predicted values for concrete with high aggregate replacement rates should continue to be investigated.

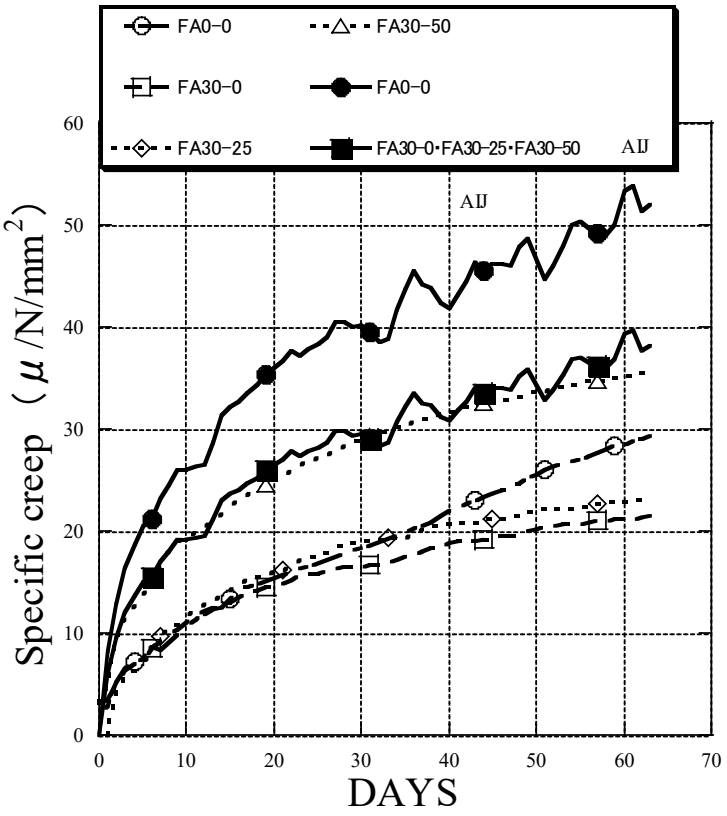

Fig. 6.11 The change over time in specific creep strain.

Table 6.7 The correction coefficients

	FA0-0	FA30-0	FA030-25	FA30-50
coefficients	0.52	0.56	0.6	0.95

6.3.5 The relationship between pore structure and compressive strength or drying shrinkage

Figure 5 illustrates the pore volume of the concrete samples. When comparing the reduction in pore volume between 7 and 91 days, it was observed that concrete containing fly ash exhibited a more significant decrease. This finding aligns with the results of compressive strength, supporting the notion that the strength enhancement in fly ash mixtures after 28 days is attributed to the pozzolan reaction. Furthermore, no substantial difference was observed when comparing FA30-25 and FA30-50, suggesting that the substitution rate of garbage molten slag has a minimal effect on the pore structure.

Figure 6 depicts the relationship between pore volume and compressive strength. Surprisingly, no discernible correlation was found between the pore volume, regardless of whether it exceeded 50 nm or encompassed the total pore volume. This indicates that the compressive strength of concrete is influenced by factors beyond the pore structure, such as the aggregate material used.

In Figure 7, the relationship between pore volume and drying shrinkage is presented. Notably, a significant correlation was observed specifically within the range of 0.003 μm to 0.1 μm pore size. Consequently, it is inferred that the pore volume within this range significantly impacts the drying

shrinkage behavior of concrete.

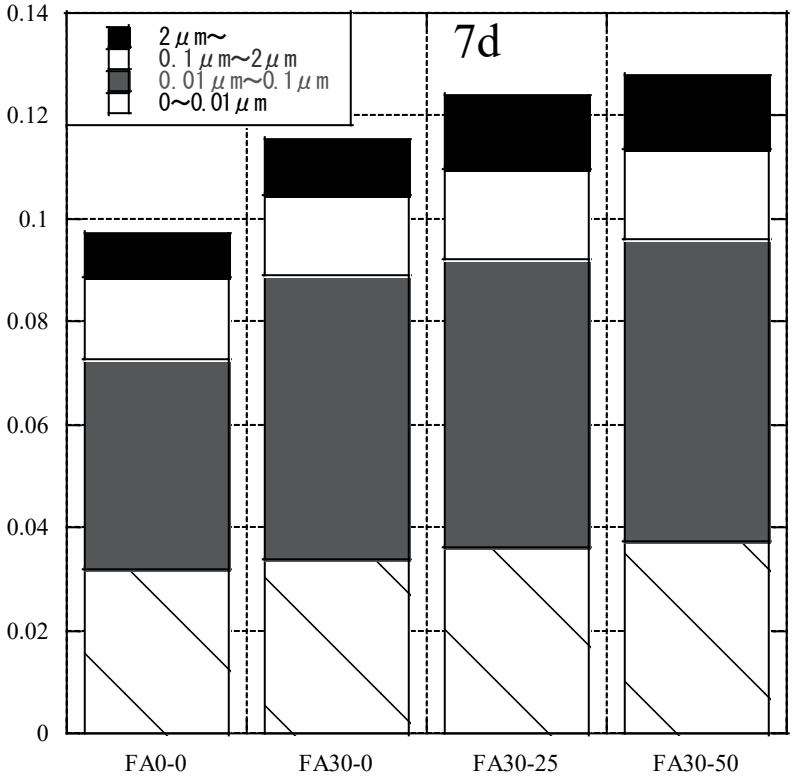

(a)

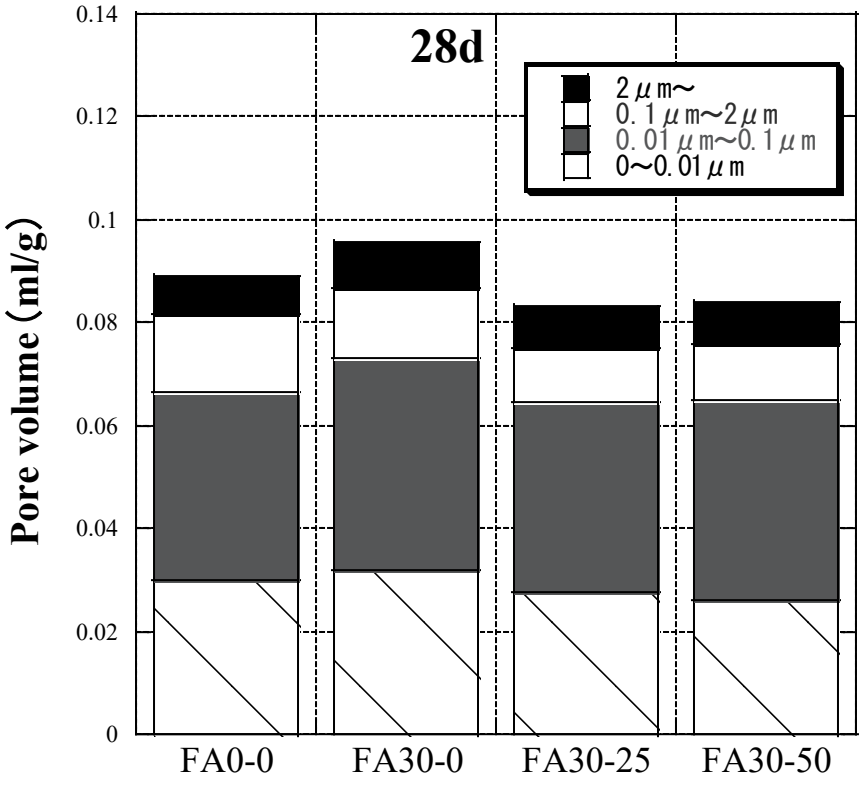

(b)

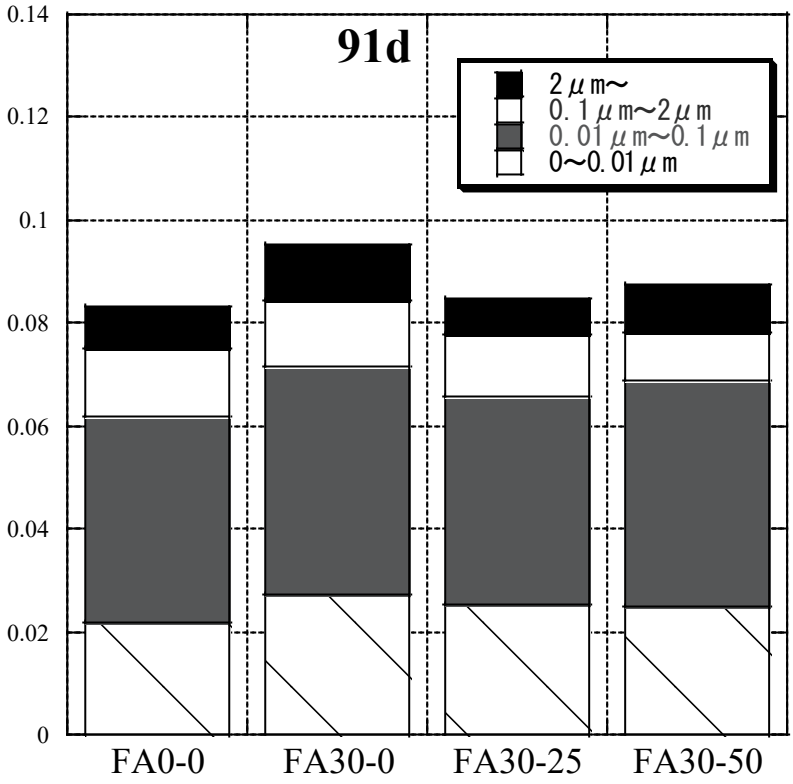

(c)

Fig. 6.12 The pores volume of concrete, (a)7d, (b)28d, (c)91d

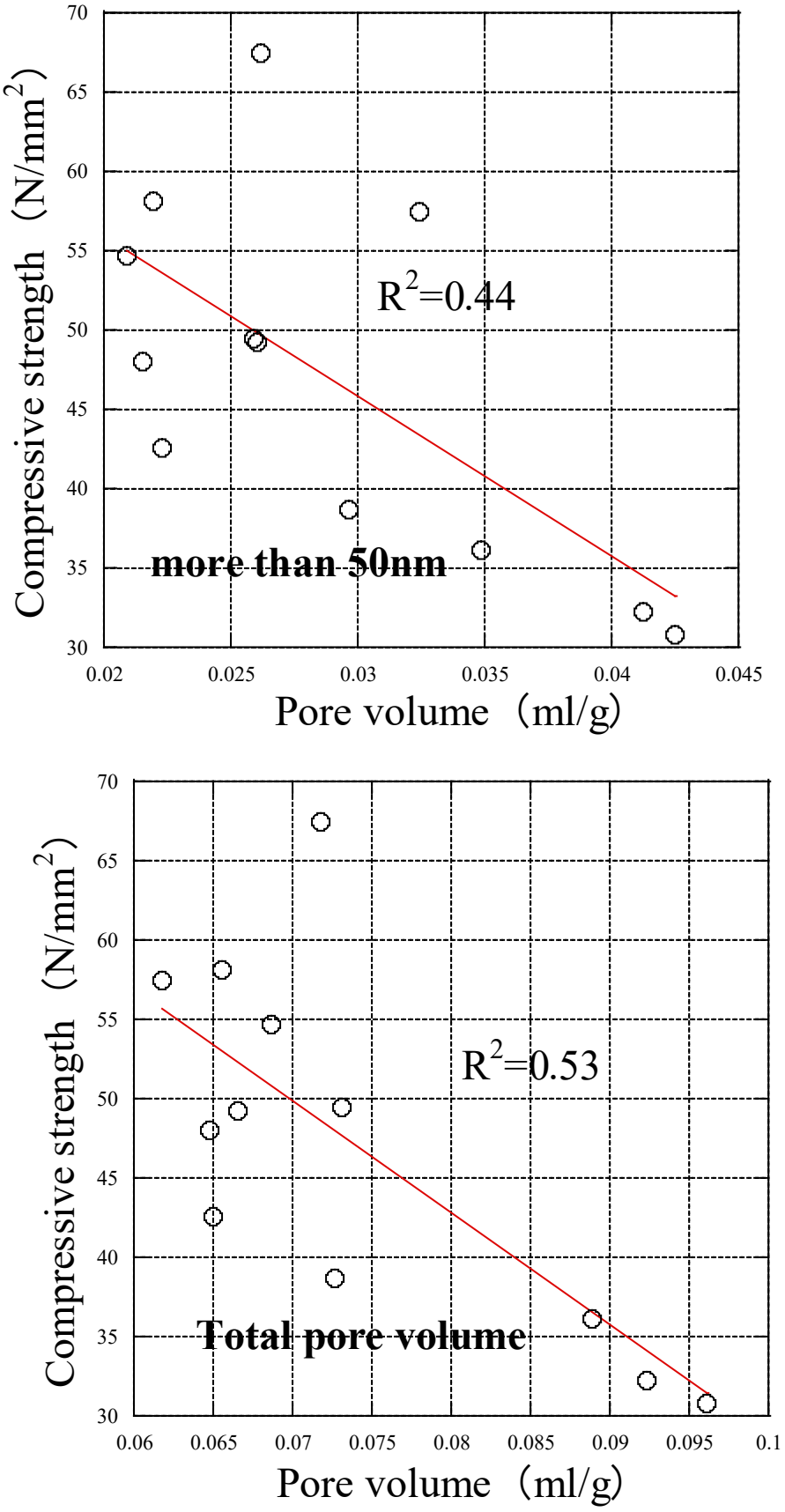

Fig. 6.13 The relationship between the pores volume and the compressive strength.

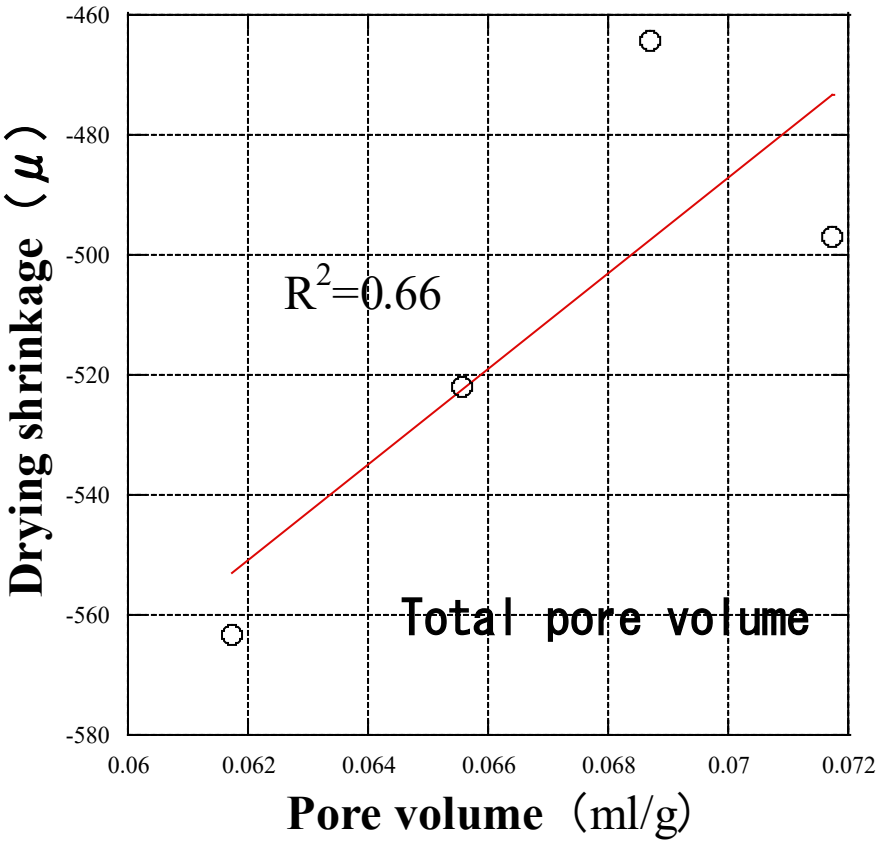

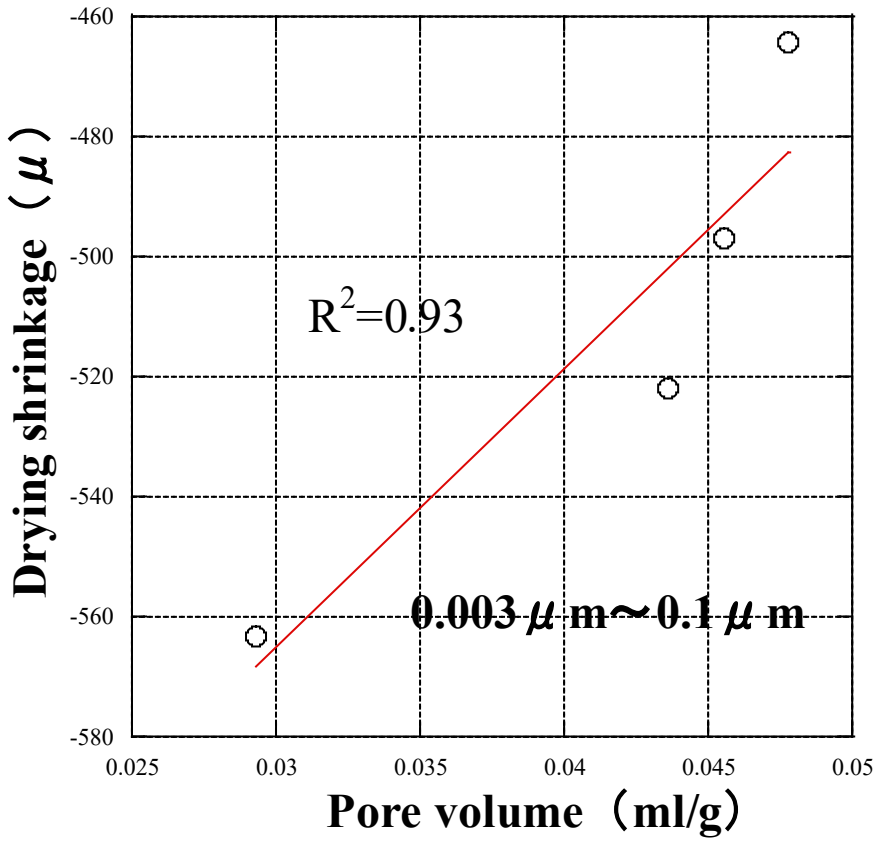

Fig. 6.14 The relationship between the pore volume and the dry shrinkage.

6.4 Conclusion

1. Incorporating fly ash at a 20% replacement ratio effectively reduced the unit creep strain in concrete. The predicted values of normal concrete obtained from the AIJ equation for unit creep strain aligned well with the measured values. The introduction of a correction factor of approximately 0.73 accounted for the influence of fly ash in the predicted values.
2. Concrete mixed with fly ash exhibited a slight increase in compressive strength after loading compared to the unloaded condition. However, the effect of loading on the compressive strength was minimal in concrete without fly ash.
3. The quantity of pores with a diameter less than 500 nm and the unit creep strain in concrete showed a consistent linear relationship regardless of the presence or absence of fly ash. This implies that as the number of pores with a diameter less than 500 nm increases, the specific creep strain tends to decrease.
4. Concerning compressive strength, FA30-0 exhibited the most significant increase in strength after 28 days, which can be attributed to the pozzolan reaction. Additionally, the inclusion of garbage molten slag demonstrated a suppressive effect on the strength increase beyond 28 days of age.
5. With regard to drying shrinkage strain, the incorporation of fly ash resulted in a tendency towards reduced drying shrinkage. Moreover, the shrinkage reduction effect achieved by replacing molten slag was found to be superior to that of fly ash.
6. In terms of unit creep strain, the addition of fly ash in concrete showcased a strain suppression effect. While the impact on creep strain at a 25% substitution rate of molten slag was relatively small, an increased substitution rate of 50% exhibited a tendency towards elevated creep strain.
7. Regarding pore volume, mixtures containing fly ash displayed a more substantial decrease in pore volume during the period between 7 and 91 days of age.

Reference

[1] Koji Takasu: Experimental study on removal of unburned carbon in fly ash by flotation and characteristics of concrete using fly ash slurry, The Architectural Institute of Japan's *Journal of Structural and Construction Engineering*, 79(697),pp.331-340,

[2] Architectural Institute of Japan: Testing methods for quality control and maintenance of reinforced concrete buildings, p214-215, 2007, 3

[3] Yoshiaki Sato: Study on prediction formula of time-dependent strain of concrete based on domestic experimental data, The Architectural Institute of Japan's *Journal of Structural and Construction Engineering*, 599, 9-15,2006.1

[4] Takeshi Yamamoto: Experimental study on tissue densification and strength development mechanism of fly ash due to pozzolanic reaction, Journal of Japan Society of Civil Engineers, E, Vol.63, No1, 52-65, 2007,1

[5] Meyer, Christian. "The greening of the concrete industry." Cement and concrete composites 31.8 (2009): 601-605.

[6] L. Evangelista, M. Guedes, J. de Brito, A.C. Ferro, M.F. Pereira, Physical, chemical and mineralogical properties of fine recycled aggregates made from concrete waste, Construct. Build. Mater. 86 (2015) 178–188.

[7] Kumar, G. S. (2019). Influence of fluidity on mechanical and permeation performances of recycled aggregate mortar. Construction and Building Materials, 213, 404-412.

[8] Heidrich, Craig, Hans-Joachim Feuerborn, and Anne Weir. "Coal combustion products: a global perspective." World of coal ash conference. 2013.

[9] De Maeijer, P.K.; Craeye, B.; Snellings, R.; Kazemi-Kamyab, H.; Loots, M.; Janssens, K.; Nuyts, G. Effect of ultra-fine fly ash on concrete
performance and durability. Constr. Build. Mater. 2020, 263, 120493.

[10] Moghaddam, F.; Sirivivatnanon, V.; Vessalas, K. The effect of fly ash fineness on heat of hydration, microstructure, flow and compressive strength of blended cement pastes. Case Stud. Constr. Mater. 2019, 10, e00218

[11] Saha, A.K. Effect of class F fly ash on the durability properties of concrete. Sustain. Environ. Res. 2018, 28, 25–31.

[12] Moffatt, E.G.; Thomas, M.D.; Fahim, A. Performance of high-volume fly ash concrete in marine environment. Cem. Concr. Res. 2017, 102, 127–135.

[13] Kristiawan, S.A.; Aditya, M.T.M. Effect of High Volume Fly Ash on Shrinkage of Self-compacting Concrete. Procedia Eng. 2015,125, 705–712

Chapter 7

THE PROPERTIES OF FLY ASH, BIOMASS FLY ASH AND GGBS BASED GEOPOLYMER CONCRETE.

7.1 Introduction

Concrete is the most widely used construction material in the world due to its versatility, durability, and cost-effectiveness. However, the production of traditional Portland cement, which is a key component of concrete, is associated with significant environmental concerns, including high energy consumption and greenhouse gas emissions[1][2]. In recent years, there has been a growing interest in developing alternative cementitious materials that can mitigate these environmental issues while maintaining or even enhancing the performance of concrete.

One such alternative material is geopolymer concrete, which is produced by activating a source of aluminosilicate material with an alkaline solution. Geopolymer concrete offers several advantages over traditional Portland cement concrete, including reduced carbon dioxide emissions and improved resistance to chemical attack and high temperatures[3-6]. Moreover, geopolymer concrete can utilize various waste materials as precursors, thereby providing a sustainable solution for waste management[7].

This research focuses on investigating the properties of geopolymer concrete incorporating three different waste materials: fly ash, biomass fly ash, and ground granulated blast furnace slag (GGBS). Fly ash is a by-product of coal combustion in thermal power plants, while biomass fly ash is generated from the burning of agricultural residues or wood. GGBS is a by-product of iron production in blast furnaces. These waste materials possess pozzolanic properties, which can contribute to the strength and durability of geopolymer concrete.

The utilization of fly ash, biomass fly ash, and GGBS in geopolymer concrete offers a twofold benefit. Firstly, it reduces the reliance on traditional cement production, thereby reducing carbon dioxide emissions and conserving natural resources. Secondly, it provides a sustainable solution for the disposal of these waste materials, minimizing their environmental impact.

The objective of this study is to evaluate and compare the key properties of geopolymer concrete incorporating fly ash, biomass fly ash, and GGBS. The properties to be investigated include compressive strength, flexural strength, workability, durability, and microstructural characteristics. By understanding the performance of geopolymer concrete with different waste materials, this research aims to contribute to the development of sustainable and environmentally friendly construction materials.

Overall, this research aims to provide insights into the potential of utilizing fly ash, biomass fly ash, and GGBS in geopolymer concrete, thereby promoting the adoption of eco-friendly construction practices. The findings of this study can help engineers and researchers in making informed decisions regarding the use of waste materials in concrete production, leading to a more sustainable and greener construction industry.

7.2 Materials and experimental programs

7.2.1 Materials properties

The fine aggregate used in this study was sourced from locally available sea sand, while the coarse aggregate was obtained from locally available crushed stone. Table 1 presents the physical properties of both the fine and coarse aggregates. Additionally, Figure 1 illustrates the particle size distribution diagram of the fine aggregate.

Table 7.1 properties of the fine and coarse aggregates

Property	Coarse aggregate	Fine aggregate
Oven-dried density (g/cm^3)	2.69	2.59
Fineness modulus	6.9	2.58
Water absorption (%)	1.14	1.04
Solid content (%)	62.1	60.9

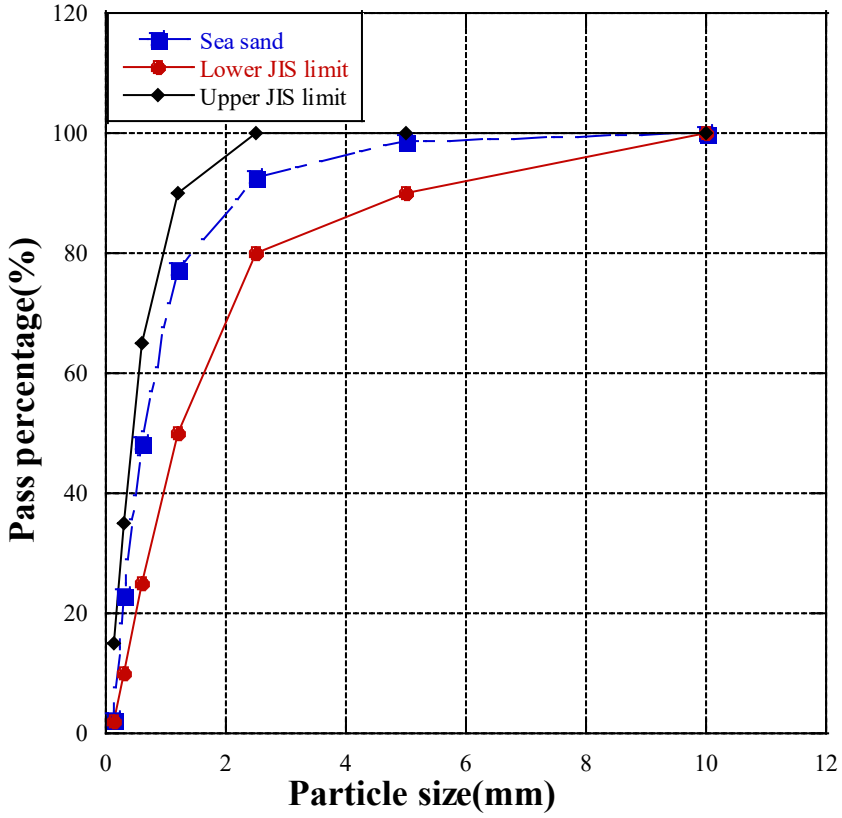

Fig. 7.1 The particle size distribution of fine aggregate

Fly ash corresponding to Class II in JIS A 6201, wood biomass fly ash and GGBS as defined in JIS A 6206 were used as mineral admixture. Table 2 shows the properties of the fly ash (FA), biomass fly ash (BF) and GGBS. Photo 1. shows the SEM image of biomass fly ash. The NaOH solution was made by dissolving caustic soda with about 98% by weight NaOH in distilled water at a concentration of 30%. The solution was left for 24 h before mixing. The Na_2SiO_3 was as a liquid with about 24.8%, 11.1% and 64.1% by weight SiO_2, Na_2O and water, respectively. The Na_2SiO_3 solution was blended with NaOH solution at a Na_2SiO_3/NaOH weight ratio of 2.5 as the alkaline solution (AS) was used in this experiment.

Table 7.2 the properties of cementitious materials

	FA	BF	GGBS
SiO_2 (%)	53.8	21.8	32.7
Al_2O_3 (%)	13.5	7.40	13.4
Fe_2O_3 (%)	13	11.82	0.5
CaO (%)	8.99	40.08	41.6
SO_3 (%)	0.489	4.24	6.9
MgO (%)	1.48	2.1	0.3
Loss on ignition (%)	2.1	3.89	0.6
Density (g/cm^3)	2.2	2.5	2.91
Blaine specific area (cm^2/g)	3270	3350	4100

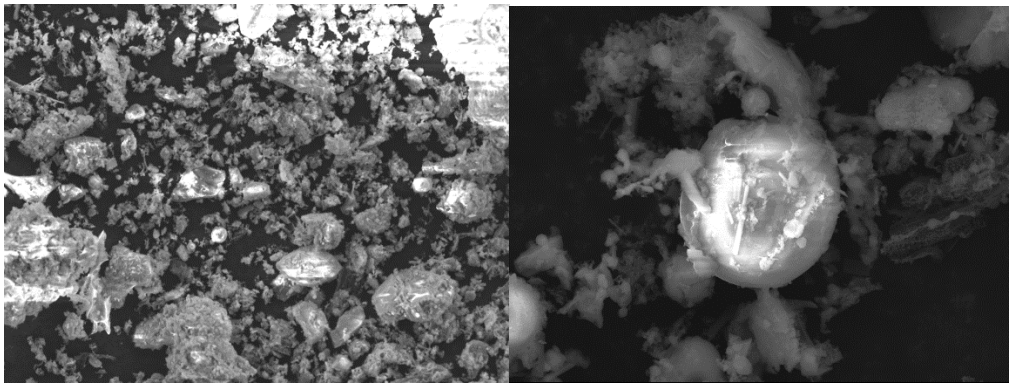

Photo 7.1 SEM image of BF (left: 500 times, right: 5000 times)

7.2.2 Mix proportion.

A total of 12 mixes of concrete and 6 mixes of mortar were prepared: five mixes based on fly ash and GGBS, the content of GGBS was 20,40,50,60,80% respectively; normal concrete of the same strength grade; six mixes based on biomass fly ash and GGBS, the content of biomass fly ash was 0, 20,40,60,80,100% respectively. The unit AS amount was 260 kg/m^3, the unit cementitious amount was 400 kg/m^3, the weight ratio of fine aggregate to cementing material is 1 to 2. The mix proportions are shown in Table 3. The alkaline activators solution (AS) was prepared by sodium hydroxide solution and sodium silicate solution. The sodium silicate solution consists of Na_2O, SiO_2, and H_2O, having 11.02%, 24.28 %, and 64.7%, respectively, with the SG of 1.4 g/cm^3 at 15 ℃. The concentration of sodium hydroxide solution is 30 percent. However, due to the insufficient amount of biomass fly ash, the biomass fly ash group conducted experiments with mortar.

Table 7.3 Mix proportions.

Type	AS/B	Unit mass(kg/m³)					
		AS	BF	FA	GGBS	Fine aggregate	Coarse aggregate
BS20	0.65	260	0	320	80	800	857
BS40	0.65	260	0	240	160	800	877
BS50	0.65	260	0	200	200	800	887
BS60	0.65	260	0	160	240	800	896
BS80	0.65	260	0	80	320	800	916
BF0	0.65	260	0	0	400	800	922
BF20	0.65	260	80	0	320	800	910
BF40	0.65	260	160	0	240	800	898
BF60	0.65	260	240	0	160	800	886
BF80	0.65	260	320	0	80	800	874
BF100	0.65	260	400	0	0	800	862

7.2.3 Experiment method

Compressive strength tests were conducted according to JIS A 1108 [48], and cylinder specimens (diameter 100 mm × height 200 mm) were prepared. The cylinders were cast in a mold and kept in a chamber at 20 °C and 60% relative humidity until the target age. The ages of the tested specimens were 3,7, and 28 days. Load was applied at a uniform rate to avoid subjecting the specimens to impact loading, with the loading rate such that the compressive stress increased by 0.6 ± 0.4 N/mm^2 per second. During each test, specimens were stored at the temperature and humidity specified for that test.

Elastic modulus was tested as following: during each strength test, a device is set up to measure both longitudinal and transverse strains around each concrete sample. The strain measurement device must possess the capability to accurately measure the longitudinal strain (strain degree) of the specimen, achieving a precision of 10×10^{-6} or better. The length of the strain measurement device should be a minimum of three times the maximum size of the coarse aggregate utilized in the concrete and at least half the height of the specimen. Once the deformations have been calculated, the value of E_c can be determined by examining the slope of the stress-strain curve. The equation for E_c, as outlined in JIS A 1149, is provided below:

$$Ec = \frac{(S1 - S2)}{(\varepsilon 1 - \varepsilon 2)} \times 10^{-3}$$

*E*c: Static elastic modulus of each specimen (kN / mm^2).
*S*1: Stress corresponding to 1/3 of the maximum load (N / mm^2).
*S*2: Stress when the longitudinal strain of the specimen is 50×10^{-6} (N / mm^2).
ε1: Vertical strain of the specimen caused by stress.
ε2: 50×10^{-6}.

As part of this research, the calculation of Ed involved conducting resonant frequency testing. Utilizing resonant frequencies to determine material properties is a relatively recent non-destructive testing method. The resonant frequency of vibration is closely linked to the density and Ed of the material. To determine the resonant frequencies of the concrete specimens, they were excited in longitudinal, transverse, or torsional modes, and the resulting free vibrations were measured. The dynamic elastic modulus experiments, involved placing a cylinder on a supportive base, allowing both ends to vibrate freely without any constraints. According to JIS A 1127, the primary resonance frequency for longitudinal vibration was defined as the frequency at which the amplified pickup's output voltage displayed a distinct maximum vibration. The dynamic elastic modulus can be calculated using the following equation:

$$E_d = 4.00 \times 10^{-3} \frac{L}{A} m f^2$$

E_d: Dynamic elastic modulus (N / mm^2).

L: Specimen length (mm).

A: Specimen cross-sectional area (mm^2).

m: Specimen mass (kg).

f: Longitudinal vibration resonance frequency (Hz).

The specimens used for the cracking and tensile strength tests were plastic cylindrical formwork of 50 x 100 mm dia. as in the compressive strength tests, and cracking and tensile strength tests were conducted according to JIS A 1113 "Method for testing cracking and tensile strength of concrete". The specimens were demolded on the first day of age, and then cured in air at 20°C until the target age 28 days.

The flexural strength tests were conducted in accordance with JIS A 1106 "Flexural Strength Test Methods for Concrete" using 40x40x160mm prismatic specimens. The specimens were unmolded on the first day of age, and then cured in air at 20°C until the target age (28 days).

7.3 Results and discussion

7.3.1 Properties of biomass geopolymer mortar

Figure 2 illustrates the compressive strength analysis of biomass fly ash geopolymer mortar. The findings revealed a decline in compressive strength at 3, 7, and 28 days as the fly ash content increased. Specifically, at 3 days, compared to BF0 (with no biomass fly ash content), the compressive strength of BF20, BF40, BF60, BF80, and BF100 decreased by 2.4%, 15.6%, 52%, 125.3%, and 309.1% respectively. Similarly, at 7 days, the compressive strength of BF20, BF40, BF60, BF80, and BF100 decreased by 14.9%, 39.4%, 80.3%, 155%, and 333% respectively when compared to BF0. At 28 days, compared to BF0, the compressive strength of BF20, BF40, BF60, BF80, and BF100 decreased by 8.3%, 13.3%, 45.1%, 111%, and 265.7% respectively.

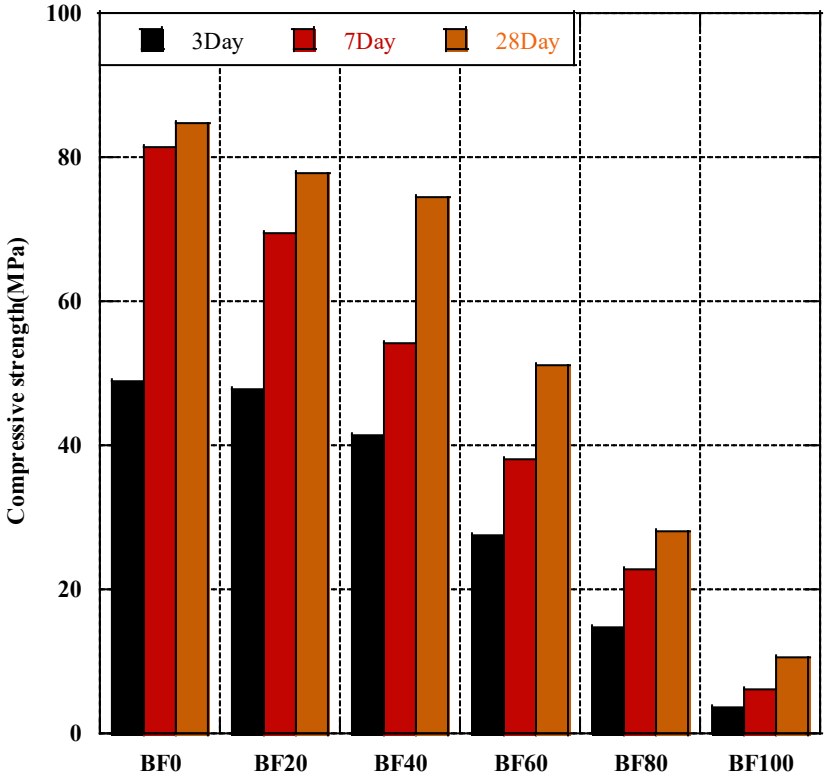

Fig. 7.2 The compressive strength of biomass fly ash geopolymer mortar

Regarding the enhancement of compressive strength for each ratio, the observed increases in compressive strength from 3 days to 7 days and from 7 days to 28 days are as follows: For BF0, there was an increase in compressive strength from 48.97 MPa to 81.52 MPa (an increment of 32.55 MPa) from 3 days to 7 days. Subsequently, from 7 days to 28 days, there was a further increase from 81.52 MPa to 84.82 MPa (an increment of 3.32 MPa). For BF20, the compressive strength increased from 47.78 MPa to 69.33 MPa (an increment of 21.55 MPa) between 3 days and 7 days. The subsequent period, from 7 days to 28 days, saw an additional increase from 69.33 MPa to 77.83 MPa (an increment of 8.49 MPa). In the case of BF40, the compressive strength exhibited a substantial increase from 41.5 MPa to 54.2 MPa (an increment of 12.7 MPa) between 3 days and 7 days. This was followed by a moderate increase from 54.2 MPa to 74.5 MPa (an increment of 20.3 MPa) from 7 days to 28 days. For BF60, there was an increase in compressive strength from 27.4 MPa to 38.1 MPa (an increment of 10.7 MPa) between 3 days and 7 days. Subsequently, from 7 days to 28 days, the compressive strength showed a slight increase from37.8 MPa to 51.2 MPa (an increment of 13.4 MPa). In the case of BF80, the compressive strength increased from 14.7 MPa to 22.7 MPa (an increment of 8 MPa) between 3 days and 7 days. From 7 days to 28 days, there was a decrease in compressive strength from 22.7 MPa to 27.9 MPa (a decrement of 5.2 MPa). For BF100, the compressive strength showed an increase from 3.6 MPa to 6.0 MPa (an increment of 2.4 MPa) between 3 days and 7 days. Subsequently, from 7 days to 28 days, there was a further increase from 6.0 MPa to 10.6 MPa (an increment of 4.6 MPa). It can be seen that the group with lower biomass fly ash content (BF0 and BF20) had faster strength growth, with higher compressive strength appearing on the seventh day and slow growth thereafter. However, the intensity increases in group BF40 and BF60 lasted until 28 days. About BF80 and BF100, although the compressive strength has been growing but still at a low level. Therefore, it can be concluded that biomass fly ash makes

the growth of strength slow.

In addition, regarding the effect of biomass fly ash on the compressive strength, a linear regression analysis was performed according to the different ages of mortar. The results are shown in Figure 3 and each coefficient of determination is greater than 0.9, and the compressive strength was linearly correlated with the content of biomass fly ash at all ages of mortar.

The regression equation of 3-day compressive is as follows:

$$y = 54.951 - 0.48588x \qquad R^2 = 0.9483$$

y: flexural strength (MPa)

x: the content of biomass fly ash (%)

The regression equation of 7-day compressive is as follows:

$$y = 83.41 - 0.76246x \qquad R^2 = 0.99801$$

y: flexural strength (MPa)

x: the content of biomass fly ash (%)

The regression equation of 28-day compressive is as follows:

$$y = 93.353 - 0.7771x \qquad R^2 = 0.93819$$

y: flexural strength (MPa)

x: the content of biomass fly ash (%)

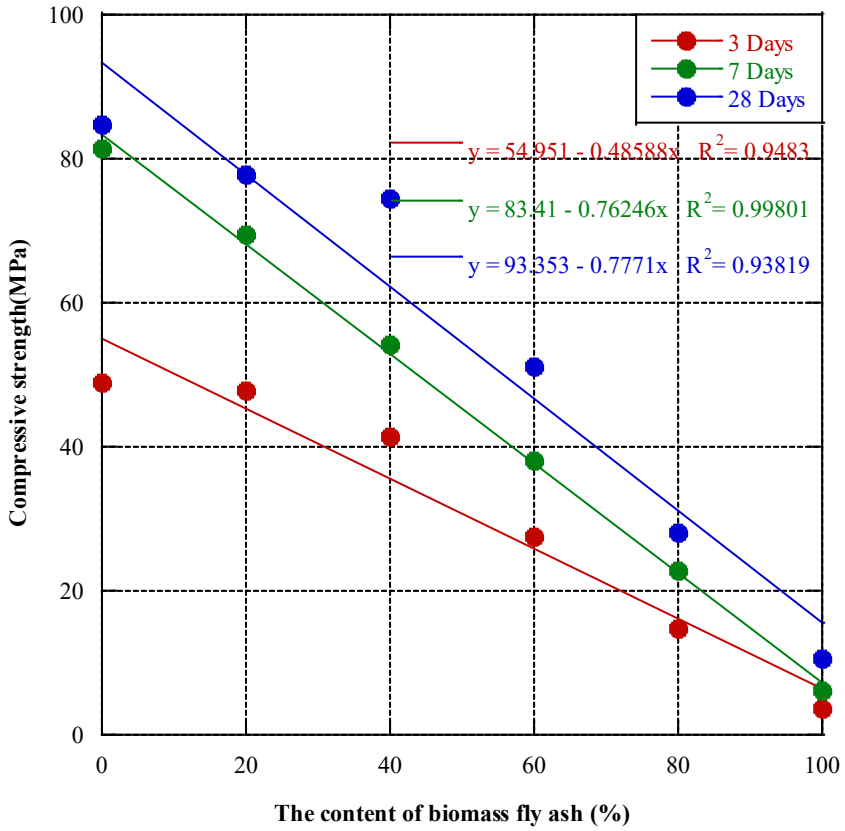

Fig. 7.3 The effect of biomass fly ash on the compressive strength

Figure 4 depicts the flexural strength analysis of biomass fly ash mortar, which is crucial for the present study. The findings demonstrate a clear correlation between flexural strength and biomass fly ash content, showing a decrease as the fly ash content increases. Notably, it was observed that the flexural strength exhibited a relatively insignificant decrease when the biomass fly ash content was increased from 20% to 60%. However, a more substantial decline in flexural strength was observed when the content was further increased to 80% or 100%.

Comparatively, in contrast to BF0 (with no biomass fly ash content), the incorporation of biomass fly ash resulted in a reduction of approximately 20% in flexural strength when blended in the range of 20-40%. Furthermore, the flexural strength of BF80 and BF100 decreased significantly, with reductions of approximately 50% and 70% respectively, as compared to BF0. These outcomes underscore the impact of biomass fly ash content on the flexural strength of the mortar specimens. The findings suggest that while the addition of biomass fly ash up to 60% may have a relatively minor influence on flexural strength, higher contents (80% and 100%) significantly impair the flexural performance. These insights contribute to the understanding of the mechanical properties of biomass fly ash mortar, particularly in terms of flexural strength, which holds significant implications for its application in construction and structural elements.

In addition, a linear regression analysis was performed on the effect of biomass fly ash on flexural strength. The regression equation is as follows:

$$y = 11.029 - 0.0719x \qquad R^2 = 0.93763$$

y: flexural strength (MPa)

x: the content of biomass fly ash (%)

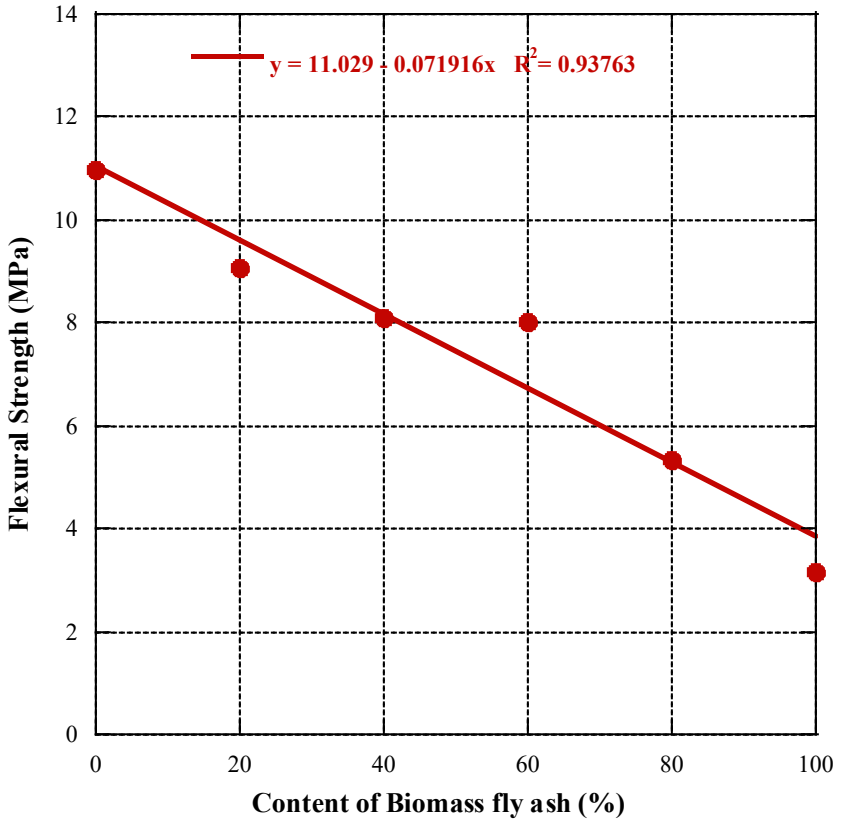

Fig. 7.4 The flexural strength of biomass fly ash geopolymer mortar

Figure 5 illustrates the analysis of splitting tensile strength in the mortar specimens, aligning with the trends observed in compressive and flexural strengths. As the biomass fly ash content increases, the splitting tensile strength experiences a noticeable decline. Similar to the patterns observed in flexural strength, the splitting tensile strength of the mortar displays a relatively insignificant decrease when the biomass fly ash content is increased from 20% to 60%. However, a more substantial decrease in splitting tensile strength becomes evident as the biomass ash content surpasses 80%. Compared to BF0 (with no biomass fly ash content), the inclusion of biomass fly ash results in a reduction of approximately 15% in splitting tensile strength when blended in the range of 20% to 40%. Furthermore, there is a significant decrease in splitting tensile strength as the biomass fly ash content reaches 80% and 100%, with reductions of approximately 37% and 73% respectively, compared to BF0.

These findings emphasize the influence of biomass fly ash content on the splitting tensile strength of the mortar specimens. The results indicate that while the addition of biomass fly ash up to 60% exhibits a limited effect on splitting tensile strength, higher contents (80% and 100%) notably impair the splitting tensile performance. These observations contribute to the understanding of the mechanical behavior of biomass fly ash mortar, specifically in terms of splitting tensile strength. Such insights hold significant implications for the appropriate utilization of this material in construction applications and the design of structural elements.

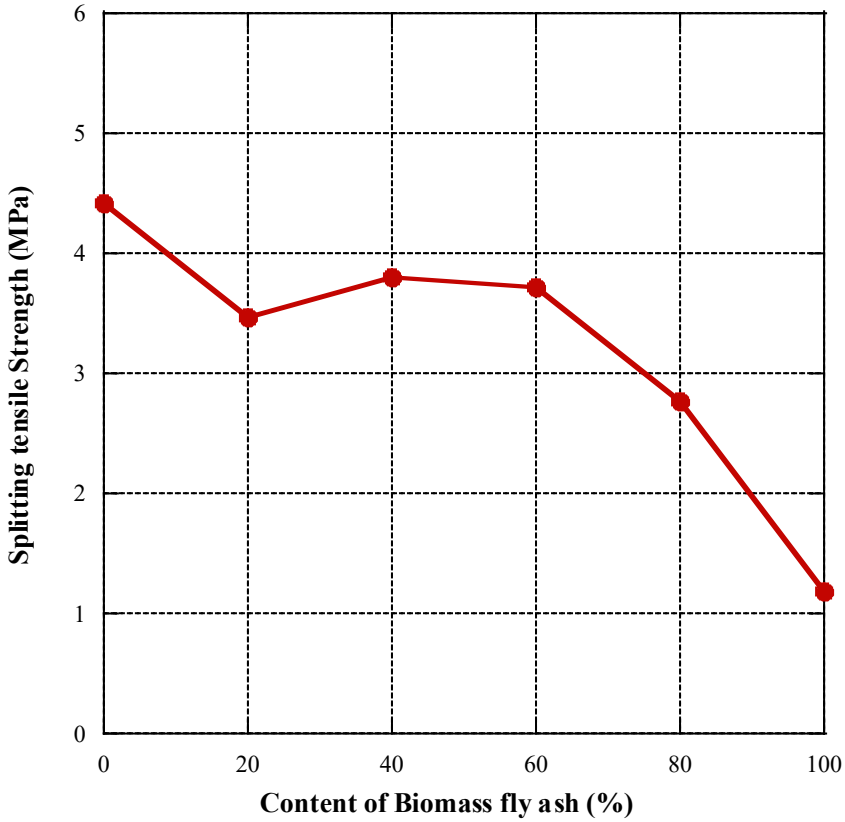

Fig. 7.5 The splitting tensile strength of biomass fly ash geopolymer mortar

7.3.2 Properties of geopolymer concrete

Figure 6 exhibits the compressive strength of the geopolymer concrete samples. The results demonstrate that all geopolymer concretes exhibit commendable compressive strengths, with the lowest strength group (BS20) showcasing a 28-day compressive strength comparable to that of the control group comprising plain concrete. Notably, the BS80 group, composed of 80% GGBS and 20% fly ash, exhibited the highest compressive strength, reaching an impressive 86 MPa at 28 days. This trend persisted across all age groups, indicating a decline in the geopolymer concrete strength as the GGBS content decreased. Specifically, the BS40 sample achieved a compressive strength of 60 MPa. Consequently, it can be deduced that a GGBS content of no less than 40% is advisable for the production of high-strength geopolymer concrete, while a GGBS content ranging from 20% to 40% is suitable for ordinary strength geopolymer concrete production. While BS20 displayed a 28-day compressive strength comparable to that of the control group, its early compressive strengths at 3 and 7 days were relatively lower. However, it is noteworthy that the geopolymer concrete exhibited a remarkable enhancement in early compressive strength as the GGBS content increased. Specifically, the early compressive strength of BS40 surpassed that of the control group at both 3 and 7 days, and its 28-day compressive strength experienced a significant 50% increase compared to the control group.

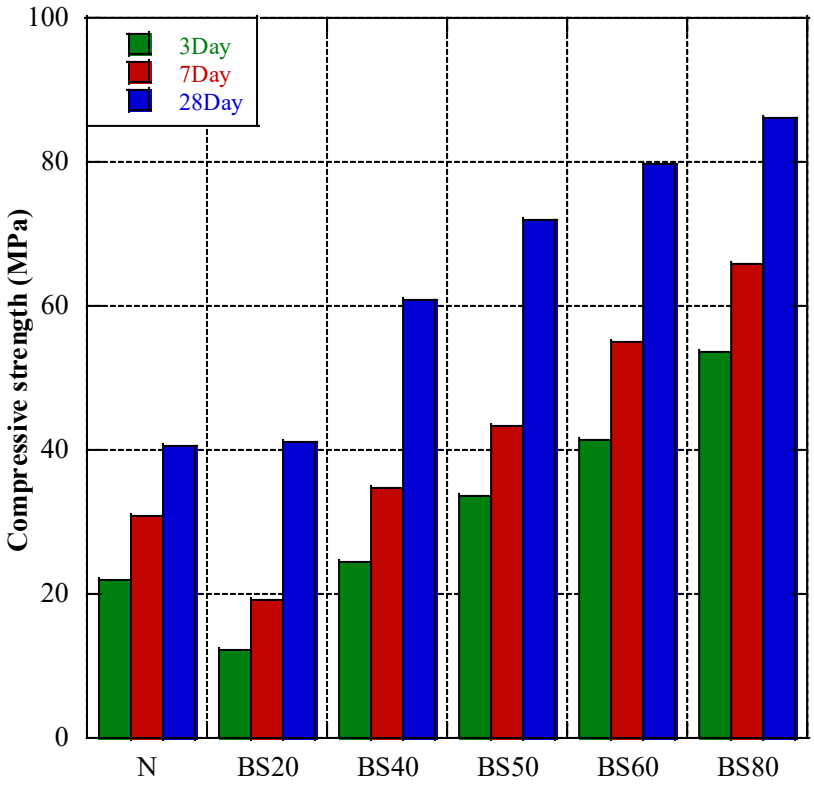

Fig. 7.6 The compressive strength of geopolymer concrete

The static modulus of elasticity of geopolymer concrete was determined through experimental analysis. The modulus of elasticity is a fundamental mechanical property that reflects the material's stiffness and ability to resist deformation under applied loads. In this study, the geopolymer concrete samples exhibited varying static modulus of elasticity values depending on their composition and curing conditions.

Figure 7 presents the static modulus of elasticity of the geopolymer concrete specimens. It can be observed that the geopolymer concretes displayed relatively lower static modulus of elasticity compared to the control group of plain concrete (with the same strength level). For example, the 28-day strength of BS20 was similar to the control group, but the static modulus of elasticity of BS20 was only about 65% of that of the control group. Among the different mix compositions, the sample with a higher content of GGBS demonstrated a higher modulus of elasticity. Specifically, the BS80 group, comprising 80% GGBS and 20% fly ash, exhibited the highest static modulus of elasticity, indicating its enhanced stiffness and resistance to deformation. Furthermore, it is worth noting that the static modulus of elasticity of the geopolymer concrete increased with curing time. At each specified curing age, the geopolymer concrete samples consistently exhibited lower static moduli of elasticity compared to the control group. This shows that the relationship between compressive strength and static modulus of elasticity of geopolymer concrete is obviously different from that of ordinary concrete, and a deeper study should be conducted for this problem.

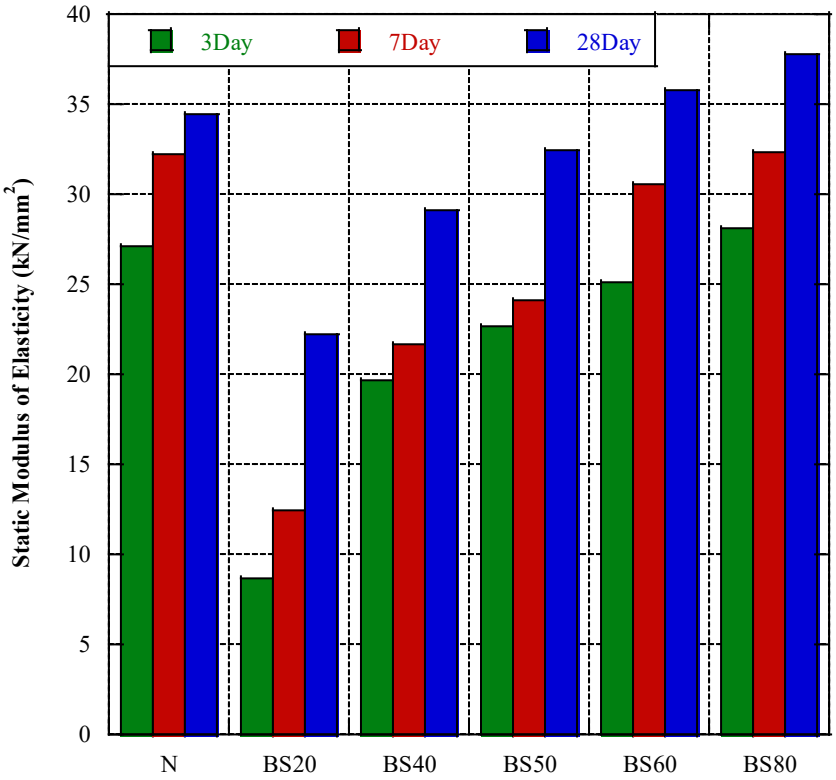

Fig. 7.7 The static modulus of elasticity of geopolymer concrete

Figure 8 depicts the dynamic modulus of elasticity of geopolymer concrete. Consistent with the observations concerning the static modulus of elasticity, geopolymer concrete samples with equivalent compressive strength levels demonstrated notably lower dynamic moduli of elasticity compared to conventional concrete. Nevertheless, it is noteworthy that the disparity between the dynamic modulus of elasticity of ordinary concrete and geopolymer concrete is comparatively smaller than that observed for the static modulus of elasticity.

Furthermore, it is important to highlight that the dynamic modulus of elasticity of geopolymer concrete exhibited an increasing trend with higher GGBS content. The BS80 group stands out with the highest modulus of elasticity value, reaching an impressive 37.7 kN/mm^2.This indicates that an elevated proportion of GGBS in the geopolymer concrete mixture contributes to the enhancement of its dynamic stiffness. These findings emphasize the distinct behavior of geopolymer concrete in terms of dynamic modulus of elasticity when compared to ordinary concrete. The dynamic modulus of elasticity serves as a critical parameter in assessing the material's ability to withstand dynamic loads and vibrations. Further research is warranted to comprehensively investigate the factors influencing the dynamic modulus of elasticity of geopolymer concrete, including the effects of various GGBS content levels and curing conditions.

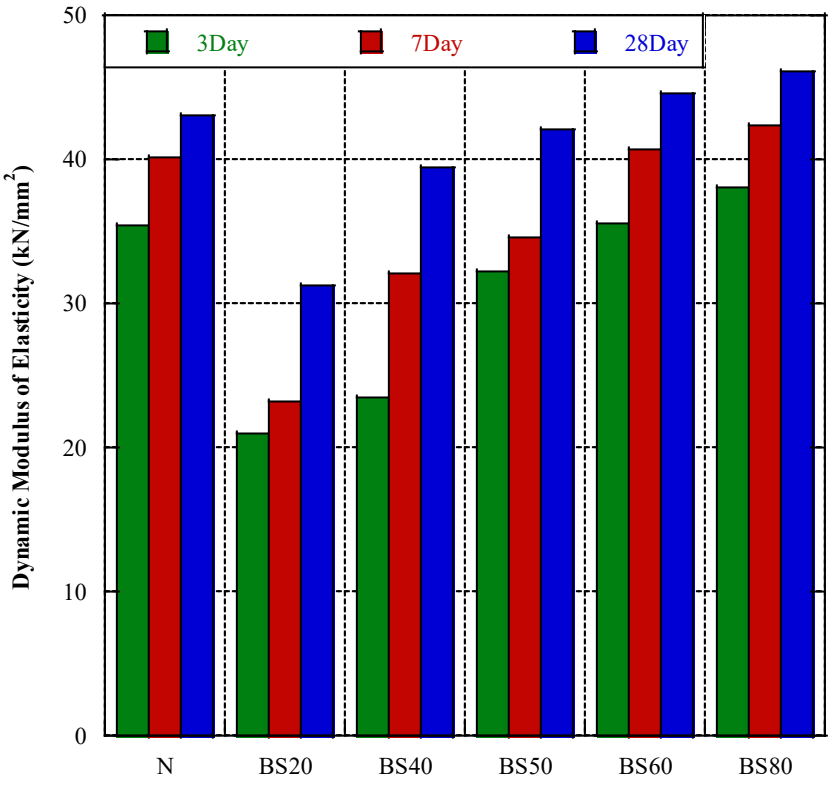

Fig. 7.8 The dynamic modulus of elasticity of geopolymer concrete

Figure 9 shows the relationship between the static and dynamic elasticity coefficients of geopolymer concrete. It is very obvious that, as with ordinary concrete, the dynamic modulus of elasticity is linearly related to the static modulus of elasticity, and the obtained R^2 value is approximately 0.95.

The regression equation is as follows:

$$y = 10.863 + 0.95124x \qquad R^2 = 0.94805$$

y: dynamic modulus of elasticity (kN/mm^2)
x: static modulus of elasticity (kN/mm^2)

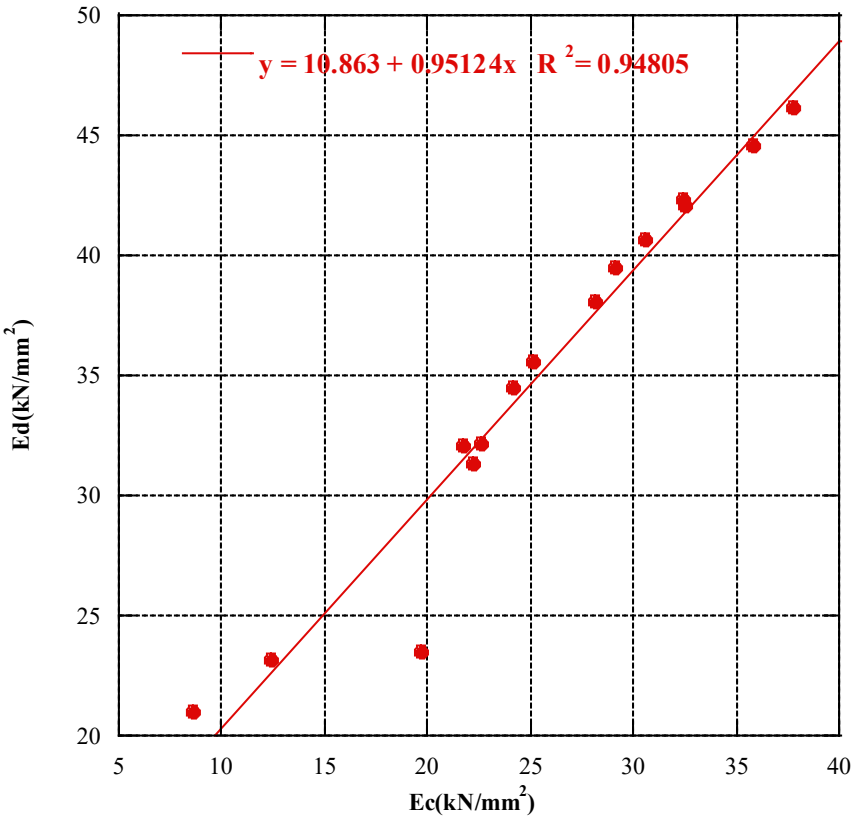

Fig. 7.9 The relationship between the E_d and E_c.

The results of compressive strength and static modulus of elasticity of geopolymer concrete show that geopolymer concrete is significantly different from ordinary concrete, so further analysis of geopolymer concrete is needed. Figure 10 shows the relationship between the compressive strength and the static modulus of elasticity of the geopolymer concrete.

A regression analysis was conducted on the experimental data, yielding an impressive R-squared value of 0.96645. The regression equation derived from the analysis is presented below:

$$y = 16x^{0.3} - 25 \qquad R^2 = 0.96645$$

y: static modulus of elasticity (kN/mm^2)
x: compressive strength (N/mm^2)

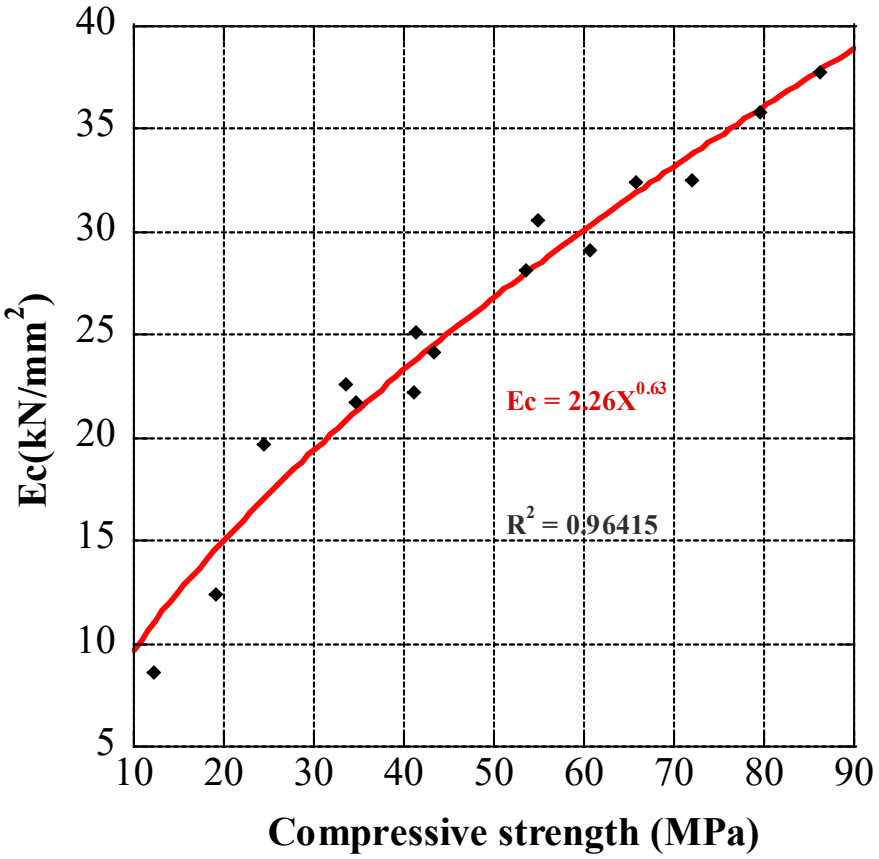

Fig. 7.10 The relationship between the E_c and compressive strength.

7.4 Conclusion

1. The analysis of the compressive, flexural, and splitting tensile strengths of biomass fly ash mortar yields significant findings regarding the impact of biomass fly ash content on the mechanical properties of the material.

The results demonstrate a consistent downward trend in strength as the biomass fly ash content increases. Specifically, the compressive strength exhibits a substantial reduction across all tested time intervals, with the most pronounced decrease observed at higher biomass fly ash contents. Similarly, the flexural strength shows a noticeable decline, particularly when the content exceeds 60%.

Interestingly, both the flexural and splitting tensile strengths display a relatively insignificant decrease when the biomass fly ash content is increased from 20% to 60%. However, a significant decrease is observed once the content surpasses 80%, indicating a critical threshold beyond which the material's performance is significantly compromised.

2. Furthermore, an investigation was conducted on the properties and performance of geopolymer concrete incorporating Ground Granulated Blast Furnace Slag (GGBS) and fly ash as binder materials, leading to several key findings.

Firstly, the geopolymer concretes exhibit high compressive strengths, with the lowest strength group (BS20) achieving comparable 28-day strength to the control group of plain concrete. Notably, the BS80 group, comprising 80% GGBS and 20% fly ash, demonstrates the highest compressive strength, reaching an impressive 86 MPa. The findings reveal that the strength of the geopolymer concrete decreases with increasing GGBS content, highlighting the influence of binder composition on the mechanical properties.

Moreover, the static and dynamic moduli of elasticity were evaluated to assess the stiffness and deformation characteristics of the geopolymer concrete. The results indicate that the geopolymer concretes exhibit lower moduli of elasticity compared to ordinary concrete, albeit with a relatively smaller disparity for dynamic modulus. Additionally, the dynamic modulus of elasticity increases with higher GGBS content, suggesting a potential for enhanced dynamic load resistance.

Regression analysis of the experimental results yields a high R-squared value of 0.96645, indicating a strong correlation among the variables studied. The resulting regression equation can be utilized for future applications to predict and optimize the properties of geopolymer concrete.

In summary, this research provides valuable insights into the utilization of GGBS and fly ash in geopolymer concrete production. The findings suggest that the selection of GGBS content should be conducted carefully to achieve desired compressive strengths, with a minimum of 40% recommended for high strength geopolymer concrete.

Reference

[1] Ecra (European Cement Research Academy). Calcined Clay: A Supplementary Cementitious Material with a Future. Available online: https://ecra-online.org/file admin/ecra/newsletter/ECRA_Newsletter_3_2019.pdf (Accessed on 02 October 2021).

[2] R. Colaço, Reduce the environmental impact of cement (Portuguese), Constr. Mag. 90 (2019) 12–14.

[3] Sathia R, Babu KG, Santhanam M. Durability Study of Low Calcium Fly Ash Geopolymer Concrete. The 3rd ACF International Conference ACF/ VCA, HO Chi Minh City, Vietnam Institue for Building materials 2008; 1153-1159.

[4] Arifln MAM, Bhutta MAR, Hussin MW, Mohd Tahir M, Aziah N. Sulfuric acid resistance of blended ash geopolymer concrete. Constr Build Mater 2013;43:80–6. https://doi.org/10.1016/j.conbuildmat.2013.01.018.

[5] Luhar S, Khandelwal U. Durability studies of fly ash based geopolymer concrete. Int J Eng Res Appl 2015;5:17–32. https://doi.org/10.14445/23488352/IJCE-V2I8P10 1.

[6] Lavanya G, Jegan J. Durability study on high calcium fly ash based geopolymer concrete. Adv in Mat Sci and Eng 2015;2015:1–7. https://doi.org/10.1155/2015/ 731056.

[7]] Ojha A, Gupta L. In: Chauhan A, Sehgal S (eds) Comparative study on mechanical properties of conventional and geo-polymer concrete with recycled coarse aggregate. Materials Today: Proceedings 2020; Chandigarh, Punjab, India https:// doi.org/10.1016/j.matpr.2020.04.811.

Chapter 8

CONCLUSION

Conclusion

A STUDY ON ENGINEERING PROPERTIES AND ENVIRONMENTAL IMPACT OF SUSTAINABLE CONCRETE WITH FLY ASH OR GGBS

The replacement of sand with fly ash or GGBS resulted in a significant increase in the compressive strength of concrete. Concrete with 30% fly ash replacement exhibited a 45% higher compressive strength compared to ordinary concrete, while 30% GGBS replacement showed a remarkable 112% increase. This suggests that fly ash and GGBS replacements can yield high-performance concrete.

Drying shrinkage was influenced by the presence of fly ash and GGBS. Concrete with 10% fly ash replacement exhibited the lowest drying shrinkage, which increased as fly ash content increased. GGBS replacements led to a significant reduction in drying shrinkage, with 30% GGBS replacement resulting in a 20% decrease.

Regarding creep behavior, concrete with 20% fly ash replacement exhibited the lowest creep strain, approximately 40% lower than control concrete. Creep strain increased with higher fly ash content (>20%), except for the 30% fly ash replacement for sand, which exhibited a 50% lower creep strain.

In terms of CO2 emissions per compressive strength ratio, concrete with GGBS replacements demonstrated lower CO2 emissions. Concrete with 30% GGBS replacement for sand showed approximately half the CO2 emissions compared to control concrete.

Analyzing widely recognized creep prediction models, an introduced parameter, KL, captured the effect of fly ash content in the AIJ Model, which displayed the highest accuracy for ordinary concrete. The low root mean square error (RMSE) obtained between experimental and predicted values using the developed model indicated the effectiveness of the introduced parameter for concrete containing fly ash.

Overall, this research provides valuable insights into the influence of fly ash and GGBS replacements on the properties of concrete, including compressive strength, drying shrinkage, creep behavior, CO2 emissions, and creep prediction models.

THE EFFECT OF BIOMASS FLY ASH AND LIMESTONE POWDER ON THE PROPERTIES OF CONCRETE

Adding limestone powder to wood biomass fly ash concrete or blend biomass fly ash concrete increases the compressive strength of concrete in all ages. In addition, the drying shrinkage and carbonization depth increase with the limestone powder content increases. The using of wood biomass fly ash or blend biomass fly ash alone also increases the compressive strength within a certain range, but it is still smaller than the original concrete, and also increases the drying shrinkage and carbonization depth. Regarding porosity, adding blend biomass fly ash or wood biomass fly ash to concrete increases the total pore volume of concrete, and adding limestone powder increases the total pore volume but reduces the pore volume of pores with large diameter. Under water curing, the decrease of pore volume with larger pore volume is more obvious. The compressive strength of concrete has a higher correlation with the volume of 0.05~36μm pores and the drying shrinkage has a higher correlation with the volume of 0.003~0.05μm pores.

THE EFFECT OF CEMENTITIOUS MATERIALS ON THE ENGINEERING PROPERTIES AND PORE STRUCTURE OF CONCRETE WITH RECYCLED FINE AGGREGATE

Adding fly ash and GGBS to RFA concrete increased its compressive strength. M50BS45 and

M50FA15BS15 exhibited similar 91-day compressive strengths with normal concrete. Therefore, the compressive strength of RFA concrete can be effectively improved by the use of cementitious materials.

Replacement of cement with fly ash or GGBS significantly decreased the drying shrinkage of the RFA concrete. The drying shrinkage of all specimens in this experiment reach the level of ordinary concrete, even lower than that of ordinary concrete. Besides, M50FA15BS15 showed 16.5% lower drying shrinkage, M50BS45 and M50FA15BS30 showed around 25% lower drying shrinkage than normal concrete.

Increasing the cementitious (fly ash and GGBS) materials content decreased the carbonation resistance of RFA concrete. Besides, fly ash had a greater effect on carbonation than GGBS.

Incorporating FA or GGBS into concrete modified the pore structure of concrete, reduced the volume of capillaries larger than 0.05μm. In addition, the compressive strength was mainly affected by the capillary pores (greater than 0.01μm or 0.05μm), and the carbonation was mainly affected by the gel pores (less than 0.01μm).

For compressive, the pores with a diameter greater than 0.05μm are considered harmful pores, 0.01-0.05μm are considered small harmful pores, and less than 0.01μm are considered harmless pores.

THE EFFECT OF FLY ASH AND GARBAGE MOLTEN SLAG FINE AGGREGATES ON THE CREEP OF CONCRETE

Incorporating fly ash at a 20% replacement ratio effectively reduced the unit creep strain in concrete. The predicted values of normal concrete obtained from the AIJ equation for unit creep strain aligned well with the measured values. The introduction of a correction factor of approximately 0.73 accounted for the influence of fly ash in the predicted values.

Concrete mixed with fly ash exhibited a slight increase in compressive strength after loading compared to the unloaded condition. However, the effect of loading on the compressive strength was minimal in concrete without fly ash.

The quantity of pores with a diameter less than 500 nm and the unit creep strain in concrete showed a consistent linear relationship regardless of the presence or absence of fly ash. This implies that as the number of pores with a diameter less than 500 nm increases, the specific creep strain tends to decrease.

Concerning compressive strength, FA30-0 exhibited the most significant increase in strength after 28 days, which can be attributed to the pozzolan reaction. Additionally, the inclusion of garbage molten slag demonstrated a suppressive effect on the strength increase beyond 28 days of age.

With regard to drying shrinkage strain, the incorporation of fly ash resulted in a tendency towards reduced drying shrinkage. Moreover, the shrinkage reduction effect achieved by replacing molten slag was found to be superior to that of fly ash.

In terms of unit creep strain, the addition of fly ash in concrete showcased a strain suppression effect. While the impact on creep strain at a 25% substitution rate of molten slag was relatively small, an increased substitution rate of 50% exhibited a tendency towards elevated creep strain.

Regarding pore volume, mixtures containing fly ash displayed a more substantial decrease in pore volume during the period between 7 and 91 days of age.

THE PROPERTIES OF FLY ASH, BIOMASS FLY ASH, AND GGBS-BASED GEOPOLYMER CONCRETE

The research findings highlight several significant conclusions regarding the utilization of biomass fly ash and GGBS in concrete production. Firstly, increasing the biomass fly ash content leads to a significant reduction in compressive strength, with the most substantial decrease observed at higher fly ash contents. The flexural and splitting tensile strengths display a relatively insignificant decrease within the range of 20% to 60% fly ash content, but a critical threshold is observed beyond 80% fly ash content, resulting in a significant decrease in strength.

Regarding geopolymer concrete incorporating GGBS and fly ash, the compressive strengths of the geopolymer concretes are high, with the BS80 group (80% GGBS, 20% fly ash) exhibiting the highest compressive strength. The strength decreases with increasing GGBS content, indicating the influence of binder composition on mechanical properties. The moduli of elasticity of geopolymer concretes are lower compared to ordinary concrete, with a relatively smaller disparity for dynamic modulus. The dynamic modulus of elasticity increases with higher GGBS content, suggesting improved dynamic load resistance.

The regression analysis shows a strong correlation among the variables studied, with a high R-squared value. The resulting regression equation can be used for future applications to predict and optimize the properties of geopolymer concrete. In summary, this research provides valuable insights into the utilization of biomass fly ash and GGBS in concrete production, emphasizing the careful selection of GGBS content for achieving desired compressive strengths in geopolymer concrete.